Forschungszentrum Karlsruhe
in der Helmholtz-Gemeinschaft

Wissenschaftliche Berichte
FZKA 6930

Similarity and Size Effects in the Quasi-Static Testing of Notched Specimens - A Review -

T. Malmberg

Institut für Reaktorsicherheit

September 2004

Forschungszentrum Karlsruhe

in der Helmholtz-Gemeinschaft

Wissenschaftliche Berichte

FZKA 6930

Similarity and Size Effects in the Quasi-Static Testing of Notched Specimens

- A Review -

Thilo Malmberg

Institut für Reaktorsicherheit

Forschungszentrum Karlsruhe GmbH, Karlsruhe

2004

Impressum der Print-Ausgabe:

Als Manuskript gedruckt

Forschungszentrum Karlsruhe GmbH
Postfach 3640, 76021 Karlsruhe

Mitglied der Hermann von Helmholtz-Gemeinschaft
Deutscher Forschungszentren (HGF)

ISSN 0947-8620

urn:nbn:de:0005-069303

Abstract

The question of similarity or non-similarity or size effects in deformation and failure is a long-standing problem which has gained recently considerable attention because of its importance for the transferability of mechanical test results of geometrically similar, scaled down structural models to full scale structures using similitude laws. Moreover, it concerns also the validity of the use of small scale laboratory type test results as a basis for the computational modelling of large scale components.

Special attention has to be given to structures with strain concentrators, such as holes or notches, which are susceptible to excessive strains, damage, and crack initiation. These mechanisms and the non-uniformity of the associated stress and strain distributions (stress and strain gradients) may induce size effects which are more pronounced than for uniform distributions.

In support of the EU-Project LISSAC ("Limit Strains for Severe Accident Conditions"), a literature survey was performed concerning mechanical test results of geometrically similar, bluntly or sharply notched specimens made of metallic materials, predominantly steel. In most cases the specimens are of relatively simple shape, such as circular tension specimens with a circumferential V- or U-notch, single-edge-notched bend specimens with rectangular cross sections, compact tension specimens, and others. The review has to be restricted to quasi-static loading conditions. Attention is focussed on test results of specimens of nominally the same material which are geometrically similar to a very large extent. Results of primary interest are:

- Records representing normalized loads or stresses versus normalized displacements or strain measures based on load-point displacement, notch opening, or crack extension.
- Specific quantities derived from these, such as absorbed energies up to fracture, maximum load, or crack initiation, normalized displacements or strains at maximum load or at a sudden load drop.
- Reduction of area or diametrical strain at a notch as well as relative notch mouth opening after fracture.
- Crack initiation and crack propagation behaviour.

Although not part of the primary interest, the size influence on characteristic quantities of Linear Elastic Fracture Mechanics and Elastic-Plastic Fracture Mechanics is also considered to some extent: The critical stress intensity factor or strain energy release rate at initiation of crack extension, appropriate for brittle response of essentially elastic materials, and the path-independent J-contour integral as well as the crack-tip opening displacement for elastic-plastic material behaviour; moreover, the size influence on records representing the J-contour integral or the crack-tip opening displacement versus the crack extension (resistance curves) are also examined where available.

A number of influences are pointed out which may affect all these results. They come from intended variations of the test conditions (e.g. temperature, testing rate, notch sharpness) or are undesirable ones and difficult to control (e.g. macroscopic material inhomogeneity, testing machine effects).

In the course of a previous literature survey, references on size effects in notched specimens had been found and this search was extended by the computerized support of several data banks. The results of about 30 research activities are reviewed selectively in chronological order, with the first publication in 1932 and the last one in 2001; but certainly, the cited

literature is not exhaustive. The annotated review closes with discussions and conclusions referring to specific results of the various publications, as related to the various issues mentioned above.

Ähnlichkeit und Größeneffekte bei quasistatischen Versuchen von gekerbten Proben – Ein Überblick

Zusammenfassung

Die Frage der Ähnlichkeit oder Unähnlichkeit bzw. des Größeneinflusses auf das Deformations- und Versagensverhalten ist ein lang anstehendes Problem. Es hat aber unlängst beachtliche Aufmerksamkeit erfahren wegen seiner Bedeutung für die Übertragbarkeit von mechanischen Prüfresultaten von Kleinversuchen auf Großversuche mit Hilfe von Ähnlichkeitsgesetzen. Darüber hinaus betrifft diese Frage auch die Gültigkeit der Verwendung von Kleinversuchen im Labormaßstab als Grundlage für die Computerberechnung von Großkomponenten.

Besondere Beachtung muss Strukturen mit Dehnungskonzentrationen, wie Löchern oder Kerben, gegeben werden, die für Dehnungsüberhöhungen, Schädigung und Rissinitiierung anfällig sind. Diese Mechanismen und die Ungleichförmigkeit der zugehörigen Spannungs- und Dehnungsverteilungen (Spannungs- und Dehnungsgradienten) können Größeneffekte verursachen, die stärker ausgeprägt sind als bei gleichförmigen Verteilungen.

Zur Unterstützung des EU-Projektes LISSAC („Limit Strains for Severe Accident Conditions“) wurde ein Literaturüberblick durchgeführt, der die mechanischen Versuchsergebnisse geometrisch ähnlicher Proben mit stumpfen oder scharfen Kerben und vorwiegend aus Stahl betrifft. In den meisten Fällen sind die Proben von einfacher Formgebung, wie z.B. runde Zugproben mit einer V- oder U-förmigen Umlaufkerbe, einseitig gekerbte Drei-Punkt-Biegeproben mit rechteckigem Querschnitt, Kompakt-Zugproben und andere. Der Überblick muss auf quasi-statische Belastungsbedingungen beschränkt werden. Beachtung wird vorwiegend Versuchsergebnissen von Proben aus nominell demselben Material gegeben, die im großen Umfang geometrisch ähnlich sind. Ergebnisse von primärem Interesse sind:

- Aufzeichnungen von normalisierten Belastungen oder Spannungen über den normalisierten Verschiebungen oder Verzerrungsmaßen, basierend auf Lastpunktverschiebung, Kerböffnung oder Rissfortschritt.
- Spezielle abgeleitete Größen wie absorbierte Energien bis zum Bruch, zur Maximallast oder bis zur Rissinitiierung; normalisierte Verschiebungen oder Verzerrungen bei Maximallast oder bei plötzlichem Lastabfall.
- Brucheinschnürung oder relative Durchmesseränderung an der Kerbe wie auch relative Kerböffnung nach dem Bruch.
- Rissinitiierung und Rissfortschrittsverhalten.

Obgleich hier nicht von primärem Interesse, wird in begrenztem Umfang auch der Größeneinfluss auf charakteristische Werte der Linear Elastischen Bruchmechanik und der Elastisch-Plastischen Bruchmechanik betrachtet: Der kritische Spannungsintensitätsfaktor oder die Verzerrungsenergiefreisetzungsrate bei Beginn der Rissfortschritts – Größen geeignet für das spröde Verhalten im wesentlichen elastischer Materialien – und das wegunabhängige J-Konturintegral sowie die Rissspitzenöffnung für elastisch-plastisches Materialverhalten. Darüber hinaus wird auch, sofern vorhanden, der Größeneinfluss auf solche Aufzeichnungen betrachtet, die das J-Konturintegral oder die Rissspitzenöffnung über dem Rissfortschritt (Risswiderstandskurven) darstellen.

Eine Reihe von Einflüssen werden aufgezeigt, die alle diese Resultate beeinflussen können. Sie rühren von beabsichtigten Variationen der Testbedingungen (z. B. Temperatur, Versuchsgeschwindigkeit, Kerbspritzenschärfe) her oder sind unerwünscht und schwer zu kontrollieren (z. B. makroskopische Materialinhomogenität, Effekte der Versuchseinrichtung).

Im Rahmen einer früheren Literaturstudie waren Veröffentlichungen über Größeneffekte in gekerbten Proben gefunden worden und diese Suche wurde erweitert mit Computerunterstützung mehrerer Datenbanken. Die Ergebnisse von etwa 30 Forschungsaktivitäten werden in diesem Bericht selektiv in zeitlicher Reihenfolge besprochen, wobei die erste Veröffentlichung von 1932 und die letzte von 2001 stammt. Allerdings ist die zitierte Literatur nicht erschöpfend. Der kommentierte Überblick schließt mit Diskussionen und Schlussfolgerungen ab, die sich auf die oben genannten speziellen Resultate der verschiedenen Veröffentlichungen beziehen.

CONTENTS

1 Introduction and Objective

The assessment of the proper function and integrity of complex structures through numerical simulations may be impossible or prohibitive because of an excessive computational effort or because the governing physical processes are insufficiently known. However, full scale experiments are often not realizable because of cost or hazards. An experiment with a geometrically similar, scaled down model may provide essential information if appropriate "similitude laws" can be obeyed in the design and performance of the small scale experiment. Then a direct transfer of the experimental results to the full scale situation is possible using the similitude laws as "transfer laws".

For such an approach to be successful, it is important to understand and to quantify the governing physical phenomena. If the appropriate balance equations and constitutive relations as well as initial and boundary conditions have been set up, the similarity laws can be obtained by transforming the governing equations in a dimensionless form which automatically yields a set of dimensionless characteristic parameters or functions. Similarity of the model- and the large scale prototype-response means that the dimensionless solutions for displacements, strains, stresses, velocities, etc. of model and prototype are identical (e.g., Malmberg (1995, [1.1])) at homologous points and scaled times. This implies the equality of the corresponding characteristic parameters or functions and these requirements represent the "similarity laws".

Aside from this approach, known as the "method of differential equations" or simply the "method of equations", other approaches, like the "method of ratio of forces, energies, etc." or the "dimensional analysis and application of the Buckingham - Π - Theorem", may be used.

A rather important case is obtained when the model uses the same material at the same temperature (replica models) as the prototype. Experience with similarity analysis in general but also for replica models shows that some of the similarity laws cannot be satisfied at all and others can be satisfied only approximately. Under these circumstances, size effects occur for replica models, i.e., the dimensionless solutions for the replica model and the prototype are not identical but depend on the geometric scale. This is the case when, for example, viscous effects come into play or when heat conduction becomes important, not to speak of fracture processes.

When inertia effects[1] are accounted for, a special situation occurs if the model and the prototype use the same classical elasto-plastic material[2] at the same temperature. Then the similarity conditions can be satisfied only if the characteristic velocities are the same (Malmberg (1995, [1.1])). This then implies that not only the strains but also the stresses and all other strain- or stress-like variables as well as volume densities of deformation energies are the same at homologous points and scaled times. In solid mechanics this case represents the traditional paradigm in considerations of similarity and its contrary (i.e., size dependence).

A further special case is obtained if inertia effects (impact, wave propagation) can be safely neglected and static or quasi-static conditions prevail. Then the similarity condition of "equal characteristic velocities" is obsolete for the replica model and prototype of the same

[1] Gravity effects are assumed to be of no importance

[2] No viscosity effects and isothermal conditions

non-viscous elastic-plastic material: the velocities (e.g., traction velocities) may be chosen at will, but such that quasi-static conditions remain valid for both model and prototype. The choice affects only the time scale.

However, if visco-plasticity becomes important under quasi-static conditions, an arbitrary choice of the characteristic velocities induces a size dependence due to the rate dependence of the material: for example, the use of the same traction velocity for the model and for the prototype increases the strain rate in the model by the factor $\lambda>1$, compared to the prototype, where λ is the geometric scale factor. For a rate dependent material, usually an increase of the strain rate yields an increase of the flow stress such that for equal stress conditions the strains will be undervalued in the replica model. Under quasistatic conditions, this can be prevented by observing the additional similarity condition, implied by visco-plasticity, of equal ratios of the characteristic velocity v_R and the characteristic length l_R, i.e., $(v_R/l_R)_m = (v_R/l_R)_p$,with the subscripts m and p denoting the model and the prototype. This is equivalent to requiring the same strain rate at corresponding points and equal time scales. Of course, this condition can also be used when the material is rate-independent and quasi-static loading is prevailing. For further details on similarity and size effects in the deformation behaviour see Ref. [1.1].

If fracture phenomena due to sharp notches or cracks occur, the theoretical concepts of Linear Elastic or Elastic-Plastic Fracture Mechanics (LEFM or EPFM) may apply to describe the instant of crack extension. These conditions at the crack tip[3] (i.e., the stress intensity factor K or the J-integral reaches a critical, material specific value – the fracture toughness) inherently imply a size dependence of stresses and strains at this instant, provided the fracture toughness value is a size invariant material characteristic constant. In fact, this is a basic premise of these fracture mechanics theories.

In connection with these fracture mechanics concepts, *different notions* of "size effect" or "size dependence" appear in the literature. On the one hand, they refer to the observation that the presumably size invariant fracture toughness value may be found to be a size dependent quantity when specimens of the same material and shape but of different size are compared. Moreover, the notion "size dependence" is also used for the influence of sole thickness variations of specimens, their in-plane geometry being geometrically similar. In fact, in this case specimens of the same material are compared which are geometrically distorted. This phenomena is properly termed "thickness effect" by some authors.

In the present review the attention is essentially restricted to the notion of similarity and its contrary due to size effects under quasi-static conditions, as found in geometrically similar specimens of the same material and at the same temperature (replica model and prototype), and as defined above. However, some results related to the two other notions are also included.

A previous literature survey (Malmberg, Tsagrakis, Eleftheriadis, and Aifantis (2001, [1.2]) on the phenomenon of "delayed yielding" (increase of yield stress under non-uniform stress distribution) and on size effects in smooth tensile specimens has been performed within the EU-project REVISA[4]. Here only two outcomes are mentioned: (i) frequently an increase of the yield stress was obtained when the size was decreased; (ii) furthermore, an increase of the strain measure "area reduction after fracture" of smooth tensile specimens was observed

[3] A theoretical singularity of the stress and strain field

[4] REactor Vessel Integrity in Severe Accidents (REVISA), EU-Contract F14S-CT96-0024, Euratom Research Framework Programme 1994-1998 "Nuclear Fission Safety"

when the size was decreased; this has also been found in corresponding experiments for the reactor vessel steel 20MnMoNi55 within the REVISA project (e.g., Devos, Auerkari, Lämmer, LeBer, Messelier-Gouze, Malmberg (2002, [1.3])).

In brittle as well as in ductile materials sharp notches or cracks (resulting from fatigue or stress corrosion) clearly represent a great risk for fracture and thus the size dependence of the fracture stress, the failure strain, and also the energy dissipation capability of geometrically similar specimens of the same material has been studied previously by experiments. These studies generally demonstrated an increased load carrying capacity and ductility with decreasing size. However, an increasing number of engineering problems require the determination of failure loads and deformations of structures containing intentionally designed strain concentrators like bore holes, perforations, or blunted notches, and no sharp notches or cracks. Testing of geometrically similar specimens of this type has also been done to some extent, and an extensive study on size effects of the reactor vessel steel 20MnMoNi55 and others has recently been completed within the REVISA project (Devos et.al. (2002, [1.3])). However, a critical review of the available literature on size effects in the quasi-static testing of sharp and blunt notched specimens had not been performed yet. Such a survey became part of the present EU-project LISSAC[5] which is, to some extent, a successor of the size-effect task of the REVISA project. It appeared that systematic testing for a variety of specimen shapes as well as over a large range of sizes (geometric scale factor larger than 10) had not been done yet and this gap promoted the realization of the LISSAC project. Within the LISSAC project the local failure strains of essential nuclear reactor vessel components as well as conventional types of specimens (bluntly notched tension and bend specimens, flat strips with circular holes, and others) are investigated, the size influence being of primary interest at room and elevated temperature and under quasi-static and dynamic conditions.

The objective of the present survey is to provide a review of mechanical test results of geometrically similar, bluntly or sharply notched specimens, predominantly made of steel. In most cases the specimens were of relatively simple shape:

- circular tension specimens with a circumferential notch;
- single-edge notched bending specimens with rectangular cross-section;
- compact tension specimens;
- some more complex configurations.

The review had to be restricted to quasi-static loading conditions. In most cases the tests have been performed at room temperature (R.T.), but tests below and above R.T. are also available.

The attention is focussed on test results of specimens of nominally the same material which are geometrically similar to very large extent. The test results of interest are, for example:

- curves representing a normalized load or stress versus normalized displacement or strain measures, such as those based on the load-point displacement, notch opening, or crack extension; alternatively, normalized bending moment versus bending angle curves
- specific quantities based on results, such as
  - absorbed energies: total (up to fracture) and partial (up to maximum load)
  - maximum normalized load, maximum nominal stress, or maximum normalized bending moment

[5] Limit Strains for Severe Accident Conditions (LISSAC), EU-Contract FIKS-CT1999-00012

  - normalized displacement, strain, or bending angle at the maximum load and at a sudden load drop
- reduction of area or diametrical strain at a notch after fracture
- notch mouth opening after fracture
- crack initiation or extension determined by visual, acoustic, or electric (e.g., potential drop) methods
- crack propagation behaviour
- J-contour integral resistance curves (e.g., J vs. crack extension Δa); J-values at crack initiation
- crack tip opening displacement (CTOD) resistance curves (e.g., $CTOD$ vs. Δa); $CTOD$-value at crack initiation
- scatter of experimental results.

A number of influences affecting the results have to be accounted for. For example,

- homogeneity of the raw block of material the specimens are cut from, i.e., the material has to be as homogeneous as possible to determine true size effects
- anisotropy of the raw material; i.e., choice of orientation of specimens
- influence of different testing machines for small and large specimens
- temperature influence
- testing rate influence
- notch sharpness and notch preparation influence.

Fracture appearance and fractographic results, such as fracture surface topography, will be only very briefly mentioned if available.

Although theoretical approaches like fracture mechanics concepts, probabilistic models, advanced continuum mechanics theories, or discrete element approaches have been and are used to interpret size effects, this review is concerned essentially with the experimental findings; the theoretical interpretation is addressed only when appropriate. In any case, the theoretical modelling and interpretation is still a rather intricate matter and no approach has universal applicability. This is also simply due to the fact that different physical mechanisms may be the reason for a size dependence of the material response, each one separately or even in a combined manner.

The review started in 2001 using references on size effects in notched and precracked specimens found in the course of the previous literature survey Ref. [1.2] and the search was then extended by computerized support of several data banks. The result of about 30 research activities are reviewed in Section 2 in chronological order, with the first publication in 1932 and the last one in 2001. It should be noted that the cited literature is not exhaustive: there is a number of reports not readily available and publications, which came late to the attention of the author: they are not cited herein.

Finally, discussions and conclusions are contained in Section 3, i.e., specific results of the various publications related to the topics listed above, are extracted and combined.

A first version of the present report was prepared under the same title as a LISSAC document (Malmberg, (2003, [1.4])).

2 Annotated Review of Relevant Literature

In view of the size effects observed in previous experimental results of notched-bar impact tests, ***Docherty (1932, [2.0])*** investigated a family of geometrically similar Izod-type specimens in an Izod test arrangement with various bending speeds ranging from "slow" to impact conditions. The specimens were similar in all respect to the standard Izod notched specimen (cross-section 10 x 10 mm, depth of 60° V-notch 2mm, notch radius ¼ mm); their dimensions are given in Tab. 2-1. Thus, a geometric scale factor of only three was realized.

The specimens were machined from ½ in. bars and this limited the maximum cross-section dimensions of the specimens. For each size about 10 specimens were fabricated, though in some cases a smaller number was realized owing to lack of material. As listed in Tab. 2-2, eight different metal materials with partially different heat treatments were investigated. However, chemical composition and tensile properties were not indicated, except the reduction of area at fracture. Also the quality and homogeneity of the stock bars were not recorded and a special cutting plan of the specimens was not mentioned.

The slow bend test equipment used is schematically illustrated in Fig. 2-1 (from Ref. [2.1]). It is designed to allow for various speeds of motion but was otherwise as close as possible to the standard Izod test. The load acting on the piston E was generated by a hydraulic ram (Buckton testing machine) not shown in Fig. 2-1. The specimen A was clamped in a vice as usually. The striker B was carried by the slider C which was guided on the back by the rollers D and on the other sides by slides. The distance of the vertical line of motion of the striking edge from the center of the notch was scaled according to the specimen size (Tab. 2-1). The slider was pushed downwards at a prescribed speed by the hydraulic ram acting on the piston E. Approximately constant speeds were maintained ranging from 150 in/min (38.1 m/min) down to 0.05 in/min (0.0127 m/min); in comparison, the average speed of the Izod test was about 7000 in/min (1778 m/min). The cylinder F, attached to the slider C, was filled with oil and the oil pressure[6] (proportional to the load) was recorded by an ordinary steam engine indicator. Further, the motion of the slider was recorded by the rotation of the indicator drum by means of the cord G. Thus, the work done in bending or fracturing a specimen was obtained from the autographic record of the load applied to the slider which was recorded on a base proportional to the displacement of the slider (work proportional to area of autographic diagram).

The speed of the striker edge (= load-point displacement rate) was held constant in each test series of geometrically similar specimens, which implied that the strain rate was not constant within each test family. A constant strain rate would be preferable since then the rate dependent part of the flow stress is approximately the same for all specimen sizes. Docherty pointed out the "speed effect", but it was decided to proceed as in previous tests since also the valve settings of the Buckton testing machine could not be altered easily. He expected that some correction could be made easily. This question will be discussed later in some more detail.

The experimental results documented in Ref. [2.0] are

[6] The leakage of oil from the cylinder was one of the chief problems in the design of the recording gear.

- the absorbed energy for plastic bending and fracture up to the instant when the recorded load drops to zero[7]; the mean values of up to 10 tests are collected in Tab. 2-3; no indication of the scatter is given;
- the diagrams (Fig. 2-2) of nominal stresses (load divided by the square of a characteristic length of the specimen) versus a dimensionless displacement of the striker, strain or bending angle; each ordinate is the mean of six typical diagrams, all of which were taken at a striker speed of 6 in/min (0.152 m/min);
- some limited information about the cracking of the specimens.

The presentation of the absorbed energy in Tab. 2-3 is not normalized; therefore, the results do not readily show the size influence. For this purpose, departing from Docherty's presentation, the data are transformed to volume specific energies by referring the raw data to a characteristic volume which, for simplicity, was chosen to be W^3 (W: depth or width of specimen). The result is shown in Tab. 2-4. If no size effect were present and if other influences (like the rate effect or material non-uniformity) are ignored, then within each test family the volume specific energy should be constant. Obviously this is not the case, instead generally a decrease with increasing specimen size is seen for all materials and speeds, except the material M (annealed phosphor bronze) where the effect is rather minor. Before discussing this apparent size effect, it is necessary to investigate the influence of the speed.

The strain rate achieved at the root of the notch is rather difficult to determine precisely and no estimate was given by Docherty. In the following a simple model is set up to provide a rough estimate. The assumptions made are

- the deformation is restricted to the notch, idealized to a section of length 2ρ where ρ is the root radius; this is certainly less than the actual deforming part of the specimen. The rest of the specimen is assumed rigid.
- This section is bent like a beam of length 2ρ and depth $W\text{-}a$ (W: depth of the unnotched section, a: depth of notch). With $1/R$ being the curvature of the neutral axis, the tension strain at the root of the notch is

$$\varepsilon = \frac{1}{R}\,\frac{W-a}{2} \,. \tag{2-1}$$

The assumption that the neutral axis does not stretch under bending implies

$$\psi \cdot R = 2\rho = const. \tag{2.2}$$

where ψ is the angle of rotation of the specimen. The displacement S of the load-point of the striking edge consists of two contributions, the displacement due to bending of the section 2ρ and due to the rotation of the rigid part of the specimen, i.e.,

$$S = S_1 + S_2 \;; \tag{2.3}$$

bending $\quad S_1 = 2R \sin^2 \psi/2$

rotation $\quad S_2 = L^* \sin \psi$

[7] This corresponded to the instant when a complete or almost complete fracture of the specimen was obtained or when the edge of the striker has slipped off the specimen due to large bending.

where L^* is the distance of the load-point from the edge of the deformable section

$$L^* = L_0 - \rho$$

L_0: half length of specimen.

For small angles of rotation ψ one gets

$$\begin{aligned} S &= 2R(\psi/2)^2 + L^*\psi \\ &= (\rho + L^*)\psi = L_0\,\psi. \end{aligned} \tag{2.4}$$

Then the strain at the root of the notch is

$$\varepsilon = \frac{1}{R}\frac{W-a}{2} = \frac{\psi}{2\rho}\frac{W-a}{2} = \frac{S}{L_0}\frac{W-a}{2\rho}\frac{1}{2} \tag{2.5}$$

and the strain rate is

$$\dot{\varepsilon} = \frac{\dot{S}}{L_0}\frac{W-a}{2\rho}\frac{1}{2} \tag{2.6}$$

With a constant speed V of the load-point one gets

$$\dot{S} = V \tag{2.7}$$

and the strain rate at the root of the notch is for small angles of rotation

$$\dot{\varepsilon} = \frac{V}{2\rho}\frac{W-a}{L_0}\frac{1}{2} \tag{2.8}$$

The smallest speed in Docherty's experiments is 0.05 in/min = 0.02117 mm/s. For the family of geometrically specimens one has $(W-a)/L_0 = 0.36\overline{36}$.

The largest specimens (cross-section 12 x 12 mm) with a root radius of 0.3 mm is subjected to a strain rate of

$$\dot{\varepsilon} = 6.415\,10^{-3}\,s^{-1}. \tag{2.9}$$

With a geometric scale factor of at most three and constant speed of the load-point, the strain rate increases by a factor of three when the specimen sizes decrease to the smallest one and thus the strain rates at the lowest speed are well within the quasi-static regime. However, the load-point displacement rate is also increased by several orders of magnitude:

$$\begin{aligned} V &= 0.05 \quad 6 \quad 50 \quad 150 \quad 7000\,(Izod) \\ \frac{V}{V_{\min}} &= 1 \quad 120 \quad 1000 \quad 3000 \quad 140\,10^3 \end{aligned} \tag{2.10}$$

Thus, for specimens of the *same size* the velocity and thus the strain rate varies over many orders of magnitude. However, the change of the volume specific energy is moderate if the speed is increased from 0.05 in/min to 6 in/min (factor 120) or to 50 in/min (factor 1000) or even to 150 in/min (factor 3000), (Tab. 2-5).

A rather similar rate influence is seen for the other specimen sizes. On the contrary, the change of the volume specific energy within a specimen family is considerable (Tab. 2-4). For the rolled mild steel (material A) the decrease in size from the 10 x 10 specimen to the 4 x 4 specimen yields an increase of 49 % accompanied by an increase of the strain rate by only a factor 2.5; increasing the strain rate by a factor of 120 (speed increase from 0.05 in/min to 6 in/min), yields only an increase of 14.6 %. Qualitatively the same observation is made for all the other families. Therefore, it is concluded that the variation of the strain rate within a test family by a factor of 2.5 or 3 has practically no effect for the speed levels considered in

these test series. The influence of size for the volume specific energy is also represented in Figs. 2-3 and 2-4, and a strain rate correction is not necessary.

In Tab. 2-6 for each material the ratio of volume specific energies of the smallest and largest specimen size is indicated for the slowest speed. This ratio is a measure for the magnitude of the size effect within the indicated size range. For the materials A and B as well as AA, the ratios are expected to be greater, as indicated, if results for the full size range (4 to 12 mm depth of the specimens) were available. These data are compared with the corresponding area reduction at fracture in tensile tests of uniform specimens. The comparison clearly shows that the size effect measure is largest (around a ratio of 2) for materials F and K which have the lowest area reduction *Z*. On the other hand, the phosphor bronze L and M have the lowest size effect measure (1.27 and 1.04) but the highest area reduction. One may conclude that the size effect is the larger the less ductile the material.

Referring to other authors, Docherty elaborates on an empirical relation between the absorbed energy *E* and a characteristic length *l* of a specimen, i.e.

$$E = Al^2 + Bl^3 \tag{2.12}$$

or

$$E = Cl^n \quad , \qquad 2 < n < 3 \quad . \tag{2.13}$$

Whereas the second relation appears to be purely empirical, the first one has a physical background: in terms of a volume specific energy, e.g., E/W^3, one gets

$$\begin{aligned} E_V := E/W^3 &= A\cdot(l/W)^2\, 1/W + B(l/W)^3 \\ &= A_V\, 1/W + B_V \end{aligned} \tag{2.14}$$

with A_V and B_V being constants for a geometrically similar test family. The second term is related to a plastic deformation energy, which is size independent, but the first term is related to surface energy prominent in fracture mechanics of brittle solids. Equ. (2.14) implies that the volume specific energy E/W^3 becomes largest for small specimens, decays hyperbolically, and approaches a constant value for large sizes. Alternatively an area-specific energy, for example

$$\begin{aligned} E_S := \frac{E}{W(W-a)} &= A\,\frac{l^2}{W(W-a)} + B\,\frac{l^3}{W^2(W-a)}\,W \\ &= A_S + B_S\,W \\ A_S = A\,\frac{l^2}{W(W-a)} &= const\,, \qquad B_S = \frac{l^3}{W^2(W-a)} = const \end{aligned} \tag{2.15}$$

may be defined. Here, the ligament area $W \cdot (W - a)$ is chosen as the reference surface (fracture area). The graph of the area specific energy E_S is a straight line and its extrapolation to small sizes *W* does not intersect the origin of the $(E_S \div W)$-diagram. This is important for the presence of a geometrical size effect. Consequently, the area specific values are determined for small speeds and are listed in Tab. 2-7 and the graphical presentations are shown in Fig. 2-3 and 2-4.

Figs. 2-3 and 2-4 demonstrate that a linear graph of the area specific energy is a reasonable approximation in most cases. Their linear extrapolation to small sizes depends in some cases on the extrapolation procedure and is thus ambiguous, but in most cases one finds $A_S > 0$. The results for the materials F, K, and AA show a rather moderate dependence on the depth *W*, especially material AA yields an almost constant area specific work, a steel which cracked in every notched bar tests. It is noteworthy that this rather moderate size dependence of the area

specific energy is accompanied with a low energy level. For the materials F and K this goes along with the lowest values for the area reduction (Tab. 2-2). The comparison of Figs. 2-3 and 2-4 shows that an increase in speed by a factor of 120 from 0.05 to 6 in/min has only a moderate influence on the size dependence of most of the tested materials, except the annealed Monel metal (material H): at the low speed 0.05 in/min the size dependence is clearly evident ($A_S \approx 0.4$ J/mm$^2 > 0$ and $E_V \neq$ const (Tab. 2-4)), but at 6 in/min a quite reduced size influence is seen ($A_S < 0.1$ J/mm^2, see also the variation of E_V in Tab. 2-4).

The observed marked size effect of the volume specific energy should also be seen in the normalized stress-strain diagrams. Docherty included a few graphs (Fig. 2-2) only for the notched specimens of materials B, L, and M and for unnotched specimens of material AA (averages of six nominally identical tests at 6 in/min). Clearly, these graphs contain more information than just the integral value of the combined deformation and fracture energy. In the diagrams for the normalized mild steel (B) and the rolled phosphor bronze (L and M) the stress maxima decrease with increasing size. Docherty attributes this to the decrease in strain rate within a test family (constant velocity tests!) which reduces the flow stress. However, as noted before, a change of the strain rate by a factor of only three is likely not sufficiently effective to explain this trends. Furthermore, the maxima for materials B and L are shifted to larger normalized displacements when the size is decreased. Also the decrease of stress beyond the maximum is more pronounced the larger the specimen (materials B and L). Docherty, referring to other authors, states that this decrease of stress indicates a "decrease in the proportion of ductile shearing in the fractures, or conversely an increase in the proportion of 'cracking'. The metals, therefore, behave in an increasing brittle manner as the size increases, but in the range of sizes tested there was no evidence that the 'cracking' became so excessive as to be audible or visible as an interruption of the smooth curve of the diagram."

It is noteworthy in Figs. 2-2a, b, c that the total normalized length of the diagrams decreases with decreasing size of the specimens, which corresponds to a shift of the sharp kink in the graphs to smaller normalized displacements the smaller the specimens. Docherty suggests that this "may also be accounted for by the increased ductility of the smaller specimens. The opening up of the fracture from the root of the notch was less; the neutral axis therefore nearer the root of the notch; there was consequently more compression on the side remote from the notch, which reduced the length of the cantilever when bending has taken place, and the striker had not to travel so far before it slipped off the end of the specimens."

It appears that this effect is likely not sufficiently effective to explain the observed trend in Figs. 2-2a, b, c. Another mechanism is possible: for those specimen which suffer an early and more extensive cracking and crack opening at the root of the notch, the load-point displacement will be mainly due to crack propagation and crack opening such that the specimen primarily rotates at the clamped edge without essential bending in the specimen outside the notch. If there is no or only minor cracking at the notch and if sufficient hardening is present, not only the notch is opened by the plastic deformation at its root but also bending may appear outside the notch. Thus, the overall shape of the specimen is curved and not almost straight. With the reasonable assumption of a constant length of the neutral axis, this mechanism yields an earlier slip off of the striker and thus the right tendency to explain the trend in Fig. 2-2a, b, c. It means that the observed trend is due to the "higher ductility", i.e., less cracking at the root of the notch and thus also more bending outside the notch. Whether this qualitative explanation is also quantitatively appropriate is unresolved. Exploratory considerations still leave some doubts.

For the material AA (0.3 % C-steel, normalized) not only notched but also unnotched specimens had been tested using a geometric scale factor of only 1.71 (7 x 7 to 12 x 12 mm). The volume specific energy (Tab. 2-4) of the notched specimens shows a definite size dependence: decreasing the size from the largest to the smallest specimen, the volume specific energy is increased by 66 %. On the contrary, the normalized load-displacement graphs (Fig. 2-2d) of the unnotched specimens tested at low speed, do not show any significant size influence. Accordingly, Docherty states that the departure from similarity, which is so marked for the notched specimens of metal AA, "is thus seen to be due to the influence of the notch, causing stress concentrations which result in brittle action taking place."

Nadai and MacGregor (1934, [2.2]) investigated the results of Kuntze (1932, [2.3]) on circular 60° V-notched tension specimens, using the theoretical elasticity results of Neuber (1933, [2.4]) who had determined the maximum stress at the tip of a notch, the profile of which was given by two branches of an ordinary hyperbola within a 60°V-notch. Keeping the radius of curvature at the apex of the notch profile (hyperbola) constant but increasing the minimum diameter at the notch from 1.8 mm to 6 mm (size factor 3.333), increased the maximum stress by about 83 % if the notch cross section area is half of the rod area. Nadai and MacGregor remarked that the sharp notches of these rods were most probably all cut with the same tool such that the same notch tip was applied to all rods. Thus, they indicated that Kuntze's belief that his notched test bars were geometrically similar was probably not quite justified. This would imply that the size dependence of the notch strength observed by Kuntze is essentially due to the increased notch sharpness when the size of the rods is increased.

To check certain similarity considerations (Barba-Kick law of proportionality) and to support the above interpretation of Kuntze's findings, Nadai and McGregor performed notched tensile tests of bars of mild steel and aluminum. A family of geometrically similar round bars with a semi-circular notch were produced from the mild steel with the radii of the notches strictly proportional to the diameters. Before machining, all bars were annealed at 900 °C for one hour. The minimum diameter at the notch ranged from ~0.088 in = 2.24 mm to 0.707 in = 17.96 mm (scale factor 8) and the radius of the semi-circular notch was such that the notch reduced the cross-sectional area by 50 %. Details are given in Tab. 2-8. It is noted that the rate of the applied stress was held constant[8]. As Tab. 2-8 demonstrates, the results for the ultimate strength at the maximum loads do not show a size dependence. This supports the consideration of Nadai and MacGregor with respect to Kuntze's findings. A second annealed mild steel family with 60°V-notches of the round bars was tested again with the radius at the tip of the notch proportional to the diameter. It is noted that the radius of curvature at the tip of the notch is somewhat smaller (~64 %) than in the first family. The diameter at the notch ranged from ~0.088 in to 0.3535 in (scale factor 4) and the notch reduced the cross-sectional area by 50 % (Tab. 2-8) as above. Again no size effect on the ultimate strength is seen. Unfortunately, no deformation data such as notch opening or area reduction at the notch at maximum load or fracture were recorded.

Among others, additional tension tests were made with a family of flat pieces cut from a hard aluminium sheet as delivered with two-sided 60°V-notches applied. The distance between the tips of the notches ranged from 0.124 in = 3.15 mm to 0.750 in = 19 mm and the thickness ranged from 0.2083 inch to 0.125 inch such that the notch reduced the cross-

[8] If linear hardening in the plastic regime applies, the strain rate is also constant.

sectional area by 50 %. The radius of curvature at the notch tip was 0.0625 in = 1.587 mm in the largest specimen and was scaled appropriately. Again no size effect was found for the flat specimens.

On the conclusion of his previous tests, ***Docherty (1935, [2.5])*** decided to carry out a few more tests with even larger notched specimens, up to section 100 x 100 mm. According to Docherty, they were the largest specimens that had been tested at that time. Slow speed three-point-bending tests were performed: the load was applied to the mid point of the span above the notch through a cylinder (2 in diameter cylinder for the 100 x 100 mm and proportionally smaller cylinders for the smaller specimens). The deflection under the load was measured by dial gauges or by multiplying levers and scales according to the size of the specimens but only a moderate accuracy was aimed at. The duration of the tests varied with size from about 2 to 10 minutes. It is believed that all specimens were tested in the same test arrangement, of course with scaled supports. Two materials (A and B) of forged mild steel were used for the fabrication of two sets of geometrically similar specimens, differing by their width (Tab. 2-9). Material A was provided in the form of a 4 in by 1 in bar, and material B in the form of a 4 in by 4 in bar. For the B-material specimens the smaller specimens were cut from the undamaged portions of the larger specimens. It was hoped that the bar would be so homogeneous that the obtained results would be comparable.

The results obtained are shown in Figs. 2-5 and 2-6. In the normalized load-deflection diagrams the ordinates are load /(area of cross section) and load-point deflection/ (depth of specimens). Except for the linear (elastic) region and the "yield point", similarity (i.e. congruence of the curves) is neither obtained for the A-type family nor for the B-type family. Docherty states that there is no evidence of tearing up to the point Y and that at the point Y tearing commences and gradually spreads from the root of the notch into the specimen. It would therefore appear that the stress at which tearing commences is practically constant, irrespective of the size of the specimen. However, no direct experimental proof by visual inspection or other means is given. Lubahn in a later publication (Ref. [2.19]) comments, "if such were the fact, one would in turn conclude that the ductility (strain when tearing = cracking sets in) is independent of specimen size." Lubahn further remarks that it is clear from the photograph Fig. 6 in Docherty's paper (dimple at the root of the notch) that considerable strains occurred prior to fracture even in the largest specimen.

Beyond the "yield point" marked differences are seen. The normalized load (nominal stress) increases steadily up to a maximum, but the maximum value and especially its related normalized deflection vary considerably. For material A there appears to be a consistent increase of the hardening with increasing specimen size, but a considerable scatter is found for the two 50 x 12.5 mm specimens (Fig. 2-5). More important, the normalized deflections associated to the maxima are shifted to larger values the smaller the specimens. Furthermore, the nominal stress for the small 10 x 2.5 and 20 x 5 mm specimens show a gradual decrease beyond the maximum. The two tests of the larger 50 x 12.5 mm specimens show a discontinuous behavior: one test yields a gradual decrease of the nominal stress, the other failed on the ascending branch at a smaller normalized deflection by cracking with an instantaneous drop of the stress. The two tests of the largest specimens of material A suffer an instantaneous failure on the ascending branch with slight scatter.

For material B the ascending part of the stress strain curve shows a considerable scatter and no size dependent trend can be seen (Fig. 2-6). However, the normalized deflection related to the absolute maxima is size dependent: the smaller the specimens the larger is the

shift to larger strain values. The 10 x 10 mm specimens yield a smooth maximum of the stress with a subsequently gradual decay. The three tests for the 20 x 20 mm specimens also yield a smooth maximum, but shortly beyond the maximum cracking and an instantaneous drop of the load is found. The largest specimens (50 x 50 and 100 x 100 mm) crack and collapse before a relative maximum is reached and the cracking in the largest specimen occurs at a normalized deflection which is about a factor of two smaller than that of the 50 x 50 mm specimen. In all cases the cracking of the largest specimens was extremely violent, the broken halves jumping several feet clear of the testing machine.

A common feature of both test families is a size dependent transition from a ductile behavior with a smoothly decaying softening part in the nominal stress-strain curves for small specimens to stress-strain curves interrupted by cracking with instantaneous drop of the load. For the A-type family this transition is around a cross-section size of 50 x 12.5 mm and for the B-type family it is between the size 10 x 10 and 20 x 20 mm. Thus, for the thicker B-type family the transition is shifted to a smaller specimen depth. Since the mechanical data are not very different (Tab. 2-10), the different widths of the specimens (a factor of four is involved) is the controlling quantity: the thicker specimens type B yield a somewhat more brittle behavior; this is related to the constraint effect in the thicker specimens type B. Docherty has brought out the different transition sizes very clearly by plotting the volume specific energy (area within the nominal stress-strain graph) versus the depth of the specimens (Fig. 2-7).

Pfender (1938, [2.6]) performed static and dynamic notched tension test for different notch shapes, temperatures, specimen sizes, and various materials. Unfortunately, only a limited account was given to the influence of size. For the quasi-static tests, U-notched round bars (unnotched diameter 15 and 25 mm, notched diameter 9 and 15 mm, radius at the root of the notch 1.825 mm and 3.125 mm) were used. The materials tested were the structural steel St 37.11 as received and aged, the tempered steel VCN 25 (annealing at 400 °C and 600 °C), as well as the Al-Cu alloy Ulminium, tempered and annealed at 300 °C. No further details with respect to the specimens were given. The quasi-static tensile tests at room temperature, however, were restricted to the determination of the area reduction at the notch. The scatter of the data is rather small and almost no size effect is observed. The latter was also found for the dynamic notch tensile tests. The author remarks that it is premature to generalize these findings to other specimen sizes and notch profiles.

Brown, Lubahn, and Ebert (1947, [2.7]) investigated the influence of the section size on the properties of a family of almost geometrically similar circular notched bars made of a normalized medium carbon steel and tested in static tension. The dimensions of the specimens are given in Tab. 2-11.
Fig. 2-8 visualizes the variation of size, the diameter D_0 of the uniform section ranging from 6.35 mm to 101.6 mm (geometric scale factor 16). The specimens possessed a 60° circumferential V-notch which removed 50 % of the cross-sectional area. They were geometrically similar, except the root radius R of the notch which in all cases was as sharp as possible (0.001 in = 0.0254 mm). Therefore, the notch sharpness $D/2R$ varied from about 90 for the smallest to 1400 for the largest specimen.

The material used was a single, 4 in-thick, commercial grade, hot rolled, fully Si killed, 0.20 to 0.30 carbon steel. The plate, as received, had been flame cut in convenient pieces (4 x 4 in, 16 in long). The pieces were subjected to heat treatment (1625°F ≈ 900°C, ~ 4 h, cooling

in still air). Since the size of the pieces was always the same, an identical cooling rate was insured.

The longitudinal axes of the notched bars were required to be parallel to the rolling direction of the plate in all cases. It was also required that the various sized specimens possess the same average notch ductility. For this purpose, the distribution of the notch ductility of the plate across the thickness was determined using 0.5 in cylindrical diameter notch specimens (60° V-notched, 50 % removed cross-sectional area) with their longitudinal axes parallel to the rolling direction and cut from various thickness positions (two tests at seven equi-distant positions across the thickness). The results show a rather uniform distribution of the notch strength (i.e., maximum load/initial notch area = 100 10^3 psi ± ~3 %). However, for the notch ductility (contraction in area at the root of the notch) a minimum is seen at the central part (about ± 0.7 in from the center). With this information the specimens of various sizes were positioned within the plate in such a manner that the average ductility of the notched cross section for any particular specimen was equal to the average ductility of notch section of the largest specimen.

The notched specimens were tension tested at slow speed. No indication was given on the speed and whether the cross-head rate was scaled.

In each test the notch strength (i.e., ratio between maximum load and initial minimum notch cross section) and the notch ductility (reduction of notch area at root of notch) were determined. Several different methods were investigated to measure initial and final notch diameter. Good agreements were obtained and the reported ductility values (area reduction) are reproducible within ±1 % strain.

Three tests for the smaller specimens and two repeat test for the three larger specimens were performed and the results are plotted in Fig. 2-9 and 2-10 versus the diameter D_0 (uniform section). Obviously the scatter is rather small. Both size dependencies follow a quasi-exponential decay. Whereas the mean notch strength decreases from the smallest to the largest specimen by about 20 %, the decrease in mean notch area reduction is almost a factor of 10 larger (from 21 % for the smallest to 2.25 % for the largest specimen). Brown et al. mention the appearance of two distinct regions of the fracture surface: a central almost circular area of cleavage type fracture and a surrounding darker area with the characteristics of shear fracture. The ratio of the brittle to the ductile area increased with increasing specimen size. Based on these latter observations the authors suggested that the specimen fractured in a progressive manner, the crack starting at the notch bottom and proceeding radially inward (observable visually). When the crack reached a certain depth, which was proportionally greater the smaller the specimen size, brittle rupture occurred over the remainder of the cross section.

Considering the influence of the increasing notch sharpness with size (non-similarity of geometry), Brown et al. stated that generally for specimens of the same size and provided with sharp notches, both the notch strength and ductility decrease with increasing notch sharpness, but the effects of notch sharpness diminish with increasing sharpness (see Sachs and Lubahn (1945, [2.8])). They concluded that the notch sharpness variation (*D/2R* from 90 to 1400) of their specimens would have a small effect on the ductility (quantitative estimate was not given). Thus, the observed large effects could be attributed only to an increase in the specimen size.

A comparison with Docherty's (Ref. [2.0, 2.5]) and Davidenkov's (Ref. [2.9, impact tests]) results was made by the authors. From the total amount of data available, they draw the following conclusions regarding the effect of specimen size as an embrittling factor: a distinct size effect exists for ductile and brittle steels which is evidenced by a decrease of both

strength and ductility or by a decrease in unit absorbed energy as the section size of geometrically similar specimens increases.

Finally, Brown et al. elaborate on explanations proposed previously to account for size effects in fracturing, such as

a) relative grain size
b) surface cold work due to machining
c) macroscopic material non-uniformity (position effect)
d) non-constant strain rate (viscous effects)
e) constant radius of crack tip
f) non-uniform stress distribution (stress gradient)
g) pre-existing defects of different sizes (statistical theory of size effect)

After comparison of results obtained with different test methods by previous experimenters, ***Shearin, Ruark, and Trimble (1948, [2.10])*** decided that the slow bend test of notched bars offered "excellent opportunities for precise study of size effects". All specimens were geometrically similar. They were of the SENB-type with a quadratic cross-section and a 90 degree notch with a semi-circular tip. The three common sizes used are given in Tab. 2-12. Thus the geometric scale factor is about 4.7. Several additional sizes (3/8, 6/8, 9/8, 12/8 and 15/8 in) were also used which fit into this family. The total lengths of the specimens were not documented in Ref. [2.10]. The specimens were machined by shaping and grinding. The notch preparation was done with special care. The tip of the 90-degree notch ended in a semi-cylindrical enlargement. The notch was cut on a milling machine and the semi-cylindrical part was lapped to size with a drill rod and abrasive eliminating milling marks.

The slow bend testing was done with a four-point roller bend tester. The load was applied to the specimen at two points by ball or roller bearings, the span between the loading bearings being twice the width of the specimen. Within this section, which contains the notch at the center, the bending moment was constant. The loading assembly was appropriately scaled according to the size of the specimens.

A first series of tests had been performed manually by applying load increments with subsequent hold times of 2 to 5 min to allow the specimens to become stabilized. The average speed of load application was 0.00023 in/s which was the same for all sizes (Tab. 2-12). The load was measured as well as the bending rotation using small mirrors attached to the specimens and scales. A typical result is shown in Fig. 2-11: the ordinate represents the "reduced bending moment" (*M:* bending moment, *b:* width of specimen, *d:* ligament length = retained depth) with the dimension of stress and the abscissa is the angle of rotation. The area under the curves is proportional to the applied work.

Subsequent testing was done making records autographically, using an in-house made equipment, with the testing machine in uniform motion. The cross head was driven at speeds proportional to the size of the specimen. The adapted sizes (nominal width) were: 3/8, 6/8, 9/8, 12/8, and 15/8 in referred to as Nos: 1, 2, 3, 4, and 5. An extensive testing program was performed using specimens made from several steels, subjected to different heat treatments, and an aluminium alloy:

(A) Central region (tempered bainite) of an 18 in-thick plate of nickel-chromium steel (~0.30 % C) with hardness variation 206 to 220 and
yield stress 77250 psi
ultimate stress 99500 psi

elongation 23.3 %
red. of area 59 %;

(A1) this material was used to investigate the influence of the specimen orientation on the size effect, i.e. long axis of specimen
OX: in rolling direction
OY: at right angle to rolling and in the plate face
OZ: normal to place face;
and notch direction
OX & OY: perpendicular to plate
OZ: parallel to OY[9]

(A2) Two blocks (3 x 6 x 12 in) of this material were heat treated to investigate its influence of embrittlement
(A2.0) as received
(A2.1) temper embrittlement: 4 h at 650 °C, furnace cooled; Brinell H 224
(A2.2) referred to as air cooled.

(B) Three materials were used to study the effect of inclusions:

(B1) a 2 in-thick nickel-chromium steel plate (~0.30 % C); very clean; tempered martensite from a heat completely killed with aluminium; BHN = 248

(B2) a 2 ¼-thick nickel-chromium plate (~0.30 % C); reported very clean; tempered martensite; BHN = 248 – 257

(B3) two blocks of a similar composition as (B2) which came from plates 1.5 to 2 in thick of fine grained tempered martensite. Their number of inclusions had been determined:

Block no.	BHN	Inclusion / in^2		Description
		Total	sharp or angular inclusion	
830	271	4750	2300	large sulphide incl.
925	271	23250	3200	small sulphide incl.

(C) 2 ½ in-thick nickel-chromium steel plate (no. 52151, 0.27 % C) and 9 sub-plates subjected to various treatments

(D) 1 ½ in aluminium alloy (24 ST) plate

Some of the results obtained for the steels are presented and discussed here. Fig. 2-11, which represents typical reduced moment-angle curves, was obtained by the manual test procedure mentioned before. The material corresponds to that mentioned under (A1); i.e., the tempered bainite region of the 18 in-thick nickel-chromium steel with the long axis of the specimen in rolling direction (OX). The two curves represent the average of three tests with 0.4 in-specimen and of four tests of the 1 ¼ in-specimens. A typical set of curves, obtained with the autographic recording for one of the specimen families of the material group (C), is shown in Fig. 2-12: the nominal stress (load/bd) is plotted as a function of the normalized displacement

[9] This choice was made to minimize the possibility that a flattened zone of inclusion or lamination could lie along the length of the notch; thus this does not show the material at its worst.

(load-point displacement[10] / ligament depth d). If similarity would prevail, the normalized curves for the specimens of all sizes should be identical. Figs. 2-11 and 2-12 reveal the following qualitative trends:

- the linear (elastic) regions and a part of nonlinear (plastic) regions before the load maximum are congruent, i.e., similarity applies;
- size effects are observed around the maxima: the smaller the specimens the larger is the shift of the maximum of the normalized load or reduced moment towards larger normalized displacements or bending angles; a significant size influence on the value of the maximum reduced moment or stress is not observed;
- the softening region beyond the maximum is more gradual and more extended the smaller the specimens. For the largest specimen (15/8 in = 47.62 mm depth, Fig. 2-12) the gradual decaying load is interrupted by an instantaneous collapse (crack) which is not observed for the two smaller specimens;
- the applied volume specific work (area under the curves), i.e., the total work as well as the work up to the load maximum, decreases with increasing specimen size. The size dependence of the work up to the load maximum, reflects essentially the size-dependent shift of the maximum along the normalized displacement axis and not a size dependence of the value of the normalized load.

This latter result is quantitatively reflected in Tab. 2-13 and Tab 2-14. Tab. 2-13 shows the volume specific work obtained from the reduced moment-angle curves of the tempered bainite material of the 18 in-thick plate of nickel-chromium steel (material A1); three test families are considered which relate to the three directions OX, OY, and OZ. Three volume specific work terms are listed, the elastic part appropriately subtracted: W_1 is the work up to the maximum load, W_2 the work in the softening region beyond the maximum, and $W = W_1 + W_2$ is the total specific work. The latter was obtained by integration up to a bending angle which corresponds to 5 % of the load maximum. Individual results of each test as well as their average are included. The authors state that the variations are due primarily to variations of material properties themselves, because measurement errors are small.

The following conclusions are deduced from Tab. 2-13:

- within a family of specimens the scatter bands related to the various sizes do not overlap; thus, the material variation is much smaller than the influence of size;
- a significant size influence is seen within each test family OX, OY, and OZ for all work terms; decreasing the size by a factor of 4.7 from 1.875 in = 47.63 mm to 0.4 in = 10.16 mm, the total work W and the partial work W_1 increase by a factor of 2 to 3 (Tab. 2-15), depending on the specimen orientation: for both work terms the largest size influence is seen for the OZ-direction (W-ratio: $(W)small/(W)large$ = 2.66; W_1-ratio: $(W_1)small/(W_1)large$ = 2.83);
- the ratio W/W_1 of the total work W to the partial work W_1 is around a factor of 2 (Tab. 2-15); for the OX-direction the largest ratio is found for the smallest specimen; for the two other directions this trend is not observed;
- for a given specimen size, the absolute values of the work densities are strongly depending on the specimen orientation: the largest values are obtained for the OX-direction and the smallest for the OZ-orientation (around a factor of 2 between the two orientations).

[10] It appears that this corresponds to the motion of the specimen loading rollers.

In Tab. 2-14 the mean data of Tab. 2-13 and the mean of the additional data (A2) as well as (B1) to (B3) are listed. Whereas the data of the material group (A2) give some indication on the influence of the heat treatments, the data for the 2 in (B1) and the 2 ¼ in (B2)-thick Ni-Cr steel plates show considerable differences in the absolute values of the work densities. However, the size effect on the work densities is almost the same for the two materials (B1) and (B2) in the OX-direction (see Tab. 2-16). The material group (B3), with two blocks containing different amounts of inclusions, show a reduction of the absolute values of the work densities when the number of inclusions per area is increased: the percentage decrease is less than 10 % for the small 0.4 in-specimens, but for the 1.25 in-specimens the percentage decrease is larger. Furthermore, the ratios of the work densities for these two blocks show that the size influence increases with the number of inclusions (Tab. 2-16). Shearin et al., however, state that from these data "no clear trends can be perceived, but they point towards the ideas that there is little connection between sulphide inclusion and size effects – at least in cases where the sulphides do not form deleterious grain boundary networks."

The material groups (C) and (D) investigated by Shearin et al. will not be commented here. It should be noted that Ref. [2.10] gives no indication of visual or instrumental investigations of crack initiation or crack propagation. Thus, it is not clear whether crack initiation occurred before, at, or beyond the load maximum; therefore, it appears to be unresolved whether the size dependence of the load maximum (shift) and of the work density W_1 is due to the presence of a crack and its propagation, or whether the size dependence of plastic deformation at large strain and strain gradients or the size dependence of damaging processes before cracking are responsible for the shift.

Shearing et al. notified that the Equ. 2.14 fits their data reasonably well. Furthermore, to explain general features of size effects, the authors resort to simple concepts, but leave detailed treatment to a later time. They mention (i) the weakening effect of flaws (probabilistic concepts), (ii) the nature of the crack tip (root radius in relation to the size), and (iii) effects of the root radius pattern of the applied stress. However, the discussion remains general and inconclusive.

With the onset of the 2nd World War, the effect of section size on fracture strength of metals and structures had become acute by serious fractures in welded steel merchant ships. Since reasons were not immediately obvious, a number of research projects had been initiated. Some of those results and salient features related to the effect of section size on the fracture strength of mild steel were presented by ***Parker (1948, [2.11]).*** They referred to

- smooth cylindrical specimens (up to 7 inches = 177.8 mm diameter);
- unnotched flat plates;
- notched flat plates with the plate thickness and notch geometry (slit) maintained constant but with different plate widths;
- geometrically similar flat plate specimens with a scaled square hole at the center;
- scale models of welded assemblies – hatch corner tests.

The results of the geometrically similar plates with a square hole are summarized here. The specimens were 3, 6, and 12 inches (76.2, 152.4, 304.8 mm) wide, 3/16, 3/8, and 3/4 inch thick (4.76, 9.52, 19.05 mm) and were 9, 18, and 36 inches (228.6, 457.2, 914.4 mm) long. The square hole at the center had sides at 45 degrees to the longitudinal axis of the specimen and the length of the side were with radii at the corners of 1/64, 1/32, and 1/16 inches (0.40, 0.79, and 1.59 mm). The specimens were machined from an annealed plate of mild steel (thickness 1 ¼ in). The raw blocks for each specimen were machined down to specimen

thickness from each face of the plate. For each size usually single tests were performed at different temperatures (0, 32, 50, 70, 74, 90, 102 °F = -18, 0, 10, 21, 23.5, 32, 39 °C) as shown in Tab. 2-17. The results listed are rather meager: the nominal stress at maximum load, the percentage reduction in thickness, and the type of fracture. No indication is given on the determination of the reduction in thickness, as defined by its maximum and minimum value. From Tab. 2-17 the following qualitative conclusions are obtained:

- the small 3 inch wide specimens are ductile with shear failure at all temperatures;
- the large 12 inch wide specimens fail by cleavage at all temperatures and show much less thickness reduction than the smaller specimens;
- the medium size 6 inch wide specimens show a transition from cleavage type fracture to shear fracture with increasing temperature (from 32 °F = 0°C to 90 °F = 32 °C);
- these results demonstrate that the transition temperature from cleavage to shear of mild steel is shifted to higher temperatures when the specimen size is increased;
- at room temperature (70-74 °F) the nominal stress at maximum load decreases with increasing specimen size in the investigated size range (scale factor 4) from about 46 psi down to 39.9 psi and the maximum percentage thickness reduction decreases from about 31.7 % to 17.9 %; the mode of fracture changes from shear to cleavage.

In view of the results for geometrically non-similar specimens, Parker remarks that "it is important to note that even geometrically similar notched specimens exhibit a marked size effect." It appears that this statement reveals a confusion which stems from an ambiguous nomenclature, which even today is not uncommon in the technical literature. One should distinguish between size effects on the one hand and shape or dimensional effects on the other hand: the first is related to geometrically similar specimens or structures in all respect for which similitude laws do not apply because of some size dependent mechanisms or processes in the material; the second, however, is related to geometrically non-similar specimens for which similitude laws principally cannot apply and which yield essentially dissimilar behavior.

With respect to the observed size effects, Parker remarks "that the first crack forms at the base of the notch considerably before the maximum load is reached, particularly with specimens that failed by shear. Consequently, the geometrical similarity is destroyed before the maximum load is reached." This is, as it stands, certainly not a sufficient explanation for the above size effects in the geometrically similar specimens. The important aspect is that, according to the laws of fracture mechanics, crack initiation and propagation are size dependent processes. If they were not, similitude could be expected.

The accidents in welded ships and bridges due to brittle fracture motivated also intensive research activities on the size dependence of fracture in Japan. ***Akita (1953, [2.12])*** investigated notched mild steel specimens under slow three-point bending over a temperature range from about –40 °C to +80 °C. The purpose was to determine the influence of size on the transition temperature, the absorbed energy, and the maximum nominal bending stress. The material used was a mild steel[11] with yield stress 21.1 kp/mm^2, ultimate stress 40.5 kp/mm^2, elongation 28.5 %. The cross sections of the notched bar specimens were quadratic with dimensions 10x10, 21x21, and 42x42 mm. The longitudinal direction of the bars was parallel to the

[11] Yawata – rimmed steel
0.19 % C, 0.41 Mn, 0.01 Si, 0.015 P, 0.032 S, 0.72 Cu, grain size 8.0 ASTM

rolling direction of the steel plate (thickness 45 mm). The 45° V-notches were machined on the edge of the mother plate perpendicular to the roll direction with a notch depth of 2, 4, and 8 mm but with different notch radii from 0.05 to 1.6 mm as shown in Tab. 2-18. For the medium size only one notch radius (i.e. 0.4 mm) was provided. The small 10x10 mm specimen with a notch radius of 0.2 mm and a span of 40 mm corresponds to the standard Charpy impact specimen. Thus, the small, medium, and large specimens with a notch radius of 0.2, 0.4, and 0.8 mm (italicized numbers in Tab. 2-18) would be similar if the tested spans would be scaled geometrically. Unfortunately, much larger spans (200 mm) for the medium and large size specimens were used because of some strange "limitation of the liquid bath". Therefore, in order to make corrections for the effect of span, series of tests with different spans for the medium and large type specimens were done at 20 °C and presumably with notch radii of 0.4 and 0.8 mm (not explicitly indicated by Akita).

The exact size of the small specimens should have been 10.5x10.5 mm for reasons of similarity, but the Charpy-type dimension was preferred. The difference appeared to be acceptable. All tests were made under the same strain rate to exclude strain rate effects (the nominal value is stated to be 0.005/min = $0.083 \cdot 10^{-3}$ s^{-1} , but it remains undefined in Ref. [2.12]).

The homogeneity of the 45 mm-thickness plate was determined by testing medium size specimens (notch radius 0.4 mm, span 200 mm) which were taken from the core and from the rim of the 45 mm-thickness plate. The absorbed energy was determined over the whole temperature range and no difference was found between material from the rim and the core. This assured that inhomogeneity through the thickness would not affect the results. Therefore, the medium and the small specimens were machined both from the rim and the core at random. Since the number of specimens was quite large, material variations along the length and the width of the plate may still be present in the test results.

The essential data -energy consumption of the specimen and the maximum load- were obtained from the load-deflection curves. The energy consumption corresponds to two terms: the "absorbed energy" and the "crack propagation energy". Although not precisely defined in Ref. [2.12], the first energy quantity should be equal to the total applied work up to fracture whereas the "crack propagation energy" is the work beyond the load maximum up to fracture. These are the two typical work terms which can be obtained as area integrals from the load-deflection curves. Unfortunately, the load-deflection curves as well as deformation measures at the notch were not reported.

The absorbed energy and the crack propagation energy are plotted versus the test temperature with the notch tip radius as parameter in Fig. 2-13 for the 10x10 mm specimens and in Fig. 2-14 for the 42x42 mm specimens. It should be noted that the data for the large specimens (Fig. 2-14) are not corrected for the overlength of the span. Figs. 2-13 and 14 show that the notch tip radius has a relatively small influence on the transition temperature (point of inflection of the energy-temperature curve). This is more directly demonstrated in Fig. 2-15. The small 10x10 mm specimen show an increase from +10 °C to +20 °C, when the notch tip radius is decreased, and almost a saturation in temperature is reached for small notch radii. For the large 42x42 mm specimen the relative notch radius *r/W* is, of course, much smaller and here no influence of the tip radius is seen. It is evident from Figs. 2-13 to 2-15 that an increase in specimen size shifts the transition temperature to considerably higher values. It should be noted that the overlength of span of the 42x42 mm specimen very likely does not effect the transition temperature.

The influence of the notch tip radius on the absorbed energy at –20 °C, +20 °C, and +80 °C is shown in Fig. 2-16 for the small 10x10 specimens. The data are obtained from the interpo-

lation curves in Fig. 2-13. It is seen that the energy increases with notch radius for all three temperatures, but the effect gets larger the lower the temperature: at room temperature (20 °C) close to the transition temperature there is a 2.3-fold increase of energy over the investigates radius range from 0.05 to 1.6 mm, but at –20 °C the increase is 4.8-fold.

The maximum load and the yield load (not precisely defined in Ref. [2.12], but expected to be the first deviation from the linear elastic load-deflection line) is plotted in Fig. 2-17 versus the test temperature for the large 42 x 42 mm specimens with the notch radius as parameter. There appears to be only a very slight change with temperature. For small notch radii the maximum load increases somewhat with temperature, but for large notch radii it decreases slightly. However, the yield load generally but moderately decreases with temperature. The influence of the notch radii at 0 °C on the maximum nominal bending stress at the root of the notch (maximum bending moment divided by section modulus of ligament section) is shown in Fig. 2-18 for the small, medium, and large specimens. Unfortunately, the medium and large size data are not corrected for the overlength of the span. Therefore, the size influence cannot be judged from these data even if data are selected with properly scaled notch radii, as done by Akita. Nevertheless, Fig. 2-18 demonstrates a considerable influence of the notch radius on the nominal maximum bending stress: generally the stress decreases with decreasing notch radius, especially for the small 10x10 mm specimens. The large 42x42 mm specimens, however, appear to approach a plateau value of the bending stress for radii less than 0.2 mm (Fig. 2-18). Such a plateau seems to be related to the fact that the relative notch radius r/w is smaller in the larger specimens.

In order to determine the proper size effect on the absorbed energy, it is necessary to correct the results of the medium and large size specimens for the overlengths of their spans because the overlength affects the maximum load, the deflection at fracture, and thus the integral of the load-deflection curve (~ absorbed energy). Medium and large size specimens with scaled notch depths and notch radii (0.4 and 0.8 mm) but different spans have been tested, obviously only at +20 °C. The absorbed energies are plotted versus the span in Fig 2-19. A considerable scatter is seen. Using the linear interpolation curve, one can infer the fractional reduction in absorbed energy if one changes the span from 200 mm to 168 mm for the (42x42)-specimens and from 200 mm to 84 mm for the (21x21)-specimens (according to Akita: for the tests at +20 °C the large specimens are to be corrected with a factor of 0.94 and the medium size with 0.64). With this correction, which apparently is assumed to be valid also for the other temperatures(!), volume specific absorbed energies were determined using a reference volume given by the "maximum cross section area (at the ligament) X loading span" which scales with the cube of the beam depth. The "corrected" energies per unit volume are plotted in Fig. 2-20 for two test temperatures[12]: +80 °C and –20 °C where the first temperature produces primarily shear fracture and the second brittle fracture. For the shear fracture curve (+80 °C tests) size independence of the volume specific energy is found for specimen depths larger than about 20 mm. For the small specimens (depth 10 mm) an about twice as large volume specific energy is necessary to obtain failure. The brittle fracture (-20 °C) case yields a more gradual decay of the volume specific energy with size and the energy per unit volume of the smallest specimen is about three times as large as that for the largest specimens. Obviously, the size effect is larger the more brittle the response (see also Docherty (1932, [2.0])]. From Fig. 2-21 it is seen that the data at 20 °C and other temperatures yield

[12] Note: the correction factors obtained from +20 °C tests were applied here.

also a more gradual decay with increasing size. It should be recalled that size invariance would require that the energy per unit volume is constant, only depending on the shape of the specimen (including notch tip radius), the temperature, and the strain rate. Although the general qualitative trends appear to be valid, the inexact correction of the non-similarity of the loading spans leaves some uncertainty of the qualitative aspects. A similar investigation should have been done for the "crack propagation energy" or alternatively, the work up to the load maximum – "crack initiation energy" (the data were available, see Figs. 2-13 and 2-14). This would have allowed to determine to which part of the total volume specific energy the size influence can be mainly attributed (see e.g. Shearin et al. (1948, [2.10]).

Wells (1955, [2.13]) published repeat tests of Docherty's notch bending tests. In Wells' test series macroscopic material inhomogeneities in specimens of different sizes were reduced as far as possible; Wells also estimated strain-energy release rates at fracture which were checked experimentally by means of the temperature-wave method.

Docherty's (1935, [2.5]) notched slow-bending tests (four-point bending) had shown a significant size influence resulting in a transition from ductile to brittle fracture when the size was increased. Wells tested geometrically similar notched bending specimens with a quadratic cross section under three-point loading. All specimens were notched to half depth with saws cutting to widths in proportion to the other specimen dimensions. The deep notch was chosen to assure initiation of fracture. The obtained notch roots showed rectangular contours with fillet radii approximately equal to one quarter of the cut width in each case. The specimen dimensions are given in Tab. 2-19, their depth (= width) ranging from 0.11 in = 2.79 mm to 1.250 in = 31.75 mm (scale factor about 11). Only a single specimen for each size was provided.

The material used was a structural-quality mild-steel plate (thickness 1 ¼ in = 31.75 mm) with composition and properties given in Tab. 2-20 (from Wells (1953, [2.14)). Thus, the depth of the largest specimen contained the material variation across the full thickness of the plate but the behavior at the tip of its notch is determined by the properties of mid-plane of the plate. The two largest specimens (no. 1 & 2) were cut from immediately adjacent portions of the plate. Subsequent smaller specimens were cut from the broken halves of the first two specimens in a successive procedure, as seen by the lengths of the specimen nos. 1, 3, 5, 7 and 2, 4, 6, 8. Thus, it was possible to ensure that the notched portions of the smaller specimens were free from prior plastic deformations of previous tests. This was because, in any one test, the zone of plastic flow was concentrated around the notched section which then became the extreme end of the next specimen. All specimens were cut with their two loading planes parallel to the rolled faces of the plate. Without explicit saying, it is believed that the smaller specimens were machined down to size such that the axis of the specimen was in the mid-plane of the original plate. Then the material at the tip of each and every notch stems from this mid-plane and thus thickness variations were excluded.

The three-point loading was applied through cylindrical bearers, whose diameters and spacing were proportional to specimen size. The testing machine was calibrated both for loading and loading rate to embrace the smallest and the largest specimen under the same rate of strain with the ratio of the load-point displacement rate and the loading span being 0.25 min^{-1} for all specimens. Close control of the temperature (20.2 °C ± 0.1 °C) was possible.

Load and central deflection were determined by marking the load-pointer at regular deflection intervals from which the nominal bending stress[13] at the root of the notch was plotted (Fig. 2-22) versus the normalized deflection (central deflection / loading span). After fracture the percentage brittle areas of the fracture surface were determined. These values, the maximum load, and the maximum nominal bending stress are given in Tab. 2-19. Wells noted that the maximum nominal bending stresses had to be corrected. The corrections arose through deviations from the correct proportions of the saw-cut dimensions; this should concern the depth of the cut or the ligament depth but not the width of the cut, as said by Wells (precise information is not given). The corrected bending stresses are given in Tab. 2-19 and are used in Fig. 2-22 and 2-23. Fig. 2-23 shows the corrected maximum bending stresses versus the specimen size ratio.

The percentage brittle area data in Tab. 2-19 show that in the four smallest specimens (nos. 5, 6, 7, 8, depth from 0.312 in = 7.92 mm to 0.110 = 2.79 mm) brittle fracture is suppressed. This is also reflected in Fig. 2-23 where the four smallest specimen show a consistently larger maximum bending stress than the larger specimens. However, the nominal stress-deflection graphs (Fig. 2-22) yield additional information and a somewhat more differentiated picture. The small specimens no. 5, 6, 7 yield a continuous and convex stress-normalized deflection curve with extended stress maxima. Identifying the end-points of these curves as the instant of complete fracture, the associated deflections are about 8.2 % of the loading span, i.e., 0.85 % of the beam depth. The smallest specimen no. 8 deviates considerably: the initial convex part is followed by a concave part. This implies over-hauling of the softening by an enhanced hardening; its maximum stress value is at the end of the concave part and the associated normalized deflection is much smaller than for the specimens no. 5, 6, and 7. However, the reviewer has some doubts about the validity of this single test.

The two largest specimens no. 1 and 2 yield convex curves with a pronounced load drop (fracture) in the ascending branch before any relative stress maximum could develop. The corresponding deflections are around 5 % of the loading span. The medium size specimens no. 3 and 4 do not show a load drop in the convex ascending branch, but a relative maximum is developed. Beyond the maximum in the softening region a small load drop occurs, followed by further bending under decreasing load; the final fracture (end-point of curves) is at normalized deflections between 7 and 8 % of the loading span. Unfortunately, no information is given on the initiation of cracking especially for specimens no. 3 to 8.

To explain the suppression of notch-brittle fracture in small specimens, Wells used the concepts of Linear Elastic Fracture Mechanics and balances the elastic energy release rate for crack extension with the surface energy required for an increase in crack length. This yields for a constant specific surface energy S (characteristic for the material) and a given remote stress σ a critical crack or notch length a above which crack propagation is induced. For cracks or notches which scale with the other dimensions of geometrically similar specimens, this implies a critical specimen size above which brittle crack propagation occurs for a given remote stress field. Wells explains the suppression of notch-brittle fracture in small specimens by the "absence of sufficient available elastic energy for propagation. This must be stored within the specimen at the instant preceding fracture." This, in fact, simply follows from the fact that the elastic energy scales with the volume of the specimen whereas the surface energy scales with the crack surface. The qualitative arguments of Wells are certainly correct for the

[13] Bending moment $M = PL/4$ divided by the section modulus $W = bl^2/6$.

idealized elastic case but because of the considerable nonlinear deformations, as seen in Fig. 2-22, the applicability of Linear Elastic Fracture Mechanics can be questioned. Further, Wells' theoretical and experimental studies concerning the surface energies will not be discussed here because of the above and other unresolved questions.

The work of ***Lubahn (1955, [2.15])*** on crack propagation and size effects in mild steel at room temperature reveals some important information which was missing in the previous studies: the size dependence of crack initiation and the related ductility, as defined by the strain up to crack initiation. For this purpose notch-bend tests (three-point bending presumably) were conducted with specimens geometrically similar to the standard V-notch Charpy impact specimen[14]. Thus, the following square cross-section dimensions were considered:

0.08 x 0.08 in	=	2.03 x 2.03 mm (miniature specimens)
0.4 x 0.4 in	=	10.16 x 10.16 mm (standard)
2.0 x 2.0 in	=	50.80 x 50.80 mm
3.5 x 3.5 in	=	88.90 x 88.90 mm.

Although not clearly stated, there are indications that the radius of the root of the V-notch is also properly scaled. The specimens were cut from two lots of 4 in-thick, hot-rolled mild steel plates. The two lots showed a rather pronounced anisotropy; although they were nominally identical, the lot I steel was found to be somewhat more anisotropic than lot II. These observations were not obtained from independent tests but are results of the size-effect tests using notched specimens with different notch orientations. Cutting plans or other information on the positioning of the specimens as well as the homogeneity of the plates were not documented in Ref. [2.15].

Lubahn discussed the definition of "ductility" to some extent and pointed out its ambivalence and arbitrariness. The concept stems from the use of the area reduction after fracture in tensile tests where the final diameter at the neck can easily be measured. However, in the case of bending Lubahn remarks that the whole process of crack initiation is so gradual that a "ductility" measure or strain at crack initiation can be assigned only with some arbitrariness: e.g., for polished surfaces at high magnification the "strain at the first crack" depends on how diligently one searches for that first crack; considerable uncertainty exists also in the observation of crack initiation in machined surfaces deformed at room temperature where a lower magnification of 20 ÷ 30 X is required to minimize the confusing effects of surface roughening because of anisotropic deformation of the differently oriented grains (orange peel). Under these conditions, Lubahn took the "ductility" as the strain at which one observed "the first crack large enough and deep enough to be certain that it really was a crack, rather than something of debatable nature, which in many cases could not even be located again after some additional bending. … Of course, the above criterion of ductility results in values which de-

[14] Standard V-notch Charpy-impact specimen dimensions:

square cross-section	0.4 x 0.4 inch
total length	2.2 inches
V-notch angle	45°
root radius	0.01 inch
notch depth	80 % of depth

pend considerably on how careful and critical the observer is, and which are therefore somewhat vague."

To improve the situation, observations were also carried out on several notch-bend specimens with the notch bottom lapped with a rotating wire. This treatment did not remove the mentioned uncertainties, but it shifted the uncertainty range to lower ductilities (strain values) since a much smaller crack could be detected in a lapped surface than in a machined surface. Thus, where a suspicion of a crack at 50 % strain developed into an assured crack at 70 % strain in a machined surface, a suspicion of a crack at 10 % strain developed into an obvious crack at 20 % strain for a lapped surface. This dependence of the critical strain values for crack initiation on the quality of the surface should be kept in mind since the absolute values of the critical strain are important for the structural assessment.

Unfortunately, Lubahn did not give further information about optical means and magnification which is certainly necessary. In most of the tests the procedure involved frequent unloading with inspection for cracks at the notch and measurement of the bend angle, etc.. No information was given about the frequency of unloading and crack detection, but some data suggest that around 15 interruptions were made up to the load maximum and about 30 during the whole test in some cases (see markers in Fig. 2-24). Also no indication was given on the speed (e.g., of the cross-head) or strain rate in the slow bend-tests and whether this was scaled according to the size of the specimen. For a special slow notch-bend test with a 2 in-wide and 0.394 in-deep specimen tested on a 4 in-span, a cross-head speed of 0.2 in/min was mentioned.

The determination of the axial strain at the root of the notch was not described in detail by Lubahn. It is mentioned that the strain was measured directly on gage lengths at the notch bottom for the largest specimen (3.5x3.5 in); the gage length was not identified, but reference was made to a General Electric report. In the smaller specimens the strain was calculated from an empirical bend angle – notch strain relationship, as described later by Lape and Lubahn (1956, [2.16]). In this reference the authors refer to earlier work of *Lequear and Lubahn (1954, [2.19])* who developed an empirical relation between the bending angle and the local axial surface strain at the root of a Charpy –V notch specimen. Since this approach is important for the proper understanding of the results, the essential details of Ref. [2.19] are briefly mentioned below.

Specimens were machined from annealed brass, mild steel, and hot forged 2 S aluminium. They were made geometrically similar to a standard Charpy impact specimen (see footnote No. 14, page 23), all dimension being 8.9 times the standard dimensions, except the span. A longer (1.92 times) span was used than that required by geometrical similitude. This would have a large effect on the forces involved, but Lequear and Lubahn expected little effect on the geometrical relation between the two geometrical quantities, bending angle and local strain at the root.

The nominal radius at the tip of the V-notch was 8.9x0.01=0.089 in = 0.226mm. The bottom of the notch was lapped by rotation of a 0.182 in diameter rod about its axis. On this lapped surface nine almost equidistant lines were scribed along the length of the notch. They were 10-12 10^{-3} in = 0.254-0.305 mm apart. Thus, four 10-12 10^{-3} in. gage lengths on each side of the centerline were provided on the curved notch bottom. The last line was about 30° up the radius from the bottom, as compared with 67° to the tangent point between the fillet radius and the straight side of the notch. The width of the scratches was about 1 or 2 10^{-3} in. The three-point bending was done presumably intermittently, to measure the permanent bend angles and the strain. For each angle of bend every gage length was measured five times at

each of three positions along the length of the notch using a microscope with a 20x-magnification. Without explicit saying, the bending tests were probably done up to a bending angle where surface cracks at the notch had not occurred yet.

The following results were obtained:

- the fillet at the bottom of the notch remained circular throughout the bending, as nearly as can be determined by matching circles;
- the circumferential strain was fairly uniform, considering that the strain measurements were made as far as 30° up from the bottom of the notch; the mean value was about 10 % less than the maximum at the root of the notch;
- within the limits of the scatter, the circumferential strain distribution was the same at points ± 0.5 in away from the center as the strain distribution at the center;
- for a given bend angle in the range up to a bend angle of 4°, approximately the same maximum engineering strains were obtained for the three materials, and the interpolation curve strain vs. bend angle was linear; beyond 6°, results were obtained only for aluminium and the linear interpolation up to almost 12° has a slightly reduced slope; thus, the circumferential engineering strain is nearly proportional to the bend angle – roughly 10 % strain per degree bend angle in the range from 0° to 12°.

Lequear and Lubahn (1954, [2.19]) remark that this fit would be very useful if it could be applied to geometrically similar small specimens, where local strain cannot be measured directly. The applicability to small specimens, however, depends on the validity on the "law of similitude" for purely plastic flow. Unfortunately, measurements on smaller specimens had not been made. It should be noted that the bending angle – notch strain relation will likely not be size independent when cracking has started and is propagating. Therefore, in the reviewer's opinion, the application of this relation to small specimens beyond crack initiation is rather questionable.

The first tests by Lubahn (1955, [2.15]) were done with specimens from lot I cut in the rolling direction of the plate. Only one large 3.5 x 3.5 in-specimen with the depth of the beam in the thickness direction (= long direction of notch in the transverse direction of the plate) was tested. The longitudinal strain at the bottom of the notch (lapped notch surface) reached 45 % when cracks appeared "high up on the notch radius on both sides." They clustered about a point somewhat above the transition between the curved and the flat notch surface. On subsequent bending the specimen broke in two with a loud sound. Inspection showed that the main crack had extended first 1/16 in approximately horizontally (parallel to the plate surface) into the steel and then went vertically (in the direction of the plate thickness) through the specimen. Lubahn notes that "even after having gone part way through the specimen vertically, the crack had considerably tendency to go horizontally … ." No cracks were observed at the bottom of notch. This abnormal fracturing appears to be related to the anisotropy of the lot I material[15]. Hence, it was suggested that the "longitudinal ductility" would be greater than 45 % without this abnormal fracture. Therefore, specimens of the standard 0.4 x 0.4 in-size with two different notch orientations were prepared. The long axis of all specimens were in the rolling direction and the long direction of the notch was in the transverse direction of the plate as before (case A, two tests) and in the plate thickness direction (case B, one test). The two specimens of case A developed cracks at the sides of the notches at longitudinal strains at

[15] It is expected that zones of weak material (e.g. segregations) are rolled out into a layered structure parallel to the plate surface. Thus cracks will have a tendency to propagate into the weak layers.

the notch bottom of 35 and 55 % (mean 45 %). Thus, the position of crack initiation and the associated longitudinal strain level at the notch bottom of these small 0.4 x 0.4 in specimens are the same as for the large 3.5 x 3.5 in specimen (Tab. 2-21). However, one specimen of case B was stretched 65 % at the notch bottom before a crack developed at the notch bottom. Thus, the anisotropy has a definite effect on the position of failure initiation and the apparent ductility in the longitudinal direction of the specimen.

The specimen sizes (0.08 x 0.08, 0.4 x 0.4, and 2.0 x 2.0 in) were provided from the lot II steel, all specimens cut again in the rolling direction. A specimen family was obtained with the long direction of the notch in the transverse direction of the plate (case A) and the number of nominally identical tests being two at most. This family covered a very large size range of 25. Furthermore, two of standard 0.4 x 0.4 in-size specimen with the notch direction in the thickness direction of the plate were also tested (case B).

Since direct measurements of the strains at the root of the notches were not made, the permanent bending angles at crack initiation were used to calculate the maximum local surface strain on the basis of the empirical relation by Lequear and Lubahn (1954, [2.19]) described above which implicitly assumes the validity of the "law of similitude". Therefore the strain values in Tab. 2-21 are actually hypothetical values. Because of the approximate linearity of the bend angle – strain relationship, the data in Tab. 2-21 are actually measures of the bending angles at the crack initiation (the reviewer).

Generally the fractures started at the notch bottom and propagated downward. The strains at crack initiation are listed in Tab. 2-21. The repeat tests show a considerable scatter and "scatter bands" are partially overlapping. Comparing mean values, the smallest specimens (0.08 x 0.08 in) yield somewhat larger "ductilities" (95 %) than the largest specimens (85.5 %). For a scale factor of 25 this appears to be only a moderate size effect. Lubahn concludes tentatively from the results of the lot I- and lot II-specimens that there is no size effect on the strain to crack initiation ("ductility"). On the other hand, the size has a very pronounced effect on the way the crack propagates: for example, the 2 x 2 in specimens of the lot II-steel tore open about 2 % of the ligament length before a sudden crack propagation occurred; the 0.4 x 0.4 in-specimen tore open about 30 %; and the smallest specimens tore to 50 % of the ligament length before exhibiting any sudden crack propagation, and then only a very small amount. Moreover, differences were seen also in the fracture surface morphology: the largest specimens showed cleavage fracture except for a very narrow band of fibrous fracture around the edges. However, the fracture surfaces of the smallest specimens were entirely fibrous except for a few tiny cleavage areas near mid-depth. Similar observations were made for the lot I-specimens.

The size effect is also reflected in the load-deflection curves. In the largest (2 x 2 in) and the smallest (0.08 x 0.08 in) specimens crack initiation occurred before the load maximum. However, in the largest specimens there was comparatively little additional deflection between crack initiation and the load maximum which was accompanied with a sudden fracture and a load drop to practically zero. In the smallest specimens the crack was tearing open gradually with increasing load but beyond the maximum with gradually decreasing load. When a sudden crack advancement occurred, there was only a minor drop in load. These characteristic differences are shown in Ref. [2.15] for a small (0.08 x 0.08 in) specimen and a large (2x2 in) specimen in two separate figures. These two graphs are combined in a single figure (Fig. 2-24) by scaling down the result of the large specimen to be comparable with the small specimen (i.e. forces are multiplied with $(0.08/2)^2$ and deflections with (0.08/2)). Unfortunately, these two specimens were not strictly similar since the span between supports was

3/8 in = 9.52 mm for the small and 11 in = 279.40 mm for the large specimen (scale factor 29.33), but all other dimensions scaled with a factor of 25. Thus, for a proper scaling, the large specimen should have a span of only 3/8 · 25 = 9 3/8 in = 238.12 mm. Accordingly, for a given load of the large specimen, the measured deflections W_1 are larger than for the properly scaled case W_2. A simple model (Appendix 1) allows to estimate this influence in the plastic regime before crack initiation. One obtains

$$\left(\frac{W_2}{W_1}\right) = \left(\frac{L_2}{L_1}\right)^{\frac{1+n}{n}} \tag{2.16}$$

where $n < 1$ is a lumped strain hardening exponent and $L_2/L_1 = 25/29.33 = 0.85227$ is the ratio of the spans. For $n = 0.1$ and 0.2 one gets $W_2/W_1 = 0.17$ and 0.38. Thus, the points of the graph for the large specimen in Fig. 2-24 should be shifted to the left by 83 % or 62 %, respectively. Therefore, except for the initial part, this curve comes close to the curve for the small specimen in Fig. 2-24. Of course, the deflection indicating crack initiation should also be shifted to the left. Assuming that the notch opening and thus the bend angle is the determining quantity, one obtains (Appendix 1)

$$\frac{W_{2c}}{W_{1c}} = \frac{L_2}{L_1} = 0.85227 \tag{2.17}$$

where W_{1c} is the deflection at crack initiation in the large specimen with a half-span $L_1 = 11/2$ in and W_{2c} the corresponding deflection with a half-span $L_2 = 3/8 \cdot 25 = 9.375$ in. With the model in Appendix 1 the corresponding loads P_{1c} and P_{2c} are related by $P_{2c}/P_{1c} = L_1/L_2 = 1.1733$. Thus, P_{2c} increases by 17 %.

These theoretical considerations show that the differences between the small and the large specimen become less in the regime of extended plastic deformation if a correction is applied to the measured results for the large specimen. However, the incident of crack initiation is shifted to smaller relative deflections than shown in the uncorrected graph in Fig. 2-24. In fact, the points of crack initiation marked in Fig. 2-24 have almost the same relative deflections (0.037 in for the small and 0.030 in for the large specimen); the theoretical correction for the latter would give 0.030 x 0.85227 = 0.025 in).

As noted by Lubahn, the size influences on the load deflection curves are similar to those noted by Docherty (1935, [2.5]): “sudden rupture is sooner and more complete in large specimens.” However, the crack initiation and gradual tearing, which precede the maximum load and the sudden rupture, were unresolved topics in Docherty’s experiments.

The subject of size effects, as related to fracturing, was taken up again by ***Lubahn (1955, [2.17]).*** He summarized some of the results for the notch-bend specimens of mild steel described in Ref. [2.15]. In addition, results of tensile tests of circumferentially notched specimens of an aluminium alloy and of a heat treated SAE 4340 steel were presented. Moreover, results for notch-bend specimens of a heat treated Ni-Mo-V steel were discussed. Three years later the results of the Ni-Mo-V-steel were reported again ***(Lubahn and Yukawa (1958, [2.18]))*** but with much more detail. Thus, the present review will combine these two sources.

The circumferentially notched tensile specimens made of the *7075-S-T6 aluminium* were provided with a 60°V-notch with a depth of about 30 % of the radius of the uniform section. The specimens were geometrically similar, except for a constant notch tip radius of

r=0.001 in[16]. A geometric scale factor of about 7.2 was used, the specimen diameter in the uniform section ranging from 0.2 in = 5.08 mm to 1.43 in = 36.32 mm. For the same range of diameters, tensile tests with unnotched specimens were also performed. The strain rate as well as the origin and homogeneity of the base material were not reported. For the notched specimens, the nominal strength, as plotted in Fig. 2-25, was defined as the maximum load divided by the initial cross section at the root of the notch; for the unnotched specimens, of course, the uniform diameter was used.

Both test families show a loss in strength for diameters larger than 0.65 in = 16.5 mm but not for smaller specimens and here the tensile strength values of both families are fairly close. For the larger specimens the size influence is definite but moderate for the unnotched specimens: the loss is about 10 %. A substantial size influence - the loss is about 35 % - is seen for the notched specimens. Since the notch tip radius was kept constant the notch sharpness increases with size and this will add to the true geometrical size effect.

The size independence in the range of small specimens was not commented by Lubahn. Since no further information is given (e.g., the nominal load-displacement curves or the mode of fracture, etc.), the following discussion is speculative. The behavior of the notched specimens is possibly due to a transition of the failure mode: the small notched specimens fail by plastic instability when plastic hardening and geometric softening (area reduction by volume conservation) are balanced. This is associated with a relative maximum σ_i of the nominal stress-displacement curves and it is usually size independent if the plastic deformation laws do not involve a size dependence, as usually. Then, to a first approximation [17], the nominal strengths of the notched and the unnotched specimens are the same. In fact, this is seen in Fig. 2-25. For specimens with a sharp notch, scaled geometrically with the gross-dimensions (e.g. minimum diameter *d,* unnotched diameter *D*), classical fracture mechanics concepts become important beyond a characteristic size d_t. For example, if the fracture is controlled by linear elasticity, the fracture stress is given by $\sigma_c = 4P_c / (\pi d^2) = (4.29 K_{IC} / \sqrt{\pi D/d}) / \sqrt{d}$ [18], the standard inverse square root decay of the fracture stress σ_c where K_{IC} is the size independent fracture toughness. Then the condition $\sigma_c = \sigma_i$ defines a characteristic diameter

$$d_t = \left[\frac{4.29\ K_{IC}}{\sigma_i} \frac{1}{\sqrt{\pi\alpha}} \right]^2, \quad \alpha = D/d = const. \tag{2.18}$$

for the mode transition. For nonlinear elastic or plastic behavior (deformation law of the form $\varepsilon \sim \sigma^n$, $n \geq 1$) at the notch tip, the inverse square root dependence changes to $(d)^{-1/n+1}$, which is a less severe size dependence than the linear elastic case. The validity of this concept would imply that crack propagation starts at the maxima of the nominal stress-displacement curves followed by a sudden local drop and that the maxima are not relative ones. This model appears to be quite plausible but further evidence is missing in Lubahns paper. A disturbing fact is the size dependence of the unnotched specimens for larger diameters. Simple fracture mechanics arguments are not applicable since a predetermined crack or notch is not present. This phenomenon may also be present in the notched specimens and superposes other size effects.

---

[16] Ref. [2.17] contains contradictory values: in the text r = 0.001 in is mentioned; however, in the Fig. 2-25 a value of r = 0.01 in is given.

[17] This is based on the assumption of a uniaxial stress distribution in the specimens.

[18] The finite opening angle of the V-notch is ignored (Ewalds and Wanhill (1984, [2.31], p. 51); here the equation for the stress intensity factor of a circumferentially notched bar needs correction).

Lubahn (1955, [2.17]) presented also notched tensile test data versus specimen diameter (Fig. 2-26) for *SAE 4340 steel* quenched to martensite and tempered to strength levels from 185000 to 290000 psi. The V-notch depth amounts to about 30 % of the specimen radius and the nominal notch tip radius was the same for all specimens and rather sharp (r = 0.001 in). Details of the material were not given, but Lubahn pointed out that the specimens were machined to size before quenching and tempering. The strength data are given in the form of the notch strength ratio, a dimensionless quantity defined as the notch stress divided by the ultimate stress of an unnotched specimen (preferably with the same diameter) and the notch stress specified as the maximum load divided by the initial cross section area at the root of the notch.

From the semi-logarithmic presentation of the results in Fig. 2-26, the following observations are made:

- the increase of the strength level (ultimate tensile strength of unnotched specimens) due to reduction of the tempering temperature
  - reduces the notch strength ratio for all sizes, but
  - increases the size dependence of the notch strength ratio; thus, for a strength level of 220000 psi the loss in notch strength ratio is about 15 % when the diameter is increased from 0.3 in = 7.62 mm to 1.5 in = 38.10 mm, but for a strength level 290000 psi the loss is about 50 %;
- for the semi-logarithmic representation and for the investigated size range the decay of the notch strength ratio is approximately linear;
- for low strength levels or small specimen sizes the notch strength ratio is greater than one.

As Lubahn remarked, the size influence in Fig. 2-26 may be partly due to an increasing notch sharpness with increasing size because of the constant notch tip radius. There may be also a metallurgical size effect since the specimens were machined before the heat treatment; thus, the larger specimens[19] may have had an inferior micro-structure.

The effect of size on the ductility and strength at room temperature of notched bending specimens of a *forged generator rotor steel* (0.30 %C, 2.53 % Ni, 0.55 % Mo, 0.07 % V) was investigated and reported by Lubahn (1955, [2.15]) and Lubahn and Yukawa (1958, [2.18]). The fabrication and the heat treatment generated a tempered bainitic micro-structure with approximately the same yield (83000 psi) and tensile strengths (108 – 110000 psi) in the radial, tangential, and longitudinal direction near the bore of the forged and heat treated cylindrical material slug. Also the same yield and tensile strengths in the radial direction were found at the outer surface. The area reduction, however, shows a considerable scatter near the bore and at the outer surface. Its mean percentage values are

at the bore $\Rightarrow$ 13 % radial, 11 % tangential, 24.5 % longitudinal,
at the surface $\Rightarrow$ 41 % radial.

This is a remarkable variation of the ductility (area reduction) along the radius.

Four families of notched specimens were prepared with the following common properties:

- generally square cross-sections, the gross depth a of the beam ranging from 0.2 inches = 5.09 mm to 9 inches = 228.6 mm covering a scale factor of 45,
- 45° V-notch with a depth of 20 % of the gross beam depth,

[19] The large specimens were tempered for four hours instead of one hour for the small ones (Fig. 2-26); whether this suffices to obtain the same micro-structure is not clear.

- the ratio of beam length to depth equals that of a Charpy impact specimen (ratio 5.5).

The differences in the four families concerned the notch root radius *r*:

I specimens geometrically similar in all respect to the Charpy impact specimen with a notch sharpness of *a/(r40) = 1*; thus, for the smallest specimens *r = 0.127* mm and for the largest *r = 5.7* mm,

II specimens geometrically similar as above but with a 10-times larger notch sharpness, *a/(r40) = 10*,

III as above but constant notch radius *r = 0.003* inch,

IV as above but constant notch radius *r = 0.001* inch.

The specimens were cut from the forged cylindrical material slug such that their long axis was radially oriented and the long direction of the notch was parallel to the forging axis (longitudinal direction of forging). Usually, the notch root was positioned near mid-radius of the forging. Some of the larger specimens required welded extensions outside the notched section. Also unnotched bending specimens of several sizes were prepared and tested.

The specimens were tested under three-point loading, loaded opposite the notch at slow rates typical for hydraulic testing machines. Obviously, the speed of the load-point was not scaled according to the size of the specimens (scale factor 45!). Also some of the 9 inch specimens were tested in a 2000 ton hydraulic press; at the beginning of the testing and during the course of test program different load calibrations were done which showed differences of 17 %. However, the consequences for the bending strength data of the very large specimens were not elucidated.

The plastic (permanent) bend angle during the test was determined either by an intermittent or a continuous method, The “ductility”, defined as the “local strain” at the notch root, was then derived via an empirical relation from the plastic bend angle. This application implied the law of similitude. Details were not given, but reference was made to the publication of Lequear and Lubahn (1954, [2.19]). See also the discussion above.

The plastic bend angle was obtained directly in the intermittent method by unloading from successive load levels and measuring the permanent rotation of the notched beam. The curve of the load versus permanent angle was then extrapolated to the measured fracture load to obtain the permanent bend angle at fracture.

In the continuous method the deflection of the notched beam was the displacement of the loading point (edge of loading knife) relative to the supports which included also the yielding at the contact points and the elastic deformation of the support. Details were not described. Lubahn and Yukawa then defined the “plastic bend angle” as the deviations from linearity which is equal to the permanent rotation which would have been observed on unloading. This was then converted to the plastic notch strain as before. A comparison of both methods showed that at large plastic strain essentially the same results were obtained.

Fig. 2-27 shows the nominal stress versus the plastic notch strain for specimens that are geometrically similar to the standard Charpy specimen. Here the nominal stress is defined by the bending moment *M* divided by the section modulus *W* of the ligament section (i.e. *M/W*) which yields a fictitious elastic bending stress at the root of the notch. The data for the specimens without welded extensions, which cover only the depth range from 0.197 inch to 1.6 inch, show a considerable scatter in the stress up to about 4 % plastic strain at the notch root; no trend related to the size is observed and thus similarity is assured. For larger notch strains, say 10 %, all data in Fig. 2-27 belong to the two small sizes (0.197 and 0.394 inch depth) except one measurement for a 1.6 inch depth specimen; all these data are fairly close and thus a

size influence is not detectable. The two largest specimens (depth 2.75 inches and 8.94 inches) have welded extension. Up to 4 % notch strain they give consistently lower stresses than the smaller specimens and for strains larger then 8 % bending stress data are missing. It cannot be excluded that some size effect is responsible for this shift to lower stress, but the welding process may have affected the notched sections, especially the largest specimens because here welds were in close proximity to the notch. According to Ref. [2.19], scribed lines had been applied to the notch root and their distance had been measured before and after welding and this revealed that high residual stresses are induced by the welding.

The influence of size on "ductility" is shown in the semi-logarithmic presentation Fig. 2-28 for specimens geometrically similar to the V-notch Charpy impact specimens. These specimens have been repeatedly loaded and unloaded (intermitted method) and this shifts the notch ductility at fracture to higher values. It should be recalled that with the intermittent method the strain at fracture is obtained by an extrapolation, as shown in Fig. 2-29 for two cycles of a 9 inch specimen. Apparently, the strain at fracture can be increased by loading and unloading to successively higher loads before fracture; reference was made to a similar effect ("coaxing") in fatigue. Only the curve with about 10 loading/unloading cycles is defined by enough points to show the trend with size. The other curves were drawn approximately parallel to this one. As seen in Fig. 2-28, the ductility decreases quasi-exponentially within the size range of the beam depth from 0.2 to 9 inches. For example, the ductility decreases from about 25 % (0.2 x 0.2 in-specimen) to about 3 % (9.9 in-specimen) if only one cycle is applied.

The results for the "ductility" or local notch strain at fracture are obviously based on the empirical relation between the bend angle and the notch strain obtained by Lequear and Lubahn (1954, [2.19]) as well as on the "law of similitude". The bend angle at total fracture, however, consists of two contributions: the plastic deformation of the notch and the crack opening and propagation. If the latter is significant, i.e., if there is considerable additional bending rotation between the instant of crack initiation and total fracture, then the "law of similitude" is likely not applicable. However, Lubahn (1954, [2.17]) pointed out that after the instant of crack initiation in this heat treated steel no increase in load or bending moment was observed and almost instantaneous cleavage fracture without previous tearing occurred, except for the smallest specimens which teared slightly at the surface before sudden rupture.

The nominal bending strength, as defined by the bending moment M_m at maximum load divided by the section modulus W of the initial ligament section[20], is plotted versus the beam depth in Fig. 2-30. In Fig. 2-30 very few tests (depth 0.2 inch and 2 inches) of unnotched bending specimens are also included. They yield roughly the same bending strength (~220000 psi) and from this Lubahn concludes that a size effect is not present. However, only a single test for the large welded specimen (2 inches) was done and this specimen failed at the weld. It appears that this result is not representative for the behaviour of the base material. It is noted that the fictitious elastic bending strength of 200000 psi is about a factor of two larger than the tensile strength in the radial direction of the cylindrical steel slug.

The two solid curves in Fig. 2-30 refer to different notch sharpnesses, as defined by the ratio of the beam depth a and the root radius r. All specimens of these two test series were geometrically similar. The tests shown in the graph with a notch sharpness *a/(r40) =1* are geometrically similar to the V-notch Charpy impact specimens, except one specimen with depth of 4 inches and a reduced thickness (1 inch). Their corresponding ductilities at fracture

[20] That is M_m/W = fictitious elastic bending stress at the root of the notch.

are depicted in Fig. 2-28. Thus, the corresponding bending strength values in Fig. 2-30 represent the data of specimens with different loading histories (repeated loading – unloading). Obviously, the repeated cycling has only a moderate effect on the bending strength (see the scatter for the (0.4 in x 0.4 in)-specimens). As seen in Fig. 2-30, this size effect – loss in bending strength – is much less (about 22 % over the range of 0.2 to 9 inches) than for the ductility shown in Fig. 2-28.

If the notch sharpness is increased by a factor of 10 *(a/(r40) = 10*, solid curve with Δ-markers), the bending strength is reduced considerably in the range of 1 to 9 inches of the beam depth. Unfortunately, no test data are available for smaller specimens because of "machining difficulties", as vaguely stated by Lubahn and Yukawa (1958, [2.18]). However, a value was determined indirectly by re-plotting the strength data of Fig. 2-30 with respect to the notch sharpness *a/(r40)* and with the depth as curve parameter (see the semi-logarithmic presentation in Fig. 2-31). The extrapolation to very small sharpness values is aided by the argument that all curves should approach the strength of unnotched bending specimens as an upper limit. For specimens with a depth of 0.4 inch the curve is well defined (Fig. 2-31) and the extrapolation to a sharpness of *a/(r40) = 10* appears to be within a reasonably "distance". This extrapolated point is marked in Fig. 2-30 by the symbol ⊗.

Aside from the shift to lower strength values, the 10-times increased notch sharpness yields an increased decay of the bending strength with size (factor of almost 1.7 in the range of 1 to 9 inches beam depth).

A complete test family, covering a depth range from 0.2 inch to 4.0 inches (scale factor 20) but with a constant notch tip radius of 0.003 inch = 0.076 mm is included in Fig. 3-30. For the smallest specimen, the notch sharpness is *a/(r40) = 1.67* which is comparable to the notch sharpness 1 (0-markers in Fig. 2-30) of the specimens geometrically similar to V-notch Charpy specimens. Clearly, for this size the bending strengths agree (≈ 205 10^3 psi). Increasing the size to 4.0 inches, the notch sharpness becomes 20-times larger which yields a bending strength of about $60 \cdot 10^3$ psi and this is just one third of the strength for the Charpy-type specimen of this size. But more important, for this large size the bending strength is also less than that for the geometrically similar test family with constant sharpness *a/(r40) = 10*, i.e., $95 \cdot 10^3$ psi. Thus, for a test family with a constant notch tip radius the strength-size curve becomes steeper for large specimens. Therefore, this greater size effect, as the size increases, is because the true size effect of geometrically similar specimens is amplified by the increase of the notch sharpness.

A few tests for large but welded specimens are also included in Fig. 2-30. Especially the strength of the 9 inch specimens are far below the unwelded ones which very probably reflects the influence of the welding in the proximity of the notch.

From the strength versus sharpness curves in Fig. 2-31 it is seen again that the reduction of strength with increasing notch sharpness becomes greater, as the specimen size increases. Further, the shape of the curves, especially for the largest unwelded specimens (9 inches), supports the suggestion that little additional loss in strength is to be expected if the notches are sharper than the sharpest one tested.

Lubahn and Yukawa presented also a few intricate arguments with respect to the influence of the depth of the notch. This discussion, however, leaves essential questions open. Finally, the authors discussed the influence of hydrogen diffusion which is more effective in small specimens than in large ones. Thus, if the steels were susceptible to hydrogen embrittlement, the size effect could be attributed to differences in hydrogen content. A test series was performed yielding the conclusion that, while hydrogen is an important factor, the size effect

observed in the bending strength cannot be explained by hydrogen diffusion, i.e., depletion in small specimens and hydrogen embrittlement in large specimens.

Notch bending and notch tension tests as well as theoretical analyses of the elastic energy release rate were done by ***Lubahn (1959, [2.20])*** to determine the critical energy release rate at fracture, presumably a material property. Some of the slow notch-bending results of Refs. [2.17, 2.18] and new, geometrically scaled notched tension test results for the same material (tempered Ni-Mo-V steel forging – rotor steel) were analysed.

Fig. 2-32 shows results from Fig. 2-30 for the notched bending specimens with very small but constant notch radii (r = 0.003 in = 0.076 mm and r = 0.001 in = 0.025 mm) in a semi-logarithmic presentation, i.e., the nominal bending strength and the plastic angle at fracture versus specimen size. For gross beam depths greater than 0.75 inch the strength data fit very well the inverse square root law of Linear Elastic Fracture Mechanics (Griffith-Irwin law) with an average critical energy release rate G_c = *131* inlb/in^2 and with maximum and minimum values of 165 and 105 inlb/in^2. For smaller specimens the measured strength data are less than the values of linear fracture mechanics and approach the bending strength value of unnotched specimens (see also Fig. 2-30).

The same Ni-Mo-V steel forging was used by Lubahn to prepare circular notched tensile specimens, their unnotched diameter nominally being D = 0.250, 0.400, 0.600, 0.900, 1.300, 2.250 inches (6.35 to 57.15 mm, scale factor 9). The 45°-V-notch depth was about 30 % of the specimen radius $D/2$, i.e., the cross-section area was reduced by 50 %. The radius at the root of the notch was required to be less than 0.003 in = 0.076 mm. Continuous measurements of the load and the change Δd of the diameter d at the root of the notch (micrometer measurements) were made. From these data curves of the average axial stress at the minimum section (load divided by the initial minimum section) versus the diametrical strain $\Delta d/d$ were obtained. Fig. 2-33 shows a few typical curves for three sizes. The initial linear part has been drawn with a slope which is the average of all tests. The elastic behaviour of the notched specimen alone should not be inferred from this slope value. The instant of complete fracture (✳-marker) was obtained by extrapolating the curve towards the measured fracture stress.

It is evident from the curves that, as the size increases, the fracture occurs at lower diametrical strain values. Thus, the smaller specimens endure considerable large plastic strains to fracture. No information on the initiation of cracking (before or almost at the instant of complete fracture) is given in Ref. [2.20]. Lubahn remarks that "size can only affect the location of the failure point on the curve; the Law of Similitude (Ref. [2.18]) requires that the shape of the stress-strain curve be independent of size." Sachs (1941, [2.21]) also stated that no exceptions to the law of similitude is known. In another paper Lequear and Lubahn (1954, [2.19]) pointed out, however, that there is little experimental evidence showing the validity of the law of similitude. Unfortunately, no systematic evaluation of this aspect has been done for the notch tensile tests.

The results for the various tests are collected in Tab. 2-22. Here S_n is the nominal notch stress at fracture and e_{sm}/e_{cl} a measure for the loading eccentricity which is low. The plastic notch strain corresponds to the permanent diametrical strain at fracture.

In Fig. 2-34 plots of the nominal notch strength and the plastic notch strain are presented. For unnotched diameters D equal to or larger than 0.9 in. = 22.86 mm, the notch strength conforms to the inverse square root law of linear fracture mechanics and the fitted graph corresponds to an average critical energy release rate G_c = 85 inlb/in^2. For the smaller sizes, the notch strength values lie below the theoretical elastic fit because of extensive plastic flow at

the notch. The extend of this plastic flow is indicated by the "notch ductility" plotted in the lower part of Fig. 2-34. It is seen that in the size range, where linear fracture mechanics applies ($D \geq 0.9$ in), the plastic notch strain ("notch ductility") is far less than 1 %. Since the material used for the notch bending and the notch tension test was the same (material A in Ref. [2.20]), a general *shape independent* validity of the linear fracture mechanics would require the same critical energy release rates. This is not the case and it signals caution with respect to the applicability of the theory. Possibly the plane strain conditions were not sufficiently realized in the notch bending tests with specimen having quadratic cross-sections.

On the track of the work of Lubahn and co-workers, ***Wundt (1959, [2.22])*** proposed a general descriptive concept of the size dependence of characteristic strength data in the presence of sharp notches or cracks, which embraces the notch-strengthening of small bars and the notch-weakening of large bars. Strengthening or weakening of a notched specimen is here understood with respect to the ultimate stress or yield stress of a smooth, unnotched specimen in a tensile test. Wundt put attention to considerable literature on the subject of increased strength of relatively small notched cylindrical tension specimens. According to the work of Sachs and co-workers (1945, [2.23]) on low alloy steels, often, after the load maximum has been reached, the load decreases until fracture. This behaviour of notched specimens indicates a degree of ductility. Under such conditions, the notch strength S_d increases linearly with the notch depth N[21]; namely, for 50 % notches the notch strength is about 50 % higher than the unnotched tensile strength S_t. For very deep notches, say almost 100 % deep, the notch strength approaches twice the tensile strength of the unnotched specimen. This applies only when the notch is made very sharp and when the notch angle is equal to or less than 60°. When the notch radius increases, the notch-strength passes through a maximum and then decreases with increasing notch depth. For still larger radii and very deep notches the notch strength may even approach the tensile strength from above. The notch strength deviates more and more from the linear strength-depth relationship if steels with higher strength are considered. If combined with very small radii, the ratio of notch strength to tensile strength may decrease below 1, especially when the notch depth is 50 to 60 %. Increased specimen size results in a more or less gradual deviation from the linear notch strength – depth relation, especially for high tensile strength steels.

On the other end of size scale, the notch-weakening of large specimens with increasing size, the geometric size effect, can be described by Linear Elastic Fracture Mechanics. In a log-log representation of the notch strength – size relation this is a straight line with slope (-½; inverse square root relation). For a specific sharply notched specimen type this is shown schematically in Fig. 2-35. According to the relation between notch strength relative to the yield strength and tensile strength, etc., a classification of the failure behaviour may be introduced: ductile, quasi-ductile, quasi-brittle, and brittle, as defined in Fig. 2-35. The experimental data for sharply notched bending and notched tension obtained by Lubahn and co-workers were represented by Wundt within this bi-logarithmic scheme.

The influence of the notch tip radius was pointed out before when the work of Lubahn and co-workers was discussed. ***Yukawa and McMullin (1961, [2.24])*** studied the effect of notch acuity (sharpness) on the fracture strength using notched bend specimen of various sizes. The

[21] N = notch depth, ratio of area removed by the notch to gross circular area

test material was a large billet of a vacuum arc remelted alloy steel[22]. This was heat treated to a coarse grained tempered bainitic microstructure to promote notch brittleness at room temperature. Uniform properties and microstructure were obtained with the mechanical properties: tensile strength =125 000 psi, 0.2 % yield strength =100 000 psi, reduction in area =51 %.

Several sets of notched beam specimens, ranging in cross section size from 0.4 x 0.4 in. = 10.16 x 10.16 mm to 3 x 3 in. = 76.20 x 76.20 mm, were machined:

Set I: 45° V-notch machined, notch depth 20 % of beam depth and constant root radius 0.005 in. = 0.127 mm for all sizes.

Set II: Normal machining of a notch then slight extension to 20 % depth by a knife-edge tool and an electric spark discharge process; this gives a root radius of about 0.004 in. = 0.102 mm, i.e., approximately the same radius as Set I; this notch preparation was limited to 1 in.-specimens only. The exact profile of the notch is not given in Ref. [2.24].

Set III: An arrested cleavage crack was produced. Starting off from blanks with a 1 x 2 in. cross section, a notch terminating in a fine saw cut was made across the 1 in.-face, then chilling with dry ice and liquid air and forcing a wedge into the notch by hammering such that cracks stopped after running a short distance; machining down of the bar to a 1 x 1 in. cross-section; use of dye penetrant to mark the crack front; considerable variation of the actual arrested crack depth. Therefore, selective choice of tested specimens with a initial crack depth of about 20 %. This set was restricted to 1 in.-specimens.

Set IV: A machined notch was provided with a short fatigue crack such that the total notch plus crack depth was about 20 % of the specimen depth. This set covered the whole size range.

Set V: A 60° V-notch with a 20 % depth and a 0.005 in. tip radius was machined as in Set I but the V-notch surface was nitrided (0.015 in. = 0.38 mm layer); nitriding did not alter microstructure outside the layer. Nitriding was done only for 1 inch-specimens. It was expected that nitriding a machined notch made it equivalent to a crack because a crack forms in the nitride layer at relatively low stress levels.

The length of the specimens was not reported but it is expected that it was proportional to the Charpy impact specimens. The specimens were tested at room temperature in slow bending under three-point loading in a hydraulic testing machine with the corresponding characteristic loading speeds (note: unscaled cross head speeds).

The primary quantity recorded during the tests was the maximum load at fracture which was converted to a nominal bending stress σ at the tip of the notch or crack using elementary beam theory ($\sigma = M/W$, M: bending moment, W: section modulus of ligament section). In Fig. 2-36 a bi-logarithmic presentation of the nominal bending stress versus specimen depth is given for all specimens with a notch or crack depth of 20 %. The fracture of all specimens larger or equal than 1 in. was brittle, i.e., at the maximum load the fracture occurred suddenly and propagated completely through the specimen (100 % cleavage type). Load deflection graphs were recorded for several specimens which are essentially linear nearly up to fracture with some plastic behaviour in some specimens prior to fracture. In the specimens with cracks

[22] Chemical composition (weight %): 0.30 C, 0.48 Mn, 0.03 P, 0.03 S, 0.22 Si, 2.6 Ni, 0.44 Mo, 0.09 V

plastic deformation was considerably less and practically non-existent in the larger pre-cracked specimens.

From Fig. 2-36 it is seen that machined as well as spark eroded notches (approximately the same root radius) yield the same bending strength for the 1 inch-specimens (as expected). However, the cracked notches and the nitrided machined notches yield considerable less strength for specimens equal to or larger than 1 inch. For the 1 inch-size roughly a factor of two in the strength is observed. In Fig. 2-36 the straight lines with slope (- ½), following the inverse square root law, are fitted to the data of specimens equal to and larger than 1 inch. The fracture toughness corresponding to the relative position of these linear graphs are, respectively, G_c = 300 and 120 lb/in.. The first value applies to the machined and eroded notches with almost the same finite root radius and the second value to the cracked notches. It should be kept in mind that the linear fracture mechanics yielding the inverse square root law is derived from linear elasticity for the case that fracture starts from a sharp crack which implies a stress and strain singularity. Of course, this is not satisfied for the machined notches.

The inverse square root law implies an increasingly higher strength as the specimen size is reduced, but the experimental data do not attain such high values. As seen in Fig. 2-36, the 0.4 inch-specimens with machined or fatigue cracked notches yield approximately the same strength which is well below the extrapolated strength according to linear fracture mechanics. It appears that the strength values for small specimens approach a limiting value (250 000 lb/in.^{2}, i.e., twice the tensile strength). Yukawa and McMullin state that this limit "results from the occurrence of gross plastic deformation wherein deformation conditions rather than fracture conditions govern the strength". No further explanation is given in Ref. [2.24]; it appears that this change is related to a failure mode transition.

The size effect at room temperature on tension properties of smooth and notched circular specimens made of 7075-T6 aluminium, 6Al-6V-2Sn titanium, and AISI 4340 steel were determined by ***DeSisto, Carr, and Larson (1963, [2.25]).*** This appears to be the first time that size effects in notched specimens were systematically investigated in conjunction with unnotched specimens of the same material. In principle this is an important approach because before size influences in notched specimens are studied, unnotched specimens with fairly uniform stress and strain distribution up to the maximum load should prove to be size independent.

The dimensions of the unnotched and notched specimens are given in Tab. 2-23. The minimum common diameter ranges from 0.113 in. = 2.87 mm to 3.57 in. = 90.68 mm which covers a very large size range (scale factor 31.6). A 60° V-notch is applied in the notched specimens with constant 50 % cross-section area reduction and a corresponding notch depth $(D-d)/D$ of about 30 %. The smooth and notched specimens represent two families of geometrically similar specimens, however, the sharp notch root radius (0.001 in. = 0.0254 mm) is kept constant. The aluminium and titanium were tested as received. However, blanks of large 5 ¼ inch diameter steel (AISI 4340) were heat treated[23] and then the specimens were machined to size. The smooth specimens were tested in the plastic regime with a constant speed (0.02 in./min) of the cross-head (platen). In the smallest specimen an average strain rate of $0.83 \cdot 10^{-3}$ s^{-1} was obtained which was reduced by more than a factor of 30 when the largest

[23] Normalized at 1600 F, 4 h, air cool; austenitized at 1550 F; 4 h, oil quench; double tempered at 1000 F, 4 h, oil quench

specimen was tested. The notched specimens were also tested with a constant but 10-times slower speed. A reason was not given by DeSisto et al. but it appears that this speed reduction compensated somewhat for the increased strain rate at the notch, as compared to the rest of the specimen. Specimens of 0.505 in. diameter and smaller were tested in a 120 000 lb hydraulic testing machine, while for the larger specimens a 2 400 000 lb hydraulic testing machine was used.

Results of the smooth and notched specimens are plotted in Figs. 2-37 to 2-41. The 0.2 % yield strength and the tensile strength of smooth specimens of all three materials show a rather moderate scatter and no size influence is observed. The area reduction and elongation at fracture, however, generally decrease with increasing size, especially for the larger specimens (see the semi-logarithmic presentation in Fig. 2-37). It is noteworthy that the area reduction appears to be size independent or increases with size for the small specimens with diameters less than about 0.5 inch whereas a decrease for larger diameters is observed. DeSisto et al. did refer to this. To the reviewers opinion, it may well be that this abrupt change in size dependence of the area reduction is related to the use of two different hydraulic testing machines, one used for specimens with diameter less than 0.5005 inch and the other for the larger specimens. Properties of the testing machine may be important for the response of the specimen in the softening regime beyond the load maximum, especially in the final phase. Thus, the change in the size dependence of the area reduction may be an indication that the system "specimen-testing machine" is not properly scaled over the whole size range.

The elongation at fracture (Fig. 2-37) of the smooth specimens, which includes the straining in the neck region and outside the neck, is less sensible to size influences which are concentrated in the neck. Only a moderate decay with size is seen in Fig. 2-37. If the length of the necked region does not scale with the size of the specimen but is approximately constant or if the average strain in the neck decreases with size, then a decrease of the elongation with size is to be expected. For further details see the review of Malmberg et al. (2001, Ref. [1.2]).

The notched tensile strength (maximum load divided by the minimum initial cross section at the notch) is plotted in the semi-logarithmic Fig. 2-38. The notch strength of the 7075-T6 aluminium remains constant for the smaller specimens, but for specimens larger than 1 inch a decrease is observed. The 4340 steel and the titanium values seemingly decrease almost linearly. For the 4340 steel the overall reduction is about 23 % (scale factor ~32).

On first sight an abrupt change of the size dependence at about 0.5 in.-diameter is not found for the latter materials, especially if the interpolation graphs are considered. However, the interpolation may be done less crude. A bi-linear interpolation is possible, for example for the titanium with an intersection of the graphs at around 0.5 in.-diameter. Thus, some influence of the change of the testing machine is likely also present in the notch tensile strength. Unfortunately, no deformation data (area reduction at the notch, notch opening) are reported by DeSisto et al.

Fig. 2-39 gives a semi-logarithmic presentation of the ratio of the notch tensile strength to the *average* 0.2 %-yield strength of the respective material. Obviously, the individual data show the same trend as the notch strength, but the interpolations are inconsistent with the previous interpolation graphs in Fig. 2-38. In any case, it is noted that for the 4340 steel the ratio is above 1.3 in the whole size range. This implies that considerable plastic deformation took place in the notch region such that Linear Elastic Fracture Mechanics is not applicable. For the two other materials the notch tensile-yield strength ratio is below 1 only for the largest specimens (diameter larger than about 2 in.) which then should follow the inverse square root law.

All data in Figs. 2-37 to 2-39 are the results of single tests for each size. The measurements for aluminium and steel are somewhat erratic. Thus, the interpolations in the figures are slightly arbitrary. Obviously, nominally identical repeat tests would have improved the situation.

DeSisto et al. used the notch tensile strength data to calculate the critical mode I stress intensity factor K_{Ic} (fracture toughness) using Linear Elastic Fracture Mechanics. The results are plotted in Fig. 2.40. If LEFM were applicable, the fracture toughness should be constant and not size dependent. It is seen that this is valid only for titanium and aluminium specimens with diameters of about 1.6 inches and larger. An exception is again the largest aluminium specimen. Inspection of Fig. 2-39 shows that notch-yield strength ratios 1.09 and 1.15 are obtained for the aluminium and titanium at the 1.60 inch-section size and these values are only slightly above the ratio 1.

Finally, the bi-logarithmic strength-size presentation of Wundt (1955, [2.22]) is used in Fig. 2-41 which demonstrates that the 4340 steel does not conform to the inverse square root law and conformity is obtained only for the largest titanium and aluminium specimens.

Wellinger and Pröger (1968, [2.26]) in their publication on size effects in notched bar tensile tests of steel specimens commented and discussed the concept of size effect and similarity to some extent. Among others, they state the following: geometrical similitude is tantamount to elasto-mechanical similitude under the same or similarly applied external specific loading; in the plastic regime the linear relation between strain and stress is lost; flow and hardening is taking over; therefore, the initial geometrical similitude and the similitude of the stresses is not present any more; consequently, a size dependence of the strength and deformation characteristics at fracture is to be expected.

This interpretation and reasoning is not correct. Classical elasticity as well as plasticity do not involve an internal length scale. Thus, both theories are not capable to describe any size effect. Beyond that, elasticity and plasticity as such are not sufficient to model fracture but must be supplemented by additional criteria which may imply a size dependence.

The essential part of the study are tensile tests of a family of geometrically scaled 60°V-notched specimens, the unnotched diameter D ranging from 180 mm down to 3 mm (scale factor 60!), with a minimum diameter at the notch of $d = 0.6\ D$, and with a nominal root radius of $\rho = 0.02\ D$ (3.6 to 0.06 mm), see Tab. 2-24.

The largest specimen was machined from a forged bar of the steel C60[24], normalized at 840 °C for 1 ½ h and cooled in air. The smaller specimens were produced successively out of the broken halves of the larger specimens. All tests were done under quasi-static conditions, but not with a properly scaled cross-head velocity to obtain a constant strain rate.

Wellinger and Pröger investigated the initiation of yielding at the root of the notch. This was defined as the first deviation from the linear elastic graph in the diagram "nominal stress at the notch versus a notch strain measure". This strain measure was either the axial strain ε_1 at the root or the circumferential strain ε_2 which both were determined by strain gages (gage length 0.8 or 0.4 mm). Using Hooke's law, the axial and circumferential surface stresses were determined as well as the v. Mises and Tresca equivalent stresses. Because of the finite size of the strain gage, this exercise was limited to few of the larger specimens, i.e., 180, 90, and 40

[24] 0.062 % C, 0.28 % Si, 0.69 % Mn, 0.034 % P, 0.030 % Si, ferritic-perlitic micro-structures; upper and lower yield stress 37.6 and 37.0 Kp/mm^2

mm diameter. Unfortunately, with gage lengths of only 0.8 and 0.4 mm the gage length of 0.4 mm used (instead of 0.8/4.5 = 0.18 mm) for the 40 mm diameter specimen was not properly scaled. Wellinger and Pröger tried to identify whether one or the other yield condition is to be preferred, but they did not come to a definite result and, curiously, they did not comment on a possible influence of the specimen size.

In Tab. 2-25 some of the results of Wellinger and Pröger are collected and obviously only for the 90 mm specimen two test results are available. The difference of the stress values for the 180- and the 90 mm – diameter specimens are quite small and the associated v. Mises-equivalent stress agrees well with the uniaxial yield stress in tension. However, for the 40 mm-diameter specimen increased (~17 %) stress values were obtained. Because of the non-uniformity of the strain at the root of the notch, even larger stresses were to be expected if a properly scaled smaller gage length had been used instead of the 0.4 mm-strain gage. The increase of the yield stress values for the smaller 40 mm diameter-specimen may be an indication of a size effect on the yield strength under non-uniform stress and strain conditions (see Malmberg et al. 2001, Ref. [1.2]). However, only a single test result for the 40 mm diameter-specimen is available and proper data for smaller notched specimens were not provided.

Wellinger and Pröger discussed also the stress-strain response of the notched specimens beyond yield initiation over a very large size range (D = 6 to 180 mm diameter). Unfortunately, the gage lengths for the strain measurement were not scaled properly within this size range and thus the results are questionable.

The essential results of the testing of Wellinger and Pröger are shown in Fig. 2-42. Here the notch strength σ_{Bk} (maximum load divided by initial notch cross-section), the true fracture stress σ_{Rk} (load at fracture divided by notch cross section at fracture) and notch area reduction ψ_{Bk} at fracture are plotted versus the diameter D. For all three quantities a quasi-hyperbolic decrease with increasing size is noted and the size influence is largest for the notch area reduction ψ_{Bk}: the notch strength decreases by about 34 %, whereas the notch area reduction reduces by 84 % down to ψ_{Bk} = 1 % within the size range from 6 to 180 mm diameter. The scatter appears to increase with decreasing specimen size, especially for the notch area reduction which, according to the authors, was not easily measured at the notch root (details were not reported).

From Fig. 2-42 (a) it is seen that the fracture stress σ_{Rk} is larger than the notch strength for small specimens. This is due to the necking of the notch beyond the maximum load until fracture. This difference decreases with increasing size and vanishes for the largest specimen where maximum load and fracture load agree without necking.

The effect of specimen dimensions on the fracture toughness of notch-bend (SENB) specimens and compact tension (CT) specimens, made of five aluminium alloys, were tested by ***Nelson, Schilling, and Kaufmann (1972, [2.27])***. In Linear Elastic Fracture Mechanics, the mode I (opening mode) stress intensity factor K_I, associated with the growth[25] of a sharp crack under plane strain conditions, is suggested to be an invariant material property denoted by K_{IC}. The ASTM testing requirements impose rigorous restrictions as to the specimen dimensions to assure plane strain conditions at the crack tip and they require specimens which are dimensionally large relative to the size of the plastic zone at the tip of the crack. For a valid K_{IC}-toughness testing, the crack length a and thickness B of the test specimen must be equal

[25] presumably in an unstable manner

equal to or greater than $2.5\ (K_{IC}/\sigma_{ys})^2$, which is about 50 times the radius of the plastic zone under plane strain conditions at fracture. Because of these specimen size limitations, there has been considerable interest in reducing the thickness limit for valid tests. To determine whether this would be appropriate for some aluminium alloys, Nelson et al. conducted a test series to investigate the influence of the specimen size on the plane-strain stress intensity factor.

Samples of five aluminium alloys with different strength levels were used, as indicated in Tab. 2-26. It is noted that the ratios of ultimate to yield strength are only slightly larger than one (low hardening) and that the elongation and reduction in area at fracture are relatively small.

Compact tension tests were made with the 2219-T851 plate material, whereas notch-bend tests were performed for the four other alloys. The notch-bend specimen dimensions are indicated in Fig. 2-43. For three of these four materials specimens with side grooving were also tested. All specimens were precracked by fatigue. Within the set of notch-bend specimens without side grooving, two families of geometrically similar specimens can be identified. Their dimensions and test results are collected in Tab. 2-27 and the further discussion will only be concerned with these specimens.

Static loading of each specimen was carried out by procedures according the ASTM method, as proposed at that time. Crack opening displacements were measured by clip gages mounted on knife edges. The load versus notch opening curves were determined and from these the load values P_Q for calculating the plane-strain stress intensity factors were determined at the 5% secant offset[26]. Values of K_Q (candidate values of K_{IC}) were calculated according to

$$K_Q = \frac{P_Q}{B\sqrt{W}} f(a/W) \tag{2.19}$$

with f being a dimensionless function for the SENB specimens. They were checked by all criteria of the ASTM method to determine whether or not they can be considered to be valid K_{IC} values. The corresponding limiting length $2.5(K_Q/\sigma_{ys})^2$ is also listed in Tab. 2-27.

From Tab. 2-27 it is seem that the specimens with the ratio $W/B=4$, which cover a thickness of ⅛ to ¾ inch (scale factor 6), satisfy the ASTM thickness limit

$$B \geq 2.5\left(\frac{K_Q}{\sigma_{ys}}\right)^2 \tag{2.20}$$

for the largest ¾ inch thickness specimens and also for the ½ inch thickness specimens. Accordingly, the candidate fracture toughness K_Q for the (⅛ inch thick) smallest specimens show the following qualitative tendencies relative to the larger specimens:

Material	**K_Q-trend (1/8 inch thickness)**
2024-T651	slightly increased
6061-T651	significantly decreased

[26] The critical load P_Q is defined in one of several ways, depending on the type of load-displacement curve (see Anderson (1995, Ref. [2.28]). In case of Type I behaviour, the load-displacement curve is smooth and deviates slightly from linearity before ultimate failure. This nonlinearity may be caused by plasticity, subritical crack growth, or both. Then one must construct a 5% secant line, i.e., a line from the origin with a slope equal to 95% of the initial elastic loading slope, to determine P_5, the load at the intersection. For this type of curve, $P_Q = P_5$.

7075-T7351	decreased
7079-T651	increased.

For the relatively thicker specimens with *W/B=2*, which cover the size range from ¼ inch to 1 ½ inch thickness (scale factor 6), the smallest specimens (¼ inch thickness) do not satisfy the ASTM thickness condition for all alloys. For the larger ½ inch thickness specimens only the alloy 6061-T651, which has the lowest tensile and yield strength (see Tab. 2-26), does not conform with the thickness limit. The K_Q-trend for the ¼ inch thickness specimens relative to the larger specimens, which satisfy the ASTM limit, is the same, as for the specimen families with the ratio *W/B=4*. Consequently, there is no uniform trend with respect to the size dependence of the K_Q-value of small, geometrically similar SENB specimens without side grooving. This observation is in contrast with the statement of the authors: "For specimens with thicknesses which are less than this stated limit, and other dimensions proportional to the thickness, values of K_Q generally increase with increasing specimen thickness".

Moreover, as noted from Tab. 2-27, the K_Q-values for sufficiently large specimens, satisfying the ASTM limit, are fairly uniform with increasing thickness, i.e., they reach a nearly constant level and thus are size invariant.

In Figs. 2-44 (a÷d) the candidate fracture toughness values K_Q are plotted versus the specimen thickness B for SENB specimens of the four aluminium alloys. These representations include the two geometrically similar specimen families as well as non-similar (non-proportional) specimens. The ASTM limit $B = 2.5\,(K_Q/\sigma_{ys})^2$ is also shown and it is generally seen that the fracture toughness of specimens satisfying the thickness limit condition become thickness invariant. It is also seen that there is no general trend of the thickness dependence of K_Q below the ASTM-limit. Therefore, among others, Nelson et al. state "there does not appear to be any basis for reducing the thickness limitation in the ASTM method".

Neale (1978, [2.29]) presented results of an experimental investigation which compared the plane strain fracture toughness K_{IC} (presumably a material constant) with the conditional fracture toughnesses K_Q[27] obtained from compact tension specimens. CT-specimens were used with the same in-plane dimensions but different thicknesses, but also geometrically similar compact tension specimens with all gross dimensions in the same ratio to each other. The present review is restricted to these latter specimens.

The 1CrMoV-steel[28] used was carefully produced including a heat treatment to ensure a homogeneous microstructure. The relevant dimensions of each geometrically similar compact tension specimen is given in Tab. 2-28 (geometric scale factor 4). Spark erosion was used to produce the slots which were extended by fatigue to give a ratio *a/W=0.5* of the nominal crack length a and specimen width W. A clip gage was mounted between knife edges rigidly bolted onto the face of the specimen across the mouth of the slot to measure the edge opening displacement. The specimens were fractured under displacement control at room temperature and a continuously recorded plot of the output of the load-sensing transducer versus the out-

[27] Here the conditional fracture toughness K_Q is the value of the stress intensity factor calculated for a precracked specimen using the initial crack length and the load corresponding to an effective crack extension of 2 %. K_Q it not necessarily a material constant.

[28] Chemical composition: 0.27 % C, 0.50 % Mn, 0.34 % Si, 0.20 % Ni, 0.95 % Cr, 0.61 % Mo, 0.29 % V, 0.01 % S; yield stress 477 MN/m^2, ultimate stress 632 MN/m^2, Young's modulus 214 GN/m^2, fracture elongation 22 %, reduction of area 61 %, hardness 207-216 VPN

put of the clip gage was produced for each of the specimens. From the load-displacement records the following characteristic data were deduced:

- P_Q, the 5 % offset load[29] at the initial elastic part of the load-displacement record
- P_{max}, the maximum failure load
- Δ_{max}, slot mouth (edge) opening displacement at maximum load (fracture).

The data are listed in Tab. 2-28 together with their corresponding nominal stresses

$$\sigma_Q: = P_Q / [B(W-a)] \quad , \quad \sigma_{max} = P_{max}/[B(W-a)] \tag{2.21}$$

and the normalized displacement

$$\delta = \Delta_{max} / a. \tag{2.22}$$

The size influence on the characteristic data σ_Q, σ_{max} and δ is evident: the nominal stresses and the normalized displacement increase by more than a factor of two when the size is reduced by a factor of four if the whole size range is considered. This is fairly close to the square root-relation between size and stress.

Neale evaluated the conditional fracture toughness K_Q according ASTM Standard E399-74 from

$$K_Q = \frac{P_Q}{BW}\sqrt{a}\ f(a/W) \qquad if\ P_{\max} / P_Q < 1.1 \tag{2.23}$$

where $f(a/W)$ is the dimensionless stress intensity coefficient given by a polynomial approximation of a/W. If $P_{max}/P_Q > 1.1$, the above equation was still used but the conditional fracture toughness was designated K_B instead of K_Q. In addition, a fracture toughness K_{max} was determined by replacing P_Q with P_{max} in the equation. Obviously, if K_Q were a material constant, the above relation implies the inverse square root dependence of the stress

$$\frac{P_Q}{BW} = \sigma_Q \cdot \left(\frac{W-a}{a}\right) \quad , \quad \frac{W-a}{W} \approx const. \tag{2.24}$$

on the size of the specimen. The corresponding fracture toughnesses calculated by Neale are collected in Tab. 2-29. Clearly, neither K_Q nor K_{max} are strictly constant. According to Neale, only the specimen A2 completely satisfied all aspects of the ASTM Standard E399-74 producing a valid plane strain fracture toughness value of K_{IC} = 59.8 MN/m$^{3/2}$. Unfortunately, only a single test for this largest size is available, so the scatter is not known. Reducing the size by a factor of two (specimens F1 to F4), increases the conditional fracture toughness K_Q by about 14 %. This qualitative trend is very well known. However, a further decrease of the size by a factor of two (specimens G2 and G3) yields a mean toughness value which is almost the same as the "valid" K_{IC}-value for the large specimen A2. All the fracture surfaces, according to Neale, indicated a brittle failure mode and none of the geometrically similar specimens produced pop-in or pop-in steps which is an important aspect of the non-similar specimens with thickness variation only. For discussion of this aspact as well as the fracture toughnesses of the other specimens, see Ref. [2.29].

The effect of specimen thickness of geometrically similar notched three-point bend specimen (SENB type) on the critical values of the crack opening displacement *COD* and the

[29] According to Neale, the 5 % offset load approximates a 2 % crack extension if 0.45 < a/w < 0.55

J-integral at fracture was studied by ***Pisarski (1981, Ref. [2.30]).*** A microalloyed carbon manganese steel plate[30] with a sulphur contend below 0.005 Wt.% was selected. The plate was 100 mm thick and was supplied in a normalized condition.

The three-point bend specimens with the full plate thickness (100 mm) were cut from the plate with their axes parallel to the rolling direction; their geometry and testing followed the British Standard BS 5447 (1977) and BS 5762 (1979), i.e., all dimensions in proportion to the depth W:

thickness $B = 0.5\ W$
loading span $S = 4\ W$
crack length a = $0.45 – 0.55\ W$ (including fatigue crack extensions).

The notches, perpendicular to the surface, were extended by fatigue and clip gages were mounted across the notch mouth. Two thicknesses (50 and 10 mm) of sub-size bend specimens were machined from the broken halves of the 100 mm thick specimens but remote from the fracture surface. The 50 mm thick specimens were made by machining equal amounts from each plate surface so that the center plane of the specimens coincided with the mid-plane of the plate. The 10 mm specimen were taken close to the mid-plane. Thus, effects of material inhomogeneity across the thickness of the plate were minimized. The tests were carried out over a temperature range of -150°C to -10°C. The testing of the 100 and 50 mm thick specimens was done in a 1.8 MN Universal testing machine, whereas the 10 mm specimen were fractured in a 100 KN screw-driven Universal testing machine. The fracture surfaces of all the specimens were visually examined or, where necessary, inspected with a low power microscope or Scanning Electron Microscope (SEM).

The critical clip gage opening displacement V_g, attained at fracture (subscript c) or at a maximum (subscript m) of the load, was used to calculate *COD* (i.e. δ_c or δ_m) according to the British Standard (see Ewalds and Wanhill (1983, Ref. [2.31], p. 152))

$$(\delta_c, \delta_m) = \delta_e + \delta_p = \frac{K_c^2(1-\nu^2)}{2E\sigma_y} + \frac{r(W-a)V_p}{r(W-a)+a+z} \tag{2.25}$$

with $r = 0.4$, V_p being the plastic part of V_g in the load P versus V_g curve and z denotes the knife edge height at the notch mouth. The values of K_c were calculated from the fracture or the maximum loads using the stress intensity factor for SENB specimens (e.g., Ewalds and Wanhill (1984, Ref. [2.31], p. 97))

$$K_c = \frac{PS}{BW\sqrt{W}} f\left(\frac{a}{W}\right). \tag{2.26}$$

These *COD* results for the three specimen sizes are shown in Fig. 2-45 as temperature transition curves.

The critical J-integral values J_c were also calculated from the critical clip gage values using a relationship due to Sumpter and Turner (1976, Ref. [2.32])

$$J_c = \frac{K_c^2\left(1-\nu^2\right)}{E} + \frac{2P_L}{B(W-a)} \frac{WV_p}{\left(r_p\left(W-a\right)+a+z\right)} \tag{2.27}$$

with $r_p = 0.4$ for $a/W > 0.45$ and $r_p = 0.45$ for $a/W < 0.45$ and the limit load P_L approximated by an energetic mean value in the nonlinear regime of the load-clip displacement curve. If

[30] British Standard B5 4360 50D

stable crack extension preceded fracture, the above equation overestimated J. Therefore a modified equation according to Sumpter and Turner (1976, Ref. [2.32]) was used which allowed for a change in the specimen compliance due to crack extension. The results of these calculations are presented in Fig. 2-46.

The J_c-data from Fig. 2-46 were transformed to fracture toughness values K_{IJ} using the relation

$$K_{IJ} = \left(\frac{J_c E}{1-\nu^2} \right)^{1/2} . \tag{2.28}$$

These data are shown in Fig. 2-47 and they represent K_{IJ}-temperature transition curves. Specimen size requirements for valid critical J-values have been proposed such as

$$B, (W-a), a \geq \gamma J_c/\overline{\sigma} \tag{2.29}$$

where $\overline{\sigma} = (\sigma_y + \sigma_u)/2$ is the mean flow stress and γ=25 to 50. The most widely used γ-value is 25. For a given thickness B and with γ=25 one can determine the maximum J_c-value or in conjunction with Equ. 2.28 the maximum K_{IJ}-value as a function of temperature if the temperature dependence of $\overline{\sigma}$ is determined. This limiting curve for the 10 mm thick specimens is shown in Fig. 2-47. Thus, all data of 10 mm specimens below this curve satisfy the size requirement Equ. 2.29 but obviously also data of thicker specimens below this curve.

On the other hand, valid K_{IC}-values for plane strain and small scale yielding require specimen dimensions which satisfy the ASME restriction

$$B, (W-a), a \geq 2.5\,(K_{IC}/\sigma_y)^2. \tag{2.30}$$

As Fig. 2-47 shows, valid plane strain values of K_{IC} were found in five of the 100 mm thick specimens tested. In spite of the scatter, Figs. 2-45 to 2-47 show that the δ_c-and J_c- or K_{IJ}-values of the 50 and 100 mm thick specimens are comparable whereas the small 10 mm specimens generally yield larger values at all investigated temperatures. This implies that the transition curves are shifted to higher temperatures if the size is increased. This shift may be as much as 50 °C.

The shift of the temperature transition curve due to changes in specimen size has been recognized before. This, of course, implies that the actual toughness of a large specimen is overestimated considerably by the data of a small specimen. Therefore, the results support previously made recommendations that "where δ_c was used for assessing allowable defect sizes in engineering structures, data should be obtained from test pieces representing the thickness of the structure of interest". Of course, there arise real difficulties in practice.

In Figs. 2-45 to 2-47 specimens are identified in which crack initiation took place by microvoid coalescence (encircled marker). In some cases clear evidence of microvoid coalescence ahead of the whole stretch zone was not present. From Fig. 2-47 it is seen (reviewer's comment) that most of the 10 mm specimens show an initial crack extension by micro void coalescence when their K_{IJ}-values are close to the limit curve of the 10 mm thick specimens. The other data of the 10 mm specimen are well below the limit curve and no definite microvoid coalescence was found. This fracture mode separation induces a considerable scatter of the small specimen data (see results at -100 °C). Unfortunately, the number of nominally identical tests for the larger specimens is much less and such a mode separation is not found.

Pisarski discussed the influence of specimen size on K_{IJ} to some extent. He stated that it is not necessary to invoke scatter in material properties to explain this effect, as done by other workers. He points out that "the present results, …, can be explained on the basis of the proposals of Milne and Chell (1979, Ref. [2.33])" which used the model of Ritchie et al. (1973,

Ref. [2.34]). In the reviewer's opinion, the verbal explanations of Pisarski but also of Milne and Chell are not intelligibly presented, partly because there is no clear distinction between the pure thickness effect and the effect of the size variation of truly geometrically similar specimens. Therefore a discussion of this aspect is not taken up here.

In the course of a catastrophic failure of a steam turbine (spontaneous brittle fracture of a low pressure turbine disc by stress corrosion cracking), the Central Electricity Generating Board (CEGB) facilitated a study by ***Shaw and Spink (1983, [2.35])*** on the post yield behavior of a series of geometrically similar specimens of varying size. Two different geometries were investigated over a temperature range (-100 °C to +100 °C) which covered all modes of failure from fully brittle to fully ductile.

The material used, a 3 % NiCrMoV-steel, came from the first and second stage low pressure turbine discs. The chemical composition and some typical mechanical properties are listed in Tab. 2-30. The two specimen types were compact tension (CT) and single-edged-notched-bend (SENB) specimens subjected to three-point-bending with a span-to-width ratio of 4:1. For both geometries three sizes were considered. Details are listed in Tab. 2-30. The notch depth-to-width ratio a/W was in the range 0.435 to 0.515, but the scale factor was relatively small: $\lambda = 4$ for the CT-specimens and $\lambda = 3.6$ for the SENB-specimens. Specimens were prefatigued and the tests were performed under load control with a constant loading rate. In the compact tension tests the load versus the crack mouth opening displacement was recorded.

In the SENB-tests both crack mouth opening and ram displacements were determined. In addition, the displacement due to the machine and uncracked body compliances were measured experimentally for each of the three SENB-specimen sizes. This allowed the load-point displacement due to cracking to be determined.

From Tab. 2-30 it is seen that the materials (two discs) used for the CT-specimens have almost the same tensile properties. However, the material for the large (B = 45 mm) SENB-specimens has rather low yield and ultimate stresses compared to the smaller SENB-specimens. Unfortunately, no cutting plan is included and a truly systematic testing of the homogeneity of the disc material is missing. This pronounced inhomogeneity will affect the interpretation of the size effect tests.

In addition to the conventional specimens, a number of three-point-bend specimens were machined from "half-discs", as removed from low pressure rotors. Since the size variation was very small, the results will not be mentioned here.

Several parameters were calculated on the basis of the load-displacement records. Among others, they are:

- The plane-strain fracture toughness K_{IC}[31],

$$K_{IC} = K_Q = \frac{P_Q}{B\sqrt{W}} f\left(a/W\right) , \tag{2.31}$$

was calculated for those tests which satisfied the stringent criteria of ASTM E 399 (see e.g., Ref. [2.28, p. 375]). For those tests which did not satisfy the thickness criterion but nevertheless displayed a linear load-displacement record and failed by cleavage instability

[31] P_Q: see ASTM E 399 standard, B: thickness of specimen, W: width of specimen, a: crack length

without shear lip formation, the stress intensity factor at failure was calculated from the maximum load ($P_Q = P_{max}$) and was also designated as K_{IC}.

- For all tests which failed by cleavage instability without prior stable ductile growth (but with plasticity resulting in a nonlinear load-displacement record; the reviewer), the J-contour integral was calculated. For the SENB specimens J was determined from

$$J = 2U / B(W-a) \tag{2.32}$$

where U is the area under the load-load point displacement record owing to cracking and $(W-a)$ is the remaining uncracked ligament. For the compact tension test allowance was made for bending and tensile components and the measured crack mouth opening displacement Δ_c was converted to a load-point displacement Δ_p using the ratio $\Delta_p/\Delta_c = 0.77$ (for details see Ref. [2.35]).

The calculated J-values were transformed to K_{IC}^J - values according to

$$K_{IC}^J = \sqrt{JE/\left(1-\nu^2\right)}. \tag{2.33}$$

- Moreover, the failure loads and stresses were determined and represented in dimensionless form. For the CT-specimens loads P_u were calculated for each specimen, including the crack, at which failure would occur by plastic collapse (use of slip line field theory):

$$P_u = m\ \sigma_u BW \tag{2.34}$$

where m is a function of a/W and $\sigma_u BW$ is the theoretical failure load of an uncracked specimen (σ_u: ultimate tensile strength) and m the ratio of failure load in a cracked specimen to the failure load in the same uncracked specimen. The actual measured failure load P_f was normalized with the plane stress plastic collapse load P_u.

In the SENB-specimens $m = 1.22\ (1-a/W)^2$ is the ratio of the moments to cause failure in cracked and uncracked bars. With $M_p = \sigma_u\ BW^2/4$ being the moment to cause plastic collapse in an uncracked beam specimen, then for a cracked beam the collapse moment is $M_{pc} = m\ M_p$. This was converted to the equivalent elastic outer fiber stress

$$\sigma_{pc} = M_{pc}/(BW^2/6) = 1.83\ \sigma_m\ (1-a/W)^2\ . \tag{2.35}$$

The fictitious elastic failure stress σ_f (at the root of the notch[32]) was then normalized to yield the dimensionless failure stress σ_f/σ_{pc}. It should be noted that the ultimate stress measured at room temperature was used throughout in the calculation. Although not made explicit in Ref. [2.35], the actual values of the various material sources were used (see Tab. 2-30) to account for the material inhomogeneity.

The test results are listed in Tab. 2-30 (II and III). For the compact tension tests a trend of generally increasing K_{IC}^J with temperature is apparent (Tab. 2-30 (II)), but there is considerable scatter between duplicate test results (except the largest specimens ($B=50$ mm). At temperatures where size dependence can be evaluated, i.e., -20 °C, 0 °C and +20 °C (all below the fracture appearance transition temperature FATT), one finds: at -20 °C and 0 °C an increase (37 % and 51 %) of the mean K_{IC}^J-value with decreasing size, at +20 °C almost size independent mean values. The fracture toughness values K_{IC}^J of the SENB-specimens (Tab. 2-30 (III)) show also a marked scatter between duplicate tests, except the largest specimens ($B=45$ mm). For this type of specimen only the data at -40 °C and -20 °C can be compared to check the size independence. At -40 °C a non-monotone decrease (≤ 26 %) of the mean value with increasing size is seen, but at -20 °C the decrease of the mean K_{IC}^J-value is 31 % when

[32] A precise definition of σ_f is not given in Ref. [2.35] but the common approach is to set $\sigma_f = M_f/W_s$ where M_f is the bending moment at failure and W_s is the section modulus of ligament section.

the thickness is reduced from 45 mm to 25 mm. These trends, however, are affected by the significant differences in tensile properties of the large and the small SENB-specimens. Summarizing, a convincing size independence of mean K_{IC}^{J}-values of these two specimen types at theses temperatures is clearly not present. This rating is in contrast with statements of Shaw and Spink.

The most definite size influence is observed for the normalized failure loads or stresses. In Fig. 2-48 the normalized load P_f/P_u of the compact tension specimens is plotted versus the temperature with the thickness B = 12.5, 25, 50 mm as parameter. A much clearer picture becomes apparent in which, for a given specimen size, the ratio P_f/P_u increases with temperature up to the transition temperature, above which the ratio becomes close to unity and decreases slightly with temperature and the scatter is much reduced. As pointed out by Shaw and Spink, the transition temperature coincides with the onset of stable ductile tearing prior to the specimen failure.

The size effect is clearly depicted in Fig. 2-48:

- Generally the normalized failure load P_f/P_u decreases with increasing size and this effect is largest below the transition temperature where the failure is characterized by cleavage instability without prior stable ductile crack growth. With increasing temperature up to the transition temperature, the size effect decreases. However, above the transition temperature the size influence on the P_f/P_u-ratio is not vanishing but almost constant.
- There is a considerable shift of the transition temperature to higher temperatures when the size is increased: for the 12.5 mm-thickness specimens the transition temperature is around 0 °C, but for the 4-times larger specimens it is 60 °C.
- Since the variation in the ultimate stresses of the material used for the compact tension specimens is small (Tab. 2-30), the size dependence of the normalized failure load is likely not caused by variations in the tensile properties.

In Fig. 2-49 a similar plot is provided (σ_f/σ_{pc}-ratio versus temperature) for the SENB-specimens. The same qualitative trends are observed, however, the difference between the 25 mm and 45 mm-thickness specimens is non-existent below the transition temperature and it is small above the transition temperature. It is, however, not clear to what extent this latter result is affected by the material inhomogeneity of the SENB-specimens; this is only partly compensated by the use of the actual σ_u-values at room temperature for the calculation of σ_{pc}.

The comparison of the CT-and the SENB-specimens (Fig. 2-48 and 2-49) shows that the transition temperature is not only depending on the specimen size but also on the shape of the specimens; e.g., for the 12.5 mm thickness CT-specimens it is about 0 °C whereas for the 12.5 mm thickness SENB-specimens it is –40 °C.

As pointed out by Shaw and Spink, the dependence of the transition temperature on size and geometry implies that the fracture behaviour of a full-sized service component could not be predicted from small scale test specimens in the transition region. Also a complicating feature of tests below the transition temperature is the extreme scatter of duplicate test results which obscured specimen size effects. The statement of the authors that “the largest specimens tended to give results toward the bottom of the scatter band” is, however, not understandable for the K_{IC}^{J}-data but only evident for P_f/P_u or σ_f/σ_{pc}-results.

The reviewer regrets that important deformation data, such as the normalized load-point displacement or the notch opening, were not presented in Ref. [2.35]. These data are at least as important for size effect considerations as characteristic loads or stresses.

The research on ship collision strength urged ***Hagiwara, Takanake, and Kawano (1983, [2.36])*** to perform bending tests on two families of almost geometrically similar specimens. The specimens were I-beams with a geometry as indicated in Fig. 2-50. The principal parts of the specimens were proportional to the thickness t_3 of the bottom flange of the I-beam (scale factor 8.7). The dimensions ℓ_2, ℓ_3, and t_4 were not exactly proportional for the convenience of testing, but the influence appeared to be small. According to the authors, the purpose of this test series was mainly to investigate the plate fracture due to strain concentration such as the scallop. Since the actual steel work may contain defects, two families of beam specimens were considered: unnotched I-beams and I-beams with notches which were applied to the top surface of the bottom flange, as shown in Figs. 2-50 and 2-51. The depth of the notches in the specimen M60N and M23N were somewhat larger than according to the scale factor. Unfortunately, the plate materials were not the same for all three sizes but differ as shown in Tab. 2-31. Thus, the 2.3 mm thickness plate material had the lowest yield and ultimate stress but the largest elongation.

The three-point bending tests were done under quasi-static conditions with continuous measurement of the load P and the deflection δ (probably the load-point displacement), but details were not reported.

Load-deflection curves of the notched and unnotched specimens are shown in Fig. 2-52 using a normalized load on the ordinate and normalized deflection on the abscissa. The normalizing was done using the largest specimen M 200 as reference such that the difference in the sizes and in the flow stress of the smaller specimens were accounted for. Thus, with $\lambda = t_3/(20\ mm)$ and $\overline{\sigma}_y$, the ratio of the average flow stress between 0 and 5 % strain of the t_3-thickness plate material to the 20 mm thickness material, the loads P are multiplied with the factor $\left(\lambda^2\overline{\sigma}_y\right)^{-1}$ and the deflection δ with λ^{-1}. From Fig. 2-52 the following conclusions are obtained:[33]

- If similarity would apply for the unnotched and the notched family, each family would be represented by a single curve. Obviously, this is generally not the case, it is valid only to a limited extent, i.e., only for normalized displacements less than about 30 mm (instantaneous fracture of the largest notched specimen M200N). There all curves, irrespective of being notched or unnotched, collapse into a single one.
- Furthermore, within each family the normalized load-deflection curves are approximately congruent up to the maximum load of their largest specimen (type M 200), but the normalized deflection corresponding to a load maximum is shifted to larger values when the size is decreased. For the unnotched specimens this shift is relatively small when the plate size is decreased from 20 mm (specimen M200S) to 6 mm plate thickness (specimen M60S), but for the 2.3 mm plate thickness (M23S) the normalized deflection at maximum load is about 2 times larger! For the family of notched specimens a very pronounced succession of the normalized deflection at the maximum load as well as of the final deflection is observed.
- Comparison of the load-deflection curves of the two families show almost no difference for the M23-specimens (plate thickness 2,3 mm), whereas the M60-curves show a slight difference. However, the large M200-specimen (20 mm thickness) yield a considerable difference: the notched specimen M200N has a smaller load maximum, but more important,

[33] These statements differ somewhat from those of Hagiwara et al.

the normalized deflection associated with the load maximum is only 1/3 of that of the unnotched specimen M200S!

- The normalized load-deflection curves in the softening regime beyond the load maximum show a gradual decrease of the normalized load for the smallest I-beams, both for the unnotched and the notched specimens. When the size is increased, the fall-off of the load becomes steeper and especially for the largest notched I-beam the fall-off is instantaneous at the maximum load which is evidence of a typical brittle fracture, quite different from the other specimens. Thus, the tendency for the notched bottom flange to fail at successively smaller normalized deflections when the size is decreased is evident. This successive decrease of the normalized deflection at the load maximum with increasing size is also seen for the unnotched specimen but to a lesser degree. This is related to the fact that the stress concentration at the center of the I-beam is reduced.
- Hagiwara et al. performed numerical calculations (details are essentially missing), using the actual stress-strain curves of the different plate materials, to determine the nominal strains in the unnotched I-beams, thus enabling the maximum nominal strain to be determined from the deflection under the maximum load. The results are given in Tab. 2-32. A comparison of these data with the uniform elongation and the elongation at fracture (Tab. 2-31) of the different plate materials shows that the size dependence of the normalized deflection at the maximum load cannot be explained by the differences in the ductility of the plate materials.
- Unfortunately, only a single test for each type of I-beam was done and no direct evidence whether it is representative is available. Nevertheless, the general qualitative trends observed in these test series are in agreement with previous findings in the testing of geometrically similar families of notched specimens.

The thickness influence on the behavior of compact tension test specimens of austenitic steel SUS 316 has revealed that the fracture under displacement control continuously propagates after the maximum load has been reached. Also the critical *J*-integral (J_c-value) at maximum load monotonically increased with the thickness of the specimen. These observations as well as safety considerations of nuclear reactors motivated ***Takeuchi, Yasunaka, and Nishijima (1985, [2.37], 1986 [2.38])*** to perform a series of systematic tests on CT-specimens where the in-plane dimensions were proportionally increased for a given thickness (in-plane similarity) and several thicknesses were considered. In the tests series a limited number of specimens can be identified which are almost fully geometrically similar.

The base material embraces several plates (1 x 0.5 m with thicknesses of 4.5, 6, and 10 mm) of the solution annealed SUS 316 L. The in-plane geometry of the CT-specimens is shown in Fig. 2-53 and nominal widths W = 200, 150, 100, 70, 50 and 30 mm were used. For each size specimens parallel and vertical to the rolling direction were produced. The width of the slot was not scaled (2 or 3 mm) and a constant radius of curvature (0.1 mm) at the tip of the 60 ° V-notch was applied. The surfaces of the specimens remained unprocessed. The quasistatic tests[34] were done at room temperature.

In addition, standard tensile test were done with specimens from all plates. They revealed approximately the same ultimate stresses and fracture elongations for all three plate thick-

[34] Load-point displacement rate: 5 mm/min for W≤ 100 mm, 10 mm/min for W≥150 mm

nesses, but the nominal fracture stress decreased with increasing plate thickness and a directional influence became apparent.

Fig. 2-54 demonstrates the influence of the in-plane size W on the nominal stress (load / $(B \cdot W)$) versus normalized pin displacement (X/W) diagrams of almost geometrically similar specimens with constant thickness B = 10 mm. From these diagrams several characteristic values were deduced:

- the maximum load F_M and the corresponding displacement X_M; the authors stated that the crack extensions started at the load maximum but no independent proof was given;
- the displacement X_H at the load level $F_H = F_M/2$ in the descending part of the load-displacement curve and these results are plotted in a normalized form in Figs. 2-55 and 2-56;
- the maximum nominal stress $(F_M/(B \cdot W)$ versus the ratio B/W for specimens with the two different orientations (L-T) and (T-L) (Fig. 2-55);
- the normalized displacements X_M/W and X_H/W for the two different orientations (Fig. 2-56).

Except for the width of the slot and the notch tip radius, full geometric similarity is obtained only for families of specimens with the same B/W-ratio. Inspection of the dimension shows that only two families satisfy gross similarity conditions:

– *family I:* $B = 6$ and 4.5 mm; $W = 200$ and 150 mm; $\frac{B}{W} = 0.03$; $\lambda = 1{,}3\overline{3}$

– *family II:* $B = 10$ and 6 mm; $W = 50$ and 30 mm; $\frac{B}{W} = 0{,}2$; $\lambda = 1{,}6\overline{6}$

Each family consists only of two specimens with geometric scale factors clearly less than two which is a rather small value. In Fig. 2-55 and 2-56 geometrically similar specimens correspond to all data with the same B/W-ratio. From Fig. 2-55 one can identify family I for the L-T orientation which yields almost the same maximum nominal stress. Moreover, the data for both orientations are within a single narrow scatter band and this implies that a size or orientation influence is not present for the maximum nominal stress. However, the geometric scale factor, as given above, is rather small and any significant effects are not to be expected.

The normalized displacements X_M/W and X_H/W are plotted in Fig. 2-56 and interpolation graphs for constant thickness specimens are also indicated. For the (L-T)-orientation narrow bands are obtained and the interpolation graphs are not arranged according to the thickness B. This implies that a significant or systematic size effect is not present for both normalized displacements of specimens with a (L-T)-orientation.

For specimens with the (T-L)-orientation (Fig. 2-56), however, a considerable spread of the interpolation curves for constant thickness specimens are obtained, but a systematic order, according to an ascending or descending thickness, is not obtained. It is noted, however, that the smallest (B=4.5 mm) specimens give the smallest normalized displacements X_m/W and X_H/W for all B/W-ratios. This is opposite to the usual size effect trend. Takeuchi et al. argue

that the processing and heat treatment differed according to the thickness (4.5, 6, 10 mm) of the plates which affected especially the crack initiation and propagation along the rolling direction.

It has been noted before that some authors did not distinguish clearly between size- and thickness effect. An example is the paper by ***Wallin (1985, Ref. [2.39])*** entitled "The size effect in K_{IC} results". Wallin summarized his paper as follows: "The size effect connected with fracture toughness results has been examined for both ductile fracture initiation and brittle cleavage fracture. The effect has been explained partly by the loss of constraint effect and partly by the statistical weakest link size effect. In the case of ductile fracture, it has been shown that the fracture initiation toughness is independent of thickness as long as the size criterion $B > \alpha\,(J_{IC}/\sigma_y)$ is fulfilled. In the case of cleavage fracture, it has been shown that the thickness effect is mainly caused by the weakest link size effect. A simple theoretical expression describing the thickness effect has been derived, and its validity has been verified for a large number of different materials. It has further been shown that the theoretical connection can also be successfully applied to describe the sharp crack ductile/brittle transition temperature shift by the thickness effect".

The experimental results Wallin presented and some of the theoretical explanations (especially for ductile fracture initiation) refer only to specimens of various thicknesses but constant in-plane dimensions. Thus, geometrical similarity was not part of Wallin's consideration. However, the loss of constraint effect is an obvious argument if only the thickness is varied, but for a size variation (by definition with geometrically similar specimens) a more elaborated argumentation is necessary.

The effect of specimen size and geometry on the ductile crack growth resistance of a C-Mn steel has been investigated by ***Gibson, Druce, and Turner (1987, [2.40]).*** The resistance, expressed in the form of J-R curves, was determined using the conventionally calculated J- or a modified J-integral in a range of specimen geometries. Thus, J-R curves of different specimen types were compared and J-integral values were correlated with different experimental characteristics of crack initiation to yield critical values. The latter were investigated with respect to their independence on specimen thickness, size, and shape to check whether they represent truly invariant material parameters. Specimen geometries such as

- compact tension (CT) specimens
- single-edge-notch bend (SENB) specimens under three-point bending
- single-edge-notch bend specimens under four-point bending
- centre-cracked tension (CCT) specimens
- double-edge-notched tension (DENT) specimens

were used. All specimens had fixed dimensions except the CT-specimens where the thickness B and the width W were varied but with an approximately constant crack length-to-width ratio a/W (see Tab. 2-33). This CT-test series contains two families of geometrically similar specimens, one without and another one with side grooves (60 ° V-notch, depth 25 % of thickness B).

The material used was a normalized C-Mn steel, British Standard 4360 43 A, in the form of a rolled plate[35]. The specimens were oriented such that the crack planes were normal to the rolling direction and the crack directions were parallel to the width direction of the plate. Six to eight specimens of each type were manufactured, as a multi-specimen approach was used to determine the J-R curve. All specimens were fatigue pre-cracked under load control at room temperature to give a final crack length-to-width ratio of between 0.5 and 0.6.

Most tests were performed at controlled temperature of 30 °C and under displacement control at a constant ram speed of 1 mm/min. During the tests load versus load-line displacement was recorded for the compact tension specimens; for the other specimens load versus ram displacement was determined. In some cases the crack tip opening displacement (CTOD) δ_a at a predefined load was also measured, forcing a silicon-rubber fluid into the crack tip region to obtain a cast of the crack tip region after a fast setting time. Moreover, the 9-point average crack extension across the specimen thickness was measured from the fracture surface. Also the plastic stretch zone[36] width *(SZW),* defined as the crack advance due to crack blunting prior to crack initiation, was measured from the fracture surface of each specimen using a Scanning Electron Microscop (SEM) with the incident electron beam normal to the fatigue crack plane. The average value was determined from readings taken at various positions across the central 2/3 of the crack front.

For the compact tension specimens a J_o-value was calculated,

$$J_o = \eta\, U/Bb_o, \qquad b_o = W\text{-}a_o, \tag{2.36}$$

where U is the area under load-load point displacement record and using η values given in the ASTM J_{1c} testing standard E 813. A crack growth correction was applied to yield the corrected J-value

$$J_r = J_o\left(1 - \frac{0.75(\eta - 1)\Delta a}{b_o}\right). \tag{2.37}$$

Corresponding formulas were used for the other specimen types. Furthermore, a J-value, modified according to Ernst (1983, [2.43]), was determined and denoted by J_m; for details see Ref. [2.40].

J_{1c}-values, approximately characterizing the onset of crack initiation, were determined from J_r-Δa or J_m-Δa data points (note: multiple specimen testing!) using the ASTM J_{1c} testing standard E 813 which assumes a $(J=2\sigma_y\Delta a)$[37]-blunting line (see also Anderson (1995, [2.28])). Moreover, $dJ/d\alpha$ was determined and taken as the linear slope through the J_r-Δa or J_m-Δa data points lying within or just outside the exclusion lines given in the ASTM J_{1c} testing standard E813; thus, $dJ/d\alpha$ corresponds to the average slope of the J-Δa curve between the crack extension (Δa)-values of 0.15 and 2 mm.

---

[35] Chemical composition Wt %: 0.22 C, 1.05 Mn, 0.04 Si, 0.08 S, 0.03 P, 0.15 Ni, <0.01 Al, 0.34 Cu, 0.03 Mo, <0.01 Ti, <0.01 V;

lower yield stress = 283 MPa, ultimate tensile stress = 494 MPa

[36] This region presumably forms prior to the incidence of extensive incipient cracking; it represents a new surface rather than an increment of crack extension (see Brothers et al. (1970, [2.41]) and, according to Broek (1980, [2.42]), it is generated by plastic slip which produces a blunted crack tip.

[37] σ_y = mean value of yield and ultimate stress

The *J*-value at the onset of crack initiation may also be determined from the stretch zone width *(SZW)* at crack initiation *(SZW_c)* and the empirical relation between *J* and *SZW* up to crack initiation described by Gibson and Druce (1985, [2.44]):

$$J = (2.21 \pm 0.05)\ \sigma_f\ SZW. \qquad (2.38)$$

According to Gibson et al., this relationship was found to be valid for both non-side grooved and side grooved CT-specimens and all other specimens. The SZW_c-values were measured from specimens which had undergone some amount of fibrous extension. The corresponding *J*-value was calculated with the above equation and was denoted as J_i.

In the following only a selected set of results is discussed. Mean values[38] and standard deviations[39] are given in Figs. 2-57 and 2-58 which show the effect of size of geometrically similar compact tension specimens without (Fig. 2-57) and with (Fig. 2-58) side grooves with a depth of 25 % of the thickness *B*. Obviously, the J_i-values obtained from the plastic stretch zone width measurements yield the least scatter and the least variation with size. Increasing the thickness from 13 mm to 50 mm (scale factor 3.85) for the non-side grooved specimens, reduces the critical value J_i from 74 KN/m down to 56 KN/m (~24 %). The critical value J_{1c} from ASTM E813 is subject to a considerable scatter and has a much less uniform size dependence. These data satisfy the size requirement $B, (W-a) \geq 25\ J_Q/\sigma_y$ of ASTM E813. Most important, the J_{1c}-values are considerably larger than the J_i-values over the whole size range; e.g., for the smallest specimens the relative difference is about 60 %.

The initial slope $dJ/d\alpha$ of the J-Δa curve is also subjected to a considerable scatter (Fig. 2-57). The mean values are almost constant up to a thickness of B = 37.5 mm but then a marked decrease with increasing size is seen.

Fig. 2-58 shows the corresponding results for the side grooved specimens. Generally the variabilities with the size of the three quantities are greatly reduced. Again the J_i-values obtained from the stretch zone measurements show the least scatter and are almost size independent. The J_{1c}-values according the ASTM testing standard E 813 are again larger than the J_i-values, in the mean by about 45 %. Furthermore, the J_i-values of side grooved specimens agree with the J_i-values of the largest (B=50 mm) non-side grooved specimens. As noted by Gibson et al., the side grooved specimens showed no lateral contraction. This suggests that the corresponding J_i-value is that for plane strain conditions.

Finally Fig. 2-59 gives an impression of the influence of the specimen shape on the critical J_i-values and the crack tip opening displacement δ_a at crack initiation for non-side grooved specimens 25 mm thick. Again the scatter for the J_i-values is rather small and clearly the specimen geometry has no influence. The δ_a-values show much more scatter, especially under four-point bending, and slight variability with specimen geometry.

From these data it appears that the J_i-values obtained from plastic stretch zone measurements is a rather size and geometry invariant quantity with small scatter for both small and large specimens. Whether these favourable properties apply to other sizes, size ranges, and other notch configurations and loadings remains to be tested. This also implies a check of the empirical relation between J_i and the critical stretch zone width SZW_c.

---

[38] The number of values (or tests) involved is not clearly indicated in Ref. [2.40]. However, according to Tab. 2-33, only two specimens of each thickness (with B/W=0.5) should be involved.

[39] According to the authors, six to eight specimens were manufactured for each type, as a multi-specimen approach was used to determine the J-resistance curve. If all these specimens were used, then it is not clear, how the standard deviation of the J_{IC}-value of this single curve was determined.

For materials with brittle behaviour the governing theory for treating the fracture of cracked or sharply notched specimens is Linear Elastic Fracture Mechanics (LEFM). Implicit in the choice of the stress intensity factor as the parameter determining fracture (fracture toughness considered as a size and shape invariant material constant) is a prediction of the size dependence of the strength (nominal fracture stress). Consider a small specimen (subscript 1) of infinite length but finite width W, weakened by a crack of length a, and under a remote uniform stress σ_1. The large specimen (subscript 2) is a scaled-up version with width λW, crack length λa and under the applied stress σ_2 ($\lambda > 1$ is the in-plane geometric scale factor). Ignoring out-of-plane effects (infinite thickness), LEFM yields at fracture for specimen 1

$$K_1 = \sigma_1^* \sqrt{\pi a} \; f(a/W) = K_{IC} \tag{2.39}$$

where K_I is the mode I stress intensity factor, $f(a/w)$ is the finite width correction factor, σ_1^* the remote nominal stress at fracture, and K_{IC} the fracture toughness, presumably a material constant. A similar relation applies for the enlarged specimen 2 of the same material which fractures under the remote fracture stress σ_2^*. Because of the geometric similarity (and the same material), the ratio of the fracture stresses is given by

$$\sigma_1^* / \sigma_2^* = \sqrt{\lambda} \qquad . \tag{2.40}$$

The "strength size effect" prediction of Equ. 2.40 is certainly in agreement with the general trend, i.e., strength increasing with decreasing size. ***Sinclair and Chambers (1987, [2.45])*** investigated the question that arises, i.e., how well Equ. 2.40 agrees with physical reality by comparing the predictions of Equ. 2.40 with a rather large amount of experimental results for steel, aluminium alloys, and others in the open literature. They placed the main emphasis on physical data featuring brittle response since these data should be in best accord with the assumptions of Linear Elastic Fracture Mechanics. They also selected those data close to perfect scaling and took strength estimates from load data directly wherever possible. In processing the data, the authors made an effort to perform data reduction procedures in a consistent manner. For this purpose they set up guidelines for including data relevant to the issue. They defined strength at fracture, placed limits on deviations from perfect scaling, including bounds on thickness effects, and they distinguished between brittle versus ductile behaviour with the intent to furnish a reasonable set of rules to filter out data not enabling a fair appraisal of the LEFM size prediction.

Some of their rules are briefly described in the following. The authors defined strength as the nominal net section stress under monotonic quasi-static loading at the onset of mode I crack growth. Here it should be noted that the size dependence in Equ. 2.40 is independent as to whether σ_i^* (i=1,2) are remote gross stresses or are based on the net section in the plane of the crack provided the two specimens are perfectly scaled. If they were not, the latter choice accounts for small deviations and was thus preferred. For truly brittle response this stress level is equal to that at total fracture; with less brittle behaviour it differs somewhat: loads at a 5 % secant offset in the load – displacement record being generally preferred, but others, such as at "pop-in", were taken when the 5 % offset stress were not available. They chose the stress at this point rather than at its maximum because the response is more linear elastic. If only maximum load levels were given, they included such data, but noted the relaxation of the definition. There was a need to define what was meant by a crack and to describe the range of

acceptable environment. With respect to the crack, their first choice were specimens with a fatigue pre-crack. However, with a view to include all pertinent data, they admitted notches whose acuity was such that the radius r at the root of the notch was one order of magnitude less than the total notch depth or crack length a, i.e.

$$r/a \leq 0.1 \,. \tag{2.41}$$

Also the flank of the notches were allowed to subtend an angle of up to 60° because the singularity orders associated with sharp re-entrant corners with opening angles less than 60° differ by less than about 3 % from that for a crack.

Concerning environments, they did not include data for environments more corrosive than air. On the other hand, some variations in temperature were tolerated since low-temperature response is quite brittle and thus in good agreement with LEFM assumptions. At temperatures other than room temperature, they allowed differences in temperature between the scaled specimens of up to *5 K*, however, with the condition that the specimen having the higher stress-intensity factor at failure were not at the higher temperature. This is required in order to avoid mixing the temperature transition behaviour with the size influence.

Aside from the requirement of overall geometric similarity, it was required that the notch acuity a/r was constant or at least the notch root radius should remain constant; thus, data where r decreases with increasing size were excluded. Furthermore, the crack length-to-width ratios, a/W, scaled within 10 %, i.e.,

$$0.9 \leq (a_1/W_1) \,/\, (a_2/W_2) \leq 1.1 \quad . \tag{2.42}$$

This was accompanied by one exception where an interpolation was performed.

Also the specimen length or span "should scale sufficiently so that a stress intensity factor calculation for the different sizes remains unaffected by any changes relative to W. Typically this just means that specimens should preserve a length which is as long, or longer than, W."

A further requirement was that thickness effects were to be excluded. Of course, this is assured if the thickness B is properly scaled with the scale factor λ. As noted before, then "whatever combination of plane stress and plane strain is present in one size is conserved in the next[40]. Alternatively test pieces can maintain a state of plane stress or plane strain exclusively by having a fixed B which is relatively small or longer, respectively". The authors then defined, in a comprehensive sense, *plane stress* as being when

$$B/a \leq 0.1, \; (B/a \leq 0.3) \tag{2.43}$$

and *plane strain* when

$$B/W \geq 0.5, \; B/a \geq 1.0 \; (B/W \geq 0.45, \; B/a \geq 0.9) \quad . \tag{2.44}$$

For the plane stress case the thickness B is an order of magnitude less than the smallest of the in-plane dimension. The authors remarked that the plane strain range is motivated by standard specimen dimensions in plane strain fracture toughness testing. It should be pointed

[40] This requires that the loading is scaled.

out that the ratios, Equ. 2.44, are consistent with the minimum size requirements with plane strain fracture toughness (K_{IC}) testing; however, there are minimum size requirements which represent lower bounds of *a, B*, and *W* which are depending on $(K_{IC}/\sigma_y)^2$, i.e., a measure of the radius of the plastic zone at the tip of the crack or notch. Thus, it may be that specimens satisfying inequalities (2.44) do not satisfy the minimum size requirements.

The classifications Equs. $(2.43)_1$ and $(2.44)_1$ exclude quite a number of configurations. Therefore Sinclair and Chambers relaxed the conditions somewhat to those given in parentheses. Finally, specimens with scaled *B* were classified as plane stress or plane strain according to which of Equ. 2.43 or 2.44 they were closest to.

An important aspect of LEFM, i.e., "the crux of the applicability of LEFM", is the question of how brittle the response is. This is meant by the authors in an engineering sense of limited plastic flow rather than microstructural fracture mechanisms. As a measure, they used the radius of the yielded region, r_y. The classical first order estimates are:

$$\begin{aligned} &\text{plane stress} && r_y = \frac{1}{2\pi}\left(\frac{K_I}{\sigma_y}\right)^2 \\ &\text{plane strain} && r_y = \frac{1}{6\pi}\left(\frac{K_I}{\sigma_y}\right)^2 \end{aligned} \qquad (2.45)$$

where K_I is the mode I stress intensity factor at the onset of crack growth and σ_y the uniaxial yield stress at the relevant temperature. Sinclair and Chambers introduced the following classifications:

$$\begin{aligned} &\text{brittle regimes}^{41} && r_y/a \;<\; 0.02 \quad (\text{or } a > 50\, r_y) \\ &\text{brittle-ductile regime} && 0.02 \;\le\; r_y/a \;<\; 0.05 \\ &\text{ductile regime} && 0.05 \;\le\; r_y/a. \end{aligned} \qquad (2.46)$$

The authors stressed the point that a considerable effort was made "to avoid comparing apples with oranges". Therefore, they applied also some supplementary rules, e.g., relaxation of the somewhat arbitrary limit *0.05* in Equ. 2.46, i.e., the transition from the brittle-ductile to the ductile regime. Also the calculation of the mean value of the stress ratio of two sets of nominally identical tests of two specimen sizes was done as follows: the authors formed all possible quotients of the fracture stresses for the small specimens divided by those for the large, noted the range of these ratios, and calculated their mean value.

The investigation was carried out for different steels, aluminium alloys, other metals, as well as non-metals. For these groups of materials tables were prepared giving the sources, types of specimen, some geometric information such as acuity, temperature, scale factors, and mean stress ratios, as well as the classification. Without distinguishing between the materials groups, plots of the strength ratio data versus scale factor together with the LEFM prediction were displayed. Fig. 2-60 shows the data for the case of plane strain, Fig. 2-61 those for the plane stress case, the bulk of the data being steels and aluminium alloys. The size of the dots reflects the number of tests involved. Among others, Sinclair and Chambers made the following general non-quantified observations concerning their guiding rules:

[41] This limit is essentially the same as prescribed in the standards for plane strain fracture toughness testing.

- Strength data based on maximum loads or stresses tend to exhibit less of a size effect than that associated with strengths at the onset of crack growth. However, where size effects are distinct for the two strength types, the maximum criterion usually involves large stresses and extensive yielding and such data fall in the ductile regime.
- There is some but little effect due to notch sharpness, provided condition Equ. 2.41 is met; typically notches with less acuity display less size dependence, but there is no clear distinction. Thus, data from both notches and fatigue precracks were used.
- Concerning the extended ranges of *a/W* similarity and *B/a* and *B/W* values for avoiding thickness effects, Equs. 2.43 and 2.44, the authors found no significant differences in strength size effects between data satisfying their strictest requirements and those only within their more relaxed limits. As a result, they combined the two types. However, variations were found in strength size effects for sets of scaled specimens which have different *a/W* values but are otherwise the same. Accordingly, such data were segregated and notified in the tables.

With reference to Figs. 2-60 and 2-61 the following observations were made:

- Generally the agreement between the LEFM prediction $\sigma_1^*/\sigma_2^* = \lambda^{1/2}$ and the bulk of the data is not "great". For example, using a least squares fit weighted by the numbers of tests involved to determine the exponent k in the fit

$$\sigma_1^*/\sigma_2^* = \lambda^k , \tag{2.47}$$

gives the following result for k

	brittle	brittle-ductile	ductile
plane strain	0.39	0.36	0.24
plane stress	0.49	0.41	0.22

in comparison to $k = 0.5$.

- The best agreement is found for the brittle case under plane stress conditions. Of course one would not expect agreement in the ductile case.
- Sinclair and Chambers stress the point that none of the curves fits any of the data distributions in any of the plots in Figs. 2-60 and 2-61 well. They comment that this "shortcoming cannot simply be dismissed as due to scatter because a significant proportion of the values plotted represent mean values themselves and, moreover, in over half of the instances where ranges can be calculated from the extreme values of σ_1^*/σ_2^*, these intervals do not even intersect the LEFM prediction, irrespective how brittle the response is".
- Generally the LEFM prediction represents on upper bound in relation to experimental data with scale factors larger than about $\lambda=5$. However, in this scale range brittle data are rare. As Figs. 2-60 and 2-61 show, the bounding property is also true for the majority of the data for scale factors less than 5. This result has implications for the practical applications of the LEFM strength size dependence prediction. If tests with scaled down models are done which yield an experimentally determined fracture stress σ_1^*, the prediction of the reduced strength $\sigma_2^* = \sigma_1^* \lambda^{-1/2}$ is conservative since the predicted strength σ_2^* of the large structure is too small, especially for large scale factors. However, if tests with scaled up models are done which yield an experimentally determined fracture stress σ_2^*, then the LEFM prediction $\sigma_1^* = \sigma_2^* \lambda^{1/2}$ for the small structures is non-conservative since the σ_1^* is too large.

Sinclair and Chambers finally introduced some measures to quantify agreement or disagreement. They quantified the effectiveness of the LEFM prediction by determining how often it does indeed predict the strength of one specimen, given the strength of another geo-

metrically similar one. The LEFM prediction is regarded as *good* if the experimental data are within ±5 % of Equ. 2.40 and are considered as useful if within ±10 %. The percentages of the data that fall within either of these two ranges are listed in Tab. 2-34 according to the different classes. Recalling Figs. 2-60 and 2-61, the insufficiency of the percentages in Tab. 2-34 are to be expected. As before, the ductile regime is worst, and, of course, should be discarded because it is out of the range of LEFM. Surprisingly, the brittle-ductile regime has higher percentages than the brittle regime. As the authors state, neither is very satisfactory, with "LEFM not being within useful agreement about half of the data". As the figures show, "a lot of what agreement there is comes from data with small scale factors $(\lambda \leq 2)$, where there is really very little to predict".

To remove the almost "automatic" agreement for low λ-values, the "size effect S",

$$S = \sqrt{\lambda} - 1, \tag{2.48}$$

is introduced. Tab. 2-35 lists the percentage of the data being in accordance with the two intervals with LEFM´s size prediction S, simply grouped according to the brittle-ductile classification. According to the authors, this is "the true key to applicability, rather than plane stress vs. plane strain". Tab. 2-35 shows that LEFM is quite ineffective to predict the size dependence, if the almost automatic agreement for small values is removed: in the brittle material response regime only 11 % of the data are within the ± 10 % deviation of LEFM and only 4.3 % are within the ± 5 % bound.

Sinclair and Chambers extended their study to investigate whether an even more restrictive set of rules would yield perhaps a more satisfactory performance of the LEFM size prediction. Therefore the data of the brittle-plane strain classification were segregated into two groups according to two different options:

1. Data which stem from valid K_{IC} testing according to ASTM standard and which thus satisfy minimum size requirements, and data which do not belong to this group.
2. Data belonging to the brittle-plane strain class but divided into two groups:
   - very brittle data when $0 \leq r_y/a < 0.01$
   - quasi brittle data when $0.01 \leq r_y/a < 0.02$.

The authors observed that it was not trivial to ascertain whether data came from valid K_{IC} test procedures since sufficient information was generally not available to check all ASTM E 399 requirements. Unless they could discover a violation of the present standards, they took the contributor's own statement for granted.

Tab. 2-36 shows the results of the two investigations. Concerning valid K_{IC} testing data, Sinclair and Chambers remark that "it would be difficult to argue that there is any significant improvement offered by the valid K_{IC} data over other plane strain brittle data". Comparing this result with the less restrictive brittle data set in Tab. 2-35, no improvement of the agreement within the ± 10 % LEFM margin is found. Tab. 2-36 also shows that the classification in *very brittle* and *quasi brittle* data does not bring about any significant improvement.

As stated by Sinclair and Chambers, there is concern about the very basis of Linear Elastic Fracture Mechanics "because there exists several hundred test results for appropriately brittle behaviour not agreeing with the LEFM prediction of strength size effects. Every one of these represents data establishing a variation in fracture toughness with size. It follows that fracture toughness is demonstrably not a material property. Thus the use of the stress intensity factor as the parameter in and of itself controlling brittle fracture needs serious examination".

In fracture mechanics the J-integral and the crack-tip-opening-displacement (CTOD) as functions of the crack extension Δa may be regarded as material characteristic relations provided certain restrictions are satisfied. The purpose of the limitation is to ensure that the J- or CTOD-resistance curves remain valid during the process of stable crack extension, independent of shape and size of the specimens. Then the crack growth process is referred to as being either J- or CTOD-controlled, whichever applies.

Results from a large experimental programme on geometry and size effects on J- and CTOD-resistance curves were performed by ***Gordon and Jones (1989, [2.46]).*** The resistance curves were obtained from single-specimen unloading compliance tests at room temperature on differently sized single-edge-notch-bend (SENB) specimens made from Ti-3Al-2V alloy.

The low tearing resistance alloy selected[42] was supplied in the form of three 50 mm thick blocks each about 300 mm square. The blocks represented adjacent samples in the original 50 mm thick plate. All SENB-specimens were in the (L-T)-orientation with respect to the rolling direction of the plate.

The specimens were side grooved[43] by 20 % and precracked by fatigue to provide an initial crack length a_o-to-width W ratio (a_o/W) of about 0.6. The loading span S-to-width W ratio (S/W) was 4.0. The dimension of the specimens were chosen such that (i) a family of geometrically similar specimens could be checked for size effects with a width W-to-thickness B ratio (W/B) of two, the thickness ranging from 10 mm to 40 mm (scale factor 4) and that (ii) specimens of constant thickness (20 mm), but with in-plane dimensions in constant proportion, could be tested. For each specimen type three room temperature unloading compliance tests[44] were performed. The dimensions are listed in Tab. 2-37.

The specimens were tested in broad agreement with "The Welding Institute"-recommended resistance-curve procedure using a computerized unloading compliance test system. The computer-controlled test procedure was done under clip gage displacement control at a load-point displacement rate of about 0.2 mm/min. During the tests, time, applied load, clip gage displacements, and ram displacement were continually measured. The load-point displacement was determined by correcting the measured ram displacement for extraneous displacements of the test machine and fixture compliance, as well as roller indentation effects.

The unloading compliance tests were terminated after the crack had grown by about 60 % of the original uncracked ligament $b_o = W\text{-}a_o$. Then the specimens were heat tinted before being cooled down to –196 °C and broken open. Both the initial fatigue crack length a_o and the stable crack growth, including the stretch zone, were determined using a weighted nine-point average along the crack front.

Several J-resistance indicators were determined:

- The standard fracture resistance J_o: for side grooved SENB specimens it is defined by

[42] Chemical composition wt % 3.13 Al, 2.41 V, 0.16 Fe, 0.01 C, <0.006 H_2, 0.006 N_2, 0.100 O_2, Ti balance; nominal yield stress = 520 N/mm^2, ultimate tensile stress = 620 N/mm^2

[43] The purpose (Ref. [2.28]) of side grooving is to obtain a straight crack front (no crack tunnelling and no shear lip formation)

[44] In this single-specimen technique the specimen is periodically unloaded by about 20 % and the elastic unloading compliance is measured. From the unloading compliances the crack lengths and, hence, crack extensions are calculated. For details see Ref. [2.46].

$$J_o = \frac{2U}{B_n (W - a_o)} \quad , \tag{2.49}$$

U = area under load versus load-point displacement curve

$B_n = 0.8\ B$ = net thickness; the factor 0.8 accounts for side grooving.

This standard J-integral value is proportional to the total deformation energy up to the instant were the crack has attained the length a, which is then referred to the initial section area of the ligament, i.e. $B_N\ (W\text{-}a_o)$ Thus, this area specific energy was not cor rected for the reduction of the ligament area due to crack extension.

- The fracture resistance J_R corrected for crack growth. An incremental approximation proposed by Ernst, Paris, and Landes (1981, [2.47]) was used for the calculation (see also Ref. [2.46]).
- The modified fracture resistance J_M according to Ernst (1983, [2.43]). This modification attempts to extend the range of crack extension over which the J-integral can be applied. As indicated by Gordon and Jones, the J_M parameter has the property that, in the limit of elastic/perfectly plastic behaviour, the rate of change of J_M is not a function of the rate of change of the crack size.

Fig. 2-62 shows three J_o-resistance curves obtained from the three nominally identical 20 x 80 mm SENB-specimens. Except for the very initial part, a considerable variability is seen. Gordon and Jones note that this scatter is typical for J_o-, J_R- and J_M-resistance curves obtained for each set of three specimens. Unfortunately, a detailed cutting plan is not provided and thus it not clear how the specimens of different dimensions were distributed within the three blocks. Also the uniformity of the material was not assessed.

The test data were analysed to determine the amount of stable crack growth up to the maximum applied load in each test. The average value Δa_m for each specimen type is listed in Tab. 2-38. For the family of geometrically similar specimens (a) in Tab. 2-38 it is seen that the crack advance up to the load maximum does not scale with the size of the specimen but increases much faster: for a three-fold increase in size (10 x 20 to 30 x 60 mm) the stable crack propagation increases 4.56 times. The data of Tab. 2-38 also show that an extrapolation to small specimens (i.e., W<20 mm) would imply a suppression of crack propagation before the load maximum is reached.

The standard J_o-resistance curves obtained for the family of geometrically similar specimens are presented in Fig. 2-63. Each curve represents the average of three nominal identical tests. The curves are almost indistinguishable up to a crack growth of about 3 mm; beyond that they fan out, but without any regular size dependence. Up to a crack growth of about 4.7 mm, when the toughness curve of the smallest specimen ends, the variation in toughness is less than about 10 %. It should be noted that the spread of the curves for the larger crack growth is comparable to the scatter of the individual tests of each size (see Fig. 2-62).

The mean J_R-resistance curves, which are corrected for crack growth, are displayed in Fig. 2-64. The mean J_R-resistance curves for the 15 x 30 mm, 20 x 40 mm, and 30 x 60 mm specimens are in close agreement over the crack growths studied and they approach a constant J_R-value after 4-5 mm crack growth. The mean curve of the largest specimen (40 x 80 mm) is in good agreement with the latter ones up to a crack growth of about 3.5 mm, but then it lies above them. The smallest specimen size shows agreement up to about 0.75 mm (at which J_R is equal to approximately 100 kJ/mm^2), but then it lies below all the others. Thus, the spread of the mean J_R-resistance curves for large crack growths is definitely larger than the J_o-resistance representation (Fig. 2-63).

The mean J_M-resistance curves are plotted in Fig. 2-65. Agreement within about 10 % variation is seen up to 3 mm crack growth, but then a considerable upswing for the 10 x 20 mm, 15 x 30 mm, 20 x 40 mm is noted. It is apparent that the J_M-resistance curves show a much larger variability for large crack growths. The upswing of the three smaller specimen sizes seem to follow the rule: the larger the size, the later the upswing. Whether this is a true size influence is not clear.

The results of the geometry effects test programme (Tab. 2-38 (b)) will not be discussed here. Also the general discussion given by Gordon and Jones will not be taken up, but several obvious statements about the above test family are made.

The mean J_o-, J_R-, and J_M-resistance curves for the geometrically similar specimen family all agree for small crack extensions (~3 mm for the J_o-curve, ~1 mm for the J_R-curve, ~1.5 mm for the J_M-curve). In the terminology of fracture mechanics, this congruence represents "size independence" up to a limited amount of crack growth which depends on the definition of the J-resistance (J_o, J_R or J_M). But the initial part (crack growth < 1 mm) of the three resistance curves appears to be insensitive to the definition of J-resistance.

It should be realized that the *J*-value represents an area specific energy, specifically J_o is twice the applied work divided by the initial ligament area. Although the initial part of the J-resistance curve is apparently size independent, the process of crack propagation is by no means size independent because under the same applied *J*-value the crack extension is the same, but the fractional or percentage crack extension relative to the initial length of the ligament is different. Thus, a 3 mm crack growth in the small 10 x 20 mm specimen corresponds to about 37.5 % of the initial ligament length but only 9.38 % for the largest specimen (40 x 80 mm).

The picture changes again if volume specific energies were considered (such as J/W or J/b_o). Therefore part of the discussion of Gordon and Jones, which argues with a uniform percentage crack extension for all specimen sizes ("..reasonable size independence up to and in many cases beyond crack growths corresponding to 50 % of the initial uncracked ligament"), is misleading.

Gordon and Jones (1989, [2.47]) also determined the effect of specimen size on the CTOD-resistance curve of the same titanium alloy. In conjunction with J-resistance testing, at each unloading the appropriate values of the standard crack tip opening displacement (CTOD) δ_o and the CTOD corrected for crack growth δ_R were calculated which was based on the measurement of the crack mouth opening displacement. The standard CTOD δ_o for SENB specimens is given by

$$\delta_o = \delta_{el} + \delta_{pl} = \frac{K^2\left(1-\nu^2\right)}{2E\sigma_{ys}} + \frac{r_p\left(W-a_o\right)}{r_p\left(W-a_o\right)+a_o+z}\,V_p \qquad (2.50)$$

where

K	stress intensity factor	
σ_{ys}	yield strength	
E, ν	elasticity constants	
r_p	plastic rotational factor	r_p=0.4
z	knife edge height	

$V_p=V-V_e$ plastic component of mouth opening displacement V obtained from the load-mouth opening displacement curve.

The plastic component δ_{pl} is obtained through a "similar triangles construction" procedure by assuming that the SENB-specimen rotates about a plastic hinge positioned in the ligament at a distance $r_p(W-a_o)$ in front of the initial crack tip.

As an indication of the variability of the CTOD-resistance curves, the δ_o-resistance curves obtained for the 15 x 30 and 20 x 60 mm SENB specimens are presented in Fig. 2-66. It is noteworthy that the small specimens show definitely less scatter than the larger specimens. The reviewer believes that the three small specimens (15 x 30 mm) were taken from adjacent positions in the raw blocks whereas the larger specimens were spread over a larger area such that macroscopic material inhomogeneity becomes more important. As noted before, testing of the material homogeneity was not reported and appropriate cutting plans are missing in Ref. [2.46, 2.47].

Fig. 2-67 shows the mean of three δ_o-resistance curves for each set of specimens. The two largest specimen types (30 x 60 and 40 x 80 mm) are in close agreement over the entire crack growth range. However, the three smaller specimen types (10 x 20, 15 x 30, 20 x 40 mm) show a considerable upswing which is largest for the smallest specimen type and decreases successively with specimen size. With decreasing crack extension, the δ_o-resistance curve of all five sizes converge to a single curve such that agreement of the curves is obtained up to a crack extension of about 1.9 mm where the δ_o-value is about 0.175 mm with a 10 % variation.

The mean δ_R-resistance curve (corrected for crack growth) is presented in Fig. 2-68. Obviously, similar trends are exhibited. An upswing behaviour becomes now also apparent for the two largest specimens.

It is also noted that the range of crack extensions, where congruence of the δ_o-and δ_R-resistance curves is obtained, is smaller (e.g., for the δ_R-curve the crack extension is about 1.5 mm and for the δ_o-curve 0.75 mm) than that for the J-resistance curves. The results of the geometry effects programme[45] will not be described here.

As noted before, in the brittle-ductile temperature transition region the fracture toughness for steels depends on specimen geometry and size. These geometry, thickness, and size effects can neither be consistently explained nor predicted and the very large scatter of the toughness data makes it difficult to determine trends in the toughness behaviour. In a study ***Landes (1992, [2.49])*** investigated the effects of thickness, size, and geometry on the basis of six sets of transition fracture toughness data from various sources. This study included also Weibull statistical modelling of transition fracture scatter and other theoretical modelling concepts. Among the data are five groups of data of geometrical similar specimens tested at distinct temperatures below 0° C. Only these will be described in the following. These steels and temperatures are:

Material	Code Name	Test Temp. °C	No. of Sizes	No. of Specimens	Source
20MnMoNi55	PVS	-60	2	23	GKSS
A533B	Morland TH	-65	4	39	UKAEA

[45] As for the J-testing, the thickness B is kept constant (20 mm) whereas the in-plane dimensions are changed in proportion with W ranging from 10 to 80 mm.

A533B	Morland SG	-35	2	30	Risley UKAEA
A533B	McCabes Data	-75	4	64	Risley ORNL
A533B	McCabes Data	-150	3	47	Oak Ridge ORNL Oak Ridge

The specimens were proportionally sized compact tension specimens (CT) without side grooving. Usually the width W equalled $2B$, in some cases $W=2.5\ B$. In all cases the ligament size $b=W-a$ was approximately equal to the thickness. Further informations on the specimens and the determination of the J-integrals were not given in Ref. [2.49], but one has to consult the original sources. The chemical composition and the room temperature tensile properties of the two reactor vessel steels 22 MnMoNi55 and A533B are comparable. No reference is given in Ref. [2.49] to the origin of the plate material, cutting plans, and homogeneity assessment.

In Figs. 2-69 to 2-73 (from Ref. [2.49]) the J-integral values for cleavage are plotted versus the thickness B for different material sources. Fig. 2-69 shows the 22MnMoNi55 data (code PVS) at -60 °C. A considerable scatter is found for both the small 20 mm thickness specimens and the 50 mm specimens (scale factor 2.5), but the decrease of the mean J-integral value with increasing size is evident.

The data for A533B at -65 °C (code: Morland TH) in Fig. 2-70 cover a thickness range from 25 to 127 mm (scale factor $\lambda\approx5$); they demonstrate the largest scatter for the smallest specimens, but the mean value is approximately size independent. Increasing the temperature to -30 °C for the same material (Fig. 2-71), a large scatter is seen for both small specimen sizes (B=12.0 and 25 mm), but a decrease of the mean value is observed at this higher temperature.

The results for a different charge of the vessel steel A533B (code: McCabes data at -75 °C and -150 °C) are presented in Figs. 2-72 and 2-73. At -150 °C a large scatter for all three sizes ($B=25,\ 50,\ 100$ mm) is seen and mean values are almost size independent. Increasing the temperature to -75 °C, a decrease of the scatter with increasing size becomes evident; also the mean value is slightly decreasing with size. However, the number of tests for the two largest specimen sizes is clearly less than that of the two small specimen types. Apparently this weakens these latter observations.

Landes remarks that three characteristics of a size influence commonly appear:

- Small specimens consistently have more scatter than large specimens.
- The mean toughness of a group of nominally identical specimens of a given size and geometry tested at a single temperature will sometimes exhibit a size effect (i.e., decrease with increasing size, Figs. 2-69, 2-71, 2-72 which include also the smallest specimens) and other times will not (Figs. 2-70 and 2-73). The small specimens seldom have a lower mean toughness value.
- Small specimens more consistently give the lowest toughness values at a given temperature than the large specimens. The reviewer notes that this result is not obvious in Figs. 2-69 to 2-73 but was obtained by Landes in a special study.

As evident from the review presented so far, the engineering community has given considerable attention to size effects in specimens with moderately sharp notches as well as rather sharp cracks (resulting from fatigue). Sharp cracks clearly are a great danger for fracture, but they are not part of the structural design. Engineering structures usually contain rather blunt

stress concentrators (holes, circular notches, transitions) and no sharp reentrant corners or even sharp cracks. Classical fracture mechanics analyses, such as Linear Elastic Fracture Mechanics (LEFM based on the concept of the stress intensity factor *K*) and the Elastic-Plastic Fracture Mechanics (EPFM based on the J-integral or the crack tip opening displacement *CTOD*), apply to pre-existing cracks and thus are not adequate for the analysis of blunt strain-concentrators. Presently, no well established theory is available to predict ductile fracture initiation and the scaling properties for the latter cases.

In an attempt to improve the situation, ***Giovanola, Kirkpatrick, and Crocker (1996, [2.50]; 1998, [2.51]; 1999, [2.52])*** applied a relatively simple, uncoupled damage mechanics model ("local approach") to experimental results of families of geometrically similar specimens with sharp cracks (CT-specimens) and to specimens with blunt notches (SENB-specimens). For both families the high strength – low hardening steel HY-130 was used. The tests with the compact tension specimens had been performed by Link (1994, [2.53]) and the notch bend specimens by Giovanola et al. (1999, [2.52]). In the following, attention is restricted to the experimental results of these two families only.

The compact tension (CT) specimens were of the 1T[46] and 4T standard size with a scale factor of 4; side grooves were applied, penetrating 20% of the gross thickness. The prefatigued crack length *a* was 0.7 to 0.71 times the width *W* ($a/W = 0.70 \div 0.71$). The specimens were tested according to the ASTM standard of J-resistance curve testing in 1994. The results of only two single tests were reported (Giovanola et al. (1996, [2.50]; 1998, [2.51])). Unfortunately, multiple experiments for each CT-specimen size were not mentioned and, therefore, conclusions of these single test results are subject to reservations. Nevertheless, it is expected that the very large scatter, as observed for J-integral values at cleavages for low temperatures (see Landes (1992, [2.493]), will likely not be present for Link's room temperature tests.

In Fig. 2-74 the normalized load[47] (P/P_L) and the corresponding normalized crack extension $(\Delta a/W)$ are plotted versus the normalized load-line displacement (δ/W) for the two specimen sizes. Fig. 2-74 shows agreement and thus similarity in the first almost linear part of the normalized load-deflection curves, but a significantly larger maximum of the normalized load (~ 33%) for the smaller specimen is seen; also the load maximum of the 1T specimen occurs at a clearly larger normalized displacement (~ 62%). Deviation from linearity of the load-displacements curves of the two specimens starts, according to Fig. 2-74, approximately at the same normalized displacement $(\delta/W \approx 9 \cdot 10^{-3})$; whether this deviation is due to plasticity and/or due to initiation of crack extension is not clear. From Fig. 2-74 it appears that Link has related the start of crack extension to the instant of deviation from linearity. Thus, the crack

---

[46] The standard 1T compact tension specimen has the dimensions: thickness B = 1 inch (25.4 mm), width W = 2 inches (50.8 mm); see also Fig. 2-53.

[47] P_L is the limit load according to Kumar et al. (1987, [2.54]).

$$P_L = 1.455\ \eta\ \sigma_y\ (W\text{-}a)\ B_N \qquad \eta = \left[\left(\frac{2a}{W-a}\right)^2 + 2\left(\frac{2a}{W-a}\right) + 2\right]^{1/2} - \left[\frac{2a}{W-a} + 1\right]$$

$B_N = 0.8\ B$ net thickness

σ_y = yield stress

extension for both specimen sizes starts before the load maximum. No explicit description of the determination of the crack extension is given, but it is believed that it was inferred from the unloading compliance of the load-displacement curves, either measured by partial unloading or using the secant method (Anderson (1995, [2.28]) which determines an effective crack size from an effective compliance.

The most significant difference of the normalized crack extension curves concerns their rate $d(\Delta a/W)/d(\delta/W)$ which is considerably larger for the large CT-specimen at small normalized crack extensions. This implies that a given normalized crack extension (say 1%) appears at smaller normalized displacements $(\delta/W \sim 14 \cdot 10^{-3})$ of the large CT-specimen than for the 4 times smaller CT-specimen $(\delta/W \sim 21 \cdot 10^{-3})$. This conforms with the general observation that for a given normalized or relative displacement cracking is more extensive in the large than in the small geometrically similar specimen of the same material. Thus, from these limited data it is concluded that similarity is restricted to the loading phase before crack extension, where, for this case, the load-displacement curve is linear.

For the experimental investigation of the U-notched three-point bend (SENB) specimens, the same HY-130 steel, a quenched and tempered alloy steel, was used. All SENB-specimens were fabricated from a single plate (381 x 762 x 50.8 mm). However, a cutting plan was not provided, so it is not clear whether the tip of the notch of all specimens is positioned at the mid-plane of the plate which is a preferable arrangement. The composition and heat treatment of the plate is given in Tab. 2-39 and mechanical properties are collected in Tab. 2-40. The yield and tensile strength data demonstrate very clearly that this is a high strength but low hardening material. Whether this is the same melt, as for the CT-specimens, is not clear. Also no indication of homogeneity assessment testing is given in the references. Three geometrically scaled sizes were considered, as listed in Tab. 2-41 and shown in Fig. 2-75. From the data it is seen that the width of the largest specimens (2T-specimens) is the same as the thickness of the plate, such that the tip of their notches are at the mid-plane of the plate.

Three specimens for each of the sizes 1T and 2T and four specimens for the size 0.5T were fabricated. The design followed the recommendation of the ASTM Standard E399-90 for three-point-bend specimens, except that they contained a straight-face notch terminated by a semi-circular tip. The nominal ratio of the notch depth to specimen width (a/W) was 0.5 for all specimens.

The loading of the specimens was done with scaled loading pins and supports (rolls). The supports were closely positioned at the ends of the specimens, i.e., loading span $S = 4\ W$ (see Tab. 2-41). Transducers included a load cell to measure the applied load, linearly variable differential transducers (LVDT) to measure the displacement of the load application point, a clip gage to measure the notch mouth opening displacement, and two acoustic emission (AE) sensors to record acoustic signals associated with fracture initiation. The two AE transducers were symmetrically installed at the two ends of the notched specimen.

In addition, the deformation at the root of the notch was monitored with a long distance microscope aimed at the mid-thickness location and a video camera to establish visually the initiation of fracture. This continuous record on video tape allowed post-test evaluation and comparison with acoustic emission data.

The tests were performed under displacement control of the hydraulic ram. A 50-ton MTS servo-hydraulic testing machine was used, presumably the same machine for all three specimen sizes. If a true displacement control was applied, this would not introduce an artificial size influence on the load-displacement records. To eliminate potential strain rate effects on deformation and fracture, scaled displacement rates of 0.3, 0.6, and 1.2 mm/min in the small,

medium and large size specimens were applied which maintained the same strain rates in all three specimen sizes. For each set of specimen scale one specimen was deformed up to the "first indication of fracture initiation", another specimen to a limited amount of crack extension, and a third specimen to a significant amount of crack extension but not to complete failure.

The video camera/long distance microscope arrangement, monitoring the fracture initiation at the mid-thickness location of the notch root, was also used to inspect the notch root over the entire thickness of the specimen at regular intervals under halted loading. This was to assure that fracture did not initiate outside the usual field of view.

The experiments were supplemented by detailed post-test analysis of the specimens, such as

(a) measurement of the residual bend angles;
(b) photography of the cracked notch root;
(c) sectioning of selected specimens normal to the notch root axis at the mid-section, and measuring the fracture penetration in the polished and etched cross section;
(d) the informations (b) and (c) were used to reconstruct the fracture process by matching the profiles of the crack faces; however, how this was done is not explained in any of the publications;
(e) selected specimens were broken open to examine the fracture surfaces and the notch root surface with a Scanning Electron Microscope (SEM).

Giovanola et. al. pointed out that in all tests the experimental data showed "a precise correspondence between the recording of the first acoustic emission event and the first visual observation of material separation at the notch root to form an open crack". This first material separation was defined as the instant of fracture initiation. It is now important to note that metallographic observations of sectioned cross sections with just-initiated cracks "suggest that cracks nucleate with a minimum initial length of 100-200 μm in all specimen sizes. Cross sections at different locations across the thickness reveal that the amount of crack penetration can vary from place to place, but that it tends to be the largest near mid-thickness, as can be expected from considerations of the stress triaxiality level". Therefore, from the reviewer's point of view, the detection of crack initiation at the mid-section is linked with a small but finite length, the minimum crack size which can be detected by the methods used and which is about the same for all sizes. This implies that possibly an artificial size effect is introduced in some of the size effects results. This point will be discussed later in somewhat more detail.

A typical set of load versus notch mouth opening records of three 1T-specimens is shown in Fig. 2-76. The records are almost indistinguishable up to the load maximum and even beyond. This proves that there is no difference in the material of these specimens and that the test is quite repeatable. The three arrows indicate the instances of crack initiation and its scatter is quite small. It is noted that for this 1T- specimen the crack initiation is close to the load maximum. Figs 2-77 and 2-78 show for the three specimen sizes the normalized load versus normalized notch mouth opening and load-line displacement curves, respectively. The normalized load is defined by P/P_L where P is the actual load and P_L the limit load according to Kumar et al. (1981, [2.54])

$$P_L = \frac{0.728\, B\, b^2\, \sigma_y}{S} \quad . \tag{2.51}$$

The notch mouth opening is normalized by dividing it by the notch root radius r and the load-line displacement is referred to the specimen width W.

Figs. 2-77 and 2-78 include also the average instances of the crack initiation (arrows) for each specimen size and their scatter bars (maximum and minimum values). The normalized curves for the three sizes clearly show almost complete agreement over a very large part before their maxima. The normalized load maxima are shifted only very slightly to larger values when the specimen size is decreased but their associated normalized notch mouth opening displacements or load-line displacement values are definitely shifted to larger values the smaller the specimens. This implies an earlier fall-off of the load when the size is increased. Moreover, following Giovanola et al., the displacement and notch mouth opening values at fracture initiation "do not scale geometrically in the scaled specimens and therefore, for HY-130 steel, there is a size effect for ductile fracture initiation at blunt notches loaded in bending".

If the normalized displacement or notch opening at crack initiation and at the load maximum are compared for each size, it appears that they agree approximately for the 0.5 T and the 1T specimen. For the 2T-specimen size it seems that crack initiation occurs somewhat before the load maximum.

Characteristic normalized data of all the scaled experiments of the blunt-notched three-point-bend specimens are collected in Tab. 2-42.

The fractographic investigations confirm the scale dependence of fracture deduced from the load-displacement data. The extent of cracking at the notch root of the geometrically similar specimens, bent to approximately the same residual angle (17-18°: specimens 0.5 T-1, 1T-3, 2T-3 normalized to the same size, see column 4 in Tab. 2-42), is shown in Fig. 2-79. The extent of cracking (crack length and opening) increases with the size of the specimen, although the global deformations are approximately the same. The fractographic investigations also showed that the main fracture was also accompanied by secondary fractures which were primarily induced by slip steps, but the main fractures consisted of a tensile opening (mode I) as well as a slip step (mode II). However, the appearance of a crack with a mode I component had been defined by Giovanola et al. as fracture initiation. By comparison of the notch surface of the small 0.5 *T*- and the large 2T-specimens at approximately the same global bending angle α, Giovanola et al. observed that separations (distances) between the ripples of the orange peel, between slip steps, and incipient crack segments were roughly size independent. This observation, of course, required that the same magnification was used for all three sizes.

For the scaled specimens in Fig. 2-79 subjected to the same residual bend angle of 17-18°, the relative as well as the absolute crack depth increases rapidly with specimen size. This is demonstrated in Fig. 2-80. In Fig. 2-80(a) the small crack in specimen 0.5 T-1 is a just-initiated submillimeter crack and metallographic investigations of other specimen sizes with just-initiated cracks (according to acoustic emission, etc.) indicate "that cracks nucleate with a minimum initial length of 100-200 μm in all specimen sizes". In fact, this is actually the minimum depth of a crack which was detected by the used detection methods (the reviewer). The metallographic cuts in Fig. 2-80 show that the planes of the initial submillimeter cracks are inclined at approximately 45° with respect to the mid-plane normal to the longitudinal axis of the specimen. Thus, according to Giovanola et al., they follow lines of maximum shear. Furthermore, in contrast to observations of other authors (see Ref. [2.52]), Giovanola et al. did not observe a distribution of voids in the vicinity of the inclined initial crack. Using the matching of cross-sectional profiles of the crack faces, the kinematic reconstruction of the crack opening proved that significant shear displacements were involved in the generation of the initial crack. Scanning Electron Microscope (SEM) studies of the fracture surfaces of the initiation region gave further evidences of shear deformations: microfracture damage, i.e.,

"smeared patches of elongated microvoids"; deeper in the specimen equiaxed dimples typical of ductile tensile fracture were found.

According to these fractographic observations, Giovanola et al. concluded that, irrespective of size, a localized shear mechanism initiated the fracture and "the weakened shear planes eventually fracture when a sufficient normal stress is applied on them and the crack continues to propagate in the classical tensile opening mode". The authors also remarked that the growths of microvoids are involved in both cracking stages but under different deformation fields.

As pointed out by the authors, Knott (1977, [2.55]) had commented that fracture initiation by shear localization is common in metals with low hardening rates. This appears to be plausible (the reviewer) because strain localization is delayed or prevented if the hardening rate of the materials is increased, which implies that the high strains are reduced and are distributed over a broader region. Then, for a low strength steel with high hardening rates many voids are generated over a broad region ahead of the notch which ultimately link up to form a crack. Therefore, the initiation of fracture for high and low-hardening materials is different. Nevertheless, the authors expect that void growth and coalescence are important in both cases.

Giovanola et al. suggest and believe to have identified those events leading to the point of fracture initiation: (1) heavy plastic deformation near the notch and extensive localized slip along planes roughly at 45° to the notch surface, (2) mixed mode (mode I and II) fracture by void nucleation and growth along the initial slip plane, and (3) mode I crack extension approximately in the direction of the notch axis. They believe that the first event with shear localization and the second event involving the growth of microvoids, primarily under shear deformation, and their linkage under superimposed tensile loading, "play a key role in controlling the scaling behaviour of fracture in notched specimens in bending, …".

Giovanola et al. extended their arguing by suggesting that the shear dominated mechanisms may introduce other characteristic size scales beyond microstructural length scales, such as inclusion size and spacing or grain size, which can affect the fracture scaling behaviour. With respect to the length scale associated to the shear localization they mention two observations:

(a) the spacing and length of slip steps in the surface of the notch root of specimens under the same bending angle are essentially independent of the specimen size;
(b) also the penetration depth of the initial crack (100-200μm) appears to be approximately size independent.

The reviewer recalls that strain (shear) localization significantly affects the strain distribution and the magnitude of the strain gradients. Moreover, the theoretical interpretation of multiple shear banding (spacing) and of the shear band width requires higher order continuum theories such as gradient plasticity, which involves at least one internal length scale characteristic for the material. Thus, observations (a) appears to be a valid argument for the suggestion of Giovanola et al.

Concerning observation (b), Giovalola et al. defined the first material separation, which they reliably identified with the acoustic emission as well as visual observations, as the point of "nucleation" of a crack with a minimum initial length, independent of the specimen size. In the reviewer's opinion, there are doubts as to whether this characteristic length is truly related to the material behaviour under these loading condition. Possibly the limited sensitivity of the acoustic emission sensor and the limited magnification of the optical systems (long distance microscope and video camera) introduce minimum lengths, which can be reliably detected, and these would be the same for both small and large specimens if the detection systems are

not changed. If this is the case, then the limited accuracy of the detection method for crack initiation introduces a small artificial length scale. This affects the identification of the instant of crack generation. If the resolutions of the detection systems were better, then mode I cracks with smaller openings and depths would be detectable and the crack initiation markers in the normalized load vs. notch mouth opening curves would shift to smaller normalized notch-mouth-openings and the shift would increase the smaller the specimens. Therefore, qualitatively the size influence on the "crack initiation" would increase. However, it is expected that the actual shift of the crack initiation markers would be rather small since the change of the notch-mouth-opening during the generation of a submillimeter crack is likely to be fairly small. A quantitative estimate is not possible since crack extension vs. notch-mouth-opening curves, such as they are provided for the CT-specimens (Fig. 2-74), were not reported.

Geometry and size effects of several cast duplex stainless steels where studied at room temperature by Besson, Devillers-Guerville and Pineau. This experimental and theoretical work was published in several articles ***(Devillers-Guerville, Besson, and Pineau (1997, [2.56]), Pineau (1997, [2.57]), Besson, Devillers-Guerville, and Pineau (2000, [2.58]))*** but some of the results were mentioned even earlier (e.g., Pineau and Joly (1991, [2.59]), Pineau (1994, [2.60]), Joly and Pineau (1995, [2.61]). Duplex stainless steels are used in the primary loop of the cooling system of pressurized water reactors (PWR's) at service temperatures between 290° C and 320° C. They contain up to 30% δ-ferrite in an austenite (γ) matrix. As pointed out by the authors, at the service temperature and after long periods of exposure (more than 10000 h) the ferritic phase of these steels is embrittled by a phenomenon known as "475° embrittlement" which increases the hardness of the ferritic phase and significantly reduces ductility and fracture toughness. Moreover, a large scatter is observed in measured values of laboratory specimens. This is due to the relatively small size of these specimens, as compared to the microstructural length scales of these materials. Therefore, a size dependence of the experimental results is observed which raises the problems of transferability of the laboratory results to structural component size.

Several duplex steels were investigated, such as that denoted by CF8M (referred to in Refs. [2.56, 2.57]) and three different heats of material denoted by Y 4331, BT and BL (discussed in Ref. [2.58]).

In what follows, attention is restricted to the experimental work only, which concerns the size effect issue but also to the influence of the notch acuity. The duplex steel CF8M is looked at first. The raw material was a centrifugally cast pipe (inner diameter 350 mm, wall thickness 40 mm) of CF8M stainless steel, its chemical composition given in Tab. 2-43; it contained about 20 % ferrite. The steel pipe was solution treated at 1115° C, water quenched, and aged at 400° C for 700 h. This induced an increase of the microhardness of the ferrite by almost a factor of two and a decrease of the ductility (elongation at fracture) from 45 to 20 %. Moreover, the Charpy impact energy KCU was reduced by more than a factor of 5 by the heat-treatment.

The chemical composition and processing route of centrifugal casting led to a specific microstructure. During the early stages of solidification large δ-ferritic grains with a columnar structure (~ 10 mm length in radial direction, 1 – 3 mm width) were formed. As cooling proceeded, the solid state transformation produced austenitic grains (γ, size ~ 1 mm) within the ferritic grains. However, some primary δ-ferrite remained untransformed within the austenitic grains and this yielded an interconnected network of both (single crystal) phases in the form of laths with thickness or spacing of about 10 μm. Therefore the duplex steel is characterized

by three distinct microstructural length scales. The mechanical tests included tensile tests of smooth and notched circular tensile specimens as well as the three-point-bending of U-and V-notched but also precracked specimens with rectangular cross sections (Charpy type).

The mechanical tensile tests at room temperature were as follows:

- Quasistatic tensile tests of smooth tensile specimens (diameter ϕ_0 = 10 mm, gage length 25 mm). Specimen axes along the tangential (T) direction of the pipe.
- Quasistatic tensile tests of notched tensile specimens (diameter at the root of the notch ϕ_0 = 10 mm, notch root radius R_d = 10, 4, and 2 mm as shown in Fig. 2-81; diameter of unnotched sections 18 mm). For R_d = 10 mm a wide notch is obtained, R_d = 4 mm is a semicircular notch and R_d = 2 mm is a narrow U-notch. Specimen axes along the tangential (T), longitudinal (L), and radial (R) direction of the pipe.
- Quasistatic tensile tests of a family of geometrically similar notched tensile specimens (diameter ϕ_0 = 6, 10, and 15 mm, notch root radius R_d = 6, 10, and 15 mm, diameter of unnotched section 10.8, 18, and 27 mm, gage length 15, 25, 37.5 mm). Specimen axes along the longitudinal (L) direction.

In all cases the tests were carried out at a (presumably overall) strain rate of $3x10^{-3}$ s^{-1}. The notched specimens were tested with a diametrical extensometer measuring the minimum diameter ϕ at the root of the notch, which allowed to calculate the logarithmic diametrical mean strain $\varepsilon = 2\ ln\ (\phi_0 / \phi)$. No indication is given along which direction the change of the diameter was measured. The diametrical mean strain ε_R to "failure" was computed by using the minimum diameter at failure. However, the instant of failure was not precisely defined in Ref. [2.56]: it may be the instant when "the load suddenly drops" or shows a marked change of its decrease in the softening regime of a load vs. displacement curve during the continuous measurement of the diameter change, or it may be simply the strain at the end of this curve. Of course, the minimum diameter, diametrical strain, or area reduction at the notch may also be determined after fracture by joining the broken halves of the specimen, but for this purpose the application of a diametrical extensometer during the test would not have been necessary.

The essential results for the smooth and notched tensile specimens are shown in Figs. 2-82 and 2-83. Fig. 2-82 shows the failure strain ε_R for the smooth specimens (presumably at the neck of the broken specimens) and at the root of the notch of the various types of notched specimens. The scatter of the nominally identical tests for the smooth specimens (ϕ_0 =10 mm, axes along the tangential (T) direction of the pipe) is considerable, ranging from 16 to 26 %. Unfortunately, no information is given about the position the specimens were taken from, e.g., mid-thickness or elsewhere.

The abscissa in Fig. 2-82 represents the theoretical stress triaxiality ratio σ_m/σ_{eq} (σ_m: mean normal (hydrostatic) stress, σ_{eq}: von Mises equivalent stress) at the center of the specimens, obtained from finite element computations. Details are missing in the references.

Fig. 2-82 shows the influence of the acuity or the radius of the root of the notch for the various notched specimens having the same minimum diameter at the notch root (ϕ_0 = 10 mm) and the same diameter and overall length outside the notch (non-similar specimens).

Devillers-Guerville et al. (1997, [2.56]) state "that the results obtained on the specimens oriented either along the pipe axes R, T, or L are almost equivalent". But obviously, Fig. 2-82 seems to exhibit more differentiated information about the diametrical failure strain ε_R at the root of the notch. For the specimens along the tangential (T) direction the scatter is largest for the 10 mm notch root radius R_d and seems to reduce with decreasing root radius. However, this conclusion appears to be uncertain since the number of nominally identical tests was considerably larger for the (R_d = 10 mm)-specimens, as compared to the other notched specimens.

But there appears to be a clear trend for the notched specimens of the T-orientation: the mean value of the failure strain ε_R reduces with increasing notch acuity over the whole range of root radii. The mean values of the failure strain ε_R for the T-, L-, and R-directions with the same notch root radius R_d = 10 mm are approximately 19.2, 18.6, and 22.4 % and are thus comparable. For the smaller notch root radius R_d = 4 mm smaller mean values are obtained for all three directions, but the values are still comparable. However, for the smallest notch root radius R_d = 2 mm the mean values for the T-, L-, and R-orientation are 8.8, 12.5, and 12.7 %; i. e., for the T-orientation a considerably lower mean value of the failure strain is seen. Moreover, whereas the mean values for the L- and R-direction are almost the same for the notch root radii 4 and 2 mm, a further decrease for the mean value of the T-direction specimens is found. Thus, orientation dependence is evident.

The results for the geometrically similar notched tension specimens are shown in Fig. 2-83. It should be recalled that the notch acuity, as measured by ϕ_0/R_d, is constant (=1), but it is the least of the three values shown in Fig. 2-82, i.e., ϕ_0/R_d = 1, 2.5, and 5. Therefore the theoretical triaxiality ratio is the same for all three sizes and equal to σ_m/σ_{eq} = 0.60.

The minimum initial diameter ϕ_0 at the root of the notch takes the value 6, 10, and 15 mm; thus the scale factor is only 2.5, a relatively small size variation. All test results shown in Fig. 2-83 are from specimens oriented along the longitudinal (L) direction of the pipe. The data seem to demonstrate that the smaller the specimen, the larger the scatter of measured diametrical failure strains. However, a considerable larger number of tests (almost a factor of 2) was done with the small specimens and therefore the limitation mentioned with respect to results in Fig. 2-82 applies also here. Devillers-Guerville et al. mentioned that the minimum values are ”almost the same for the three different sizes, but as the diameter increases, the maximum values are reduced. Consequently, the mean value of ductility decreases with specimen size”. This argument is generally valid only if the distribution is symmetric. The actually calculated mean values are shown in Fig. 2-83 and they indeed prove the decrease of the mean ductility value with increasing size: the decrease of the ductility is about 31 % (relative) if the minimum diameter is increased from 6 to 15 mm. Devillers- Guerville et al. (1997, [2.56]) suggested the conventional qualitative probabilistic explanation: “the bigger the specimen, the greater the probability is of finding a very damaging cluster which will lead to the premature failure of the material.”

The test of the notched beam specimens (standard cross section 10x10 mm) under three-point-bending did not include families of geometrically similar specimens. The notch acuity was varied by using (i) Charpy U-, V-, and precracked notched specimens with otherwise the same dimensions, and (ii) Charpy V-notched specimens of varying thickness (5, 10, and 20 mm),as shown in Fig. 2-84. The axis of the specimen was in the tangential (T)-direction, the axis of the notch in the longitudinal (L)-direction, and the crack propagation in the radial (R)-direction. As seen from Fig. 2-84, the notch tip radii but also the notch depths were considerably different; thus a single parameter variation was not done. For the slow bending tests, the notch (crack) mouth opening was measured with a clip gage extensometer, but also the load versus displacement (presumably the load-point displacement) curves were recorded. All slow three-point bending tests were done with the same ram rate of $5\text{x}10^{-3}$ mm s^{-1}. From the load-displacement records the fracture energy was determined as the area under the load-displacement curves. From this an area specific energy was calculated by dividing the work by the (initial) ligament area ahead of the notch or crack. This area specific energy was separated into two parts: the energy up to the load maximum and the energy beyond the load maximum up to total fracture. Devillers-Guerville et al. state that the energy before reaching

the maximum load corresponds to the “crack initiation energy”, as it was shown by ”electrical determination of the crack initiation and by observations of sections of interrupted specimens”. Accordingly, the “macro-defect” initiates when the maximum load is reached. Since this is a very important statement and by no means an obvious matter, the authors should have given convincing details of the experimental basis of this finding.

The results of the energy partition are shown in Figs. 2-85 and 2-86. Fig. 2-85 shows the scatter and mean values of the area specific work for “crack-initiation” and “crack-propagation” of the U-, V- notched, and the precracked specimens with 10x10 mm cross-sections. A considerable scatter of the crack initiation energy of the U-notched specimens was obtained (16 tests). This scatter is not only due to the scatter of the maximum load but obviously also due to scatter of the corresponding load-point displacement, as seen in Fig. 2-87 which depicts, among others, experimental results of load versus notch mouth opening curves of nominally identical U-notched specimens. Fig. 2-85 seems to prove a reduction of the scatter of the crack initiation energy with increasing acuity, but the number of tests was not well balanced and the depth of the V-notch was not comparable with the two other specimen types. Furthermore, the mean value of the crack initiation energy significantly decreases with increasing acuity, especially if one compares the U-notched and the precracked specimens which have the same notch or crack depths. On the other hand, the mean value and the scatter of the crack propagation energy are almost equivalent for all three geometries. Therefore, for these notch geometries the influence of the notch acuity on the total area specific fracture work is due to the sensitivity of the crack initiation energy.

Fig. 2-86 displays the area specific crack initiation and propagation energies for U-notched Charpy type specimens when only the specimen thickness is varied (5, 10, and 20 mm, non-similar specimens). The crack initiation energy of the thin (5 mm) specimens are subject to an extreme scatter (from about 12.5 to 42.5 J/cm^2) which decreases when the thickness is increased. Here an unbalance of the number of tests is not an argument which jeopardizes this finding (compare the 5 and 10 mm thickness specimens in Fig 2-86). This decrease of the scatter of the crack initiation energy with increasing thickness appears to the plausible (the reviewer) from a probabilistic point of view: the crack initiation at the tip of the V-notch is controlled by finding a damaged zone in front of the notch and the degree of damage may vary, which makes the initiation sensible to the position a thin specimen was taken from; if the thickness is increased, various types of damaged zones are in front of the notch and their number increases; this makes the initiation less sensible.

Fig. 2-86 shows that the mean value of the crack initiation energy decreases when the thickness is increased from 5 to 10 mm, which is the well known thickness effect, but then it remains constant. Here the probabilistic weakest link argument may be used as a plausible explanation. The scatter and mean value of crack propagation energy, however, is fairly insensitive to the change of the specimen thickness. Devillers-Guerville et al. use the weakest link argument to explain this trend: ”crack growth is a rather averaging process, since all the damaged grains ahead of the crack tip contribute to the crack propagation process”. As a consequence the total area specific fracture energy is thickness dependent, especially for thin specimens and this is only due to the thickness dependence of the propagation energy. Unfortunately, these energy partition considerations have not been done for a family of geometrically similar Charpy type specimens and also not for the notched circular tensile specimens, where the data should have been available.

In their conclusions Devillers-Guerville et al. state among others: “Size effect is essentially related to crack initiation. Scatter is reduced when the specimen size increases, but the mini-

mum measured values remain almost the same". However, recalling the previous discussion, here again size and thickness effects are not clearly distinguished.

In fact, it has only been shown that the "thickness effect" is important for the area specific work up to the load maximum which is interpreted (the so called "crack initiation energy") as the instant of crack initiation, but convincing experimental facts for this interpretation were not presented. The reduction of scatter with size was shown for the diametrical failure strain at the minimum section of notched tensile specimens, but this seems to be still uncertain since the test numbers were not well balanced. The reduction of scatter with increasing thickness, however, was shown for the so called crack initiation energy of U-notched Charpy type specimens but only for thin specimens. Moreover, so far the results are restricted to this cast duplex stainless steel.

Besson, Devillers-Guerville, and Pineau (2000, [2.58]) presented further experimental and theoretical results on scatter and size effects in ductile fracture of three allegedly different cast duplex stainless steels which also had been thermally embrittled. They extended also their qualitative description of the microstructural damage process: microcleavage cracks nucleate in the embrittled ferritic laths, and then stop at the interface with the austenite; they subsequently grow into the austenite accompanied by plastic deformation of the austenite and form cavities; eventually, these cavities coalesce to produce a macrodefect. A typical feature of the damage nucleation is that the microcracks are not uniformly distributed but are grouped in clusters of about 1 mm^3 (Ref.[2.56]). These clusters match with specific austenitic grains which are preferential oriented for single slip (see Ref. [2.56] and references cited therein).

The three investigated heats are characterized as follows. Similar to the material studied in Ref. [2.56], the first material, denoted by Y4331, is described to be part of a centrifugally cast pipe (external diameter 400 mm, thickness 40 mm) with the a similar microstructure as the material CF8M (columnar structure). The two other heats (denoted by BT and BL) are statically cast ingots (215x65x45 mm). The ferritic laths in the material Y4331 are much larger than in the materials BT and BL. However, in contrast to Y4331, the microstructure of BT and BL is equiaxed and isotropic. The chemical compositions are listed in Tab. 2-44. The materials were aged at 400 °C for 700 h (Y4331) or 30 000 h (BT and BL).

The mechanical testing included:

- Quasistatic tensile testing of smooth and notched axisymmetric bars similar to the testing of the material CF8M:
  Material Y4331
  Specimens cut out along the tangential (T) direction of the pipe
  Smooth specimens: diameter ϕ_o= 10 mm, gage length 25 mm
  Notched specimen: minimum diameter ϕ_o= 10 mm,
  notch root radius R_d = 10, 4, 2 mm
  the notation AEχ (AE10, AE4, AE2) is used with

$$\chi = 10\frac{R_d}{\phi_o};$$

  diameter outside the notch = 18 mm

Materials BT and BL
Specimens taken from the center of the ingots (microstructure equiaxed and isotropic) and cut in the plane of the mould along the longest direction (65 mm).
Smooth specimens: diameter ϕ_o= 6 mm, gage length?
Notched specimens: minimum diameter ϕ_o= 6 mm
notch root radius R_d = 6, 2.4, 1.2 mm
χ = 10, 4, 2

- Quasistatic tensile tests of a family of geometrically similar specimens of only material Y4331; the direction of the specimen was not explicitly indicated. Same dimensions as for CF8M (Ref. [2.56]).
- Quasistatic three-point bending of non-similar Charpy type U- and V-notched as well as precracked specimens. Geometry as for material CF8M (see Fig. 2-84). For the pipe material Y4331 the axes of the specimens were in the tangential (T)-direction, the axes of the notches in the longitudinal (L)-direction and the crack propagation in the radial (R)-direction (same as for material CF8M). For the ingot materials BT and BL "the crack direction corresponds to the second longest dimension of the ingot"[48].
- Quasistatic three-point bending of non-similar Charpy type U-notched specimens of material Y4331 with varying thicknesses (5, 10, 20 mm). Geometry as for material CF8M (see Fig. 2-84). No indication of specimen orientation in the pipe.
- Quasistatic testing of a set of nominally identical compact tension (CT) specimens of material Y4331 according to the ASTM E873-89 standard; determination of the J-integral at crack initiation $J_{0.2}$ (crack growth of 0.2 mm) and the tearing moduls dJ/da. Description of the specimen preparation and results insufficient.

The results for the smooth and non-similarly notched tension specimens are collected in Fig. 2-88 which represents the diametrical failure strain $\bar{\varepsilon}_R$ at the root of the neck or notch, respectively, for the three materials.

The data for the smooth tension specimens of material Y4331 (5 tests) are almost exactly the same as those obtained for the pipe material CF8M (Fig. 2-82). Comparison of the data of the non-similarly notched tensions specimens (AE10 $\triangleq$ R_d = 10 mm, AE 4 $\triangleq$ R_d = 4, AE 2 $\triangleq$ R_d = 2 mm) of the pipe material Y4331 (Fig. 2-88) with the corresponding data of the pipe material CF8M (Fig. 2-82) shows again perplexing agreement if all CF8M data are combined without discrimination of the T-, L-, and R- orientation. From this one may conclude that the two materials and test series are identical. In fact, the same agreement is found when the Y4331-data for the geometrically similar family of notched specimens (Fig. 2-89) are looked at and are compared with the results of the pipe material CF8M (Fig. 2-83), provided again, no discrimination is made for the specimen direction of the CF8M data (failure strain for ϕ_o = 10 mm in Fig. 2-88 includes all CF8M data for ϕ_o = 10 mm). In the reviewer's opinion, the ignorance of directional influences is not acceptable because this introduces an artificial extension of the scatter and mixes effects.

A comparison of the chemical composition of material CF8M (Ref. [2.56], Tab. 2-43) and material Y4331 (Tab. 2-44) shows slight differences and also the dimensions of the cast pipe

[48] This statement is not compatible with the dimensions of the specimens (Fig. 2-84) and the dimensions of the cross section of the ingots (65x45 mm).

do not completely agree. Unfortunately, the origin of the chemical data was not outlined. Possibly one set was provided by the manufacturer and the other was generated by the laboratory. This inconsistency will be discussed later.

Summarizing, the Y4331-data for the smooth and non-similarly notched tensile specimens as well as the data for the geometrically similar notched tension specimens are the same as those published in Ref. [2.56] for the pipe material CF8M. The only new data are those for the ingot materials BT and BL in Fig. 2-88. For each type of test only two experiments were performed and also their diameter ϕ_o was less than that of the Y4331 or CF8M material ($\phi_o = 6$ instead of 10 mm) because of limited availability of ingot materials. Due to the different diameter ϕ_o, a quantitative comparison between the ingot materials (BT and BL) and the pipe material Y4331 (CF8M) should be made only with caution. In this connection one should recall that the decrease of the diameter of even smooth specimens increases the area reduction or diametrical strain at fracture of ferritic and austenitic steels (main size effect in smooth tension specimens; see Malmberg, Krompholz, Solomos, Aifantis (1999, [2.62]).

The BT- and BL-data show a considerable scatter and their mean values do not compare well with those of the pipe material Y4331. However, the general qualitative trend – decrease of the mean value of the diametric failure strain $\bar{\varepsilon}_R$ with increasing notch acuity ϕ_o / R_d – is also seen here and seems to be even more pronounced than that of the pipe material Y4331 (CF8M).

Similarly to material CF8M, the results for Charpy type specimens under three-point bending are presented for materials Y4331, BT, and BL in Figs. 2-90 (a, b, c). Fig. 2-90 (a) shows the initiation, propagation, and total energies only for the U-notched specimens of the three materials. The scatter bands of material Y4331 agree with those of material CF8M in Fig. 2-85, the only difference being that Fig. 2-90 (a) gives the individual measurements. Thus, the new data in Fig. 2-90 (a) are those of the materials BT and BL which yield comparable results as those of Y4331 or CF8M.

Fig. 2-90 (b) depicts the influence of the notch tip acuity on the initiation, propagation, and total energy of material Y4331 and these scatter bands agree again completely with those of material CF8M shown in Fig. 2-85. Finally, Fig. 2-90 (c) shows the influence of the specimen thickness for U-notched specimens of material Y4331, again in agreement with the results for CF8M in Fig. 2-86. Therefore, the results for material Y4331 are the same as for material CF8M (Ref. [2.56]), except that in Fig. 2-90 (a, b, c) each measured value is indicated. Thus, a further discussion of Figs. 2-90 (a, b, c) is superfluous.

Besson et al. (2000, [2.58]) presented also the $J_{0.2}$- and dJ/da-data for CT-specimens of material Y4331, i.e., 81 ± 31 (kJ/m^2) and 65 ± 20 (MPa), based on two groups of tests (altogether nine tests), which, however, remain undefined. Also the definition of the range is not clear. From this Besson et al. state that "in agreement with results on Charpy specimens, dispersion is more important on initiation than on crack propagation".

In the reviewer's opinion this statement is fairly premature if not erroneous. First of all, looking at the individual $J_{0.2}$-and dJ/da-measurements [Ref. 2.58], one finds roughly a ± 50 % variation with respect to the mean value if maximum and minimum values of both quantities are considered. Secondly, CT-specimens are usually precracked by fatigue (see Anderson (1995, [2.83])) and therefore a comparison with Charpy type specimens under three-point bending should be made only if they are precracked, too. However, observing Fig. 2-90 (b), the precracked 10x10 mm Charpy specimens do not prove that dispersion is more important on initiation than on crack propagation, but the opposite is seen. Thus, the above conclusion of Besson et al. is not acceptable.

The experimental and theoretical work of this French research group has put similar attention to a carbon-manganese steel ***(Decamp, Bauvineau, Besson, and Pineau (1997, [2.63]))*** used in pressurized water reactors (PWR's; e.g., secondary piping components at a service temperature of 300 °C). To a large extent, the type of notched tension specimens and testing was similar to the previous work. Uniaxial tensile tests were performed at 300 °C on axisymmetric notched specimens. As previously, two types of tensions tests were realized:

- Quasistatic tensile tests on notched specimens where the acuity of the notch was increased, but other dimension were held constant: minimum diameter at the root of the notch $\phi_o = 10$ mm, diameter outside the notch in the uniform sections $\phi_e = 18$ mm, overall gage length not indicated, notch root radius $R_d = 10$ (AE10), 4 (AE4), and 2 (AE2) mm where the notation AEχ is defined as before (Fig. 2-91). The specimens were cut from a secondary piping component with the axes along the tangential direction (T) of the pipe.
- Quasistatic tensile tests of a family of geometrically similar notched tensile specimens: minimum diameter ϕ_o= 3.75, 6, 10, and 15 mm, notch root radii R_d = 1.5, 2.4, 4, and 6 mm, diameter outside notch ϕ_e= 6.75, 10.8, 18, 27 mm (Fig. 2-91). Note that the size range includes a smaller specimen (ϕ_o=3.75 mm), as compared to the previous investigations; thus a size factor of 4 is involved. Moreover, the acuity ϕ_o/R_d = 2.5 is increased, as compared to the previous value ϕ_o/R_d =1. The specimen axes are also along the tangential direction of the pipe, but specimens were cut from a different part of the pipe component.

The specimens were instrumented with a diametrical extensometer to determine the minimum diameter at the notch. From this the diametrical strain was defined[49] as $\bar{\varepsilon} = 2 \log (\phi_o/\phi)$. Of course this was accompanied by the load measurement. All tests were performed at 300 °C with a mean strain rate[50] of $5 \cdot 10^{-4}$ s^{-1}.

The chemical composition of the C-Mn steel is given in Tab. 2-45. The mechanical properties at 300 °C and a strain rate of $5 \cdot 10^{-4}$ s^{-1} of specimens in the tangential direction are reported to be: yield stress 190 MPa, ultimate stress 500 MPa, elongation at fracture 28 %, and area reduction 52 %. However, the pipe material is not perfectly uniform, as demonstrated by the stress strain curves in Fig. 2-92 of standard tensile specimens from two different parts of the component (GU2: material for the notch radius variation – geometry effect – and GV2: material for size variation). Unfortunately, the position influence beyond the load maximum was not reported. The two curves in Fig. 2-92 likely represent results of single tensile tests. Whether the variation in Fig. 2-92 is due to a true positional effect, is not known, since the scatter of neighbouring specimens was not documented.

Microstructural investigations revealed ferritic-pearlitic bands and elongated inclusions resulting from hot - rolling conditions of the pipe manufacturing. A majority of inclusions were MnS particles which are due to the relatively high sulphur content (210 wt.ppm). It was shown that the inclusions were concentrated in clusters producing zones of high inclusion densities. The average dimension of MnS inclusion ranged from 3 to 28 μm, depending on the

[49] Note that in Ref. [2.56] and [2.58] the natural logarithm was used.

[50] Decamp at al. state that the "mean" strain rate is $5 \cdot 10^{-4}$ 5^{-1} . There are doubts that the diametric strain $\bar{\varepsilon}$ is controlled in the tests. Possibly the strain rate value corresponds to the mean overall strain rate within the gauge length along the axis.

direction within the pipe (radial, tangential and longitudinal). Considerable work was done to determine histograms showing the distribution of inclusion volume fractions, since the inclusions are responsible for the initiation of the ductile rupture.

The experimental "ductilities" are presented in Fig. 2-93 and 2-94. The ductility shown in the figures corresponds to the diametrical strain at the root of the notch when "the load suddenly drops". This is, in fact, not a very precise definition because, first of all, it may depend on the kind of presentation of the load history, i.e., load vs. time, load vs. diameter change, or other; secondly, after the load maximum a continuous decrease of the load is observed and the instant where the fall-off of the load is faster is not necessarily sharp (see also the discussion of the point of "failure" in the work of Devillers-Guerville et al. on page 70).

Fig. 2-93 shows the influence of the notch radius variation (or acuity) on the "ductilities" (diametric strain at the root of the notch at "failure") versus the stress triaxiality σ_m/σ_{eq}. The theoretical value σ_m/σ_{eq} was determined by finite element calculations which depend, of course, on a set of assumption not explained in Ref. [2.63]. The triaxiality depends nonlinearly on the notch radius. As the acuity, defined by the ratio ϕ_o/R_d, increases, the stress triaxiality increases, too. Fig. 2-93 depicts a decrease of the mean value of the ductility. A decrease of the scatter with increasing acuity is not clearly evident from these results, especially because of the very low ductility value for the AE2-specimen which possibly is an "outlier". The decrease of the mean ductility is about 38 % (relative) when the notch acuity is increased from ϕ_o/R_d =1 to ϕ_o/R_d =5. The results of the duplex stainless steel CF8M, shown in Fig. 2.82 for the same specimen geometries (!), show a similar qualitative trend of the mean values (in the tangential direction) but for much smaller ductilities and smaller stress triaxiality factors. Note that this is related to the different mechanical properties of the two steels (Tab. 2-47).

The size effect is depicted in Fig. 2-94. A quasi-hyperbolic decay of the mean ductility with increasing size but constant acuity ϕ_o/R_d = 2.5 (and constant stress triaxiality σ_m/σ_{eq}=1.0) is seen: for a size factor of 4 the ductility of the smallest specimen (ϕ_o =3.75 mm) decreases with size, especially when the very small and the largest specimens are compared (decrease: 20 % relative). It appears that further increase in size would not yield a further reduction of the ductility. Also an apparent decrease of scatter with increasing size is seen, but again the number of tests is rather unbalanced. Here once more, the authors use the weakest link probability argument to give a qualitative explanation of the decrease of the ductility with size.

Fractographic investigations were also done to examine the damage process of the ductile rupture, i.e., in situ SEM tensile test were performed with smooth specimens at R.T. and 150 °C with the tensile axis in the transverse direction. MnS inclusion cracking and debonding were observed during the early stages of plastic deformation. Therefore, void nucleation was negligible and void growth was the main damage mechanism. This observation was important for the theoretical modelling of the facture process. Following the general understanding, the authors described the fracture process by growth and coalescence of voids (related to the MnS inclusions) caused by localized shear failure (shear localization) of the matrix material between the cavities. For further details of the fractographic results the reader should consult Ref. [2.63].

A similar carbon manganese steel was used by ***Marini, Carassou, Wident, and Soulat (1998, [2.64])*** to determine the diametrical strain at failure of a family of geometrically similar notched tension specimens. This result was used to calculate the theoretical critical volume fraction of cavities at fracture or equivalently the critical relative cavity radius $(R/R_o)_c$. R_o and

R are, respectively, the initial and the instantaneous cavity radii. With this result the fracture toughness $J_{0.2}$ (at crack initiation) of CT-specimens of the same material was calculated and then compared with the experimental results of a family of geometrically similar CT-specimens. The easy understanding of the paper is limited since the actual experimental failure strains of the notched tensile specimens were not reported. Instead derived quantities were documented and for their explanation Marini et al. referred extensively to previous publications which were not consulted by the reviewer. Thus, some of the involved premises remain unclear.

The chemical composition of the C-Mn steel is given in Tab. 2-45. Obviously, this steel is fairly similar to the C-Mn steel used by Decamp et al. (1997, [2.63]). This similarity is also found for the microstructure: the material is an hypo-eutectoid steel and has a banded ferritic-perlitic microstructure. The high sulphur content and its low solubility leads to MnS-inclusions which are dominant and which tend to form clusters. The pipe component, which was the material source for the specimens, contained inclusions strongly anisotropic in shape due to the pipe manufacture: the average lengths were 21, 9, and 3 μm in the longitudinal (L), the transverse (T, tangential), and the short-transverse (S-T, radial) direction, respectively. The average distance of the clusters was 250 μm and the average volume fraction was around $1.5 \cdot 10^{-3}$.

The characteristic tensile and impact *(KCV)* data at 100 °C in the longitudinal and the radial direction of the pipe are collected in Tab. 2-47. Whereas the 0.2 % yield stresses and the ultimate stresses are independent of the orientation, the uniform elongation and the elongation at fracture show a reduced ductility in the radial direction. This is even more pronounced for the reduction of area *(Z = R.O.A.)* at fracture and the Charpy-V notch impact energy *KCV*. Although the yield and ultimate stresses are the same for the two directions, the different uniform elongations (strain at maximum stress) imply that the stress-strain curves are different, especially for large plastic strains: the data imply an increased strain-hardening in the radial direction.

Tensile tests were performed on notched circular specimens at 100 °C under displacement control with a servo hydraulic tension machine, presumably under constant strain rate (information not available). The procedure followed the recommendations of the European Structural Integrity Society (ESIS) for this type of test. The reduction of the notch root diameter was measured during the tests (clip gages attached) and the diametrical logarithmic strain at "fracture" was calculated according to

$$\varepsilon_r = 2 \ln\left(\frac{\phi_o}{\phi_r}\right)$$

where ϕ_o and ϕ_r *are* the initial and the "final" notch root diameter. The precise instant of failure or fracture in this continuous measurement is not defined in the article of Marini et al.

The geometrically similar family of specimens is shown in Fig. 2-95. The specimen geometry corresponds to that of the specimen families used by Decamp et al. (Ref. [2.63], see Fig. 2-91 in this report) and Besson et al. (Ref. [2.58]), except for the notch root radius of the smallest specimen (3.6 mm instead of 3.75 mm). The specimens were cut from the pipe component along the longitudinal (L) and the radial (S-T short-transverse) direction.

The measured diametrical strain values were not documented in Ref. [2.64] but were used for the critical cavity radius ratio $(R/R_o)_c$. According to theoretical modelling, the authors employed a relation between the average plastic strain ε_r at fracture and the critical cavity radius ratio $(R/R_o)_c$ given by

$$ln\ (R/R_o)_c = 0.283 \int_{\varepsilon n}^{\varepsilon r} exp\left(\frac{3}{2}\ \frac{\sigma_m}{\sigma_{eq}}\right) d\ \varepsilon_{eq}\ \ . \qquad (2.53)$$

Here ε_n is the strain at which cavity nucleation starts and σ_m/σ_{eq} is the stress triaxiality factor. The determination of the integral requires numerical evaluation during the whole deformation process with some finite element model if the triaxiality factor changes due to large deformations. Actually the equation should represent a spatially local relation. The application to the tension of notched specimens (nonuniform stress and strain distribution) and the use of the average diametrical strain ε_r as the upper limit of the integral requires an appropriate modification to be applicable. Possibly an average value of the triaxiality factor within the cross section was used in Equ. 2.53, but the authors give no information. The nucleation strain ε_n was set to zero since for the C-Mn steel the cavity expansion starts as macroscopic plasticity arises.

The result of the integration process is seen in Fig. 2-96 which shows the calculated natural logarithm of the ratio of the cavity radii versus the instantaneous diametrical strain. Then the measured diametrical strain ε_r at fracture determines the critical ratio $(R/R_o)_c$ as a derived quantity shown in Fig. 2-96. The theoretical plasticity model is not described by the authors, but it is said that conventional incremental plasticity was used. This would imply that the plastic response is not coupled to the porosity evolution. In any case, the theory as such obviously does not involve an internal length scale and yields therefore size independent stress and strain fields. Thus, the curve in Fig. 2-96 is size independent by assumption, i.e., it applies to all members of a geometrically similar specimen family. Unfortunately, the authors did not comment on the finite element modelling of the notched round specimens. The choice of a mesh size is necessary and actually the mesh should be scaled according to the size of the specimens to prevent its influence on the solution if calculations were done for all specimen sizes. However, the reviewer believes that Marini et al. performed only a single calculation for one specimen size within this family since only a single curve is shown in Fig. 2-96. For further comments on this issue see the reviewer's remarks on the calculations for the CT-specimens below.

The critical cavity ratio criterion, i.e., the theoretical failure criterion, implies (Ref. [2.64]) that "this critical value is assumed to be an intrinsic characteristic of the material for a given testing direction and is considered to be independent of the stress state". Thus, changing just the size of the specimen with dimensions in proportion, the constant critical ratio $(R/R_o)_c$ would yield the same fracture strain ε_r, provided the stress fields and therefore also the triaxiality factors are the same (theoretical similarity!) and this is, in fact, the case as pointed out above.

Fig. 2-97 depicts the derived critical ratio $(R/R_o)_c$ versus the specimen size (i.e., the initial minimum diameter at the root of the notch) for the longitudinal (L) and radial (S-T) direction. Since the obvious size dependence and scatter of $(R/R_o)_c$ is solely determined by the size dependence and scatter of the measured diametrical strain ε_r at fracture, Fig. 2-97 represents indirectly the size dependence and scatter of the fracture strain ε_r. Clearly, the size dependence is strongly depending on the specimen orientation: for the longitudinal (L) direction a quasi-hyperbolic decay with increasing size is seen and the scatter apparently decreases with size; for the radial (S-T) direction almost no effect is observed. The size dependence of the fracture strain ε_r or the critical cavity radius ratio $(R/R_o)_c$ definitely prove that the used theoretical concepts are not appropriate. Marini et al. state that this effect is due to the heterogeneous distribution of the inclusion which "can be interpreted using a probability local approach presented elsewhere" (see Ref. [2.64] and references cited therein).

In a second test series Marini et al. determined the fracture toughness[51] $J_{0.2}$ (ASTM Standard E813-87 for J_{IC}-testing) and the (initial) slope[52] dJ/da of the J-resistance curve[53] of a family of geometrically similar side grooved compact tension (CT) specimens with sizes 1/2T, 1T, and 2T[54]; the actual relative crack lengths are not indicated. The specimens were cut along the longitudinal (L) and the short-transverse (S-T, i.e., radial) direction of the pipe component but a precise definition of the crack orientation was not given. Probably the orientation was L-S and S-T according to the terminology in Fig. 2-98. For each size three nominally identical specimens were tested. The average fracture properties at 100 °C for all three sizes and the two directions are listed in Tab. 2-48.

The $J_{0.2}$-data for the longitudinal direction show almost no size dependence for crack initiation but the slope dJ/da or tearing modulus[55] clearly is size dependent: it decreases by 43 % when the size is increased from the small (½ T) to the largest (2T) CT-specimen. Since the tearing modules is a measure for the stability of the crack propagation, the dJ/da-data demonstrate that larger CT-specimen are more susceptible to unstable crack propagation.

The data for the short-transverse direction encompass only the two sizes ½ T and 1T. These fracture data are much smaller than those in the longitudinal direction, but a size dependence is seen for the $J_{0.2}$-value and an inverse tendency for the dJ/da-value.

Since the scatter of the data is not indicated at all and the size variation involves only a factor of two, it is difficult to assess this result. Marini et al. simply state that the "fracture toughness $J_{0.2}$ is very different in the two directions, but for a given direction, no size effects are measurable". Although fracture data are very different in the two directions, the fractographic investigation (SEM) showed a ductile fracture mode for all (!) specimens.

These experimental data have been compared with a theoretical approach based on the critical cavity radius ratio obtained from the tension tests on the notched round specimens described above.

Marini et al. referred to theoretical results of Mudry (see Marini et al., Ref. [2.64]) who derived a relation between the fracture toughness $J_{0.2}$ and the critical cavity radius ratio $(R/R_o)_c$ for small scale yielding as follows:

$$J_{0.2} = k\, L_c\, \sigma_y\, ln\, (R/R_o)_c\ ; \tag{2.54}$$

here k is a material constant depending on the hardening coefficient, L_c is a characteristic length frequently taken to be the average distance between inclusions, and σ_y is the yield stress. For large scale yielding as in this study, however, Equ. 2.54 did not apply at fracture initiation and finite element calculations were needed. Since the CT-specimens were side grooved, a two dimensional calculation was sufficient.

---

[51] J-value at 0.2 mm offset line of the J-resistance curve, see Ref. [2.28].

[52] dJ/da is proportional to the tearing modulus $T_R = \frac{E}{\sigma_y^2}\frac{dJ}{da}$.

[53] J vs. Δa curve.

[54] 1T specimens: thickness B=1 inch, width W=2 inches, relative crack length 0.5≤a/W≤0.7.

[55] The tearing modulus describes the change of the fracture resistance (J-resistance) with increasing crack extension Δa.

Finite elements at the crack tip were squares, their side length set equal to the average spacing of inclusion clusters (250 μm); without explicit saying, this element form and size was kept constant for all sizes of the CT-specimens. As Marini et al. pointed out, this inclusion cluster spacing "is a characteristic distance for the ductile fracture of the material: crack propagates from clusters to clusters by localization of the strain between a damaged cluster and the crack tip." This instant of localization was assumed to be attained when the critical cavity radius ratio was reached.

As mentioned before, conventional incremental plasticity (without coupling to a porosity model) was used. The instantaneous ratio R/R_o was obtained from Equ. 2.53 for a (crack tip) finite element after averaging the stress and strain field over the element in the CT-specimen. The instantaneous *J*-value was obtained from an internal routine of the finite element code. Thus, a numerical relation between the instantaneous values of R/R_o and *J* was obtained for a CT-specimen. Since the finite element meshes were the same for both the small and the large CT-specimens, this solution is possibly mesh dependent, especially if softening occurs due to large deformations. Then an artificial size-dependence is introduced and the numerical relation between R/R_o and *J* would depend on the specimen size. Marini et al. did not comment on this aspect at all. It is very likely that they did only a calculation for a single specimen size, e.g., the 1T-specimen as shown in Fig. 2-99, implying that the solutions were mesh independent. Marini et al. state that "these calculations are independent of the testing directions because the stress-strain law is independent of these directions". However, the uniform elongation in Tab. 2-47 clearly shows that the strain hardening for the longitudinal direction is less than for the short-transverse (radial) direction; therefore different stress-strain laws should have been used, specifically for larger plastic strains.

Presumably a single numerical *J* vs. R/R_o curve was obtained (Fig. 2-99), the size dependent critical ratios $(R/R_o)_c$ for the notched round specimens in Fig. 2-97 yield a wide set of predicted fracture toughness values ranging from 110 to 245 kJ/m^2 for the longitudinal direction, whereas the experimental data show a very small variation (177 to 184 kJ/m^2 (Fig. 2-100). Therefore, using small notched round specimens to determine the critical cavity radius ratio yields fracture toughness values for CT-specimens which are too large and are thus nonconservative. However, the use of large notched round specimens gives conservative fracture toughness values (Fig. 2-100). Obviously, some intermediate size must be chosen.

In the reviewer's opinion the predictive capability of this theoretical approach is fairly weak. Moreover, the reviewer conjectures that the validity of the correlation of the failure processes in the round notched specimens and in the CT-specimens is questionable for ductile materials. The experimentally determined average failure strain ε_r of the notched round specimens, a strongly size dependent quantity, is related to a catastrophic unstable instant, i.e., when the load "suddenly drops"[56] after passing the load maximum. The experimentally determined $J_{0.2}$-value for the CT-specimens, however, corresponds to the beginning of stable crack propagation which was found to be size independent for the longitudinal direction. But the slope *dJ/da* was definitely size dependent and since it determines the instant of unstable crack propagation (see comment above), this instant would also be size dependent, with the consequence that the global strain at this instant would decrease with increasing size. This possibly implies that the instant of crack nucleation in the notched round specimens, which

[56] See Decamp et al. (1997, [2.63]; note that a precise definition was not given in Ref. [2.64]. At this instant a crack has already been formed in the centre of the specimen.

occurs before the load suddenly drops, and the correlated average diametrical strain at the root of the notch could have been more appropriate measures, which are possibly even less size dependent. For example, acoustic sensors or the potential drop method to detect this instant are conceivable approaches, but this increases the experimental effort considerably.

The long-standing problem of similarity and non-similarity or size effects has gained new impetus in recent years because of the needs of safety assessments in reactor engineering. Worth mentioning is its importance for: (i) the transferability of mechanical test results of geometrically similar scaled down structural reactor models to the full scale structures using similitude laws and (ii) the validity of small scale laboratory type test results and their use as a basis for the computational modelling of large scale components.

In support of small scale tests of reactor structures and to improve and extend basic knowledge, a joint experimental and theoretical activity of several institutions[57] has been performed as part (Task 5- "Size Effects") of the recent ***EU-project REVISA***[58]. All activities of the REVISA-project have been summarized by ***Devos, Auerkari, Lämmer, LeBer, Messelier-Gouze, and Malmberg (2002, [2.65] and [2.66])***[59] in an abbreviated as well as in an extended report.

The experimental part of the size effect studies consisted of screening material tests up to failure of different families of geometrically similar specimens for different temperatures and strain rates. Three different nuclear steels were investigated:

- the ferritic-bainitic LWR-reactor vessel steel 20MnMoNi55;
- the austenitic steel X6CrNiNb1810 used for upper internal structures of the vessel;
- the ferritic steel 26NiCrMo146 used for the bolting of the reactor vessel head.

The tests included tensile tests of smooth and blunt-notched circular specimens with a diameter from 3 to 30 mm, three-point bending tests of U-notched bars (width: 10, 25, 140 mm), tension creep of smooth circular specimens and others. In this review attention will be restricted to the testing results of notched specimens under tension and three-point bending of the ferritic reactor vessel steel 20MnMoNi55 subjected to quasi-static strain rates. These test configurations are similar to some of the test results reviewed above and allow comparisons.

The ferritic steel was cast from a single heat in the form of a single bar. Sawing and forging produced eight plates (1000x500x70 mm). Detailed cutting plans were provided such that the specimens of different type and size were distributed over the plates, the larger specimens positioned at the midplane, the smaller ones through the thickness (70 mm). Unfortunately, for manufacturing reasons the small specimens were grouped together in small sections of the plates such that generally the smallest specimens were not located in the neighbourhood of the largest ones. Standard tensile and Charpy impact specimens of one size were also distributed over the plates, and were used for quality assurance and homogeneity assessments (QS-specimens). These specimens were located at the ends (position 01 and 03) and at the mid-

[57] Forschungszentrum Karlsruhe, Germany; Paul Scherrer Institut, Villigen PSI, Switzerland; European Commission, Joint Research Centre, Ispra, Italy; Aristotle University of Thessaloniki, Greece

[58] REVISA: Reactor Vessel Integrity in Severe Accidents, contract F14 S-CT96-0024

[59] The reviewer was group leader of Task 5-„Size Effects" of the REVISA Project and was strongly engaged in the theoretical work (gradient plasticity and size effects), but he was also extensively involved in the evaluation and discussion of a large part of the experiments. Therefore, the reader is asked to be indulgent towards the reviewer for this part of the review if his criticism is possibly insufficient sometimes.

point (position 02) of one diagonal of each plate. All specimens were oriented parallel to the long edges of the plates.

Quality control and homogeneity assessment consisted of chemical analysis, metallography, hardness tests, as well as tensile and Charpy impact tests at R.T. and 300 °C (Krompholz, Kamber, and Kalkhof (1999, [2.67]); Malmberg, Dolensky, and Krompholz (2000, [2.68])). The results obtained for the 20MnMoNi55-plates confirmed the specifications and any significant inhomogeneity could not be derived from the standard chemical analyses and metallography, nor from the hardness tests. However, metallographic investigations of the undeformed parts of used tensile specimens done later revealed bands of brittle carbide segregations parallel to the long edges of the plates (Materna-Morris, Graf, Zimmermann, and Malmberg (2002, [2.69])); these segregations appear to be typical for this steel. Moreover, the tensile test with the QS-specimens demonstrated position dependent material properties within the ferritic plates and through their thicknesses, as well as from plate to plate. At room temperature almost all plates show at position 01 a reduced 0.2 %-yield stress, an increased ultimate stress and a decreased area reduction at fracture, as compared to positions 02 and 03 (position effect). For example, for plate 2 the corresponding average percentage deviations are 15 % reduction of the yield stress, 3.6 %[60] increase of the ultimate stress, and 9 % reduction of the area reduction (Devos et al. (2002, [2.66]). This systematic inhomogeneity is a consequence of the manufacturing procedure of the eight plates from a single long bar. At 300 °C, however, the inhomogeneity is reduced, especially the area reduction becomes rather uniform. When the size effect tests are evaluated, this systematic position influence must be properly accounted for to prevent misinterpretations.

The families of geometrically similar specimens and their test conditions are briefly described as follows:

- Tensile tests at room temperature (R.T.) and 400 °C of blunt-notched (T-type) circular specimens (Fig. 2-101; diameter D_o = 3, 9, and 30 mm; gage length-to-diameter ratio = 6); circumferential semicircular notch at the center (notch radius R_o =notch depth, R_o/D_o = 1/10); average strain rates are $2 \cdot 10^{-5}s^{-1}$ and $10^{-3}s^{-1}$ and refer to the gage length. In addition, tensile tests of smooth (R-type) specimens with the same gross dimensions and test conditions were made to assess similarity or size dependence under a quasi-homogeneous strain distribution.
- Three-point bending tests at R.T. of U-notched (S-type) bars with rectangular cross section (Fig. 2-102; thickness *B*-to-width *W*-to-length *L* ratio 1/2/5.5; U-notch depth-to width *W* ratio 3/10 and notch radius *R*-to-width *W* ratio 1/10; width *W*: 10, 25, 140 mm); scaled supports (span $S = 4\ W$); testing with two sets of scaled cross-head speeds, however, differing in magnitude only by a factor of 5.

As mentioned before, size effect studies of specimens with non-uniform strain distributions due to strain concentrators should be accompanied by tests of smooth specimens to assess whether size influences are already present under quasi-uniform strain conditions. Therefore, such an experimental investigation (tensile tests of R-type specimens) was an integral part of this project (***Krompholz, Kamber, Groth, and Kalkhof (2000, [2.70]))***. The main results are briefly summarized here ***(Malmberg, Krompholz, Solomos, and Aifantis (1999, [2.62]))***. By well-contrived comparisons of different tensile tests, pseudo-size effects due to positional

[60] Some references state a value of 6 % which appears to be a misprint: according to the data by Malmberg, et al. (2000, [2.68]), an average increase of 3.6 % is calculated.

influences on the tensile characteristics were unambiguously identified and could be separated. Thus, the main conclusions are:

(i) The ultimate stress and the uniform elongation are essentially size independent.

(ii) The hardening is essentially similar up to the ultimate stress but deviations and size effects occur when necking sets in.

(iii) Whereas the fracture elongation does not show a consistent trend when the diameter is increased from 3 to 30 mm, the reduction of area after fracture shows no or a slight decrease with diameter change from 3 to 9 mm; but an increase from 3 to 30 mm yields a relative decrease of the area reductions of at most 8 % at R.T.; at 400 %C the relative decrease is about 15 %.

(iv) The normalized radius of curvature R/D_o of the meridional neck contour after fracture shows a non-monotonous (first increase then decrease) size dependence for both strain rates and temperatures; generally, however, the lowest values were found for the largest specimens.

(v) Generally, the smallest specimens fail with cup and cone fracture at both strain rates and temperatures. But the largest specimens fail with a milling cutter type fracture at R.T.. This appears to be induced by carbide segregations (Krompholz et al. (2000, [2.70]); Materna-Morris et al. (2002, [2.69]).

In qualitative terms, the experimental findings agree with observations reported in the literature (Malmberg, Tsagrakis, Eleftheriadis, and Aifantis (2001, [2.71])), the most definite finding being the decrease of the area reduction at fracture with increasing size (Fig. 2-103). An exception is, however, the non-monotonous size dependence of the normalized meridional radius of curvature of the neck after fracture which disagrees with previous observations (monotonic increase with size; Malmberg et al. (1999, [2.62]); Malmberg et al. (2001, [2.71])).

The experimental procedures, the evaluation and the results of the tensile testing of the blunt-notched (T-type) specimens were reported in several publications ***(Krompholz, Kamber, Groth, Kalkhof, and Malmberg (2001, [2.72]); Malmberg, Krompholz, Kalkhof, Solomos, and Aifantis (2001, [2.73]; Devos et al. (2002, [2.66]))***, the most detailed one being the report by Krompholz et al. (2001, [2.72]).

The tensile testing of the blunt-notched (T-type) specimens at R.T. involved the continuous measurement of the load, the gage elongation, and the diameter change at the root of the notch, as well as the notch opening using a video-extensometer. At 400 °C continuous measurements of the notch deformations could not be made. After fracture the gage elongations and the notch deformations were recorded by joining the broken halves of the specimens.

The small specimens (type T1 = 3 mm ∅) came mainly from position 01 of a single plate (plate 2). This required special considerations in order to account for the associated material inhomogeneity when the experimental results were interpreted. Hereinafter, the following findings and conclusions were obtained.

(i) The nominal stress-strain diagrams (engineering stress at the root of the notch vs. average strain in the gage section) show an overlapping scatter for the medium and large specimens in the whole strain range; this is true for R.T. and 400 °C and for both strain rates ($2 \cdot 10^{-5}$ and $10^{-3}s^{-1}$). The small T1-specimens, however, disclose a larger maximum nominal stress and a softening regime which differs markedly from that of the larger specimens (Figs. 2-104 and 2-105). This increase of the maximum stress can be interpreted as a

pseudo-size effect since the small specimens came from a plate position with increased strength. However, the shift of the stress maximum of the small T1-specimens to larger global strains and their larger softening regimes reflect a size effect, which at R.T. is possibly even partially masked by the reduced ductility of these specimens.

(ii) The nominal stress vs. the quasi-local strains at the notch, namely, the diametrical strain and the relative notch opening measured at R.T. only, show similar trends but, as expected from some theoretical considerations (Tsagrakis, Malmberg, and Aifantis (1998, [2.74]); Malmberg, Tsagrakis, Eleftheriadis, and Aifantis (2001, [2.75])), even more pronounced size influences with a definite pattern (Figs. 2-106 and 2-107): the small T1-specimens show the most extended softening range whereas the ranges of the medium size and large size specimens are successively decreased. The difference between the notch strains at the lowest comparable stress level of the small and the largest specimens amounts up to a factor of 2. The authors suggested that the shift of the maximum of the nominal stress to larger global as well as quasi-local notch strains is due to the size dependence of softening inducing damage processes occurring before the maximum load is reached and leading to crack extension. Unfortunately, steps were not taken to detect crack initiation.

(iii) The quasi-local notch deformation measure after fracture (i.e., the area reduction Z at the root of the notch) is shown in Figs. 2-108 and 2-109 for the fast strain rate ($10^{-3}s^{-1}$) at R.T. and 400 °C and similar results are obtained for the slow strain rate (Krompholz et al. (2001, [2.72]). The results for the area reduction reveals that the quasi-local strain measure of the small T1-specimens tested at R.T. accumulate around two different mean values (Fig. 2-108). As the authors indicate, they are mainly related to two sets of small specimens which come from two adjacent sections (section 0206: data around $Z = 0.7$, section 0204: data around $Z = 0.5$ and below) about 50 mm apart at position 01 of plate 2. Obviously, the results at 400 °C (Fig. 2-109) do not reveal this scatter of the small specimens since, as stated by the authors, they come only from one section and since heterogeneities at this elevated temperature are partially equalized. The authors state that the area reduction and, of course, also the correlated diametric strain show an approximately linear decay with increasing size if the group of the small, less ductile specimens in Fig. 2-108 are excluded. However, it appears that a quasi-hyperbolic decay is a more appropriate description for the size dependence. On the other hand, if all data are included, the size dependence at R.T. flattens out in the range of small specimens. This result very clearly demonstrates that positional influences due to material inhomogeneity may affect the scatter considerably and thus may change the qualitative size dependence of the mean values.

(iv) Another quasi-local notch deformation measure is the relative notch opening. Fig. 2-110 shows the data for the various sizes at R.T. and for the fast rate ($10^{-3}s^{-1}$). Similar results were obtained for the slow rate (Krompholz et al. (2001, [2.72]). As expected, the data for the small T1-specimens separate into two groups for the same reasons as the area reduction data in Fig. 2-108. The three higher data (around 2.0) came from section (0204) whereas the data below (around 1.3) came from section 0206. This implies that the small specimens from section (0204), which yield less area reduction than the small specimens from section (0206), give larger relative notch openings than the specimens set from section (0206). Therefore, the two notch strain measures do not yield the same trend.

Accounting for all small specimens, the mean value of the relative notch opening at R.T. is to some extent insensitive to a change in size. However, at 400 °C (Fig. 2-111), where

positional influences are less important for the small specimens, the qualitative picture of the size dependence of the relative notch opening changes drastically: whereas there is no difference between the medium and the large size specimens of type T2 and T3 and no influence of the strain rate is seen (Krompholz et al. (2001, [2.72]), the small specimens of type T1 (from section (0206) yield a mean relative notch opening which is more than 1.8-times larger. This rather steep decay of the size dependence of small specimens has not been observed for the other quasi-local strain measures. Also the temperature rise from R.T. to 400 °C has only a moderate influence on the medium and large size specimens but a significant influence on the smaller specimens.

(v) A further measure of the notch deformation is the radius of curvature R of the meridional contour of the notch after fracture. Its determination involves the fitting of a circle to the shadow contour of the deformed notch profile after fracture which is a subtle procedure. The reviewer thinks that this may be rather subjective if not the range of the contour and the fitting rules are uniquely prescribed. In Ref. [2.72] the procedure is not described in detail, but from the information given (Fig. 2a in Ref. [2.72]) it appears that the whole contour of the notch is used for the fit. The authors state that in all cases segments of circles could laid into the notch after fracture.

Therefore, starting with a semicircular notch at the beginning of the test, the notch retains approximately its circular contour, but the center of the circle moves outwards. At R.T. and for both strain rates the mean of the normalized radii of curvature R/D_{omin} (D_{omin}: minimum initial diameter at the root of the notch, initial value $R_o/D_{omin} = 0.125$) is relatively insensitive to a change in size (Fig. 2-112). The data for the small T1-specimens again separate into two groups, the high values (>0.4) belonging to specimens from section (0204) and the low data related to section (0206). This is, as expected, the same trend as for the area reduction or diametrical strain of the small T1-specimens at R.T.

At 400 °C, however, there is almost no difference between the small and the medium size specimens but the large specimens yield considerably reduced normalized radii for both quasi-static strain rates.

It is noted that the number of tests results at R.T. is generally larger than those at 400 °C since these tests were easier to perform. However, in the reviewers opinion this is a shortcoming because this unbalance may induce some distortion in the size effect trend of the mean values at the high temperatures.

The experimental techniques, the evaluation, and the results of the three-point bending testing of the U-notched S-type specimens were reported in detail by ***Krompholz, Kalkhof, and Groth (2001, [2.76])*** and also by ***Malmberg et al. (2001, [2.73])*** and ***Devos et al. (2002, [2.66]).***

The testing was performed at R.T. up to some instant beyond the maximum load but without reaching complete fracture. To obtain the same nominal strain rates at the roots of the notches, the cross-head velocities v_k were scaled (geometric scale factor $\lambda = 14$). Apart from the load, the load-point displacement δ and the notch opening u were recorded with a video-extensometer. Moreover, the crack initiation was detected by the D.C.-potential drop technique. In addition, the crack extension at termination of the experiment was determined by heat tinting and subsequent fracture at liquid nitrogen temperature.

Among others, the results of the continuous measurements were presented as curves showing the

- normalized load (load divided by the limit load) vs. the normalized load-point displacement δ/W or bending angle,
- nominal stress σ_n (load divided by initial ligament area $(W-K)B$) vs. the relative notch opening $(u-u_o)/u_o$ where u_o is the initial notch width,
- the instances of crack initiation according to the potential drop technique,
- characteristic normalized data (i.e. load at crack initiation, maximum load, displacement and bending angle at the load maximum, and especially applied energies up to crack initiation) vs. the size (e.g., width W) of the specimens.

As described in Ref. [2.76], the analysis of the experimental results was done under considerations of positional effects due to the macroscopic material inhomogeneities. The following observations and conclusions were obtained (Ref. [2.76] and [2.73]):

(i) The scatter bands of the nominal stress σ_n vs. the relative notch opening for each specimen size are well separated, except for the very first part (Figs. 2-114 and 2-115): in the elastic regime and for small plastic deformations with relative notch openings of about 15 %, the results are within a single scatter band (Fig. 2-114). This implies that the classical geometric scaling applies within this regime (Malmberg (1995, [1.1]). Beyond this and even before the markers for crack initiation, the results for the three different sizes are clearly separated such that for a given relative notch opening the small specimens yield the largest nominal stress which reduces successively for the medium and large size specimens. The maxima follow the same pattern, which is a decay function with increasing size (Fig. 2-116). The maxima of the largest specimens are only about 70 % of that of the smallest one. The positional effects, observed for yield and ultimate stresses by the homogeneity assessment, can certainly not explain this difference.

(ii) The relative notch openings corresponding to the stress maxima show a considerable scatter for the small S1-specimens in Fig. 2-114. These specimens come from position 01 with the reduced ductility. Therefore, the authors suggest that this influence suppresses their deformation ability. Nevertheless, a clear pattern is observed: the small specimens yield the largest average of the relative notch openings, the medium size somewhat smaller values, and the larger size distinctly smaller values. The relative notch openings of the small specimens are about a factor of 3 larger than those of the largest specimens. The results for the slow speed tests (Fig. 2-115) show a more pronounced pattern for the S1-and S2-specimens. As the authors state, these specimens are not affected by the material heterogeneity. This behaviour is also reflected by the size dependence of the bending angle at maximum load (Fig. 2.117).

(iii) For the instant of crack initiation (arrow markers in Figs. 2-114 and 2-115) the small S1-specimens require larger relative notch openings than the medium size S2-specimens and the critical openings for the large S3-specimens are the smallest. The difference between the relative notch openings at crack initiation for the various sizes, however, is relatively small. In terms of the relative notch opening it is noted that crack initiation in the small specimens occurs long before the maximum stress is reached whereas in the large specimens the maximum stress is obtained shortly after crack initiation.

(iv) The normalized load vs. the normalized displacement δ/W essentially reflects the same trends as above. This is due to the fact that the overall bar deformation is primarily controlled by the notch deformation.

(v) The applied work for crack initiation was determined by integrating the normalized load-displacement curve up to the instant of crack initiation. The corresponding area specific work A_s is obtained by dividing the applied work by the initial ligament area. The data

and their linear regression line are shown in Fig. 2-118 as a function of size. It is noteworthy that the linear interpolation is quite representative. It has a non-zero extrapolated value for very small specimens. Dividing the area specific work A_s by the notch width $2R$ (Fig. 2-102), the required work A_v for crack initiation and per active ligament volume $(W-K)B2R$, assumed to a parallelepiped, is obtained. This volume specific work is plotted in Fig. 2-119 which shows a non-linear decay with increasing specimen size. Obviously, the volume specific work A_v consists of two energy terms:

(a) A size dependent hyperbolic decay term; this corresponds to the Linear-Elastic Fracture Mechanics of brittle materials where a critical specific surface energy, a material constant, determines the initiation of crack extension.

(b) A size independent constant term; this corresponds to classical size independent plasticity.

For the smallest specimens tested (type S1, notch radius R = 1 mm), about 28 % of the total volume specific energy A_v is contributed by the first energy term (a). From Figs. 2-114 and 2-115 it is also seen that the size dependence of the volume specific work A_v for crack initiation consists of two size dependent effects:

- The increase of the nominal stress σ_n for a given relative notch opening before crack initiation when the size is decreased; equivalently, this is seen in normalized load vs. load-point displacement curves (Ref. [2.74]). The authors stress the point that this size dependence has not been observed for the blunt-notched tension specimens. They suggest that the highly non-uniform strain field in front of the U-notch (combined bending and notch effect) may explain the difference, if the plastic material behavior is size dependent due to gradient effects; moreover, a likely other cause may be the (gradient dependent; the reviewer) size dependence of the damage phenomena which lead to crack initiation.
- The second size influence on the volume specific work A_v at crack initiation is seen in the shift of the instant of crack initiation to larger relative notch openings or normalized displacements when the size is decreased (Figs. 2-114 and 2-115)

A crucial aspect of the findings and interpretations related to the instant of crack initiation is the accuracy of the potential drop method and its application. The authors point out in Ref. [2.76] that under ideal conditions the onset of crack growth is correlated with a definite increase of the time derivative of the voltage. But plastic deformation and the associated cross section changes as well as temperature variations affect the change of voltage, too. This introduces uncertainties. Beyond that, the voltage vs. time curves given in Ref. [2.76] illustrate the difficulty to uniquely determine the instant of a "change in the voltage". In the reviewers opinion this determination is susceptible to subjective choices. Therefore, as the authors state, this determination needs considerable expertise. It appears that other methods (e.g. acoustic emission methods) should also be tried.

Independently of the method used, there remains the question what "crack initiation" actually means in an originally uncracked specimen.

In Ref. [2.73] the results of the testing of smooth and blunt-notched tensile specimens as well as the U-notched bending specimens of the ferritic reactor vessel steel 20MnMoNi55 within the REVISA project were summarized. Accordingly, they have revealed size dependencies of various degrees. The influence of material heterogeneity (position effect) could be accounted for, at least in a qualitative sense, due to an extensive homogeneity assessment testing. Under quasi-static conditions the nominal stress-strain diagrams of the smooth and blunt-

notched tensile specimens (R-and T-type) as well as the U-notched bending specimens (S-type) show a certain trend on a phenomenological level:

- The smooth R-type specimens, subjected to a macroscopic uniform strain distribution up to the maximum load, do not reveal a size dependence in this range when the position effect is properly accounted for. However, when necking sets in and a non-uniform strain distribution and damage are developing, the size dependence becomes apparent, e.g., the area reduction at fracture reduces with increasing size.
- The blunt-notched T-type specimens under tension do not show a definite size effect in the nominal stress-strain curves in the first part before the maximum and also in the values of the stress maxima, provided the position effect is taken into consideration. However, the stress maxima of the small specimens are definitely shifted to larger strains and their softening regimes (decaying stress range beyond the stress maximum) are much more extended. Also a size dependent pattern of the softening part is observed with the tendency that, for a given stress level, smaller specimens yield larger deformations.
- Whereas for the above specimens types the size influence apparently does not affect the first part of the nominal stress-strain curves, for the U-notched S-type bending specimens almost the whole nominal stress-strain (e.g., relative notch opening) diagram, even before crack initiation, is affected with the tendency that smaller specimens are "stronger" than larger ones. Only the elastic and a range of "small" plastic strains appear to be size invariant. Also crack initiation is shifted to larger strains when the size is decreased.

The authors make the conjecture that the high non-uniformity of the strain distribution at the root of the notch due to the combined bending and the notch effect produces this behaviour.

The testing results of the various specimen types also demonstrate that for size effect investigations it is necessary to determine the complete nominal stress-strain diagrams (preferably with quasi-local strains) than only stress maxima and quantities after fracture, as done in so many previous studies. This allows to detect when the size influence becomes evident. Since it is well known that the propagation of macroscopic cracks induces size effects on stress and strain quantities, it is necessary to determine the initiation of cracks. This would allow to detect whether significant size influences are present before the initiation of cracks, i.e., in the range where plastic deformation and damage evolution are the governing processes. It seems that the results of the three-point-bending tests of the U-notched specimens have shown this.

3 Discussion and Conclusions

The objective of this study was to provide a limited review of mechanical test results of geometrically similar, sharp- or blunt-notched specimens, predominantly made of steel, and under quasi-static loading conditions. Generally, the specimens were of relatively simple shape:

- circular tension specimens with a circumferential notch;
- single-edge-notched bend (SENB) specimens with a rectangular cross section;
- compact tension (CT) specimens;
- several non-standardized specimens and structures.

The early investigations of size effects on notched specimens under quasi-static testing conditions concentrated on load-displacement or bending moment-bend angle records and characteristic data derived from them, such as absorbed energies, maximum loads, characteristic displacements, etc. From the mid-fifties the size invariance or size dependence of typical fracture mechanics quantities, like critical *K*-, *J*-, or *CTOD*-values, became also of interest. As explained in Section 1, this is a different and new concept of size dependence. This will be briefly discussed at the end of this section. In the following some of the main qualitative trends, as related to specific topics and as observed in the cited literature, are emphasized and several open issues are discussed.

The ***energy absorption*** capability of a structure is of special engineering concern in safety considerations. However, it has found rather limited attention under quasi-static testing conditions, whereas it is of primary interest in notched bar impact tests. The quasi-static tests of Docherty (1932, [2.0]), Shearin et al. (1948, [2.10]), Akita (1953, [2.12]), and Krompholz et al. (2001, [2.76]) concerned the influence of specimen size on volume or area specific energies, whereas Devillers-Guerville et al. (1997, [2.56]) studied the influence of specimen thickness and notch acuity.

The absorbed energy E is obtained by integrating a suitable load-displacement curve up to fracture or up to a fast load drop or up to some other characteristic displacement (e.g., associated with maximum load or crack initiation).

The slow and fast bending tests of Izod-type notched bar specimens (V-notch with scaled root radius, relative notch depth = 0.2) performed by Docherty (1932, [2.0]) on various metals (steel, brass, bronze, Monel metal) revealed the following findings:

- A definite increase of the total absorbed energy per unit volume (see footnote 7, page 6) exists when the size is decreased (Tab. 2-4) for a scale factor of λ=3 (cross section 4x4 to 12x12 mm); the ratio of the volume specific energy of the small to the large specimen depends on the material and ranges between 1.0 and 2.2 (Tab. 2-6) for the slowest speed (quasi-static).
- A comparison of this ratio – a measure for a size effect up to fracture – with the area reduction Z (45 % < Z < 85 %) after fracture in a quasi-static tensile test (Tab. 2-6) clearly shows that this size effect is larger the less ductile the material is.
- The volume specific energy $E_v = E/W^3$ (W: width of specimen) can be represented by
$$E_v = A_v/W + B_v \tag{3.1}$$
where A_v and B_v are constants. The first term characterizes the size dependence, the second describes the size invariance; this corresponds to a hyperbolic decay of E_v with increasing size.

- The corresponding total area specific energy, defined by $E_s = E/S$ with S being the ligament area, can be represented by

  $$E_s = A_s + B_s W$$

  where A_s and B_s are constants. In most cases this linear graph of the area specific energy is a reasonable approximation for the data (Figs. 2-3 and 2-4). For some materials an almost constant area specific work is found and this is accompanied by a low energy level as well as by the smallest area reduction values.
- An increase in testing speed (0.005 in/min to 6 in/min) shifts the total volume specific energy to higher values. However, two orders of magnitude in speed are necessary to increase the volume specific energy by at most 16 % (with one exception; Tab. 2-5). Thus, quasi-static testing of the geometrically similar specimen families (λ=3) with unscaled strain rates has almost no effect on the results.

The research of Shearin, Ruark, and Trimble (1948, [2.10]) on the absorbed energy of notched bar specimens (scaled notches) of several steels under bending referred not only to the total work up to fracture but also to the work up to the load maximum. Further, the authors determined also the influence of the specimen orientation in a 18 in thick tempered martensite plate. The observed trends are as follows:

- The scatter of the response of nominally identical tests is much smaller than the influence of size (cross section 0.4x0.4 to 1.875x1.875 in, $\lambda \approx 4.7$, relative notch depth 0.2; Tab. 2-13).
- The total absorbed energy w per unit volume reduces with increasing size whatever orientation the specimens have; for the scale factor $\lambda \approx 4.7$ the ratio of the volume specific energies $(w)_{small}/(w)_{large}$ of the small to the large specimen depends on specimen orientation and material and ranges between 2 and 3; the largest size influence is seen for specimen axes normal to the plate face.
- The same trend is observed for the absorbed volume specific energy w_1 up to the load maximum. Ratios $(w_1)_{small}/(w_1)_{large}$ are also between 2 and 3, but for 2 in-thick Ni-Cr steel plates also ratios of about 1.5 have been determined.
- The absolute values of the volume specific energies w and w_1 depend strongly on the specimen orientation; they may differ by more than a factor of two. The smallest values were obtained for the direction normal to the plate face.
- The ratio w/w_1 of the total volume specific energy to the partial energy up to the load maximum is around a factor of two (Tab. 2-15, 18 inches plate (Tab. 2-14); tempered martensite). For the different Ni-Cr steel plates (18, 2, 2 ¼ in thickness; Tab. 2-14) a definite size effect is seen for specimens in the rolling direction (OX): the work ratio w/w_1 is largest for the smallest specimens. With $w_2 = w\text{-}w_1$ being the work density beyond the load maximum up to fracture, the work ratio w_2/w_1 will also take the largest values for the smallest specimens.

The work of Akita (1953, [2.12]) on 60° V-notched mild steel specimens (cross section 10x10 to 42x42 mm, notch depth 20 % of width) under slow three-point bending (scaled displacement rates) added further insight: the author studied the influence of temperature (-40 °C to +80 °C) and of the notch tip radius (0.05 to 1.6 mm) on the total absorbed energy and on the "crack propagation energy". The latter is defined as the work beyond the load maximum up to fracture. The dimensional variations included also partially similar specimen families which required an empirical length correction for similarity.

With respect to the energy terms, the following trends are observed:

- The total absorbed energy per unit volume decays quasi-hyperbolically with increasing size (Fig. 2-20); at +80 °C shear fracture is observed and the volume specific work approaches a size independent value for specimens larger than 20 mm width. For the small 10x10 mm specimens (notch radius 0.2 mm, notch depth 2 mm) an almost twice as large volume specific energy is necessary. At -20 °C brittle fracture is found for all sizes at a considerably less energy level; the decay with size is also quasi-hyperbolically but more gradual. A size invariant energy level is not yet reached.
- The increase of temperature for fixed specimen dimensions raises the absorbed and the crack propagation energy from a low to a high energy level (temperature transition curve; Figs. 2-13 and 2-14). For the small 10x10 mm specimen the increase is almost threefold and for the similar large 42x42 mm specimen it is almost six fold.
- The variation of the notch tip radius (0.05 to 1.6 mm) has a very small influence on the point of inflection (transition temperature), except for small specimens with the larger notch tip radii.
- The transition temperature for the total absorbed energy is somewhat lower (by ≤10 °C) than for the crack propagation energy for small notch tip radii; for large radii the relation is reversed.
- An increase in specimen size (gross dimensions) with scaled or non-scaled notch tip radii shifts the transition temperature to higher values (for λ=4.2 from +20 °C to +60 °C; Figs. 2-13 and 2-14). Moreover, the temperature sensivity of the absorbed energy around the transition temperature increases when the size is increased. This implies a considerable size dependence of the volume specific energy in the temperature transition region.

The absorbed energy up to the instant of crack initiation is a further energetic quantity of interest. As defined by an integral of the load-displacement curve, it depends on the definition and the method of determination of the instant of crack initiation or extension. Krompholz et al. (2001, [2.76]) tested a geometrically similar family (width W = 10, 25, 140 mm, relative notch depth 0.3, acuity K/R = 3, λ = 14) of U-notched SENB-specimens of the reactor vessel steel 20MnMoNi55 under three-point bending at room temperature. Among others, crack initiation was determined by the potential drop technique and was found to be size dependent: the smaller specimens required larger relative notch openings (Figs. 2-114 and 2-115). The same trend has been found (Fig. 2-77) by Giovanola et al. (1999, [2.52]) testing U-notched SENB-specimens with deeper and more acute notches but with a smaller geometric scale factor (width W = 12.7 to 50.80 mm, relative notch depth 0.5, acuity a/r ~ 4, λ = 4); here visual and acoustic techniques for the detection of the crack initiation were used and the material was a high strength-low hardening steel.

Moreover, the results of Krompholz et al. showed, except for an initial part, that the nominal stresses became larger the smaller the specimens are at the same relative notch mouth openings, even before crack initiation (~9 % at ω~0.25, λ = 14; Fig. 2-114). For the low-hardening material used by Giovanola, however, this trend has not been observed: the nominal stress vs. relative notch mouth opening curves are congruent up to crack initiation of the largest specimen; this may be related to the different hardening behaviour, but also the geometric scale factor was much larger in the test series of Krompholz et al. (λ = 14 instead of 4).

The two size dependent phenomena, as seen in the normalized load-displacement curves for the SENB-specimens of Krompholz et al., imply the following findings:

- The absorbed work A_s per unit initial ligament area $B \cdot (W\text{-}K)$ up to crack initiation is strongly size dependent. It increases with specimen size and a linear interpolation

$$A_s = \alpha_s + \beta_s W \qquad (3.2)$$

α_s, β_s: constants

is quite appropriate. This area specific work does not vanish when extrapolated to very small specimens, i.e. $\alpha_s \neq 0$.

In analogy to Linear Elastic Fracture Mechanics of brittle materials the first term may be interpreted as a size independent critical surface energy for the generation of free surfaces in the material such as voids or microcracks. The second term, which is linearly size dependent, is related to a size independent volume specific energy typical for classical elasticity or plasticity.

The term $E_i = 2\ A_s$ corresponds to the J-integral value of SENB-specimens with deep sharp cracks (singular crack tip). For this case and according to EPFM, this value should be equal to a size invariant material constant characterizing crack extension. Obviously, a (J = const.)-type or (A_s = const.)-type criterion for crack initiation is not valid for blunt-notched specimens.

- A volume specific work A_v for crack initiation is obtained by dividing the area specific work A_s by the notch width $2R$, for instance. It is found that A_v decreases non-linearly with increasing size and approaches a constant value. Quantitatively it consists of a size dependent hyperbolic decay term and a size independent constant term:

$$A_v = \alpha_v + \frac{1}{W}\,\beta_v \qquad (3.3)$$

α_v, β_v: constants

where

$$\alpha_v = \alpha_s \frac{W}{2R},\ \beta_v = \beta_s \frac{W}{2R}$$

with β_v being the size independent volume specific work typical for classical elasto-plasticity.

- The two-term representations of the area specific work A_s and the corresponding volume specific work A_v agrees formally with the two-term energy representations of Docherty (1932, [2.0]) for complete fracture of various steels and metals. Whereas such a representation appears to be plausible for Docherty´s tests, which involve extensive free surface generation by crack propagation as well as plastic deformation, this is not so evident for the absorbed energy up to the "beginning of a crack formation".
- A crucial aspect of these findings and interpretations is the accuracy of the method of determination of crack initiation, i.e., the potential drop method. There is still some uncertainty. Other methods, allowing a cross check, are recommended.

Energetic quantities were also determined in a joint activity by Devillers-Guerville et al. (1997, [2.56]) and Besson et al. (2000, [2.58]). These referred to the "crack initiation energy" and to the "crack propagation energy", i.e., the area specific work up to the load maximum and the work beyond the load maximum up to complete fracture with the ligament area as the reference area. SENB-specimens (width W = 10 mm, thickness B = 5, 10, 20 mm, relative notch depth $a/W \leq 0.5$, acuity $a/R \geq 5$) of different notch acuities (U-, V-, and precracked) were tested under three-point bending, as well as U-notched specimens with varying thickness; geometrically similar specimens were not included in these test series. The materials

used were thermally embrittled duplex steels. The following qualitative observations were made:

- For the test series (10x10 mm specimens) with variation of only the acuity (Fig. 2-85), the mean value of the area specific work up to the load maximum ("crack initiation energy") decreases considerably (factor of about 3) with increasing acuity (U-notched specimen with a = 5 mm, R = 1 mm to precracked specimen with a = 5 mm). The largest scatter is found for the U-notched specimens. As seen from load-displacement curves (Fig. 2-87), this is not only due to some scatter of the maximum load but also due to distinct scatter of the corresponding load-point displacement. The scatter of the crack initiation energy decreases significantly with increasing acuity.
- The mean values and the scatter of the area specific work beyond the load maximum ("crack propagation energy") are almost equivalent for all three acuities.
- If only the thickness is varied for U-notched specimens (Fig. 2-86), qualitatively similar trends are observed. However, the minimum measured values (lower ends of scatter bands) are almost thickness independent.
- As a consequence, the influence of the acuity as well as thickness variation on the total area specific energy reflects the sensitivity of the "crack initiation" energy on these variations.

One of the primary information to be extracted from size effects tests are the ***load-displacement records***. To be comparable for specimens of the same material and same shape but different size, the load has to be normalized with respect to a common reference load (e.g., limit load) to obtain a dimensionless quantity or has to be transformed to a suitable nominal stress. Similarly, the displacement has to be normalized, too, to be dimensionless or suitable strain measures (e.g. elongation, diametrical strain, area reduction, relative notch opening, etc.) have to be used. Alternatively, the various load-displacement records can be transformed to a reference size (i.e., the smallest or the largest specimen) using scaling factors. If no size effect is present, then these curves are congruent.

Appropriate normalized load-displacement curves or nominal stress-strain curves have been published for families of geometrical similar specimens of various types and for different steels and non-ferrous metals by Docherty (1932, [2.1]; 1935, [2.5]), Shearin et al. (1948, [2.10]), Wells (1955, [2.5]), Lubahn (1955, [2.15]); 1959, [2.20]), Hagiwara et al. (1983, [2.36]), Giovanola et al. (1998, [2.51]; 1999 [2.52]), and recently within the EU-Project REVISA. Their results are shown in Figs. 2-2, 2-5, 2-6, 2-11, 2-12, 2-22, 2-24, 2-33, 2-52, 2-74, 2-76 to 2-78, 2-104 to 2-107, 2-114, and 2-115. From these figures, the review in Section 2, and the related references, the general trends are quite obvious:

- The initial linear (elastic) response and a considerable part of the non-linear (plastic, etc.) response before reaching the load maximum are size independent, i.e., the normalized load-displacement curves are congruent. An exception appears to be the results of Krompholz et al. (2001, [2.76]) of the three-point bending of U-notched specimens of a reactor vessel steel (Figs. 2-114 and 2-115) where the congruence is limited to the linear and a relatively small range in the non-linear regime.
- The maximum normalized load or nominal stress value remains approximately the same or decreases when the size is increased. In some cases, depending on the brittleness of the material, the absolute size, and the magnitude of the scale factor, the decrease is considerable and is accompanied with an abrupt load drop, i.e., fracture (Figs. 2-6, 2-24, 2-33, 2-52, 2-114 and 2-115).

- The normalized displacement associated with the load maximum decreases with increasing size. Frequently this size influence is clearly more pronounced than the influence on the normalized load or nominal stress (Figs. 2-2, 2-5, 2-11, 2-12, 2-22, 2-52, 2-104 to 2-107, 2-114 and 2-115).
- The shift of the normalized displacement or nominal strain at maximum stress to larger values when the size is decreased is combined with an increasingly gradual load decay after the maximum and an increasing extension of this softening region, i.e., the final normalized displacements increase with decreasing specimen size.
- In some cases (Figs. 2-5 to 2-7, 2-23) and for a large scale factor ($\lambda > 10$) an almost abrupt transition occurs at a distinct specimen size between the more ductile behaviour with gradual load decay of the smaller specimens and a brittle behaviour with a sudden load drop of the larger specimens. This implies also a sudden change in the volume specific energy consumption (Fig. 2-7) or a change in the maximum stress (Fig. 2-23).

More detailed investigations on the size dependence of the ***maximum normalized load or stress*** are contained in references by Nadai et al. (1934, [2.2]), Sachs et al. (1945, [2.23]), Brown et al. (1947, [2.73]), Parker (1948, [2.11]), Akita (1953, [2.12]), Wells (1955, [2.13]), Lubahn and Lubahn et al. (1955, [2.17]; 1959, [2.20]; 1958, [2.18]), DeSisto et al. (1963, [2.25]), Wellinger (1968, [2.26]), Neale (1978, [2.29]), Shaw et al. (1983, [2.35]), Takeuchi et al. (1986, [2.83]), and Krompholz et al. (2001, [2.76]). From these the following qualitative findings may be stated:

- Whereas some authors did not observe any size influence on the maximum stress (notch strength) even for a large scale factor ($\lambda = 8$, Tab. 2-8) but relatively small absolute sizes, frequently a decrease (possibly quasi-hyperbolic or exponential) with size is seen (Figs. 2-9, 2-18, 2-25, 2-30, 2-32, 2-34, 2-36, 2-38, 2-39, 2-42, 2-116).
- The results of Lubahn (Figs. 2-25, 2-26, 2-32, 2-34), Lubahn et al (Fig. 2-30), Yukawa et al. (Fig. 2-36), and DeSisto et al. (Fig. 2-38) show that there is a transition in the size dependence: for small specimens there is no or only a moderate decay with size, but beyond a certain small size interval a strong decrease is observed which may be characterized by the inverse square-root dependence of LEFM. This qualitative change appears to be related to a failure mode transition: apparently size independent plastic instability of the small specimens and size dependent unstable crack propagation for the larger specimens. In the latter size range a number of influences are important:
    - The transitions observed in the results of DeSisto et al. (Fig. 2-38) are possibly due to the change of the testing machine: specimens of 0.505 inch diameter and smaller were tested in a different hydraulic testing machine. Such an influence draws attention to the requirement that the system "specimen-testing machine" should be properly scaled over the whole size range. Usually this aspect is not mentioned or even discussed in the reviewed references.
    - Accompanying testing of geometrically similar smooth tensile specimens should be done to assess not only the homogeneity of the raw material but also to assure the size independence of the ultimate stress. The results of Lubahn (Fig. 2-25) demonstrate that already the nominal strength of smooth tensile specimens under quasi-homogeneous stress conditions may be size dependent. Thus, this effect will add to the size effect induced by the presence of a notch.

- An increase of the strength level (ultimate stress in a tensile test) by heat treatment (tempering) yields a reduction of the notch strength ratio (notch strength divided by the strength level) and increases the size dependence of the notched tensile specimens (SAE4340, V-notch, notch tip radius constant, Fig. 2-26). Thus, the high strength material is more susceptible to notches and more sensible to size variations.
- A complete geometric similarity of the specimens requires, of course, also similarity of the notch (i.e., depth *a* and root radius *r)* such that the acuity *a/r* is constant. An increase of the acuity (by decreasing the root radius) decreases the maximum stress (e.g., nominal bending stress in SENB-specimens) considerably for large sizes (Fig. 2-30). But for large notch sharpnesses the maximum stress appears to approach a finite value (Fig. 2-31). Moreover, the size dependence of the maximum stress is clearly reduced when the notch sharpness is reduced (Fig. 2-30).
- If the notch tip radius *r* is held constant, then the notch sharpness increases with increasing size. This yields an additional size influence by shifting the maximum stresses to lower values, as compared to the data of geometrically scaled notches (Fig. 2-30), and the size dependence is increased.
- The notch tip acuity and preparation has a significant influence on the maximum stress if specimens are sufficiently large. Bend specimens (SENB type) with notches (20 % of width) prepared by machining a constant 0.005 inch (0.127 mm) tip radius showed (Yukawa et al., Fig. 2-36) consistently the largest maximum stress in the whole size range (10.16 x 10.16 mm to 73.2 x 76.2 mm cross section), as compared to specimens with fatigue cracked notch tips. However, differences were rather small (less than about 10 %) for the smallest specimens. Much larger differences were observed for the larger specimens. Spark erosion, giving an approximately constant tip radius of about 0.004" (0.10 mm), produced the same maximum stresses as machining (single size – 1.0 x 1.0 inch = 25.4 x 25.4 mm test series). Other techniques to generate a sharp crack tip (i.e., arrested cleavage cracking machining (0.005 inch = 0.127 mm tip radius) with subsequent nitriding which induces cracks in the nitride surface layer at already low stress levels) caused reduced maximum stresses approximately comparable to fatigue cracking (single size testing only). The maximum stress appears to approach a size independent limiting strength for small specimens and the influence of the notch tip sharpness is vanishing.
- The influence of temperature on the size dependence of the maximum stress, among others, has been documented by Parker (Tab. 2-17) and Shaw and Spink (Tab. 2-30, Figs. 2-48 and 2-49). Whereas the data of Parker (flats plates with square hole, scale factor $\lambda = 4$, temperature range -18 to +39 °C) do not show significant temperature influences on the maximum stress, the results between -100 °C and +100 °C of Shaw and Spink are more conclusive. They showed all modes of failure from fully brittle to fully ductile. At low temperatures geometrically similar prefatigued CT- and SENB-specimen families showed an increase of the normalized load (Fig. 2-48) or normalized stress (Fig. 2-49) with increasing temperature for all three sizes (thickness 12.5, 25, 50 or 45 mm), the small specimens giving the largest values. Beyond a transi-

tion temperature the temperature dependence is greatly changed (i.e., is flattened out) and the normalized load decreases slightly (CT-specimens) with temperature or remains constant (SENB-specimens). For both specimen families the transition temperature is shifted to higher values when the size is increased; the shift may be as much as 60 °C or 40 °C over the whole size range ($\lambda = 4$). CT- and SENB-specimens of the same thickness do not yield the same transition temperature, i.e., this temperature is also shape dependent.

Below the transition temperature a considerable scatter is observed when nominally identical tests (usually two test at most) are performed, whereas above the transition temperature fairly consistant results are determined.

The size dependence of the ***normalized displacement or strain at the load maximum*** became already evident in several normalized load-displacement curves discussed above. Apart from this, some explicit results were also documented by Neale (1978, [2.29]) and Takeuchi et al. (1985. [2.38]) for CT-specimens, by Gordon and Jones (1989, [2.46]) and Krompholz et al. (2001, [2.70]) for SENB-type specimens, and by Hagiwara et al. (1983, [2.52]) for scalloped I-beams with and without notches. These findings are as follows:

- The results of Takeuchi et al. (Fig. 2-56, CT-specimens, thickness 4.5, 6, and 10 mm, scale factor 2.2) are almost size independent (L-T specimens) or do not yield a consistent trend (T-L specimens).
- The findings of Neale (Tab. 2-28, CT-specimens, thickness 12. to 50.5 mm, scale factor 4), however, referring to the slot mouth opening displacement at maximum load, and also the results of Link (Fig. 2-74, CT-specimens, side grooved, thickness 25.4 and 101.6 mm, scale factor 4) cited by Giovanola et al. (1999, [2.52]) demonstrate a significant decrease with size of these characteristic normalized displacements at maximum load.
- Although the used materials and absolute sizes are different, it is felt that the scale factor is the main reason for the qualitative difference: a scale factor of about two is too small to obtain a definite conclusion on the existence of a size influence on any of the relevant quantities.
- A definite decrease of the normalized load-line displacement or bending angle at maximum load was also obtained by Krompholz et al. (Fig. 2-117) for blunt-notched (U-notched) SENB-specimens of a reactor vessel steel, covering a very large scale factor ($\lambda = 14$, thickness 10 to 140 mm, relative notch depth 0.3).
- Moreover, the normalized stable crack advancement (indirectly determined by compliance measurements) up to the load maximum, obtained by Gordon and Jones (Tab. 2-38, SENB-specimens, sharp notch, side grooved, thickness 10 to 45 mm, relative notch depth 0.6), does not scale with the size but increases much faster: for a threefold increase of size, the stable crack propagation increases 4.56-times. The data also show that a linear extrapolation to small specimens (thickness < 10 mm) would imply a suppression of crack propagation before the load maximum is reached.
- Based on calculations of the maximum nominal strain as a function of the deflection of a scalloped but unnotched I-beam, Hagiwara et al. (Tab. 2-32) obtained the nominal strain associated to the deflection at the maximum load. The data in Tab. 2-32 but also Fig. 2-52 show the reduction of the maximum nominal strain or normalized deflection at maximum load when the size is increased for specimens without or with a notch and that application of the notch increases the size influence.

Whereas several influences, such as temperature and notch acuity, on the size dependence of the maximum normalized load or stress have been investigated, unfortunately, these influences on the size dependence of the normalized displacement or relative notch mouth opening at the maximum load have not found attention. The probable reason is that under quasi-static conditions the traditional interest in engineering is primarily oriented towards stress-like design limits and rules.

Besides the normalized load or stress maximum, the most investigated quantities are ***strain type measures at or after fracture***, such as the area reduction, diametrical strain, or relative notch mouth opening. Results on this issue were published by Brown et al. (1947, [2.7]), Parker (1948, [2.11]), Lubahn (1958, [2.18]); 1959, [2.20]), Wellinger et al. (1968, [2.26]), Neale (1978, [2.29]), Decamp et al. (1997, [2.63]), Devillers-Guerville et al. (1997, [2.56]), Marini et al. (1998, [2.64]), Besson et al. (2000, [2.58]), and Krompholz et al. (2001, [2.72]) within the REVISA project.

Although the definition of « failure strain » varies and occasionally is not very well defined (e.g., "sudden load drop"), the following qualitative observations may be stated:

- The average permanent failure strain (e.g., area reduction or diametrical strain of notched tensile specimens, relative notch opening of tensile and CT-specimens, bend angles (and "strains" derived from this) of three-point bend specimens and relative thickness changes of plates) generally decreases with increasing size, frequently quasi-hyperbolically in linear representations (notched tension specimens: Figs. 2-10, 2-34, 2-42, 2-83, 2-89, 2-94, 2-97, 2-108 to 2-111; notched bending specimens: Figs. 2-28, 2-32; flat plate with hole: Tab. 2-17; CT-specimens: Tab. 2-28). For a sufficiently large size range, small almost constant strain measures are approached and in some cases almost vanishing permanent failure strains are obtained for the large sizes (fully brittles response: Figs. 2-32,-2-34).
- Notch acuity was varied for tensile specimens with constant minimum notch diameter and a constant unnotched diameter (Figs. 2-81, 2-82, 2-88, 2-93, duplex stainless steel): increasing the acuity implied a reduction of the failure strain[61]. Unfortunately, systematic tests on the influence of size on the failure strain for different notch acuities apparently do not exist.
- Depending on the production process of the raw material (e.g. plate, pipe), the orientation of the specimen in the raw material may have not only a considerable influence on the absolute values of the failure strain (Figs. 2-82, 2-97) but also on the size dependence (Fig. 2-97). This was found to be related to the anisotropy of the microstructure (e.g. columnar grains, layered microstructure, banded segregations due to forging or rolling)
- Frequently, failure strains of only two or three nominally identical tests are available. Test results for blunt-notched tension specimens (Figs. 2-83, 2-93, 2-97, 2-108, 2-110) with more test results demonstrate repeatedly a decrease of the failure strain scatter with increasing size. Often this finding is somewhat unbalanced since the number of

[61] A correlation with the stress triaxiality factor σ_m/σ_{eq} determined at the specimen centre, as suggested by Figs. 2-82 and 2-92, seems not to be assured by these data since, among others, the position of fracture initiation depends on the acuity: for smooth specimens or small acuities it starts at the specimen centre but for large acuities it may start at the root surface of the notch (the reviewer).

repeat tests is considerably smaller for the large specimens. This may distort conclusions with respect to the mean values. In one case (Figs. 2-108, 2-110) the large scatter of the smallest specimens is related to a macroscopic material inhomogeneity (position effect).

- Very few results concerning the influence of temperature on the size dependence of the failure strain are available. The tests of Parker (Tab. 2-17) for a mild steel plate with a hole, done within a small temperature range (-18 to +39 °C), show a significant influence of size on the mode of failure and the plate thickness reduction:
    - The small specimens (3/16 inch = 4.76 mm thick) fail by shear fracture at all temperatures and the percentage thickness reduction is at a high ductile level independent of temperature.
    - The large specimens (3/4 inch = 19.05 thick) fail by cleavage at all temperatures at a considerably lower strain level almost independent of temperature.
    - The intermediate size specimens (3/8 inch = 9.53 mm thick) show a transition from cleavage type to shear type fracture with increasing temperature. This transition temperature is at +10 °C for this material and size. The transition in fracture type is accompanied by a transitional increase of the percentage reduction in plate thickness at fracture.
    - The results imply that the transition temperature from cleavage to shear fracture is shifted to higher temperatures when the specimen size is increased.

  Tests of notched tensile specimen by Krompholz et al. (Figs. 2-108 to 2-111), covering a scale factor of 10, were performed at two temperatures only, R.T. and 400 °C. Apart from some increase of the absolute values of the area reduction at the notch with the rise of the temperature, the size dependences of the area reduction and the relative notch opening appear to increase at the higher temperature, notably for the relative notch opening after fracture of the small specimens (Fig. 2-111).
- The change of the mode of fracture with increasing specimen size, as pointed out by Parker (Tab. 2-17) for a mild steel plate, was also remarked by Brown et al. (1947, [2.73]) for notched tensile specimens and was quantitatively determined by Wells (Tab. 2-19) for mild steel notched slow-bend specimens (width 0.110 to 12.50 in = 2.79 to 31.75 mm, λ = 11.4): the percentage brittle area of the largest specimen was 95 %; decreasing the size, a gradual decrease of the percentage brittle area was found, but for the four smallest specimens an almost complete suppression of brittle fracture was clearly shown. Moreover, the results of Lubahn (1955, [2.15]) for geometrically similar V-notched bending specimens (thickness: 0.08 to 3.5 in = 2.03 to 88.9 mm) of mild steel showed the same tendencies under a very large scale factor: the largest specimens showed cleavage fracture, except for a very narrow band of fibrous fracture around the edges; however, the fracture surface of the smallest specimen was entirely fibrous, except for a few tiny cleavage areas near mid-depth.

As seen from the above discussion, in the quasi-static size effect investigations attention was placed primarily to the maximum normalized load or stress and to some strain measures at fracture, quantities which can be determined without excessive effort. But the size dependence of ***crack initiation and the related "ductility"***, as defined by a strain accumulated up to crack initiation, merits equally strong attention, not only for basic scientific reasons but also for design oriented safety assessments. For sharply notched or precracked specimens the fracture mechanics theories (LEFM and EPFM) are possible means to describe initiation of crack

extension and propagation and this will be discussed briefly later on. For blunt-notched but crack-free specimens the review has revealed only a few experimental studies of the size influence on crack initiation (i.e., Lubahn (1955, [2.15]), Giovanola et al. (1999, [2.52]), and Krompholz (2001, [2.72])). All three studies used single-edge-notched bending specimens of different size ranges and materials, as well as different detection methods. As discussed above in the annotated review, the definition of "crack initiation" in a crack-free body with a strain concentrator is not an unambiguous matter (see Lubahn (1955, [2.15])). It depends on the size of the defect to be considered as a small initial crack, which can be detected, and on the method of detection.

The qualitative trends observed in these different tests series are as follows:

- The results of Lubahn (Tab. 2-21) for mild steel, showing the calculated notch root strain of V-notched bending specimens at the "appearance of first surface cracks" at the notch (visual inspection), are subject to a considerable scatter. The relatively small number of repeat tests do not show a definite size dependence. Also the indicated notch root strains are based on an almost linear empirical relation between bending angle and notch root strain, obtained for large size specimens, the relation assumed to be size invariant. Therefore, the data in Tab. 2-21 are actually measures of the bending angle at initiation.
- However, as noted by Lubahn, the (stable) crack propagation following the initiation showed a pronounced size dependence (lot II steel): the smallest 0.08 in-thick specimens tore open 50 % of the ligament length before exhibiting any sudden crack propagation, the 0.4 in-thick specimens tore open about 30 %, and the large 2 in-thick specimens tore open only 2 % of the ligament length before sudden crack propagation. Therefore, the relative crack advancement before the start of complete (unstable) fracture reduces with increasing size of the specimen.
- The initiation of cracking in geometrically similar U-notched bending specimens (width 12.7 to 50.8 mm, relative notch depth 0.5) of a high strength-low hardening steel, studied by Giovanola et al. (Tab. 2-42, Figs. 2-77 and 2-78) with visual and acoustic methods, displays a very definite size dependence: that is, the normalized notch mouth opening displacement and the normalized load-line displacement at initiation decrease with increasing size, their scatter bands almost not overlapping. Based on metallographic observations, Giovanola et al. suggest that cracks nucleate with a minimum initial length of 100-200 μm in all specimen sizes, a minimum crack length (or depth) which they reliably identified by their methods. There are still some doubts, as to whether this characteristic length is truly related to the material behaviour (material intrinsic length) or to the sensitivity of the detection methods (the reviewer).
- The results of Giovanola et al. also demonstrate that the extent of cracking up to a same (!) bending angle (without complete fracture) increases with specimen size (Tab. 2-42, Fig. 2-79 and 2-80).
- The initiation of cracking in geometrically similar U-notched bending specimens (width 10 to 140 mm, relative notch depth 0.3) of a ferritic reactor vessel steel, investigated by Krompholz et al. (Tab. 2-49, Figs. 2-114 and 2-115) with the potential drop technique, also exhibits a clear size dependence, i.e., the associated normalized notch openings or bending angles decrease when the size is increased (23 % on an average for $\lambda = 14$); also their scatter bands are almost not overlapping (Tab. 2-49). For this very large size range (geometric scale factor 14) the influence on the relative notch openings or bending angles at crack initiation is relatively small. A crucial aspect of

the determination of the instant of crack initiation is still the accuracy of potential drop method and its application.

The few results on the size dependence of crack initiation in nominally crack-free specimens suggest the following further work:

- A comparison of different methods for the detection of crack initiation using the same set of scaled test specimens should be done.
- Crack initiation studies should be extended to initially uncracked specimens with different strain concentrators and shapes.

In the following the size invariance as well as size dependence of ***critical fracture mechanics quantities*** related to different fracture mechanics concepts are briefly examined. To mention are critical values of the stress intensity factor K or the strain energy release rate G, appropriate for brittle response of essentially elastic materials, and for elastic-plastic material behaviour the path-independent contour integral J and also the crack-tip opening displacement δ. Theoretically, these characteristics apply only to sharp pre-existing cracks and they intend to characterize the initiation of the crack extension. Ideally, the critical values represent size and shape invariant material specific constants. Their size invariance would then inherently imply the size dependence of nominal stresses and strains at initiation of crack extension, as it has been discussed in the first part of this section.

However, there is a growing interest in fractures at unavoidable strain concentrators when pre-existing cracks are not present. In this problem area the fracture mechanics concepts which require the pre-existence of a dominant sharp crack are not appropriate. But theoretical concepts and models of continuum damage mechanics, a precursor to the fracture mechanics regime, possibly represent appropriate tools to describe and predict failure and also its size dependence, provided an internal length scale is introduced. This issue of failure of specimens with design typical blunt strain concentrators and its size dependence is exactly the primary topic of the EU-project LISSAC[62] (see Section 1, P.3); the present literature survey was performed in support of this project. Within this project the interest in the size invariance or size dependence of fracture mechanics quantities, such as critical K or G, J or δ values, is quite limited. Therefore, only a rather concise discussion of these fracture mechanics topics is included in the present review.

Critical values of the ***stress intensity factor K or the strain energy release rate G*** have been determined by Lubahn (1959, [2.20]), Yukawa and McMullin (1961, [2.24]), DeSisto et al. (1963, [2.25]), Nelson et al. (1972, [2.27]), Neale (1978, [2.29]), and Shaw and Spink (1983, [2.35]) for families of geometrically similar specimens, such as notched circular tension specimens, single-edge-notched bending (SENB) specimens, and compact tension (CT) specimens. The following qualitative trends were observed:

- In a number of cases the size dependence of the nominal bending strength or notch tension strength follows the inverse square-root law of Linear Elastic Fracture Mechanics (LEFM) with an almost size independent ***strain energy release rate G_c***, provided that the specimens are sufficiently large (Figs. 2-32, 2-34, 2-36), e.g., in these cases larger than about 1 inch in width or diameter. The relative notch depth was equal

[62] The LISSAC project very recently has been completed and was documented in an extended and a short report (Krieg and Seidenfuß (2003, [3.4]; 2003, [3.5])).

to or larger than 20 % and the V-notches were machined with root radii not scaled but equal to 0.003 inch and less (Figs. 2-32 and 2-34) or 0.005 inch (Fig. 2-36). In all three cases, for small specimens the size dependence of the nominal fracture stress decreases when the specimen size is reduced, and the nominal fracture stress apparently approaches a limiting strength value.

- The individual ***G_c-data*** of each tension test for specimens of 0.9 to 2.25 inches diameter (Tab. 2-22) show a moderate scatter. However, a slight decrease of the average G_c-value (i.e. 91.5, 84.5 and 79 inlb/in^2) with increasing size is observed. The overall average value is G_{CT} = 85 inlb/in^2. This is fairly different from the average strain energy release rate G_{CB} = 131 inlb/in^2 of the notched bending specimens. Since the material used for the notch bending and the notch tension tests was the same (material A), a general shape independency would require equal strain energy release rates. This is not the case. Since $G_C \sim K_C^2 \sim \sigma^2 a$ and G_{CB}/G_{CT} = 1.54, an uncertainty of about 25 % arises for the fracture stress if LEFM is used to correlate notch tension tests with notch bending tests. Thus, following Lubahn (1959, [2.24]), the correlation of different types of tests by means of LEFM (Griffith-Irwin concept) should be performed with great caution.
- The results of Yukawa and McMullin (Fig. 2-36) for notched bending specimen with different notch tip preparations (especially: machined notches with constant 0.005 inch root radius and fatigue cracked notches) show that the sharper notch tip (fatigue crack at the notch root) reduces the nominal notch strength and the strain energy release rate G_C considerably from 300 (machined notch) down to 120 inlb/in^2 (pre-cracked by fatigue).
- The critical stress intensity factor for mode I cracks ***(fracture toughness K_{IC})***, determined by DeSisto et al. (Fig. 2-40) for geometrically similar notched tension specimens (constant notch root radius 0.001 inch), show that almost size independent toughness values for a titanium and an aluminium alloy are obtained for specimens larger that 1.6 inches in diameter; an exception is the largest aluminium specimen. The K_{IC}-data for the 4340 steel show a strong size dependence in the whole regime of investigated sizes (unnotched diameter 0.16 to 5.05 inches, λ = 32). The bi-logarithmic Wundt-type representation of the notch strength vs. gross diameter (Fig. 2-41) demonstrate that all notch strength data of the 4340 steel are above yield and even ultimate tensile strength (U.T.S); this implies extensive plastic deformation such that LEFM is clearly not applicable. This notch-strengthening effect is seen for the smaller-titanium and aluminium specimen, but the larger specimens with notch strengths below or somewhat above the yield strength (Fig. 2-39) follow the linear decay graph, i.e., the inverse square root law with constant fracture toughness of LEFM.
- Fracture toughness tests with fatigue pre-cracked specimens of different aluminium alloys were performed by Nelson et al. (Tab. 2-27, Fig. 2-44) to investigate whether the stringent ***dimension requirements*** on crack length a and thickness B (i.e. $a,\ B \geq 2{,}5\ (K_{IC}/\sigma_{ys})^2$, see Brown and Scrawley (1969, [3.1])) for valid ***K_{IC}-toughness testing*** could be relaxed. The set of notch-bend specimens without side grooving contained two families of geometrically similar specimens with different width-to-thickness ratios (Tab. 2-27). With K_Q being the candidate fracture toughness value, there is no uniform material independent trend (Tab. 2-27) with respect to the size dependence of the K_Q-value of small geometrically similar SENB-specimens, their dimensions a and B violating the ASTM dimension limit. However, for the larger specimens almost uni-

form toughness values are obtained for all alloys. These trends are also seen in Fig. 2-44, representing K_Q vs. specimen thickness B, based on the results of geometrically similar but also non-proportional SENB-specimens.

- Among others, ***provisional fracture toughness values K_Q*** for a family of geometrically similar pre-cracked compact tension (CT) specimens of 1Cr-MoV-steel were determined by Neale (Tab. 2-28, 2-29) with a thickness range from 12.7 to 50.5 mm. Only the largest specimen (A2) satisfied all aspects of the ASTM standard. Reducing the size, first a slight increase of the conditional K_Q-value is seen followed by a further decrease. This non-uniform trend has also been seen for the thickness variations of small aluminium alloy specimens (Fig. 2-44).
- As described above, in a number of cases almost ***size invariant critical mode I stress intensity factors and strain energy release rates*** have been obtained if the specimens were sufficiently large such that crack tip plasticity is small, especially if the ASTM minimum dimension requirements are satisfied. Even then some results showed that LEFM should be applied with caution (e.g., Lubahn (1959, [2.20])).

A very embracing investigation of the ***"strength size effect" according to LEFM*** was performed by Sinclair and Chambers (1987, [2.45]); they used published results of geometrically similar specimens. For a mode I fracture toughness K_{IC}, assumed to be a true (i.e., size invariant) material constant, one obtains theoretically for the ratio of the nominal fracture stresses

$$\frac{\sigma_1^*}{\sigma_2^*} = \sqrt{\lambda}$$

where the subscript 1 refers to the small and 2 to the large specimen and $\lambda > 1$ is the geometric scale factor. Sinclair and Chambers introduced classifications according to plane stress and plane strain conditions and they defined brittle, brittle-ductile, and ductile regimes, and even further subclassifications. Among others and with the view to include all pertinent data, the authors admitted notches whose acuity was such that the radius r at the root of the notch was an order of magnitude less than the total notch depth or crack length a (i.e., $r/a \leq 0.1$). They compared the experimental results within these classes with the above predictions, especially for materials and configurations exhibiting brittle response which is the situation in best accordance with the assumption of LEFM theory.

- The result of the comparison is seen in Figs. 2-60 and 2-61 and Tabs. 2-34 to 2-36. From Figs. 2-60 and 2-61 it is seen that generally the LEFM prediction represents an upper bound for most but not all of the data. Therefore, if tests with scaled down models are done which yield an experimental determined fracture stress σ_1^*, the prediction of the reduced strength $\sigma_2^* = \sigma_1^* \lambda^{-1/2}$ is frequently conservative since the predicted strength of the large structure is too small; but clearly in many cases a significant over-conservatism is involved.
- Since a lot of data come from tests with small scale factors ($\lambda \leq 2$) "where there is really very little to predict", Sinclair and Chambers introduced the "strength size effect" quantity

  $$SSE = \sqrt{\lambda - 1}$$

  and they regarded a prediction as *good* if the experimental data are within ± 5% of the prediction *SSE* and as *useful* if within ± 10%. Restricting the investigation to different types of brittle response, results are obtained, as shown in Tab. 2-36. It is seen that of the 231 tests, which are in accordance with the conditions for valid K_{IC}-testing (ASTM

standard E399 (1982, [3.27])), only 11% of the predictions are considered as useful and only 6.2% as good. As stated by the authors, there is concern about the very basis of Linear Elastic Fracture Mechanics "because there exist several hundred test results for appropriately brittle behaviour not agreeing with the LEFM prediction of strength size effects. Every one of these represents data establishing a variation in fracture toughness with size. It follows that fracture toughness is demonstrably not a material property."

- Nevertheless, in a number of investigations, admittedly with dimension or size variations of usually not more than a factor of four, a reasonable constant K_{IC} has been found. A more quantitative estimate was given by Brown and Srawley (1969, [3.1]), when preparing a basis for formulating recommended practices for K_{IC}-testing. Data obtained by the NASA-Lewis Research Centre for three heats of maraging steel with different yield strengths using different specimen types and dimensions[63] (Ref. [3.1]) revealed the mean $\overline{X}$ and standard deviation S of the K_{IC}-tests as shown in Tab. 3-1. Ratios $S/\overline{X}$ between 0.0478 and 0.0555 were obtained for the three strength levels. If the measured K_{IC}-values follow a normal distribution, then about 68% of the K_{IC}-data are between $\overline{X}+S$ and $\overline{X}-S$ (e.g., Kreyszig (1975, [3.5])), and 95.5% between $\overline{X}+2S$ and $\overline{X}-2S$, i.e., a ± 5% or ± 10% variation of the fracture toughness, provided $S/\overline{X}$ is about 0.05. In this case a quite better picture of the usefulness of LEFM is obtained.

For moderately large elastic-plastic deformations at the crack tip ***critical values of the J-integral and the crack-tip-opening displacement*** have been determined or collected for geometrically similar specimens by Pisarski (1989, [2.30]), Shaw and Spink (1983, [2.35]), Gibson et al. (1987, [2.40]), Gordon and Jones (1989, [2.46]), Landes (1992, [2.49]), and Marini et al. (1998, [2.64]):

- For geometrically similar, fatigue pre-cracked, notched three-point bend (SENB) specimens *critical values of the crack opening displacement δ and the J-integral* at fracture were determined by Pisarski (Figs. 2-45 to 2-47) for a carbon manganese steel in the temperature range of -150 °C to -10 °C. The specimen thicknesses were 10, 50, and 100 mm with a relative crack length (including fatigue crack extension) of around 50 %. The crack opening displacement δ_c and J_c at unstable fracture were determined using critical notch mouth opening values and are represented vs. temperature in Figs. 2-45 and 2-46. Also fracture toughness values K_{IJ} were determined by converting the J_c-values according to Equ. 2.28 and these are shown in Fig. 2-47. Without going into details, it is seen that the characteristic values increase progressively with increasing temperature. In spite of the scatter and the scanty amount of data of the larger specimens at the same temperature, the 50 and 100 mm thick specimens give comparable critical values. This gives reason to expect a confirmed size independence in this size range if more data were available. However, the mean values of the small 10 mm thick specimens generally yield considerably larger critical δ_c-, J_c-, and K_{IJ}-values, but the scatter is substantial. To a large amount, the scatter is caused by a fracture mode change (with and without microvoid coalescence) of the small specimens. The increase of the critical values of the small specimens implies a shift of the transition temperature curve to higher temperatures if the size is increased; the shift may be as

[63] Geometrically similar specimen were not explicitly identified.

much as 50 °C. From Fig. 2-47 it is also seen that K_{IJ}-values obtained for 10 mm thick specimens overestimates valid K_{IJ}-values of 100 mm thick specimen. These size dependent results support the recommendation that "data should be obtained from test pieces representing the thickness of the structure of interest". Of course, then real difficulties arise in practice.

- The behaviour of geometrically similar compact tension (CT) and single-edged-notched bend (SENB) specimens under-three-point-bending of a NiCrMoV-steel was investigated by Shaw and Spink (1983, [2.35]) over a temperature range from -100 °C to +100 °C. Three sizes were considered ranging from 50 mm thickness to 12.5 mm with a relative depth of the pre-fatigued notches in the range of 44 % to 52 %. Among others, the *equivalent critical stress intensity values* K_{IC}^{J} were determined by converting critical *J*-values (Tab. 2-30). There is a considerable scatter between duplicate test results. For the CT-specimens the K_{IC}^{J}-values generally increase with temperature for all three sizes, but this is not so evident for the SENB-specimens, partly because the investigated temperature range is smaller and different. The size independence of the K_{IC}^{J}-values can be checked only for a few temperatures, i.e. -20 °C, 0 °C, and +20 °C for the CT-specimens, and -40 °C and -20 °C for the SENB specimens. The comparison shows that there are variations of the mean values up to 50 % such that a convincing size independence of average K_{IC}^{J}-values of these two specimen types at these temperatures is not present. This rating is at variance with statements of Shaw and Spink.
- The effect of specimen size and geometry on the ductile crack growth resistance (J-resistance curves) of a C-Mn steel was investigated by Gibson et al. (1987, [2.40]). All various specimen types had fixed dimensions, except the CT-specimens which included also two families of geometrically similar specimens with thicknesses between 13 mm and 50 mm and fatigue pre-cracked V-notches of a relative total depth between 50 % and 60 %: one family was without, the other with 25 % side grooving. The *critical J-integral values* J_{1c} were determined according to the ASTM J_{1c} testing standard E818 on the basis of a J-resistance curve which included a correction for crack growth. In addition, the *initial slope dJ/da* of the J-resistance curve was determined. Moreover, the *J-value* at the onset of crack initiation was also *determined from the stretch zone width SZW* at initiation of crack extension using an empirical relation between *J* and *SZW*. The corresponding value was denoted by J_i. The results, mean values and standard deviations, are contained in Figs. 2-57 and 2-58. Obviously, the J_i-values yield the least scatter and the least variation with size. The critical value J_{1c} is subject to considerable scatter and has a much less uniform size dependence. Moreover, they are considerably larger than the J_i-values for both non-side grooved and side grooved CT-specimens. Fig. 2-57 demonstrates that all the quantities decrease with increasing size, especially the initial slope *dJ/da*, if no side grooving is applied. For side grooved CT-specimens, the J_i-value is almost perfectly size invariant; this suggests that the corresponding J_i-value is that for plane strain conditions. Fig. 2-59 demonstrates that the same J_i-values are obtained for different specimen types but with the same thickness of 25 mm. The crack-tip-opening displacement values δ show much more scatter, but the mean values exhibit only a slight variability for different specimen geometries with the same thickness. From these data it appears that the J_i-values obtained from plastic stretch zone measurements is a rather size and geometry

invariant quantity with small scatter for both small and large specimens. Whether these characteristics of J_i can be generalized, remains to be tested.

- From J-resistance curves *the critical $J_{o.2}$-values and initial slopes dJ/da* were also determined by Marini et al. (1998, [2.64]) at +100 °C for a family of geometrically similar side grooved CT-specimens with sizes ½ T, 1 T, and 2 T (1 T specimen: thickness B = 1 in, width W = 2 in, relative crack length $0.5 \leq a/W \leq 0.7$). The material was a C-Mn steel used for piping and specimens were taken from two directions of a pipe component. The average $J_{o.2}$-data of three nominally identical specimens for the longitudinal direction show almost no size dependence, whereas the slope *dJ/da* decreases significantly (by 44 % when the size is increased from ½ T to 4 T; Tab. 2-48). The short-transverse direction cover only a small size range. The mean data are much smaller and trends are clearly different. This demonstrates the importance of orientation influence (anisotropy) on fracture mechanics data. A comparison of the longitudinal data with the data of Gibson et al. for side grooved CT-specimens with the same gross dimensions (Fig. 2-58) shows fairly different size effect trends, especially for the *dJ/da*-values.
- The experimental results of a programme of geometry and size effects on *J- and CTOD-resistance curves* of Gordon and Jones (Figs. 2-62 to 2-68) add a new aspect because extended resistance curves of geometrically similar SENB-specimens with large crack growths can be compared. The specimens were side grooved by 20 % and pre-cracked by fatigue with an initial relative crack depth of about 60 %, width-to-thickness ratio of two, and thicknesses ranging from 10 to 40 mm. The material was a titanium alloy. *Several J-resistance indicators* were determined, i.e. the standard fracture resistance J_o not corrected for crack extension, the fracture resistance J_R corrected for crack growth using an incremental approximation, and a modified fracture resistance J_M to extend the range of crack extension over which the J-integral can be applied. The results are plotted in Figs. 2-63 to 2-65. The curves represent averages of three nominally identical tests. Each of the average J_o-, J_R-, and J_M-resistance curves for the various geometrically similar SENB-specimens agree very well for small crack extensions (up to ~ 3 mm for the J_o-curve, ~ 1 mm for the J_R-curve, ~ 1.5 mm for the J_M-curve). In the terminology of fracture mechanics, this congruence represents "size independence" up to a limited amount of crack growth which depends on the definition of the J-resistance (J_o, J_R or J_M). Moreover, the initial part (crack growth < 1 mm) appears to be not sensible to the definition of the J-resistance.

  Although the initial parts of the J-resistance curves are size independent, the process of crack extension is by no means size independent because under the same applied *J*-value the crack extensions are the same, but the percentage crack extensions relative to the initial length of the ligament are different, i.e., a 3 mm crack growth in the small specimen corresponds to about 38 % of the initial ligament length (8 mm) but only about 9 % for the largest specimen.

  Comparing the J_o-resistance curves for larger crack extensions, a considerable spread is seen, with the smallest spread corresponding to the standard J_o-resistance curve. This spread is comparable with the scatter of the nominally identical repeat tests (Fig. 2-62). Thus, for the standard J_o-resistance a reasonable approximate size independence is also exhibited for crack extension larger than 3 mm.
- Gordon and Jones (Figs. 2-66 to 2-68) determined also *CTOD-resistance curves*. The standard crack-tip opening displacement (CTOD) δ_o and the CTOD corrected for

crack growth δ_R were calculated using the measured crack mouth opening displacements. Fig. 2-67 depicts the mean of three δ_o-resistance curves for each size. The two largest specimen sizes are in close agreement over the entire crack growth range, whereas the three smaller sizes show a considerable upswing which increases when the specimen size is decreased. However, if crack extensions are small, all five δ_o-resistance curves converge to a single curve so that size independence is obtained up to about 1.9 mm crack extension. The mean δ_R-resistance curves, presented in Fig. 2-68, exhibit similar trends. It is noted that the range of crack extensions where congruence of δ_o- or δ_R-resistance curves is obtained is somewhat smaller than that for the J-resistance curves.

- Whereas for most of the presented results the number of nominally identical repeat tests was fairly small (usually one to three tests), Landes (1992, [2.49]) presented ***J_{1c}-data*** for cleavage fracture of geometrically similar CT-specimens of two reactor vessel steels which allow a much better ***assessment of the scatter*** (Figs. 2-69 to 2-73). The data of the two reactor vessel steels 20MnMoNi55 and A533B were collected from different sources. The specimens were without side grooving and the ligament length was approximately equal to the thickness. A geometric scale factor between 2.5 and 8 was used. The test had been done far below 0 °C, i.e., between –150 °C and – 30 °C. According to previous results (e.g. Shaw and Spink, Figs. 2-48 and 2-49), at these low temperatures considerably more scatter is to be expected than at elevated temperatures, especially above the transition temperature.

  As Figs. 2-69 to 2-73 show, several characteristics, depending on material and temperature, appear:

  - Small specimens have frequently more scatter than large specimens (Figs. 2.69, 2-70, 2-72, 2-73). However, the number of tests for the very large specimens are usually smaller such that a comparable picture of their scatter is impaired.
  - The mean toughness of a group of nominally identical specimens of a given size and geometry and tested at a single temperature will sometimes exhibit a size effect (i.e., decreases with increasing size; Figs. 2-69, 2-71, 2-72) and other times will not (Figs. 2-70, 2-73). The cases showing a size effect included specimens with thicknesses less than or equal to 20 mm, whereas in the other cases the minimum thickness was larger, i.e., 25 mm.
  - As stated by Landes, small specimens more consistently give the lowest toughness values at a given temperature than large specimens. This result, however, is not obvious in Figs. 2-69 to 2-73. It was obtained by Landes in a special study.

In closing this review on size effects in notched specimens under quasi-static conditions, which covered result between the years 1932 and 2001, it is recalled that some problems of size effect have a long history, e.g., Galileo (1638, [3.63]) pointed out: "For we can demonstrate by geometry that the large machine is not proportionally stronger than the small", but systematic testing under impact conditions set in before and during the World War I (e.g., Stribeck (1912, [3.7]), Stanton and Batson (1920, [3.8])).

Summarizing, the review has exemplified the size dependence of a number of characteristic quantities, as obtained in the quasi-static mechanical testing of families of geometrically similar, notched specimens made of nominally the same metal material.

Investigated were primarily the normalized load-displacement curves and characteristic data derived from them, such as: (i) volume specific absorbed energies up to fracture, maximum load or crack initiation, (ii) maximum normalized load or stress and their associated normalized displacements or strains, (iii) crack initiation and associated "ductilities" (strain measures) as well as (iv) strain type measures at the notch (area reduction, diametrical strain, or relative notch month opening) at or after fracture. In fairly cursory and rough terms, the tendency is that the larger the specimens are the more these characteristic quantities decrease: i.e., strength and deformability and thus energy absorption capability reduce, crack initiation sets in earlier (at smaller strains) and cracking is more extended. Thus, the traditional characterization of materials as being ductile or brittle using laboratory tests may be misleading because a size dependent mechanism may induce a transitional behaviour, i.e., ductile response with extensive plastic deformation for small specimens and brittle response with elastic and almost no or very localized plastic deformation for large specimens. If no size dependence were present, then, in contrast to the above, all stress, strain, and volume specific energies, etc. would be the same as in classical elasticity and plasticity theories.

Some of the results, e.g., the decrease of the nominal fracture strength of relatively large specimens with increasing size can be described by concepts of Linear Elastic Fracture Mechanics and others by Elastic Plastic Fracture Mechanics, concepts which are based on the assumption of size invariant, material specific critical fracture mechanics quantities, such as the critical stress intensity factor K (fracture toughness) or energy release rate G, or the path-independent contour integral J as well as the crack-tip opening displacement. It appears that the size invariance of these quantities is a reasonable assumption under limited conditions, but considerable caution is advised; one study even suggests" that fracture toughness is demonstrably not a material property", i.e., is size dependent. This, of course, is a different notion of "size effect" as that related to the nominal stresses, strains, and volume specific energies mentioned above.

Theories to model the size dependence, such as fracture mechanics, requiring a preexisting dominant crack, and more advanced damage mechanics theories, involving an inherent length scale and describing the precursor processes, as well as higher order continuum mechanics models are the subjects of quite a number of studies, especially for non-metallic materials (see e.g., Mazars and Bazant (1989, [3.9]); Mühlhaus (1995, [3.10]); Carpinteri (1996, [3.11]); Bazant and Chen (1997, [3.12]); Bazant and Planas (1998, [3.13]); Bazant and Rajapakse (1999, [3.14])). Moreover, a number of theoretical investigations modelling size effects were also done within the EU-project LISSAC (see Krieg and Seidenfuß (2003, [3.3], 2003, [3.4])). A review of these concepts is a challenging task, but this was definitely outside the scope of the present study.

Also the comparison of the experimental results, as described in this report, with the recent experimental findings of the LISSAC-project, unfortunately, is outside the frame of this EU-project with its limited support. Yet, such a comparison is worth to be done and would show, how the experimental LISSAC results fit into the general picture of size effects in notched specimens obtained earlier. Nevertheless, this is a task for the future.

Acknowledgement

Part of this work was financially supported by the EU under the project “Limit Strains for Severe Accident Conditions (LISSAC)”, Contract No. FIKS-CT1999-00012. The lasting support of the Department of Library and Communication Services of the Forschungszentrum Karlsruhe is gratefully acknowledged. The author also expresses his thanks to B. Dolensky for preparing figures and Mrs. Schwartz and Mrs. Strehlau (all FZK-IRS) for typing the text and tables. Especially the author is indebted to G. Solomos (Joint Research Centre, IPSC-ELSA, Ispra) and R. Krieg as well as V. Heinzel (both FZK-IRS) for their thorough critique and painstaking proofreading of a first version of this report. Above all, my thanks go to my wife, Irene, for her continuous patience and understanding for many years and in particular during the writing of this report.

References

Section 1

[1.1] Malmberg, T.: Aspects of similitude theory in solid mechanics, Part I: Deformation behaviour, Forschungszentrum Karlsruhe, Scientific Report FZKA 5657, Dec. 1995

[1.2] Malmberg, T., Tsagrakis, I., Eleftheriadis , I., Aifantis, E.C.: On the gradient plasticity approach to size effects, Part I: Reviews, EU-Project REVISA, Milestone Report INV-REVISA(00)-P006, Dec. 2000, Forschungszentrum Karlsruhe, Scientific Report FZKA 6321, March 2001

[1.3] Devos, J., Auerkari, P., Lämmer, H., Le Ber, L., Messelier-Gonze, C., Malmberg, T. : REVISA-Project – Final Report (Extended Version), EU-Contract F14S-CT96-0024, Milestone Report INV-REVISA(01)-P006, CEA Rapport DM2S – Report SEMT/DIR/RT/02-002/A, March 2002

[1.4] Malmberg, T.: Similarity and size effects in the quasi-static testing of notched specimens – A review, EU-Project LISSAC, contract No. FIKS-CT1999-00012, LISSAC Document SAM-LISSAC-DO37, Aug. 2003

Section 2

[2.0] Docherty, J. G.: Bending tests on geometrically similar notched bar specimens, Engineering vol. 133, pp. 645-647, June 1932

[2.1] Docherty, J. G.: The effect of velocity of tests on notch brittleness, Engineering vol. 126, pp. 597-600, Nov. 1928

[2.2] Nadai, A., Mac Gregor, C. W.: Concerning the effect of notches and laws of similitude in material testing, Proc. ASTM vol. 34, pp. 216-228, 1934

[2.3] Kuntze, W.: Kohäsionsfestigkeit (see p. 13, Fig. 12 – 13), Mitteilungen der dt. Materialprüfungsanstalten, Sonderheft 20, Berlin, Springer-Verlag, 62 p., 1932

[2.4] Neuber, H.: Elastisch-strenge Lösungen zur Kerbwirkung bei Scheiben und Umdrehungskörpern, Zeitschrift für angewandte Mathematik und Mechanik, No. 6, p. 422, 1933

[2.5] Docherty, J. G.: Slow bending tests on large notched bars, Engineering vol. 139., pp. 211-213, Feb. 1935

[2.6] Pfender, M.: Das Verhalten der Werkstoffe bei behinderter Verformungsmöglichkeit, Archiv für das Eisenhüttenwesen vol. 12, pp. 595-606, June 1938

[2.7] Brown, W. F., Lubahn, J. D., Ebert, L. J.: Effects of section size on the static notch bar tensile properties of mild steel plate, Welding J. vol. 26, pp. 554s-559s, 1947

[2.8] Sachs, G., Lubahn, J. D.: Effect of triaxiality on the technical cohesive strength of steels, J. of Appl. Mech. vol. 12, p. 241, 1945

[2.9] Davidenkov, N., Shevandin, E., Wittmann, F.: The influence of size on the brittle strength of steel, J. of Appl.. Mech. vol. 14, pp. A63-A67, 1947

[2.10] Shearin, P. E., Ruark, A. E., Trimble, R. M.: Size effects in steel and other metals from slow notch bend tests, Fracturing of Metals, A.S.M., Cleveland Ohio, pp. 167-188, 1948

[2.11] Parker, E. R.: The effect of section size on the fracture strength of mild steel, Fracturing of Metals, A.S.M., Cleveland Ohio, pp. 82-89, 1948
[2.12] Akita, Y.: Scale effects in notch brittleness, Welding Research Supplement vol. 2, pp. 475s-480s, 1953
[2.13] Wells, A. A.: The geometrical size effect in notch brittle fracture, Trans. N. Coast Inst. Eng. Shipbuilding vol. 71, pp. 278-290, 1955
[2.14] Wells, A. A.: The mechanics of notch brittle fracture, Welding Research vol. 7, no. 2, p. 34r-56r, April 1953
[2.15] Lubahn, J. D.: Room temperature crack propagation and size effect on mild steel, Welding Research Supplement vol. 34, pp. 518s-528s, 1955
[2.16] Lape, E. M., Lubahn, J. D.: On the relation between various laboratory fracture tests, Trans. Am. Soc. Mech. Eng. vol. 78, pp. 823-835, 1956
[2.17] Lubahn, J. D.: Effect of section size on fracturing, Proc. of the Sagamore Army Materials Research Conf., Syracuse, NY 1955, pp. 143-161, 1955
[2.18] Lubahn, J. D., Yukama, S.: Size effect in slow notch-bend tests of a nickel-molybdenium-vanadium steel, Proc. Am. Soc. Test. Mater. vol 58, pp. 661-677, 1958
[2.19] Lequear, H. A., Lubahn, J. D.: Root conditions in a V-notch Charpy impact specimen, Welding Research Supplement, pp. 585s-588s, Dec. 1954
[2.20] Lubahn, J. D.: Experimental determination of energy release rate for notch bending and notch tension, Proc. ASTM vol. 59, pp. 885-913, 1959
[2.21] Sachs, G.: Some fundamentals of the flow and rupture of metals, Trans. Am. Inst. of Mining and Metallurgical Engineers vol. 143, pp. 12-29, 1941
[2.22] Wundt B. M.: A unified interpretation of room temperature strength of notched specimens as influenced by their size, ASME Publ., paper no. 59-Met-9, 13 p., 1959
[2.23] Sachs, G., Lubahn, J. D., Ebert, L. J.: The effect of notches of varying depth on the strength of heat treated low alloy steels, Trans., Am. Soc. for Met. vol. 34, pp. 517-544, 1945
[2.24] Yukawa, S., McMullin, J. G.: Effects of specimen size and notch acuity on the brittle fracture strength of a heat treated steel, Trans. ASME, J. Basic Eng. vol. 83, pp. 541-544, 1961
[2.25] DeSisto, T. S., Carr, F. L., Larson, F. R.: Influence of section size on mechanical properties and fracture toughness of 7075-T6 aluminum, 6Al-6V-2Sn titanium, and AISI 4340 steel, Proc. ASTM vol. 63, pp. 768-778, 1963
[2.26] Wellinger, K., Pröger, M.: Size effects in notched bar tensile tests on steel (Größeneffekte beim Kerbzugversuch mit Stahl), Materialprüfung vol. 10, no. 12, pp. 397-404, 1968
[2.27] Nelson, F. G., Schilling, P. E., Kaufmann, J. G.: The effect of specimen size on the results of plane-strain fracture-toughness tests, Eng. Fracture Mech. vol. 4, pp. 33-50, 1972
[2.28] Anderson, T.L.: Fracture Mechanics-Fundamentals and Applications, CRC Press, Boca Raton, London, New York, Washington D.C., 1995
[2.29] Neale, B. K.: An investigation into the effect of thickness on the fracture behaviour of compact tension specimens, Int. J. of Fracture vol. 14, no. 2, pp. 203-212, 1978
[2.30] Pisarski, H.G.: Influence of thickness on critical crack opening displacement (COD) and J values, Int. J. of Fracture vol. 17, no. 4, pp. 427-440, 1981
[2.31] Ewalds, H.L., Wanhill R.J.H.: Fracture mechanics, Edward Arnold & Delftse Uitgevers Maatschappij., 1984

[2.32] Sumpter, J.D.G., Turner, C.C.: A method for laboratory determination of J_c, ASTM STP 601, pp. 3-18, 1976
[2.33] Milne, J., Chell, G.G.: Effect of size on the J fracture criterion, in: Landes, J.D., Begley, J.A., Clarke, G.A.: Elastic-Plastic Fracture, ASTM STP 668, pp. 358-377, 1979
[2.34] Ritchie O., Knott J.F., Rice, J.R.: On the relation between critical tensile stress and fracture toughness in mild steel, J. Mech. and Phys. of Sol. vol. 21, pp. 395-410, 1973
[2.35] Shaw, N.B., Spink, G.M.: The effect of temperature, specimen size, and geometry on the fracture toughness of a 3 pct NiCr MoV low pressure turbine disc steel, Metallurgical Transactions A vol. 14A, pp. 751-759, 1983
[2.36] Hagiwara, R., Takanabe, H., Kawano, H.: A proposed method of predicting ship collision damage, Int. J. Impact Eng. vol. 1, no. 3, pp. 257-279, 1983
[2.37] Takeuchi, T., Yasunaka, T., Nishijima, S.: Size effects on the load displacement curves of compact specimens of SUS316-steel (Japanese), Trans. Japan Soc. Mech. Eng. vol. 51, no. 465, pp. 1385-1392, 1985
[2.38] Takeuchi, T., Yasunaka, T., Nishijima, S.: Size Effect on the load-displacement curves of compact specimens of SUS316 steel (English), Bulletin of JSME vol. 29, no. 247, pp. 22-28, 1986
[2.39] Wallin, K.: The size effect in K_{IC} results, Eng. Fracture Mech. vol. 22, no. 1, pp. 149-163, 1985
[2.40] Gibson, G.P., Druce, S.G., Turner, G.E.: Effect of specimen size and geometry on ductile crack growth resistance in a C-Mn steel, Int. J. of Fracture vol. 32, pp. 219-240, 1987
[2.41] Brothers, A.J., Hill, M., Parker, M.T., Spitzig, W.A., Wiebe, W., Wolf, O.E.: Correlation of fracture toughness, K_{IC}, with fractographically derived plastic stretched zone width-a report of ASTM E-24/II task group, ASTM STP493, pp. 3-19, 1971
[2.42] Broek, D.: Elementary engineering fracture mechanics, Martinus Nijhoff Publ., Doodrecht, Boston, Lancaster, 1986
[2.43] Ernst, A.E.: Material resistance and instability beyond J-controlled crack growth, ASTM STP803, pp. 191-213, 1983
[2.44] Gibson, G.P., Druce, S.G.: ASTM STP856, pp. 166-182, 1985
[2.45] Sinclair, G.B., Chamers, A.E.: Strength size effects and fracture mechanics: what does the physical evidences say? Engineering Fracture Mech. vol. 26, no. 2, pp. 279-310, 1987
[2.46] Gordon, J.R., Jones R.: The effect of specimen size on the J-R curve behaviour of a titanium alloy, Fatigue Fracture Eng. Mat. Struct. vol. 12, no. 4, pp. 295-308, 1989
[2.47] Gordon, J.R., Jones, R.L.: The effect of specimen size on the CTOD R-curve behaviour of a titanium alloy, Fatigue Fracture Eng. Mat. Struct. vol. 12, no. 4, pp. 309-321, 1989
[2.48] Ernst, H.A., Paris, P.C., Landes, J.D.: Estimation on J-Integral and tearing modulus T from a single specimen test record, ASTM STP743, pp. 476-502, 1981
[2.49] Landes, J.D.: The effect of size, thickness and geometry on fracture toughness in the transition, GKSS-Forschungszentrum Geesthacht GmbH, Report GKSS92/E/43, 1992
[2.50] Giovanola, J.H., Kirkpatrick, S.W., Crocker J.E.: Investigation of scaling effects in elastic-plastic ductile fracture using the local approach, Journal de Physique IV, Colloque C6, supplement an Journal de Physique III, vol. 6, pp. C6-513 – C6-520, 1996
[2.51] Giovanola, J.H., Kirkpatrick, S.W.: Using the local approach to evaluate scaling effects in ductile fracture, Int. J. of Fracture vol. 92, pp. 101-116, 1998

[2.52] Giovanola J.H., Kirkpatrick, S.W., Crocker, J.E.: Fracture of geometrically scaled, notched three-point-bend bars of high strength steel, Eng. Fracture Mech. vol. 62, pp. 291-310, 1999

[2.53] Link, R.E.: Private communication to Giovanola et al., US Naval Academy, Annapolis, 1994

[2.54] Kumar, V., German, M.D., Shih, C.F.: An engineering approach for elastic-plastic fracture analysis, Electric Power Research Institute, EPRI NP-1931, Research Project 1237-1, Topical Report, July 1981

[2.55] Knott, J.K.: Micro mechanisms of fracture and the fracture toughness of engineering alloys, Fracture vol. 1, pp. 61-92, 1977

[2.56] Devillers-Guerville, L., Besson, J., Pineau, A.: Notch fracture toughness of a cast duplex stainless steel : modelling of experimental scatter and size effect, Nuclear Engineering and Design vol. 168, pp. 211-225, 1997

[2.57] Pineau, A.: Modelling of scatter and size effects in ductile and brittle fracture, Trans. 14th Int. Conf. Struct. Mech. in Reactor Technology (SMiRT-14), Lyon, France, Aug. 17-22, Plenary Session 4, pp. 77-88, 1997

[2.58] Besson, J., Devillers-Guerville, L., Pineau, A.: Modelling of scatter and size effect in ductile fracture : application to thermal embrittlement of duplex stainless steels, Engineering Fracture Mechanics vol. 67, pp. 169-190, 2000

[2.59] Pineau, A., Joly, P.: Local versus global approaches to elastic-plastic fracture mechanics. Application to ferritic steels and cast duplex stainless steels, in: Assessment in Components-Fundamentals and Application, Blauel, J.G. and Schwalbe, K.H. (eds.), ESIS/EGF9, Mechanical Engineering Publications, London, pp. 381-414, 1991

[2.60] Pineau, A.: Modelling micromechanisms and statistical features of ductile fracture, in: ECF10-Structural Integrity: Experiments, Models and Application, Schwalbe, K.H., and Berger, C. (eds.), Warley: EMAS, pp. 37-51, 1994

[2.61] Joly, P., Pineau, A.: Modelling of the effect of thermal aging of duplex stainless steels on their fracture toughness, Scand. J. Metal. vol. 24, pp. 226-236, 1995

[2.62] Malmberg, T., Krompholz, K., Solomos, G., Aifantis, E.C.: Investigations on size effects in ferritic and austenitic materials, Trans. of the 15th Int. Conf. on Structural Mechanics in Reactor Technology (SMiRT-15), Seoul, Korea, Aug. 15-20. 1999, vol. X, paper L06/5, pp. X299 - X306, 1999

[2.63] Decamp, K., Bauvineau, L., Besson, J., Pineau, A. : Size and geometry effects on ductile rupture of notched bars in a C-Mn steel : experiments and modelling, Int. J. of Fracture vol. 88, pp. 1-18, 1997

[2.64] Marini, B., Carassou, S., Wident, P., Soulat, P.: Evaluation of the fracture toughness of a C-Mn steel using small notched tensile specimens, in: Small Specimen Test Techniques (Corwin W.R. et al., eds.), ASTM-STP1329, pp. 513-522, 1998

[2.65] Devos, J., Auerkari, P., Lämmer, H., LeBer, L., Messelier-Gouze, C., Malmberg, T.: REVISA Project-Summary Final Report, EU-Contract F14S-CT96-0024, Milestone Report INV-REVISA(01)-P007; CEA Rapport DM2S-Report SEMT/DIR/RT/02-001/A, March 2002

[2.66] Devos, J., Auerkari, P., Lämmer, H., LeBer, L., Messelier-Gouze, C., Malmberg, T.: REVISA Project-Final Report (Extended Version), EU-Contract F14S-CT96-0024, Milestone Report INV-REVISA(01)-P006, CEA Rapport DM2S-Report SEMT/DIR/RT/02-002/A, March 2002

[2.67] Krompholz, K., Kamber, J., Kalkhof, D.: A preliminary study of material homogeneity for size effects investigations, Paul Scherrer Institut, PSI-Report No. 9903, June 1999, EU-Project REVISA Technical Report INV-REVISA(99)-P022, June 1999

[2.68] Malmberg, T., Dolensky, B., Krompholz, K.: Supplementary evaluation of material homogeneity in six plates of the ferritic steel 20 MnMoNi 55, Forschungszentrum Karlsruhe, Paul Scherrer Institut, EU-Project REVISA, Technical Report INV-REVISA(00)-P014, Dec. 2000

[2.69] Materna-Morris, E., Graf, P., Zimmermann, H., Malmberg, T.: Investigations of size and strain rate Influences on fracture surfaces of smooth tensile specimens of austenitic X6CrNiN6 1810 (1.4550) and ferritic-bainitic steels 20 MnMoNi 55 (1.6310), Forschungszentrum Karlsruhe, Scientific Report FZKA 6525, Dec. 2002

[2.70] Krompholz, K., Kamber, J., Groth, E., Kalkhof, D.: Size effect studies on smooth tensile specimens at room temperature, Paul Scherrer Institut, PSI-Report No. 00-02, June 2002, EU-Project REVISA, Technical Report INV-REVISA(00)-P005, July 2000

[2.71] Malmberg, T., Tsagrakis, I., Eleftheriadis, I., Aifantis, E.C.: On the gradient plasticity approach to size effects, Part I: Reviews; Forschungszentrum Karlsruhe, Scientific Report FZKA 6321, March 2001, EU-Project REVISA, Milestone Report INV-REVISA(00)-P006, Dec. 2000

[2.72] Krompholz, K., Kamber, J., Groth, E., Kalkhof, D., Malmberg, T.: Size effect studies on notched tensile specimens at room temperature and 400 °C (revised version), Paul Scherrer Institut & Forschungszentrum Karlsruhe, REVISA-Project document INV-REVISA(00)-P015, July 2001

[2.73] Malmberg, T., Krompholz, K., Kalkhof, D., Solomos, G., Aifantis, E.C.: Size effects in deformation and fracture of a ferritic reactor pressure vessel steel, Trans. 16th Int. Conf. Structural Mechanics in Reactor Technology (SMiRT-16), Washington D.C., USA, Aug. 12-17, 2001, Division F, paper no. 1224

[2.74] Tsagrakis, I., Malmberg, T., Aifantis, E.C.: Gradient plasticity and size effects, Proceedings of the 5th National Congress on Mechanics, Joannina, Greece, Aug. 1998, vol. 2, pp. 953-960, (Theocaris, P.S., Fotiadis, D.I., Massalas, C.V. eds.) Publ. by the University of Joannina Press, 1998

[2.75] Malmberg, T., Tsagrakis, I., Eleftheriadis, I., Aifantis, E.C.: On the Gradient Plasticity Approach to Size Effects, Part II: Applications, Forschungszentrum Karlsruhe, Scientific Report FZKA 6321, March 2001; EU-Project REVISA, Milestone Report INV-REVISA(00)-P006, Dec. 2000

[2.76] Krompholz, K., Kalkhof, D., Groth, E.: Size effect studies on geometrically scaled three-point bend type specimens with U-notches, Paul Scherrer Institut, PSI-Report No. 01-03, Feb. 2001; EU-Project REVISA, Technical Report INV-REVISA(00)-P016, Feb. 2001

Section 3

[3.1] Brown, W.F., Srawley, J.E.: Plane strain crack toughness testing of high strength metallic materials, ASTM Special Technical Publ. No. 410, ASTM, 1962

[3.2] 1982 Annual Book of Standards, Part 10, ASTM, 1982

[3.3] Krieg, R., Seidenfuß, M.: Limit strains for severe accident conditions, Final Report of the EU-Project LISSAC, Contract No. FIKS-CT1999-0012, Forschungszentrum Karlsruhe, Scientific Report FZKA 6854, Oct. 2003

[3.4] Krieg, R., Seidenfuß, M.: Limit strains for severe accident conditions, Synthesis Report of the EU-Project LISSAC, Contract No. FIKS-CT1999-00012, Forschungszentrum Karlsruhe, Scientific Report FZKA 6914, Oct. 2003

[3.5] Kreyszig, E.: Statistische Methoden und ihre Anwendungen, Vandenhoek & Ruprecht, 1977

[3.6] Galilei, G.: Dialogues concerning two new sciences (engl. tranl.), first publ. 1914 by the Macmillan Comp., reprint by Dover Publications Inc., New York; original publ.: In Leida, Appresso gli Elsevirii. M.D.C.XXXVIII.

[3.7] Stribeck, R.: Die Kerbschlagprobe und das Aehnlichkeitsgesetz (the notched-bar impact specimen and the law of similarity), Stahl und Eisen, 35 Jahrg., Nr. 15, pp. 392-369, 1915

[3.8] Stanton, T.E., Batson, R.G.: On the characteristics of notched-bar impact tests, Proc. Inst. C.E. vol. 211, pp. 67-100, 1920

[3.9] Mazars, J., Bazant, Z.P.: Cracking and damage; strain localization and size effect, Proc. France-US Workshop, Laboratoire de Mecanique et Technology, Cachan, France, Sept. 6-9, 1988 ; Elsevier Applied Science, London, New York, 1989

[3.10] Mühlhaus, H.-B. (Ed.): Continuum models for materials with microstructure, John Wiley & Sons, Chichester, New York, Brisbane, Toronto, Singapore, 1995

[3.11] Carpinteri, A. (Ed.): Size-scale effects in the failure mechanism of materials and structures, Proc. of IUTAM-Symposium, Oct. 3-7, 1994, Politecnico, Turin, Italy; E & FN SPON, London, Glasgow, Weinheim, New York, Tokyo, Melbourne, Madras, 1996

[3.12] Bazant, Z.P., Chen, E.-P.: Scaling of structural failure, Appl. Mech. Rev. vol. 50, pp 593-627, 1997

[3.13] Bazant, Z.P., Planas, J.: Fracture and size effect in concrete and other quasibrittle materials, CRC Press, Boca Raton, Boston, London, New York, Washington D.C., 1998

[3.14] Bazant, Z.P., Rajapakse Y.D.S. (Eds.): Workshop on fracture scaling, University of Maryland, June 10-12, 1999; Special Issue of the Int. J. of Fracture vol. 95, 1999

Appendix 1: Qualitative Estimations

Appendix 1

Qualitative Estimations for the Correction of the Load-Deflection Curve of a Notched Three-Point-Bend Specimen with Overlength of the Span.

Lubahn (1953, [2.15]) performed slow bend tests under three-point loading of V-notched bar specimens. Among others, two specimen sizes were considered with unnotched cross sections 0.08 x 0.08 in = 2.03 x 2.03 mm and 2 x 2 in = 25.4 x 25.4 mm and geometrically similar V-notches (geometric scale factor $\lambda = 25$). For the small specimens the loading span was 3/8 in = 9.53 mm and for the large specimen an overlength span of 11 in = 279.4 mm (scale factor $\lambda_{span} = 29.33$ was used; the length of a properly scaled span would be 3/8 λ = 9.375 in = 238.13 mm. For the small specimen the load-deflection curve is shown in Fig. 2-24. The load-deflection curve of the large specimen (with overlength span!) was scaled down to be comparable with the small specimen by multiplying the loads with $(0.08/2)^2$ and the deflections with (0.08/2). The result is also shown in Fig. 2-24, but because of the overlength span, this result is distorted.

In the following, a simple model will be used to indicate the qualitative change of the load-deflection curve of the large specimen when the span is reduced to the properly scaled length.

It is assumed that under three-point loading all the plastic deformation is concentrated in the notched region with rigid behaviour of the rest of the bar. Thus, the specimen will be represented by two rigid bar sections of length L simply supported at the ends, but connected in the centre by a plastic hinge transmitting moments. If P is the load at the centre, then the moment at the hinge is

$$M = P\,L/2. \qquad \text{(A1-1)}$$

With $\varphi = 2\,\alpha$ being the rotation angle between the two rigid segments (Fig. A1-1), it is assumed that the bending moment M is a power function of the angle φ, i.e.,

$$M = C\,\varphi^{n} \quad , n < 1 \qquad \text{(A1-2)}$$

where the constant C depends on the cross section at the notch and the material. The exponent n is depending on the material, i.e., the hardening exponent $m < 1$ of the uniaxial stress-strain relation $\sigma \sim \varepsilon^m$, but also on the cross section at the notch, e.g., the depth of the notch. However, these relations are not known, and their determination would require a more detailed model. In any case, the two parameters C and n approximately do not depend on the length of the specimen. It should be noted that this model appears to be reasonable only up to the instant of crack initiation.

For small deformations, the centre-deflection w is given by

$$w = L \sin\alpha \approx L\,\alpha = L\,\varphi/2 \quad . \qquad \text{(A1-4)}$$

Thus

$$M = C^{*}\,(w/L)^{n},\ C^{*} = C2^{n}$$

and the load-deflection relation is given by

$$P = \frac{2}{L} C^{*} \left(\frac{w}{L}\right)^{n} . \qquad \text{(A1-4)}$$

For two different spans

$$L_1 > L_2 \ ,$$

one has

$$P = \frac{2C^*}{L_1}\left(\frac{w}{L_1}\right)^n, \qquad P = \frac{2C^*}{L_2}\left(\frac{w}{L_2}\right)^n.$$

Applying the same load

$$P = P_1 = P_2$$

to the two specimens, one gets

$$\frac{P_2}{P_1} = \frac{L_1}{L_2}\left(\frac{w_2}{L_2}\right)^n\left(\frac{L_1}{w_1}\right)^n = \left(\frac{L_1}{L_2}\right)^{1+n}\left(\frac{w_2}{w_1}\right) = 1$$

which yields

$$\frac{w_2}{w_1} = \left(\frac{L_2}{L_1}\right)^{\frac{1+n}{n}}. \qquad \text{(A1-5)}$$

With $(1+n)/n > 1$ and $L_2/L_1 < 1$ one gets

$$\frac{w_2}{w_1} < 1. \qquad \text{(A1-6)}$$

This implies a shift of the deflection to smaller values under the same load when the length of the span L_1 is reduced. This result simply reflects the consequence that reducing the length L ($L_1 > L_2$) brings down the moment M for the same load which then yields a reduction of the rotation φ, Equ. (A1-2), and also the displacement w, Equ. (A1-3).

The ratio L_2/L_1 is given by

$$L_2/L_1 = \frac{3 \cdot 25}{8 \cdot 11} = 0.8523.$$

Since the exponent $m < 1$ is not known, some parameter calculations (Tab. A1-1) demonstrate the tendencies for the ratio w_2/w_1. It should be noted that the ratio w_2/w_1 is not affected whether the deflections w_1 and w_2 for the large specimen are scaled down with the factor (0.08/2) or not. Therefore, with increasing nonlinearity, i.e., exponent n, the shift of the P-w curve to the left for the (2 x 2 in) specimen (Fig. A1-1) will increase considerably.

The deflections indicating crack initiation are also marked in Fig. 2-24. However, for the (2 x 2 in) specimen this instant should also be shifted to the left. With the crack-tip-opening-displacement concept in mind (CTOD-concept, see Anderson (1995, [2.28], Equ. (3.9)), it is assumed that the crack initiation is controlled[1] by the notch opening angle or equivalently w/L. Thus, for the large specimen with overlength L_1, the ratio w_{1C}/L_1 is a measured quantity where w_{1C} is the critical deflection at crack initiation. With Equ. (A1-4) one gets

$$P_{1C} = \frac{2}{L_1}C^*\left(\frac{w_{1C}}{L_1}\right)^n.$$

For the properly scaled large specimen with reduced length L_2, one obtains

$$P_{2C} = \frac{2}{L_2}C^*\left(\frac{w_{2C}}{L_2}\right)^n$$

and since

[1] One should not imply that this is generally valid for geometrically similar specimens of different size!

$$\frac{w_{1C}}{L_1} = \frac{w_{2C}}{L_2} \qquad \text{(A1-7)}$$

at crack initiation, one finds

$$\frac{w_{2C}}{w_{1C}} = \frac{L_2}{L_1} = 0.8523 < 1$$

and

$$P_{1C}L_1 = P_{2C}L_2$$

which simply means that crack initiation occurs under the same moment. Consequently,

$$\frac{P_{2C}}{P_{1C}} = \frac{L_1}{L_2} > 1,$$

i.e., the critical load increases. With $L_1/L_2 = 1.17\overline{3}$, the increase is 17 %.

Tab. A1-1
Influence of the lumped hardening exponent n on the deflection ratio w_1/w_2 of two beams with a centered plastic hinge , same cross sections and loadings, different lengths: $L_2/L_1 = 0.8523$

Exponent n	0.05	0.10	0.20	0.30	0.50	1.00
Deflection Ratio w_2 / w_1	0.0348	0.1723	0.3832	0.5002	0.6191	0.7264

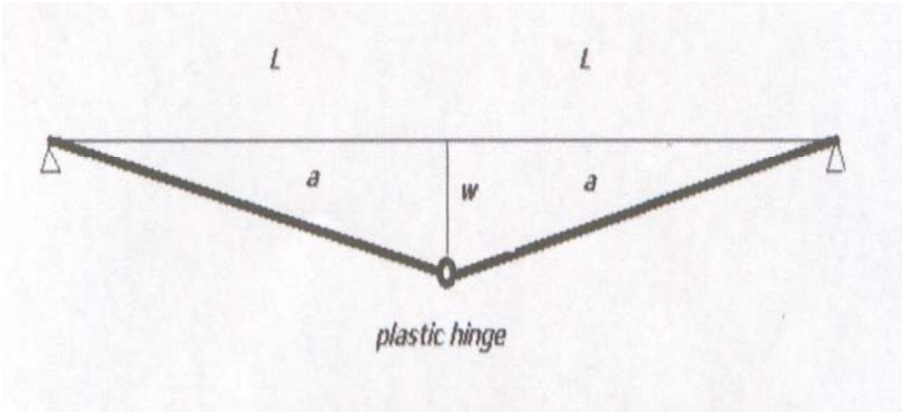

Fig. A1-1
Ersatz-model for notched bending specimen

Appendix 2: Tables

Tab. 2-1
Nominal dimensions of geometrically similar Izod-type specimens; based on Ref. [2.0]

Width x height mm	V-notch depth mm	Ligament mm	Root radius mm	Overhang* mm	Distance of load point from notch mm
4x4	0.8	3.2	0.1	11.2	8.8
7x7	1.4	5.6	0.175	19.6	15.4
10x10	2.0	8.0	0.25	28.0	22.0
12x12	2.4	9.6	0.3	33.6	26.4

* half length of specimen

Tab. 2-2
Area reduction after fracture in a tensile test; data extracted from Fig. 6 of Ref. [2.0]

A:	mild steel, as rolled	Z = 60%
B:	mild steel, normalized	64%
F:	3% Ni-steel, normalized	45.5%
H:	Monel metal, annealed	70%
K:	naval brass, annealed	45.5%
L:	phosphor bronze, as rolled	81%
M:	phosphor bronze, annealed	84.5%
AA:	0.3% C-steel, normalized	60%

Tab. 2-3
Size effect on absorbed energy of notch bend specimens of different metals and load point displacement rates; from Ref. [2.0]

Metal.	Size. mm.	Energy Absorbed (ft. lb.) at Speed of				
		Izod.	150 in./min.	50 in./min.	6 in./min.	0·05 in./min.
A. Mild steel as rolled	4 × 4	6·4	6·3	5·92	5·84	4·96
	7 × 7	30·2	26·9	26·7	25·9	22·7
	10 × 10	75·8	65·8	61·9	59·6	52·0
B. Mild steel normalised	4 × 4	6·6	5·93	5·68	5·39	4·98
	7 × 7	30·2	26·1	25·8	24·8	21·9
	10 × 10	71·2	64·1	62·1	60·0	51·9
F. 3 per cent. Ni steel normalised	4 × 4	2·44	2·58	2·58	2·72	2·5
	7 × 7	7·5	8·56	8·56	8·3	7·5
	10 × 10	15·4	22·4	23·8	23·5	21·5
	12 × 12	24·7	33·5	34·2	35·4	30·5
H. Monel metal annealed	4 × 4	8·04	8·02	7·64	7·43	6·74
	7 × 7	41·3	39·1	39·2	38·4	28·3
	10 × 10	120 (about)	117·2	116·1	113·5	67·5
	12 × 12	—	195·0	189·0	185·0	116·0
K. Naval brass annealed	4 × 4	2·69	2·5	2·49	2·37	2·01
	7 × 7	9·82	8·64	8·21	7·96	6·69
	10 × 10	23·6	22·5	20·8	19·8	17·8
	12 × 12	40·0	36·2	35·1	33·6	29·6
L. Phosphor bronze as rolled	4 × 4	5·8	5·84	5·55	5·37	4·81
	7 × 7	26·4	28·1	27·5	26·7	24·2
	10 × 10	75·9	73·4	—	72·0	66·4
	12 × 12	116·0	112·8	112·9	109·8	102·0
M. Phosphor bronze annealed..	4 × 4	4·5	4·3	4·2	4·0	3·9
	7 × 7	22·0	21·7	21·4	20·6	19·4
	10 × 10	67·3	65·8	—	62·3	58·4
	12 × 12	112·5	112·3	110·6	106·7	101·3
AA. 0·3 per cent. C. steel normalised ..	7 × 7	12·6	15·9	15·7	15·1	14·9
	10 × 10	19·5	30·5	30·2	28·0	29·2
	12 × 12	35·2	52·8	51·4	49·5	45·3

Tab. 2-4

Volume specific absorbed energy (10^{-3} J/mm^3); reference volume = W^3; data based on Ref. [2.0]

Material	Size WxW mm	Speed in/min				
		Izod	150	50	6	0.05
A	4x4	135.582	133.464	125.413	123.719	105.008
	7x7	119.375	106.331	105.541	102.378	089.729
	10x10	102.771	89.213	83.923	80.806	70.503
B	4x4	139.819	125.625	120.329	114.185	92.789
	7x7	119.375	103.169	101.983	98.030	86.567
	10x10	96.535	86.908	84.196	81.349	70.367
F	4x4	51.690	54.656	54.656	57.622	52.962
	7x7	29.646	33.836	33.836	32.808	29.646
	10x10	20.880	30.370	32.369	31.862	29.150
	12x12	19.380	26.284	26.834	27.775	23.931
H	4x4	170.325	169.901	161.851	157.402	142.785
	7x7	163.252	154.556	154.951	151.789	111.865
	10x10	162.698	158.902	157.410	153.886	91.518
	12x12	-	153.001	148.293	145.154	91.016
K	4x4	56.987	52.962	52.750	50.208	42.581
	7x7	38.799	34.152	32.453	31.465	26.444
	10x10	31.997	30.506	28.201	26.845	24.134
	12x12	31.385	28.403	27.540	26.363	23.225
L	4x4	122.871	123.719	117.575	113.762	101.898
	7x7	104.355	111.074	108.703	105.541	95.658
	10x10	102.907	99.517	-	97.619	90.026
	12x12	91.016	88.113	87.877	86.151	80.031
M	4x4	95.331	91.094	88.976	84.739	82.620
	7x7	86.926	85.776	84.591	81.428	76.685
	10x10	91.247	89.213	-	84.468	79.180
	12x12	88.270	88.113	86.779	83.719	79.482
AA	4x4	-	-	-	-	-
	7x7	49.806	62.850	62.059	59.688	58.897
	10x10	26.438	41.353	40.946	37.963	39.590
	12x12	27.619	41.428	40.329	38.839	35.543

Tab. 2-5
Percentage increase of volume specific energy with increase in speed for constant size 10x10 specimens; data based on Ref. [2.0]

Material	Speed factor		
	6/0.05=120	50/0.05=1000	150/0.05=3000
A	14.6 %	19 %	26.5 %
B	15.6 %	19.7 %	23.5 %
F	9.3 %	10.7 %	4.2 %
H	68.1 %	72 %	73.6 %
K	11.2 %	16.9 %	26.4 %
L	8.4 %	-	-
M	6.7 %	-	12.7 %
AA	-4.1 %	2.7 %	4.5 %

Tab. 2-6
Area reduction and magnitude of size effect; data based on Ref. [2.0]

Material	Area reduction * %	Magnitude of size effect -	Size range mm
M	84.5	1.04	4 ÷ 12
L	81	1.27	4 ÷ 12
H	70	1.57	4 ÷ 12
B	64	> 1.32	4 ÷ 10
A	60	> 1.49	4 ÷ 10
AA	60	> 1.65	7 ÷ 12
F	45.5	2.2	4 ÷ 12
K	45.5	1.83	4 ÷ 12

* Quasistatic tensile tests of smooth specimens

Tab. 2-7
Area specific absorbed energy (J/mm^2); data based on Ref. [2.0]

Material	Size WxW mm	Speed in/min	
		6	0.05
A	4x4	0.61893	0.52538
	7x7	0.89581	0.78513
	10x10	1.01009	0.88128
	12x12	-	-
B	4x4	0.57093	0.51797
	7x7	0.85776	0.75746
	10x10	1.01687	0.87959
	12x12	-	-
F	4x4	0.28811	0.26481
	7x7	0.28707	0.25940
	10x10	0.39827	0.36438
	12x12	0.41663	0.35896
H	4x4	0.78701	0.71392
	7x7	1.32815	0.97882
	10x10	1.92357	1.14397
	12x12	2.1773	1.36524
K	4x4	0.25104	0.21291
	7x7	0.27531	0.23139
	10x10	0.33557	0.30167
	12x12	0.39545	0.34837
L	4x4	0.56881	0.50949
	7x7	0.92348	0.83701
	10x10	1.22024	1.12533
	12x12	1.29227	1.20047
M	4x4	0.42369	0.41131
	7x7	0.71249	0.67099
	10x10	1.055845	0.98975
	12x12	1.25578	1.19223
AA	4x4	-	-
	7x7	0.52227	0.51535
	10x10	0.47454	0.49487
	12x12	0.58258	0.53315

Tab. 2-8
Dimensions and test results of tension tests of semicircular- and V-notched round bars of mild steel; from Ref. [2.2]

Test Specimen	Ratio of Sizes of Bars	Diameter at Notch, in.	Radius of Groove at Notch, in.	Average Speed of Loading, lb. per min.	Tensile Strength, lb. per sq. in.
GROUP A, SEMICIRCULAR NOTCH (FIG. 4)					
No. 1	8	0.707	0.125	3100	74 300
No. 2	8	0.707	0.125	3100	74 000
No. 3	4	0.353	0.0625	763	72 600
No. 4	4	0.353	0.0625	763	72 900
No. 5	1	0.0883	0.0156	48.4	75 900
No. 6	Broke prematurely				
No. 7	1	0.0883	0.0156	48.4	76 900
No. 8	1	0.086	0.0156	48.4	77 400
GROUP B, V-NOTCH (FIG. 3)					
No. 9	4	0.3535	0.040	763	76 800
No. 10	4	0.3535	0.040	763	75 900
No. 11	1	0.0883	0.010	48.4	76 800
No. 12	1	0.0883	0.010	48.4	75 700

[a] For all test specimens in this table the notch factor was the same: $K = 0.5$.

Tab. 2-9
Dimensions of three-point bend specimens; material: forged mild steel; data based on Ref. [2.5]

Material	Height x width mm	V-notch depth mm	Root radius mm	Span mm
A	10x2.5	2	0.25	44
	10x5	4	0.5	88
	50x12.5	10	1.25	220
	100x25	20	2.5	440
B	10x10	2	0.25	44
	20x20	4	0.5	88
	50x50	10	1.25	220
	100x100	20	2.5	440

Tab. 2-10
Tensile test data of material A and B; data from Ref. [2.5]

Material	R_m tons/sq.in.:	A %	Z %	Izod test ft.-lb.
A	28.0	27	62.5	33
B	27.9	39	64.0	40/45

Tab. 2-11
Dimensions of notched tension specimens of a medium carbon steel; from Ref. [2.7]

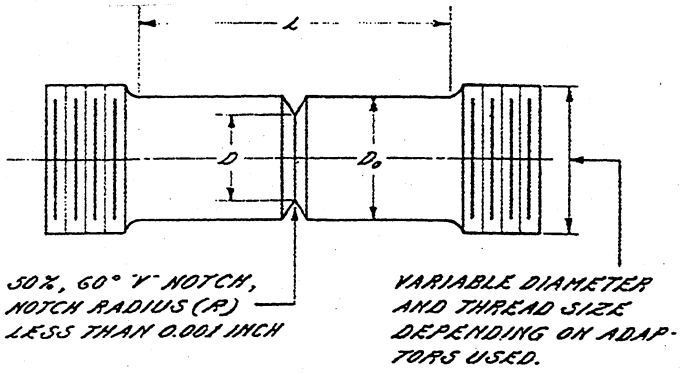

DIMENSIONS OF NOTCHED TENSILE SPECIMENS				
SECTION SIZE -IN.	CYLINDRICAL DIA. (D_o) -IN.	NOTCH DIA. (D) -IN.	CYLINDRICAL LENGTH (L) -IN.	NOTCH SHARPNESS D/2R
1/4	0.250 ± 0.001	0.177 ± 0.001	5/8 ± 1/64	90
1/2	0.500 ± 0.001	0.353 ± 0.001	1 1/4 ± 1/64	180
1	1.000 ± 0.002	0.707 ± 0.002	2 1/2 ± 1/32	350
2	2.000 ± 0.002	1.414 ± 0.002	5 ± 1/32	700
4	4.000 ± 0.003	2.830 ± 0.003	10 ± 1/32	1400

Tab. 2-12
Dimensions of four-point-bend specimens (SENB-type) and tolerances; from Ref. [2.10]

Nominal size in	0.4	1 1/4	1 7/8
Width			
in	0.395 ± 0.004	1.250 ± 0.010	1.875 ± 0.010
mm	10.03	31.75	47.62
Depth			
in	0.400 ± 0.005	1.250 ± 0.010	1.875 ± 0.010
mm	10.16	31.75	47.62
Notch diam.			
in	0.024 ± 0.001	0.076 ± 0.002	0.114 ± 0.002
mm	0.61	1.90	2.90
Retained depth after lapping	80 % of depth ± 2 %		

Tab. 2-13
Volume specific work densities from moment-angle curves; material (A1): 18 in-thick Ni-Cr steel plate (tempered bainite region); different specimen directions; from Ref. [2.10]

(W_1 and W_2 Regions Are Separated by Sloping Lines)

Specimen Size and Direction	No.	Work Density, Ft-Lb./Cu. In. W_1	W_2	W
0.4" OX	F6A	687	907	1594
	F6B	753	920	1673
	F6C	719	931	1650
	F6D	668	959	1627
	Mean	707	929	1636
1.25" OX	F4A	501	485	986
	F4B	480	476	956
	F4C	515	476	991
	Mean	499	479	978
1.875" OX	F6A	367	340	707
	F6B	320	319	639
	Mean	343	330	673
0.4" OY	211D	554	678	1232
	221C	652	683	1335
	221D	653	617	1270
	Mean	620	659	1279
1.25" OY	211	415	345	760
	221	323	381	704
	Mean	369	363	732
1.875" OY	F4A	251	316	567
	231	237	282	519
	Mean	244	299	543
0.4" OZ	112B	360	455	815
	121C	404	460	864
	121D	412	446	858
	133B	411	485	896
	Mean	397	462	858
1.25" OZ	113	240	206	446
	121	203	246	449
	132	194	246	440
	Mean	212	232	444
1.875" OZ	F1A	136	133	269
	F1B	143	231	374
	Mean	140	182	322

Tab. 2-14
Mean volume specific work densities of different steels; from Ref. [2.10]

Specimen Size and Direction	No. Specs.	Work Density, Ft-Lb./Cu. In. W_1	W_2	W	W/W_1
18-Inch Thick Plate—Tempered Martensite					
0.4" OX	4	707	929	1636	2.31
1.25" OX	3	499	479	978	1.96
1.875" OX	2	343	330	673	1.96
0.4" OY	3	620	659	1279	2.06
1.25" OY	2	369	363	732	1.98
1.875" OY	2	244	299	543	2.23
0.4" OZ	4	397	462	858	2.16
1.25" OZ	3	212	232	444	2.09
1.875" OZ	2	140	182	322	2.30
18-Inch Thick Plate—Tempered Martensite—Special Heat Treatments. ("As-Received" material located adjacent to two plates receiving special treatments.)					
"As Received"					
0.4" OX	4	665	1000	1665	2.50
1.25" OX	3	442	530	973	2.20
"Temper Brittle"					
0.4" OX	4	772	1003	1775	2.30
1.25" OX	3	485	589	1074	2.21
"Air-Cooled"					
0.4" OX	4	505	829	1334	2.64
1.25" OX	3	245	424	669	2.73
2-Inch Thick Ni-Cr Steel					
0.4" OX	5	546	984	1530	2.80
1.25" OX	3	406	550	956	2.35
1.875" OX	1	367	460	827	1.79
0.4" OY	6	453	619	1072	2.37
1.25" OY	3	246	299	545	2.22
1.875" OY	2	214	265	479	2.24
2¼-Inch Thick Ni-Cr Steel					
0.4" OX	4	492	661	1153	2.69
1.875" OX	3	320	359	679	2.12
Inclusion-Count Blocks					
Block 830					
0.4" OX	4	397	529	926	2.33
1.25" OX	2	294	258	552	1.88
Block 925					
0.4" OX	4	364	502	866	2.34
1.25" OX	2	221	261	482	2.18

Tab. 2-15
Work ratios for notched bend specimens; nickel-chromium steel (tempered bainite); data decluced from Tab. 2-13

Direction	$\frac{(W_1)_{0.4"}}{(W_1)_{1.875"}}$	$\frac{(W)_{0.4"}}{(W)_{1.875"}}$	Size in	$\frac{W}{W_1}$
OX	2.06	2.43	0.4	2.31
			1.25	1.96
			1.875	1.96
OY	2.54	2.36	0.4	2.06
			1.25	1.98
			1.875	2.23
OZ	2.83	2.66	0.4	2.16
			1.25	2.09
			1.875	2.30

Tab. 2-16
Work density ratios for notched bend specimens; data deduced from Tab. 2-14

Material	Direction	Size range (in)	$\frac{(W_1)\ small}{(W_1)\ large}$	$\frac{(W)\ small}{(W)\ large}$
(B1)	OX	0.4" ÷ 1.875"	1.49	1.85
	OY		2.12	2.24
(B2)	OX	0.4" ÷ 1.875"	1.54	1.70
(B3) 830	OX	0.4" ÷ 1.25"	1.35	1.68
(B3) 925	OX		1.65	1.80

Tab. 2-17
Tension tests of geometrically similar flat plates with a square hole; summary of results; from Ref. [2.11]

Size, In.	Temp. of Test, °F	Type of Fracture	Nom. Stress at Max. Load, Psi	Reduction in Thickness, %: Maximum	Reduction in Thickness, %: Minimum
3" Wide	0	Shear	47.9	30.0	18.9
9" Long	32	Shear	45.2	26.7	15.6
3/16" Thick	74	Shear	47.7	30.0	18.5
	74	Shear	45.8	33.3	(a)
6" Wide	32	Cleavage	45.5	22.3	9.0
18" Long	50	Shear and Cleavage	44.2	23.1	7.8
3/8" Thick	70	Shear	44.5	25.7	15.1
	90	Shear	44.4	25.6	17.7
12" Wide	32	Cleavage	40.9	16.2[b]	1.4
36" Long	70	Cleavage	39.9	17.9[b]	1.4
3/4" Thick	102	Cleavage	39.1	19.7[b]	1.7

(a)—Not completely broken.
(b)—At base of notch.

Tab. 2-18
Dimensions of 45 °-V-notched bend specimens; from Ref. [2.12]

Size	*Small*	*Medium*	*Large*
Cross section, mm	10 x 10	21 x 21	42 x 42
Rim or core		Rim and core	
Notch radius, mm	0.05	...	0.05
	0.1	...	0.1
	0.2	...	0.2
	0.4	*0.4*	0.4
	0.8	...	*0.8*
	1.6	...	1.6
Notch depth, mm	2	4	8
Tested span, mm	40	200	200
Correct span, mm	40	84	168

Tab. 2-19
Dimensions and strengths of geometrically similar notched bend specimens; mild steel; from Ref. [2.13]

Spec. No.	*Loading Span L in.*	*Max. Load P tons*	*Specimen Width b in.*	*Ligament depth l in.*	*Sawcut Width in.*	*% Brittle area*	*Maximum Nominal Stress*		*Calculated Surface Energy* $\frac{\sigma_2 l}{114}$ *lb./sq. in.*
							σ *tons /sq. in.*	*Corrected*	
1	12·0	1·49	1·250	0·610	0·055	95	57·7	62·8	17·8
2	8·5	0·738	0·883	0·430	0·035	80	57·6	58·1	12·5
3	6·0	0·415	0·625	0·314	0·024	45	60·5	59·8	10·1
4	4·25	0·205	0·440	0·221	0·015	25	61·0	55·6	7·2
5	3·00	0·113	0·312	0·154	0·011	2	68·8	64·9	6·4
6	2·12	0·053	0·221	0·107	0·0088	0	67·0	67·5	—
7	1·30	0·022	0·156	0·074	0·0073	0	58·3	66·1	—
8	1·06	0·013	0·110	0·053	0·0039	0	66·6	62·7	—

All specimens were tested at 20·2°C. ± 0·1°C.

All specimens were tested at $\frac{\text{loading rate (in./min.)}}{\text{loading span (in.)}} = 0{\cdot}25$

Tab. 2-20
Composition and properties of structural-quality mild-steel plate material; from Ref. [2.14]

Investigator	Thickness (in.)	Material Designation	Mechanical Properties				Chemical Constituents (per cent.)							
			Yield Point (tons per sq.in.)	Ultimate (tons per sq.in.)	Reduction of Area (per cent.)	Transition Temperature (deg. C.)	C	Mn	Si	P	S	Ni	Cr	Others
Tipper	0·339	Fractured plate U.S. Samzona	20·6	28·0	45·0	15	0·20	0·38	<0·02	0·038	0·034	Trace	0·10	Cu = 0·10
	0·410	S.D. 413	17·0	26·5	61·0	−20	0·18	0·33	0·05	0·022	0·040	,,	Trace	Cu = 0·20
	0·560	1. Basic O.H.	16·2	28·4	59·0	−20	0·19	0·58	0·07	0·010	0·028	0·13	0·05	Cu = 0·08
	0.560	5. Acid O.H.	16·8	28·0	48·0	0	0·17	0·41	0·06	0·050	0·039	0·14	0·05	Cu = 0.10
	0·510	4. Acid O.H.	19·4	32·0	49·0	−10	0·22	0·72	0·17	0·039	0·045	0·21	0·09	Cu = 0·13
Bagsar	¾	12.	16·5	27·0	—	>22	0·33	0·55	0·02	0·014	0·035	—	—	—
	1¼	13.	13·9	25·8	—	>22	0·26	0·46	0·01	0·015	0·030	—	—	—
	1	15. Semi-killed	13·6	26·5	—	46	0·20	0·45	0·07	0·019	0·029	—	—	—
	1	17. Semi-killed	14·7	28·8	—	27	0·19	0·42	0·07	0·015	0·030	—	—	—
	1	18. Semi-killed	14·0	27·4	—	40	0·20	0·63	0·07	0·020	0·033	—	—	—
	¼	21. Rimmed	19·7	29·4	—	−23	0·21	0·43	0·02	0·010	0·028	—	—	—
	15/16	23. Semi-killed	14·9	28·3	—	43	0·25	0·45	0·05	0·015	0·024	—	—	—
Thomas and Windenburg	¾	A Semi-killed	16·1	26·8	57·5	0	0·26	0·50	0·03	0·012	0·039	0·02	0·03	—
	¾	B_r Semi-killed	14·9	25·5	64·5	−11	0·18	0·75	0·07	0·008	0·030	0·05	0·03	—
Carpenter and Roop	¾	B_n Semi-killed normalised	15·6	25·5	63·5	−2	0·18	0·73	0·04	0·011	0·030	0·06	0·03	—
	¾	C Semi-killed	16·1	29·0	56·5	34	0·24	0·48	0·05	0·012	0·026	0·02	0·03	—
	¾	D_r Killed	16·8	29·0	53·9	−10	0·22	0·55	0·21	0·013	0·024	0·16	0·12	Cu = 0·22
Boodberg and collaborators	¾	D_n Killed normalised	15·5	26·6	59·0	−10	0·19	0·54	0·19	0·011	0·024	0·15	0·12	Cu = 0·22
	¾	E Rimmed	13·4	25·4	56·4	27	0·20	0·33	0·01	0·013	0·020	0·15	0·09	Cu = 0·18
Wilson and collaborators	¾	H Killed	15·9	28·3	63·5	−15	0·18	0·76	0·16	0·012	0·019	0·05	0·04	Al = 0·053
		N Alloy	25·8	35·7	64·5	−50	0·17	0·53	0·25	0·011	0·020	3·39	0·06	Al = 0·077 Cu = 0·19
Robertson	¾ and 1	A, C and D	—	—	—	7 to 20	0·20/0·31	1·02/1·44	—	—	—	—	—	—
Wells	3/16	Spring	36·0	55·5	26·0	>20	0·54	0·87	2·01	0·025	0·035	0·06	0·03	—
	¾	Ship	19·8	28·6	59·2	−15	0·20/0·30*	—	—	—	—	—	—	—
⇒	1¼	Structural	17·9	27·6	54·0	>20	0·185	0·57	0·05	0·023	0·030	—	—	—

* Estimated from micrograph.

Tab. 2-21
Notch root strain at crack initiation in slow notch-bend tests of mild steel specimens, long axis of specimens in rolling direction, different notch orientations; from Ref. [2.15]

Material	Nominal size in	Longitudinal strain %	
	width x depth	(A) notch in transverse direction	(B) notch in normal direction
Lot I (anisotropic)	0.08x0.08	-	-
	0.4x0.4	(35/55) → 45[(1)]	65
	2.0x2.0	-	-
	3.5x3.5	45	-
Lot II (slightly less anisotropic)	0.08x0.08	(86/104) → 95 [(1)]	-
	0.4x0.4	76	(67/105) → 86[(1)]
	2.0x2.0	(79/92) → 85.5[(1)]	-
	3.5x3.5	-	-

[(1)] mean value

Tab. 2-22
Size effect in tension tests of V-notched circular specimens; tempered Ni-Mo-V steel forging, rotor steel; from Ref. [2.20]

Material	Un-notched Diam-eter, in.	Notch Diameter, in.	Net Area, sq in.	Notch Area, per cent	P_{max}, lb	S_n, psi	e_{sm}/e_{cl}	Plastic Notch Depth Change at Fracture, in.	Plastic Notch Strain, per cent	G_c in-lb per sq in.
A.....	0.250	0.1775	0.02475	50	3 750	151 000	1.16	0.0025	2.8	...
A.....	0.252	0.1781	0.02492	50	3 720	149 000	1.16	0.0033	3.7	...
A.....	0.402	0.2838	0.0633	50	9 000	142 000	1.10	0.00215	1.5	...
A.....	0.3985	0.2852	0.0639	49	8 880	139 000	1.05	0.0031	2.2	...
A.....	0.599	0.4193	0.1380	51	18 100	131 000	1.09	0.0015	0.7	...
A.....	0.598	0.4203	0.1386	51	18 800	136 000	1.07	0.0018	0.9	...
A.....	0.900	0.6360	0.3177	50	40 400	127 000	1.10	0.00095	0.3	94
A.....	0.899	0.6339	0.3155	50	39 000	124 000	1.08	0.0009	0.3	89
A.....	1.3005	0.9200	0.6647	50	71 400	108 000	1.08	0	0.0	98
A.....	1.300	0.911	0.6520	51	69 800	92 000	1.06	0	0.0	71
A.....	2.250	1.593	1.993	50	146 000	73 000	1.00	0.0002	0.0	78
A.....	2.250	1.600	2.011	49	148 000	74 000	1.11	...	...	80
WC.....	2.250	1.591	1.989	50	143 000	72 000	1.02	0.0005	0.1	76
WC.....	2.250	1.590[a]	1.986	50	190 000	96 000	1.07	0.0005	0.1	143

[a] 4-mil root radius.

Tab. 2-23
Dimensions of smooth and notched circular tension specimens; from Ref. [2.25]

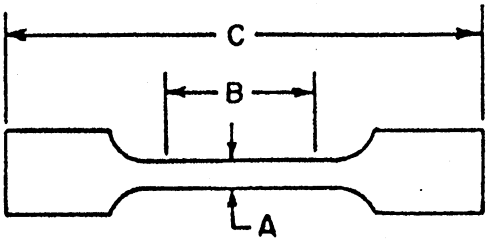

A	B	C
0.113	0.4	1⅝
0.160	0.64	2¼
0.252	1.0	3
0.357	1.4	3½
0.505	2.0	4½
1.13	4.0	16¼
1.60	6.4	20
2.52	10.0	24
3.57	14.0	28

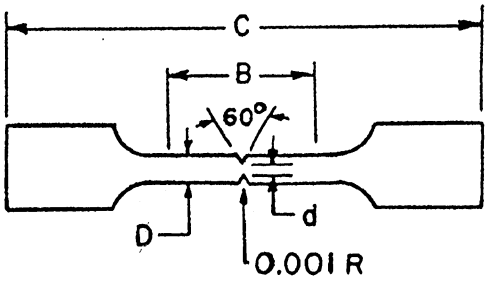

B	C	d	D
0.64	2¼	0.113	0.160
1.00	3	0.160	0.225
1.4	3½	0.252	0.357
2.0	4½	0.357	0.505
2.75	16¼	0.505	0.714
6.4	20	1.130	1.600
10.0	24	1.600	2.250
14.0	28	2.520	3.570
20.0	34	3.570	5.050

Tab. 2-24
Nominal dimensions of geometrically similar 60 ° V-notched round tension bars of C60-steel; from Ref. [2.26]

Specimen type no.	D mm	d mm	t mm	ρ mm	ξ -
1	180	108	36	3.6	
2	90	54	10.8	1.8	
3	60	36	7.2	1.2	
4	40	24	4.8	0.8	0.066
5	20	12	2.4	0.4	
6	10	6	1.2	0.2	
7	6	3.6	0.72	0.12	
8	3	1.8	0.36	0.06	

D: unnotched diameter
d: notched diameter
T: depth of V-notch
ρ: radius of curvature at root of V-notch
ξ: = ρ /(d/2) notch sharpness

Tab. 2-25
Principal and equivalent stresses at root of the 60 °V-notch at yield initiation (1), C60-steel; from Ref. [2.26]

Specimen No	D mm	Gauge length mm	σ_1	σ_2	σ_{VGEA}	σ_{VSA}
			kp/mm^2			
1	180	0.8	41.1	14.0	36.241.1	
2	90	0.8	42.7	13.9	37.842.7	
2	90	0.4	42.9	14.1	37.842.9	
3	40	0.4	47.9	15.5	42.447.9	

D: unnotched diameter
σ_1: axial stress at root of notch
σ_2: circumferential stress at root of notch
σ_{VGEA}: v. Mises equivalent stress
σ_{VSA}: Tresca equivalent stress
(1) Yield initiation defined in nominal stress versus axial strain ε_1 diagram

Tab. 2-26
Tensile properties of aluminium alloys; from Ref. [2.27]

Alloy and temper	Tensile strength, ksi	Yield strength, ksi	Elongation in 2 in., %	Reduction of area, %
2024-T851	70·8	64·4	7·2	14
2219-T851	65·8	49·3	10·0	20
6061-T651	51·0	43·4	12·0	25
7075-T7351*	68·2	56·8	11·8	24
7079-T651	82·5	72·8	11·2	16

*Met specification properties when fabricated although it does not meet current properties for 7075-T7351 plate.

Tab. 2-27
Notch-bend fracture-toughness tests of aluminium alloy plate; from Ref. 2-27

Nominal thickness, B, in.	Nominal width, W, in.	Ratio W/B	2024-T651 Actual thickness, in.	2024-T651 Crack length, a_0, in.	2024-T651 K_Q, ksi$\sqrt{in.}$	2024-T651 $2{\cdot}5\left(\frac{K_Q}{\sigma_{YS}}\right)^2$, in.	6061-T651 Actual thickness, in.	6061-T651 Crack length, a_0, in.	6061-T651 K_Q, ksi$\sqrt{in.}$	6061-T651 $2{\cdot}5\left(\frac{K_Q}{\sigma_{YS}}\right)^2$, in.	7075-T7351 Actual thickness, in.	7075-T7351 Crack length, a_0, in.	7075-T7351 K_Q, ksi$\sqrt{in.}$	7075-T7351 $2{\cdot}5\left(\frac{K_Q}{\sigma_{YS}}\right)^2$, in.	7079-T651 Actual thickness, in.	7079-T651 Crack length, a_0, in.	7079-T651 K_Q, ksi$\sqrt{in.}$	7079-T651 $2{\cdot}5\left(\frac{K_Q}{\sigma_{YS}}\right)^2$, in.
⅛	½	4	0·126	0·245	22·2	0·297	0·125	0·243	16·1	0·343	0·126	0·243	23·7	0·434	0·126	0·252	28·4	0·381
			0·127	0·238	21·5	0·279	0·125	0·237	14·2	0·269	0·126	0·233	22·7	0·401	0·126	0·245	23·1	0·252
			0·126	0·245	20·9	0·266	0·125	0·230	14·8	0·292	0·126	0·237	24·7	0·471	0·126	0·257	24·9	0·292
			0·125	0·243	22·1	0·294					0·126	0·237	24·0	0·446	0·127	0·243	23·7	0·265
					21·8				15·0				23·7				26·7	
¼	½	2	0·250	0·248	20·7	0·259	0·250	0·252	14·6	0·284	0·250	0·254	24·8	0·475	0·248	0·257	25·8	0·313
			0·250	0·258	22·7	0·310	0·250	0·248	14·6	0·284	0·250	0·258	26·2	0·531	0·250	0·260	27·8	0·366
			0·250	0·259	22·5	0·306	0·250	0·247	13·3	0·234	0·250	0·250	25·7	0·510	0·250	0·275	25·5	0·306
					22·0				14·2				25·4				26·4	
	2	8	0·251	0·993	20·6	0·255	0·250	0·977	25·1	0·839	0·251	0·970	26·0	0·493	0·251	1·097	23·6	0·262
			0·251	1·012	22·9	0·315	0·250	0·992	25·5	0·862	0·249	1·017	28·9	0·609	0·251	1·030	26·2	0·324
			—	—	—	—	—	—	—	—	0·251	0·972	25·8	0·485	0·250	0·943	23·1	0·251
					21·8				25·3				26·9				24·3	
	3	12	0·251	1·493	20·4	0·251	0·252	1·485	25·9	0·894	0·251	1·507	28·1	0·576	0·250	1·457	27·3	0·317
			0·249	1·407	18·0	0·195	0·250	1·483	25·7	0·877	0·248	1·478	30·6	0·682	0·248	1·475	26·3	0·327
			—	—	—	—	0·250	1·502	26·3	0·921	0·252	1·553	31·0	0·700	0·251	1·612	23·5	0·261
					19·2				26·0				29·9				25·7	
½	1	2	0·500	0·512	20·6	0·257	0·500	0·495	22·7	0·687	0·499	0·505	24·8	0·476	0·500	0·486	21·9	0·226
			0·500	0·512	21·3	0·274	0·500	0·482	24·8	0·817	0·500	0·489	26·4	0·542	0·500	0·487	25·1	0·298
			0·500	0·503	19·3	0·225	0·500	0·475	23·4	0·725	0·500	0·502	24·9	0·481	—	—	—	—
					20·4				23·6				25·4				23·5	
	2	4	0·497	1·040	20·3	0·247	0·501	1·012	25·9	0·893	0·498	0·990	28·2	0·579	0·501	1·047	24·2	0·277
			0·500	0·922	20·1	0·244	0·502	0·933	30·2	1·208	0·500	0·935	25·6	0·477	0·502	1·003	24·7	0·288
			—	—	—	—	0·502	0·985	23·6	0·740	0·501	0·013	28·3	0·583	0·501	1·030	24·1	0·274
					20·2				26·6				27·4				24·0	
	3	6	0·500	1·712*	23·4	0·331	0·502	1·510	27·5	1·003	0·499	1·567	27·3	0·545	0·501	1·503	24·0	0·272
			0·503	1·527	23·9	0·344	0·502	1·628	30·9	1·269	0·499	1·492	29·3	0·627	—	—	—	—
			0·501	1·500	20·4	0·251	0·502	1·462	27·5	1·002	—	—	—	—	—	—	—	—
					22·2				28·6				28·3				24·0	
¾	1½	2	0·751	0·856*	24·0	0·347	0·750	0·680	26·0	0·897	0·750	0·782	26·6	0·549	0·750	0·757	23·5	0·261
			0·750	0·777	22·4	0·302	0·750	0·693	27·7	0·017	0·751	0·792	27·3	0·579	0·751	0·781	24·9	0·292
			—	—	—	—	—	—	—	—	0·749	0·763	26·5	0·544	—	—	—	—
					22·4				26·8				26·8				24·2	
	2	2⅔	0·752	0·918	20·5	0·252	0·750	0·970	24·3	0·785	0·752	0·985	26·8	0·525	0·753	0·943	24·6	0·285
			0·752	0·902	19·1	0·220	0·751	0·982	28·2	1·055	0·751	0·935	28·1	0·574	0·753	0·873	22·6	0·242
			—	—	—	—	—	—	—	—	0·751	1·003	26·6	0·513				
					19·8				26·2				27·2				23·6	
	3	4	0·752	1·498	19·7	0·235	0·751	1·547	27·4	0·994	0·753	1·528	27·8	0·561	0·752	1·478	23·1	0·253
			0·746	1·500	21·2	0·270	0·752	1·528	26·3	0·919	0·753	1·500	28·1	0·575	0·752	1·532	24·1	0·273
			0·752	1·535	20·6	0·255	0·750	1·500	27·3	0·980	0·753	1·515	27·9	0·567	—	—	—	—
					20·5				27·0				27·9				23·6	
1	2	2	0·999	0·977	20·2	0·245	0·998	1·025	26·0	0·897	1·001	1·035	27·7	0·593	1·000	1·078	22·8	0·246
			0·999	0·995	19·6	0·233	1·000	0·995	27·2	0·982	1·001	1·015	27·0	0·565	1·002	1·128	18·6	0·163
			0·997	0·986	20·9	0·262	1·002	1·018	26·6	0·940	1·001	1·065	28·9	0·646	1·001	1·034	23·3	0·257
					20·2				26·6				27·9				21·6	
	3	3	0·998	1·512	20·4	0·250	1·000	1·505	25·8	0·887	1·000	1·477	27·8	0·560	0·999	1·550	23·9	0·270
			1·005	1·472	20·8	0·261	1·000	1·563	27·5	1·002	0·999	1·482	27·1	0·536	—	—	—	—
			1·000	1·490	20·1	0·244	—	—	—	—	0·999	1·522	27·7	0·559	—	—	—	—
					20·4				26·6				27·5				23·9	
1⅜ or 1½	3	~2	1·388		20·2	0·245	1·480	1·810*	32·3*	1·384	1·381	1·557	28·9	0·646	1·385	1·677	23·6	0·263
			1·385		20·5	0·252	1·479	1·443	25·4	0·855	1·389	1·498	27·6	0·588	1·380	1·617	22·3	0·234
			1·387		20·1	0·244	1·479	1·508	27·6	1·014	1·385	1·538	28·1	0·613	1·380	1·628	24·3	0·278
					20·3				26·5				28·2				23·4	

*Crack length too long or too short, K_Q omitted from average.

Tab. 2-28
Characteristic data of the load-slot mouth opening displacement curve of geometrically similar compact tension specimens; 1 CrMoV-steel; room temperature; based on Ref. [2.29]

Spec. Code	B mm	W mm	B/W -	a mm	a/W -	P_Q kN	σ_Q N/mm^2	P_{max} kN	σ_{max} N/mm^2	Δmax mm	δ -
A2	50.5	101.7	0.4966	55.1	0.5418	87.0	36.97	87.0	36.97	0.53	$9.619 \cdot 10^{-3}$
F1	25.5	50.8	0.5020	24.9	0.4902	40.0	60.56	46.6	70.56	0.52	20.88 "
F2	25.4	50.9	0.4990	25.6	0.5029	43.2	67.22	46.0	71.58	0.59	23.05 "
F3	25.4	.50.8	0.5000	25.3	0.4980	41.6	64.23	42.4	65.46	0.48	18.96 "
F4	25.4	49.9	0.5090	28.4	0.5691	30.4	55.67	33.4	61.16	0.51	17.96 "
G2	12.7	25.5	0.4980	13.3	0.5216	12.0	77.45	12.0	77.45	0.31	23.30
G3	12.7	25.4	0.5	13.5	0.5315	11.3	74.77	11.3	74.77	0.29	21.48

Tab. 2-29
Fracture toughness of geometrically similar compact tension specimens; 1 CrMoV steel; room temperature; from Ref. [2.29]

Specimen code	a/W	P_Q kN	K_Q $MN/m^{3/2}$	K $MN/m^{3/2}$	K_{max} $MN/m^{3/2}$
A2	0.542	87.0	59.8	-	59.8
F1	0.490	40.0	-	64.9	75.6
F2	0.503	43.2	73.2	-	78.0
F3	0.497	41.6	69.3	-	70.7
F4	0.570	30.4	65.3	-	71.8
G2	0.523	12.0	61.3	-	61.3
G3	0.530	11.3	59.4	-	59.4
Mean			68,12		74.03

Tab. 2-30

Material composition and mechanical properties of 3% NiCrMoV low pressure turbine disc steel; fracture results of CT- and SENB-specimens; from Ref. [2.35]

Typical Composition

Element	Wt Pct
C	0.23 to 0.30
Si	0.16 to 0.27
Mn	0.39 to 0.49
Ni	2.57 to 2.94
Cr	0.56 to 0.71
Mo	0.18 to 0.28
V	0.10 to 0.13
S	0.01 to 0.038
P	0.01 to 0.031

Mechanical Properties

Material	0.2 Pct PR Stress MN m^{-2}	U. T. S. MN m^{-2}	Elongation 5.65$\sqrt{A}$ Pct	FATT °C
Discs used for the compact tension specimens	644	770	19	40
	613	780	18	50
45 mm T single-edge-notch bend specimens	627	763	17	23
25 mm T and 12.5 mm T single-edge-notch bend specimens	720	840	17	58

Tensile properties measured at 20 °C

Results for Compact Tension Specimens

(a) Width W = 100 mm, Thickness B = 50 mm

T °C	a/W	Pf MN	K_{IC} MN m$^{-3/2}$	$K_{IC}{}^{J}$ MN m$^{-3/2}$	Pu Pl. Stress MN
−20	0.447	0.192	101	104	0.393
0	0.435	0.197	100	107	0.412
0	0.477	0.225	128	133	0.348
20	0.517	0.232		183	0.286
20	0.447	0.285		183	0.393
40	0.448	0.342		230	0.388
40	0.462	0.292		194	0.367
60	0.477	0.352		327	0.348
60	0.453	0.383		333	0.380
80	0.455	0.365			0.378
80	0.463	0.360			0.374
100	0.453	0.375			0.380
100	0.482	0.316			0.399

(b) Width W = 50 mm, Thickness B = 25 mm

−80	0.493	0.036	61*	59	0.081
−80	0.457	0.033	51*	49	0.094
−60	0.461	0.062	95	96	0.093
−60	0.454	0.057	86	86	0.095
−40	0.452	0.039	58*	56	0.099
−40	0.443	0.074	108	112	0.101
−20	0.457	0.090		160	0.094
−20	0.463	0.045	70	68	0.092
0	0.520	0.054	99	98	0.071
0	0.462	0.101		199	0.093
20	0.465	0.100		202	0.092
20	0.467	0.084		154	0.091
30	0.451	0.105		222	0.096
30	0.460	0.105		218	0.093
40	0.451	0.093			0.096
40	0.443	0.107			0.101
60	0.457	0.105			0.094
60	0.459	0.097			0.093
80	0.461	0.099			0.093
80	0.461	0.099			0.093
100	0.456	0.100			0.095
100	0.458	0.097			0.094

(c) Width W = 25 mm, Thickness B = 12.5 mm

−80	0.473	0.0161	72	67	0.0221
−80	0.499	0.0127	62	59	0.0199
−60	0.525	0.0167		96	0.0177
−60	0.474	0.0175		84	0.0221
−40	0.465	0.0135	59	51	0.0228
−40	0.453	0.0265		142	0.0238
−20	0.457	0.0282		160	0.0235
−20	0.455	0.024		125	0.0236
0	0.462	0.0270		157	0.0230
0	0.466	0.0271		206	0.0228
20	0.479	0.0255			0.0216
20	0.477	0.0225			0.0220
40	0.478	0.0258			0.0218
40	0.485	0.0235			0.0208
60	0.466	0.0260			0.0228
60	0.470	0.0249			0.0223
80	0.486	0.0230			0.0208
80	0.481	0.0239			0.0211
100	0.441	0.265			0.0254
100	0.463	0.0260			0.0230

*ASTM E399 valid tests

Results for Single-Edge-Notch Bend Specimens

(a) Width W = 90 mm, Thickness B = 45 mm

T °C	a/W	σf MN m^{-2}	K_{IC} MN m$^{-3/2}$	$K_{IC}{}^{J}$ MN m$^{-3/2}$	σpc MN m
−40	0.469	287	140	158	394
−40	0.470	273	131	139	393
−20	0.467	338		201	397
−20	0.472	342		228	389
0	0.469	330	159	165	394
0	0.472	308		183	388
20	0.476	348			383
20	0.471	355			390

(b) Width W = 50 mm, Thickness B = 25 mm

−60	0.459	158	55*	61	450
−60	0.459	343	120	116	450
−40	0.459	372		136	450
−40	0.459	250	87	84	450
−20	0.453	432		176	460
−20	0.509	295	120	120	371
0	0.455	391		144	456
0	0.459	434		186	450
20	0.457	420			453
20	0.457	442			453
40	0.459	437			450
40	0.458	442			451
60	0.452	451			462
60	0.460	422			449
80	0.457	437			453
80	0.458	420			451
100	0.463	403			443
100	0.455	427			456

(c) Width W = 25 mm, Thickness B = 12.5 mm

−100	0.472	440		127	428
−100	0.469	173	44*	47	434
−80	0.473	303	78	73	427
−80	0.471	323	82	74	430
−60	0.468	453		133	435
−60	0.475	288	74	69	424
−40	0.480	419		108	415
−40	0.461	468		142	447
−20	0.468	451			435
−20	0.469	457			434
0	0.476	405			422
0	0.468	422			435
20	0.468	438			435
20	0.473	453			427
40	0.476	453			422
40	0.460	451			449
60	0.469	447			434
60	0.456	476			455
80	0.465	447			440
80	0.463	459			443

*ASTM E399 valid test

Tab.2-31
Tension properties of plate materials for I-beams; from Ref. [2.36]

Material	Plate thickness t (mm)	Yield stress (*Proof Stress) σ_y (kgf mm^{-2})	Ultimate strength σ_B (kgf mm^{-2})	Uniform elongation (%)	Elongation E_l (%)
KAS Specified by NK Rule	20	29.6	46.7	~ 22	30.5
SPHC JIS. G3131	6	28.3	35.9	~ 15	24.8
SPCC JIS. G3141	2.3	15.9*	28.5	~ 25	40.1

Tab. 2-32
Maximum nominal strains calculated from the deflection under the maximum load(1); different I-beams; from Ref. [2.36]

Plate thickness, material	Maximum nominal strain	
	Notched	Unnotched
20 mm, KAS	0.05	0.12
6 mm, SPHC	0.18	0.23
2.3 mm, SPCC	0.24 ~ 0.25	

(1) Obtained from the experiments (Fig. 2-52)

Tab. 2-33
Dimensions of compact tension (CT) specimens; based on Ref. [2.40]

Thickness B(mm)	B/W	Width W (mm)	Average initial crack length a (mm)	a/W	Sidegroove depth (%)
13	0.5	26	15.1	0.58	0
13	0.5	26	15.3	0.5885	25
13	0.26	50	27.2	0.544	0
13	0.173	75	42.2	0.5626	0
13	0.13	100	58.6	0.586	0
25	0.5	50	27.7	0.554	0
25	0.5	50	26.7	0.534	25
25	0.25	100	54.4	0.544	0
37.5	0.5	75	43.2	0.576	0
37.5	0.375	100	54.9	0.049	0
50	0.5	100	58.6	0.586	0
50	0.5	100	54.1	0.541	25

Tab. 2-34
LEFM strength prediction; from Ref. [2.45]

Thickness classification	Material response regime	No. of tests involved	Percent within ±10% of LEFM	Percent within ±5% of LEFM
Plane strain	Brittle	784	37	19
	Brittle–ductile	341	50	30
	Ductile	1691	18	9
Plane stress	Brittle	109	47	25
	Brittle–ductile	152	48	35
	Ductile	771	21	10

Tab. 2-35
LEFM size prediction; from Ref. [2.45]

Material response regime	No. of tests involved	Percent within ±10% of LEFM	Percent within ±5% of LEFM
Brittle	893	11	4.3
Brittle–ductile	493	20	8.7
Ductile	2462	7.2	3.6

Tab. 2-36
LEFM size prediction for different types of brittle response; from Ref. [2.45]

Classification	No. of tests involved	Percent within ±10% of LEFM	Percent within ±5% of LEFM
Valid K_{Ic}	241	11	6.2
Not K_{Ic}	593	11	3.1
Very brittle	177	9.0	6.8
Quasi-brittle	387	10	5.2

Tab. 2-37
Dimensions of SENB specimens; from Ref. [2.46]

Specimen dimensions				
Specimen numbers	Thickness, B (mm)	Width, W (mm)	Net thickness, B_n (mm)	Ligament, b (mm)
(a) Size effects programme				
1-3	10	20	8	8
4-6	15	30	12	12
7-9	20	40	16	16
10-12	30	60	24	24
13-15	40	80	32	32
(b) Geometry effects programme				
16-18	20	10	16	4
19-21	20	20	16	8
7-9	20	40	16	16
22-24	20	60	16	24
25-27	20	80	16	32

Tab. 2-38
Average crack extension (Δa_m) prior to maximum load; from Ref. [2.46]

Specimen Size (mm)	Δa_m (mm)
(a) Size effects programme	
10x20	0.25
15x30	0.41
20x40	0.98
30x60	1.14
45x90	1.62
(b) Geometry effects programme	
20x10	0.16
20x20	0.24
20x40	0.98
20x60	1.25
20x80	1.72

Tab. 2-39
Composition of HY-130 steel plate; from Ref. [2.52]

C	Mn	P	S	Cu	Ni	Cr	Mol	V	Ti
0.1	0.73	0.008	0.003	0.13	4.97	0.54	0.40	0.081	0.002

Heat treatment: austenitized at 899 °C for 129 min, water quenched; austenitized at 843 °C for 120 min, water quenched; tempered at 627 °C for 126 min, water quenched

Tab. 2-40
Mechanical properties of HY-130 steel plate; from Ref. [2.52]

Orientation	Yield strength (MPa)	Tensile strength (MPa)	Elongation (% in 50 mm)	Reduction of area (%)	21°C CVN (J)	−18°C CVN (J)	Fracture toughness J_{Ic} (kJ m^{-2})[a]
Longitudinal	992	1016	16.0	66.1	124	118	154
Long transverse	986	1022	16.0	64.8	132	126	–

[a] Measured at SRI with cracked round bar specimens

Tab. 2-41
Dimensions of scaled blunt-notched three-point-bend specimens; from Ref. [2.52]

Size	Nominal span, S (mm)	Nominal width, W (mm)	Nominal thickness, B (mm)	Nominal ligament, b (mm)	Actual ligament, b (mm)	Nominal notch radius, r (mm)
0.5 T	50.80	12.70	12.70	6.35	6.50	1.6
1 T	101.60	25.40	25.40	12.70	12.45	3.2
2 T	203.20	50.80	50.80	25.40	25.40	6.4

Tab. 2-42
Normalized characteristic data of scaled experiments on blunt-notched three-point-bend specimens, material: high strength-low hardening HY-130 steel; from Ref. [2.52]

1	2	3	4	5	6	7	8
Specimen no.	Normalized NMOD at initiation[a]	Normalized load-line displacement at initiation[b]	Residual bend angle (degrees)	Normalized continuous crack length[b]	Normalized discontinuous crack length[b]	Normalized residual CMOD[a]	Normalized crack depth[b]
0.5 T-1	2.064	0.276	17.8° ×	0.263 ×	0.417	0.079 ×	0.013 ×
0.5 T-2	2.048	0.275	24.9°	0.682	0.682	0.429	
0.5 T-3	1.92	0.265	15.0° ××	0.093 ××	0.328	0.048 × ×	0.011
0.5 T-4	2.112	0.289	23.2°	0.617	0.617	0.206	0.084
1 T-1	1.752	0.265	15.8°	0.372	0.516	0.096	
1 T-2	1.856	0.276	14.7° ××	0.161 ××	0.464	0.032 ××	0.007
1 T-3	1.672	0.250	18.0° ×	0.555 ×	0.555	0.152 ×	0.050 ×
2 T-1	1.388	0.203	14.3° ××	0.429 ××	0.550	0.120 ××	
2 T-2	1.268	0.189	11.3°	0.168	0.358	0.052	0.009
2 T-3	1.484	0.218	17.0° ×	0.671 ×	0.671	0.424 ×	0.207 ×

[a] Normalized by the notch root radius. [b] Normalized by the specimen width

×, ×× approximately equal residual bend angles

Tab. 2-43
Chemical composition of CF8M duplex stainless steel (wt. %); from Ref. [2.56]

C	Mn	Si	S	P	Ni	Cr	Mo	Cu	Co	Nb	N
0.045	0.74	1.25	0.002	0.026	9.84	20.61	2.61	0.14	0.04	0.23	0.046

Tab. 2-44
Chemical composition of the different duplex steels (wt. %) and ferrite volume fraction (f_v); from Ref. [2.58]

	C	N	Cr	Ni	Mo	Si	Mn	f_v (%)
Y4331	0.036	0.051	21.25	9.70	2.50	1.06	0.89	20.0
BL	0.040	0.032	21.18	9.66	2.60	1.15	0.58	22.1
BT	0.038	0.045	20.45	10.86	2.58	1.10	0.51	14.4

Tab. 2-45
Chemical composition (weight %) of the investigated C-Mn steels; from Ref. [2.63]

C	Si	Mn	P	S	Cr	Ni	O	Al	N	Ref.
0.20	0.23	0.97	0.022	0.021	0.10	0.12	0.008	0.007	0.0011	[2.63]
0.167	0.21	1.1		0.032	0.07	0.1			0.011	[2.64]

Tab. 2-46
Tensile properties of the duplex stainless steel CF8M (Y4331) and the C-Mn steel; from Ref. [2.58] and [2.63]

Material	$R_{0.2}$ (MPa)	R_m (MPa)	A (%)	References
CF8M (Y4331)	327	722	20	[2.58]
C-Mn steel	190	500	28	[2.63]

Tab. 2-47
Tensile and impact properties along two directions of a pipe component of a C-Mn steel at 100 °C; from Ref. [2.64]

Direction	**Y.S. $_{0.2}$ (MPa)**	**U.T.S. (MPa)**	**Uniform Elongation (%)**	**Total Elongation (%)**	**R.O.A. (%)**	**KCV (J)**
Longitudinal	248	397	20	36	74	97
Short-Transverse	247	391	13	16	19	21

Tab. 2-48
Effect of CT-specimen size on fracture properties along two directions within a pipe component of a C-Mn steel at 100 °C; from Ref. [2.64]

Direction	CT size	$J_{0.2}$(kJ/m²)	dJ/da (MPa)
Longitudinal	½ T	184	162
	1 T	181	124
	2 T	177	90
Short-Transverse	½ T	38	22
	1 T	29	38

Tab. 2-49
Size influence on characteristic data at crack initiation of U-notched bending specimens at R.T.; material: ferritic steel 20 MnMoNi 55; based on Ref.[2.76]

Specimen	W_o *mm*	v_k *mm/min*	F_i *kN*	σ_i *MPa*	t_i *s*	α_i *deg*	$2A_S$ kJm^{-2}	$2A_V$ kJm^{-3}
S1001	10	0.31	5.562	158.9	412	9.18	360	180000
S1002	10	0.31	5.506	157.3	403	9.78	440	220000
S1004	10	0.31	5.504	157.4	366	8.28	425	212500
S1006	10	0.06	5.724	163.4	1941	10.43	390	195000
S2001	25	0.77	32.826	150.1	373	8.52	824	164800
S2002	25	0.77	31.425	143.8	356	8.00	806	161200
S2003	25	0.77	31.416	143.7	395	8.27	804	160800
S2004	25	0.15	32.120	147.0	1838	8.13	783	156600
S2005	25	0.15	31.407	143.6	1845	8.46	792	158400
S3001	140	4.29	943.75	137.6	96.3	7.62	3945	140893
S3002	140	4.29	896.13	130.6	257	6.99	4166	148786

W_o : nominal width of three-point-bend specimen

v_k : speed of load pin

F_i : load at crack initiation

σ_i : twofold ligament shear stress at crack initiation

t_i : time at crack initiation

α_i : bending angle at crack initiation

A_S : area specific work at the ligament up to crack initiation

A_V : volume specific work in ligament volume $2RB(W-K)$ up to crack initiation

Tab. 3-1
Statistical data of valid[a] K_{Ic}-test results; from Ref. [3.1]

Material	Heat Treatment	Yield Strength, ksi	K_{Ic} Tests			
			Number of Tests, n	Mean K_{Ic}, $\bar{X}$, ksi·(in.)$^{1/2}$	Standard Deviation, S, ksi·(in.)$^{1/2}$	$S/\bar{X}$
Maraging steel (300)	900 F, 3 hr	285	38	51.75	2.47	0.0478
Maraging steel (250)	900 F, 3 hr	259	23	68.4	3.51	0.0515
Maraging steel (300)	850 F, 3 hr	242	44	84.5	4.67	0.0555
Aluminum 7075 (½-in. thick)	T651	79	24	26.8	1.32	0.0495

[a] Valid according to the criteria suggested in Ref. [3.1]

Appendix 3: Figures

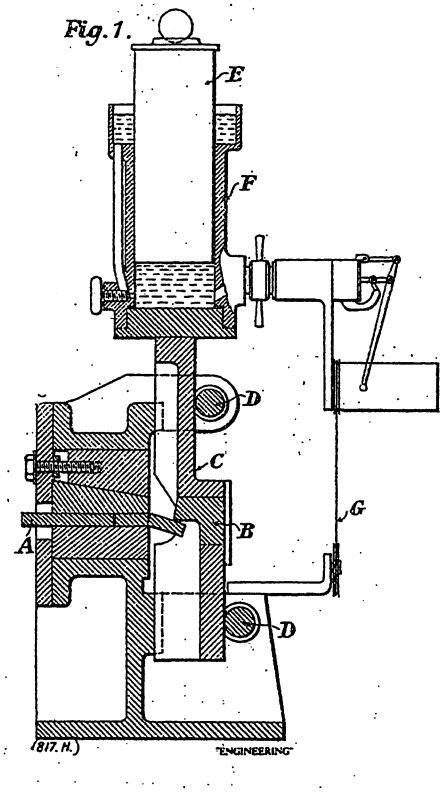

Fig. 2-1
Machine for bending tests with variable speed of Izod-type notched specimens; from Ref. [2.1]

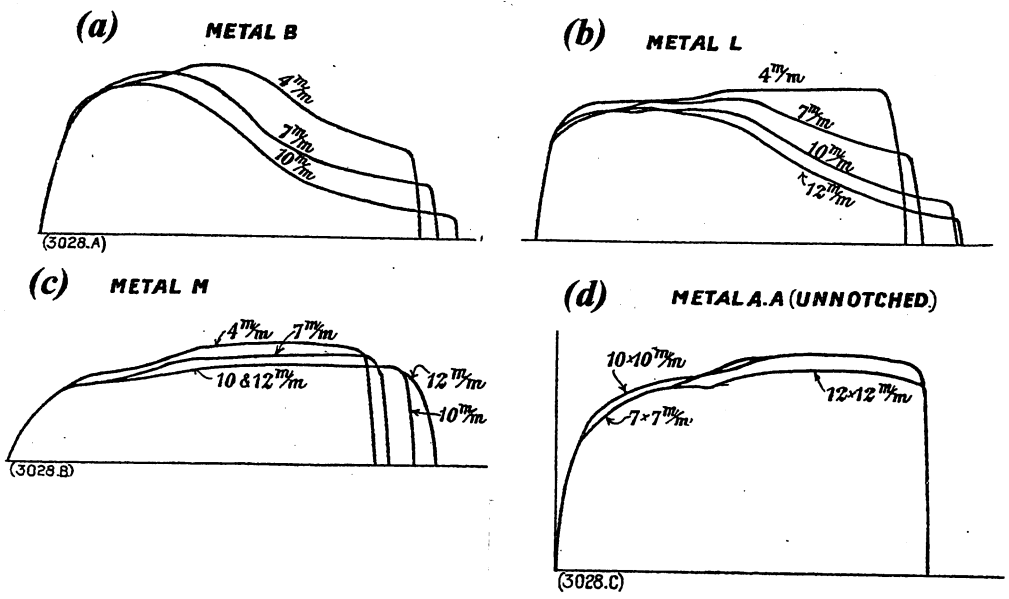

Fig. 2-2
Size effects on normalized load vs. load-point displacement curves of Izod-type notched specimens ((a), (b), (c)) and un-notched bend specimens (d); four different metals; from Ref. [2.0]

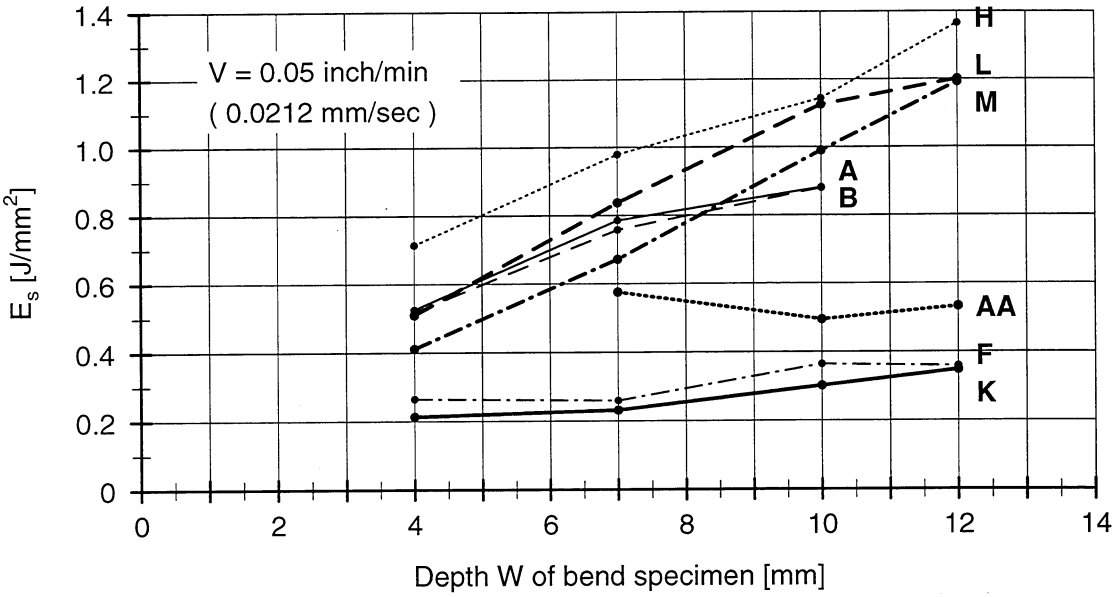

Fig. 2-3
Area specific absorbed energy (obtained from load-load point displacement curves) vs. specimen depth W for constant load point displacement velocity v=0.05 in/min; different metals; based on Tab. 2-7

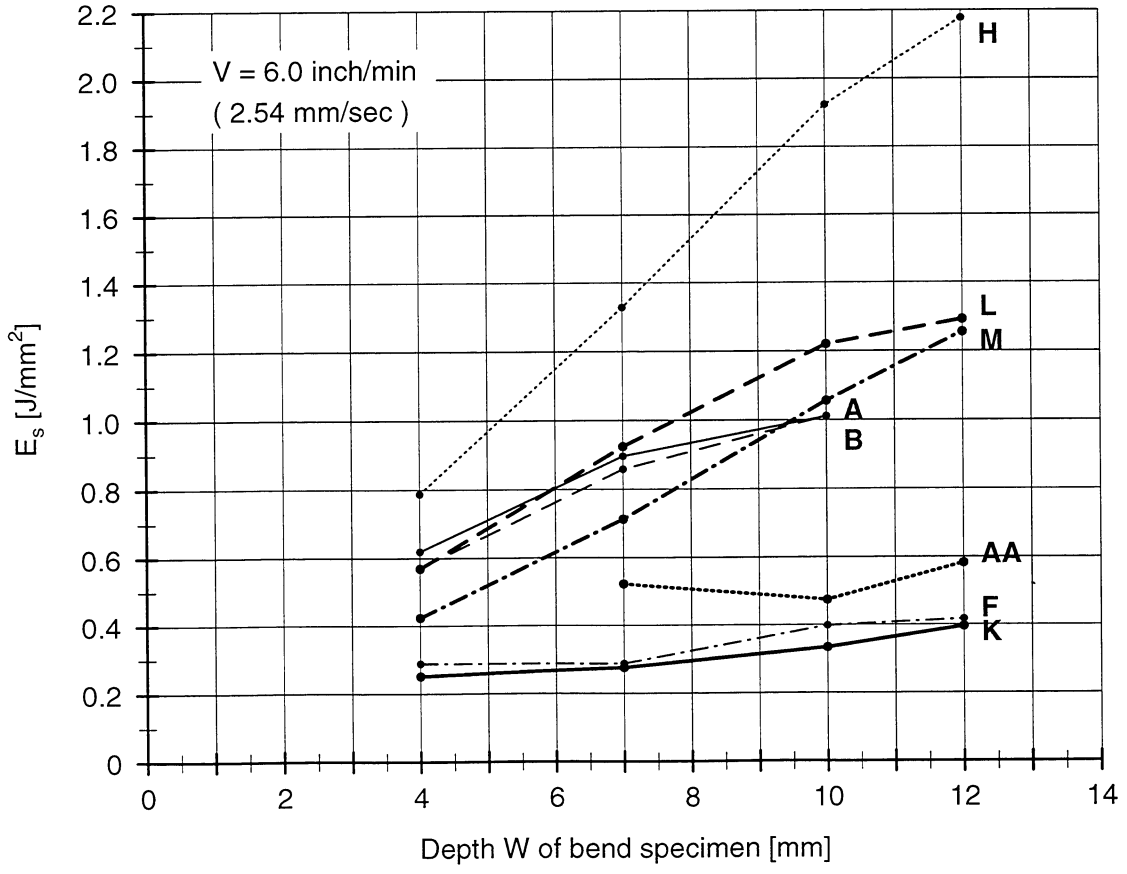

Fig. 2-4
Area specific absorbed energy (obtained from load-load point displacement curves) vs. specimen depth W for constant load point displacement velocity v=6 in/min; different metals; based on Tab. 2-7

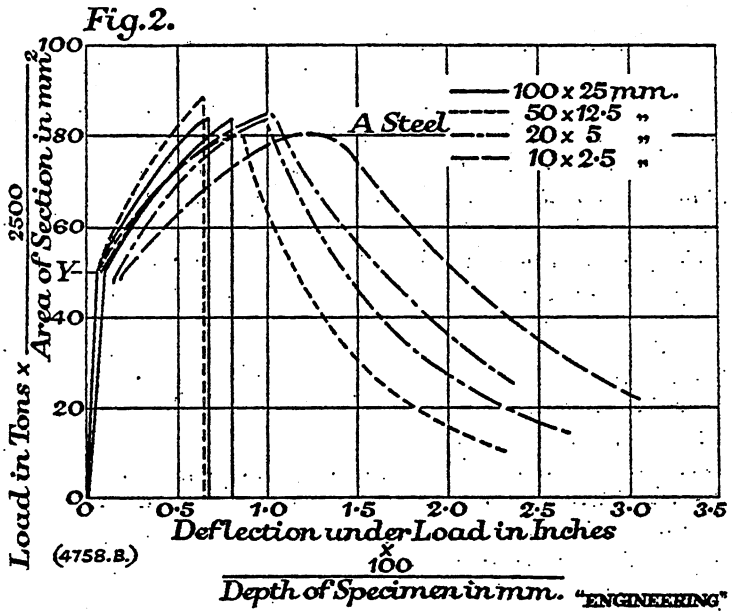

Fig. 2-5
Normalized load-deflection diagrams for three-point-bending of notched beams; forged mild steel A; from Ref.[2.5]

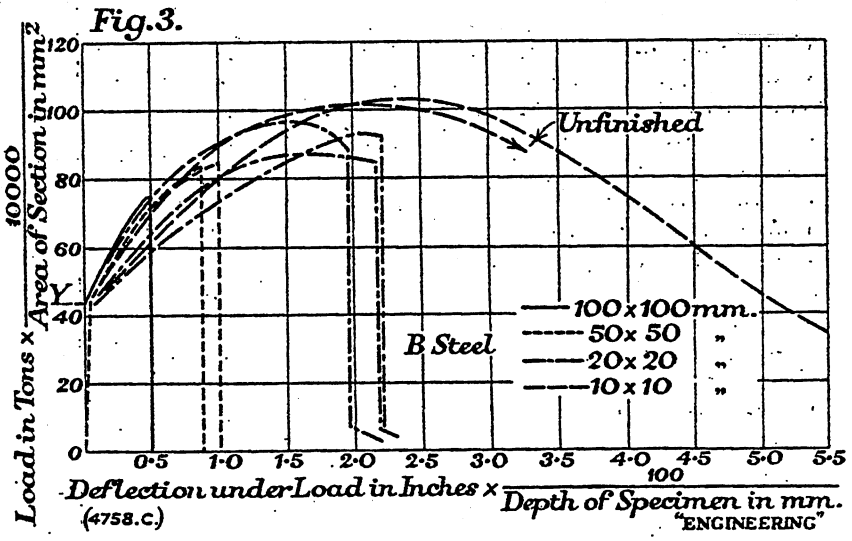

Fig. 2-6
Normalized load-deflection diagrams for three-point-bending of notched beams; forged mild steel B; from Ref.[2.5]

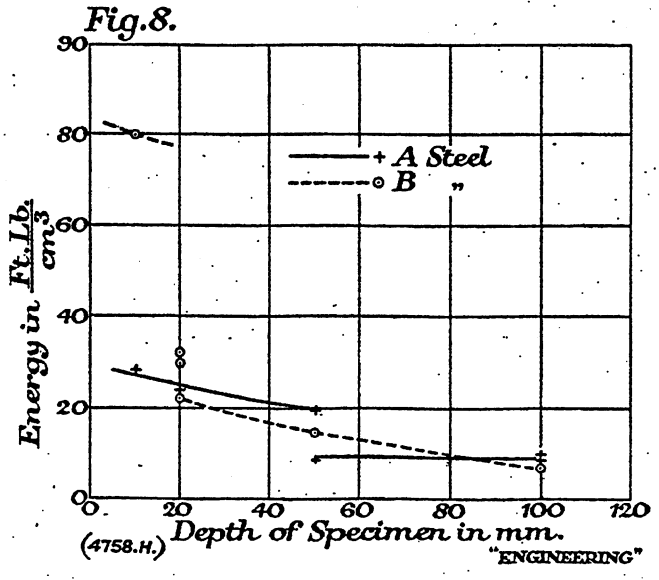

Fig. 2-7
Volume specific energy vs. depth of specimen, three-point-bending of notched beams; forged mild steel A&B; Ref.[2.5]

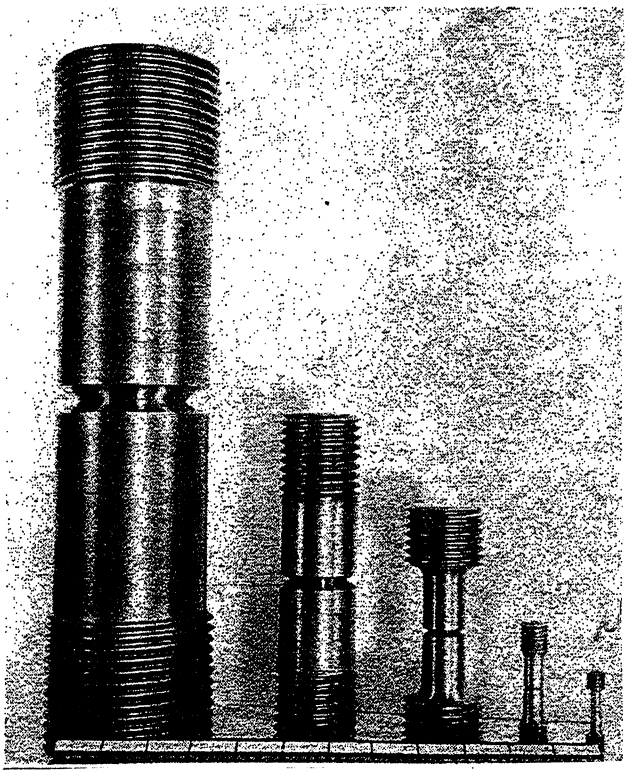

Fig. 2-8
Geometrically similar V-notched tension specimens; constant notch tip radius; normalized medium carbon steel; from Ref.[2.7]

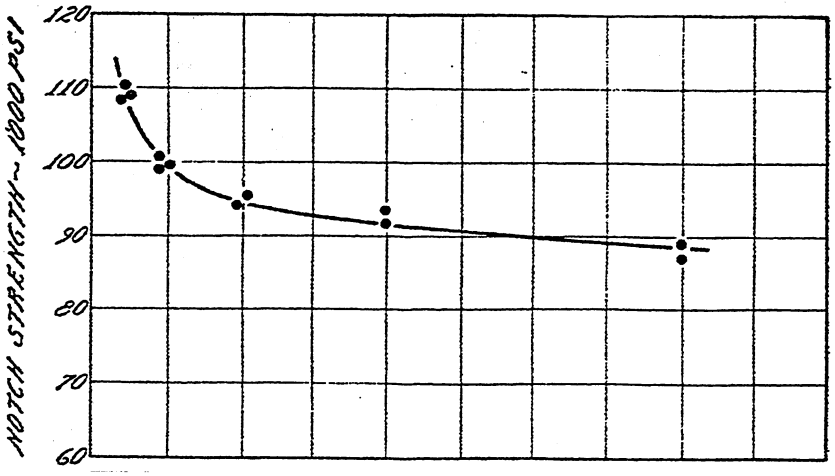

Fig. 2-9
Notch strength vs. specimen diameter of the uniform section; 60°V-notched tension specimens; tempered medium carbon steel; from Ref.[2.7]

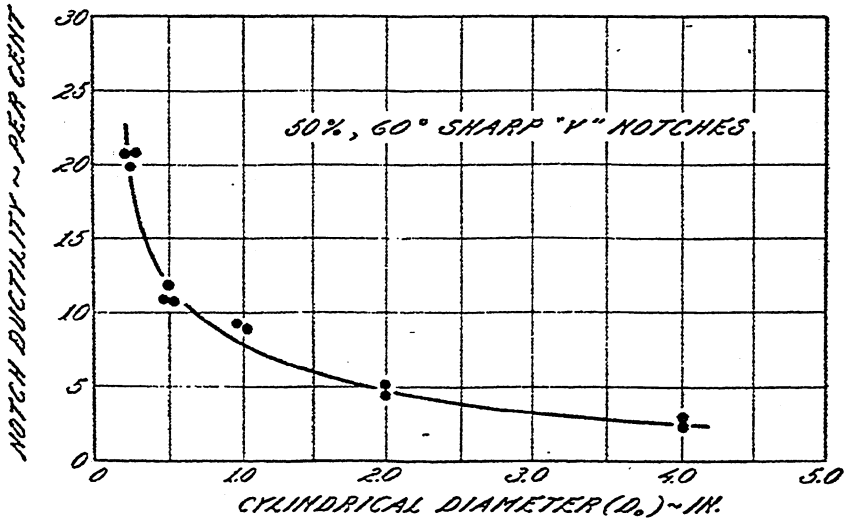

Fig. 2-10
Area reduction at the root of the notch after fracture vs. specimen diameter of the uniform section; tempered medium carbon steel; from Ref.[2.7]

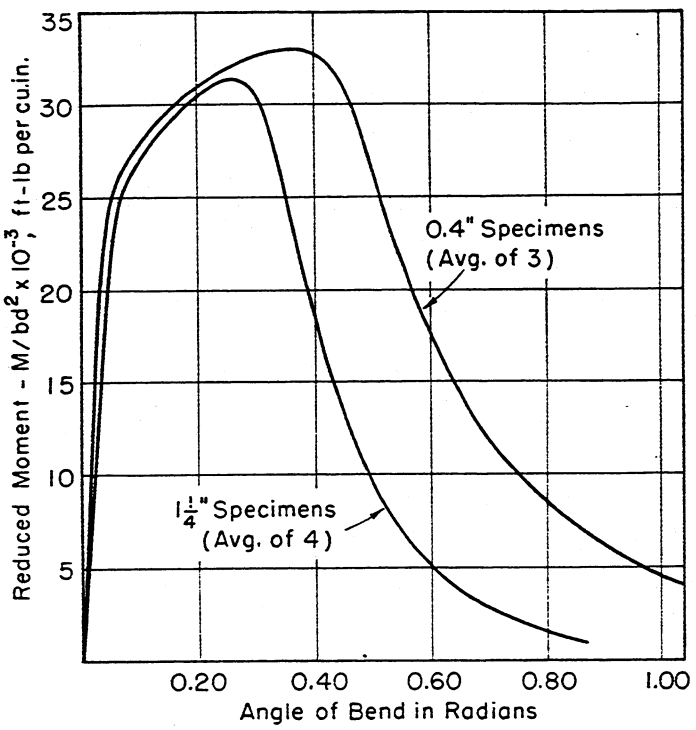

Fig. 2-11
Reduced moment-angle curves from slow bend tests of notched specimens; material (A2.1), specimens from OX-direction; from Ref. [2.10]

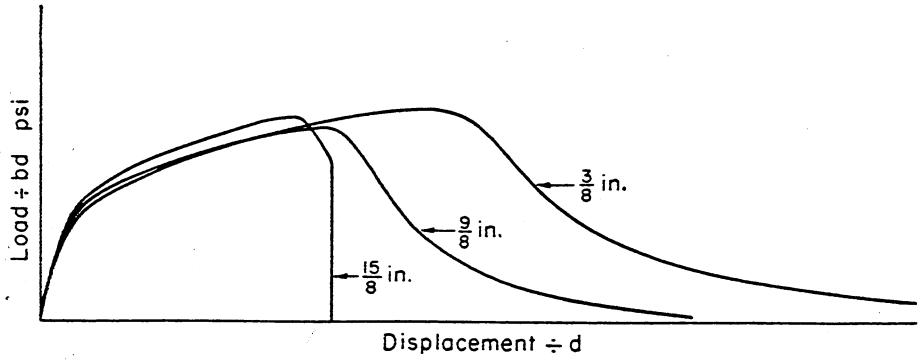

Fig. 2-12
Nominal stress vs. nominal displacement from slow bend tests of notched specimens; autographic records; material of group (C); from Ref. [2.10]

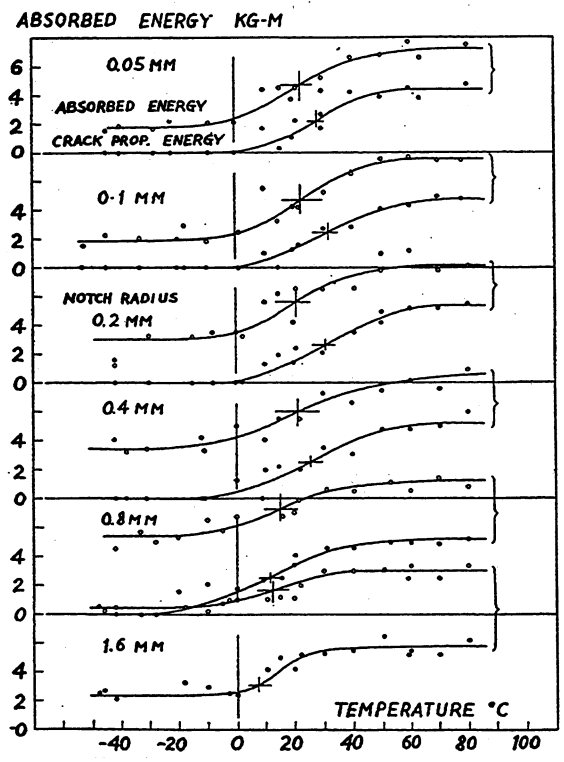

Fig. 2-13
Absorbed energy and crack propagation energy in small specimens (10 x 10 mm) with various notch radii; mild steel; from Ref. [2.12]

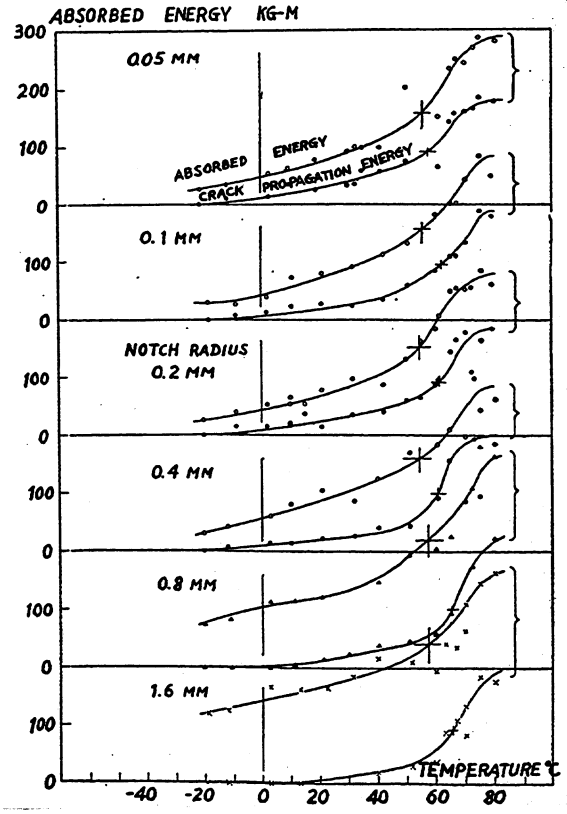

Fig. 2-14
Absorbed energy and crack propagation energy in large specimens (42 x 42 mm) with various notch radii; uncorrected for over-length of span; from mild steel; Ref. [2.12]

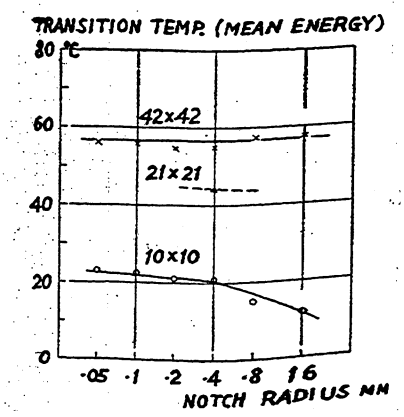

Fig. 2-15
Transition temperature obtained from mean absorbed energy against notch radius, uncorrected; mild steel; from Ref. [2.12]

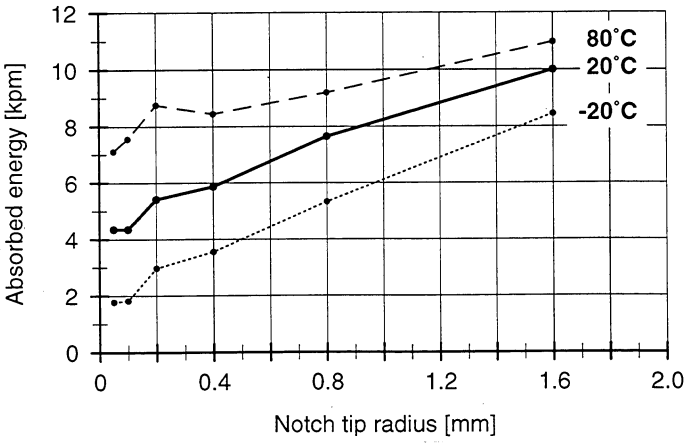

Fig. 2-16
Absorbed energy in small (10 x 10 mm) specimens versus notch tip radius; mild steel; based on data from Ref. [2.12]

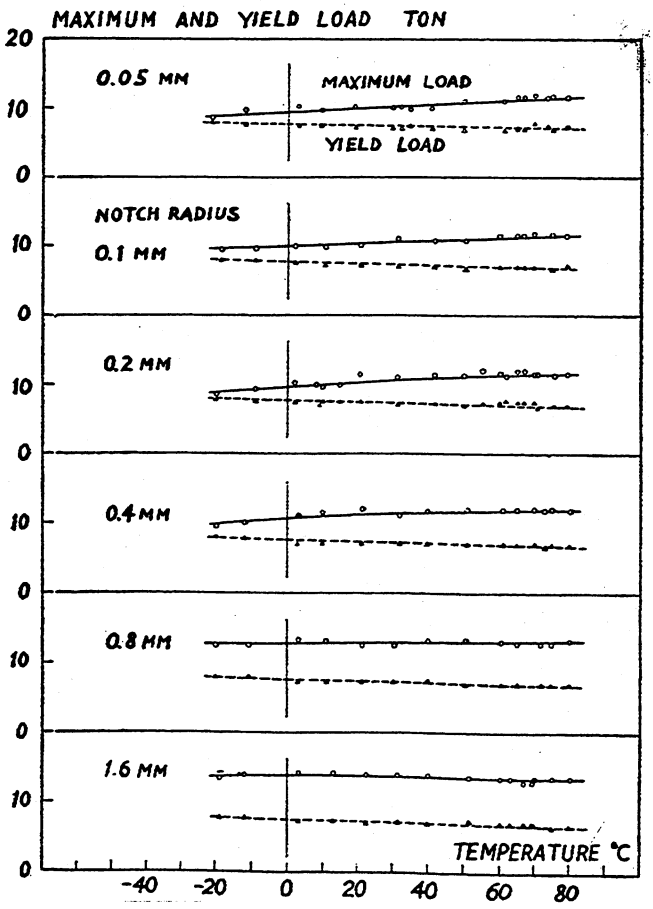

Fig. 2-17
Maximum and yield load vs. test temperature in large specimens (42 x 42 mm) with various notch radii, uncorrected; mild steel; from Ref. [2.12]

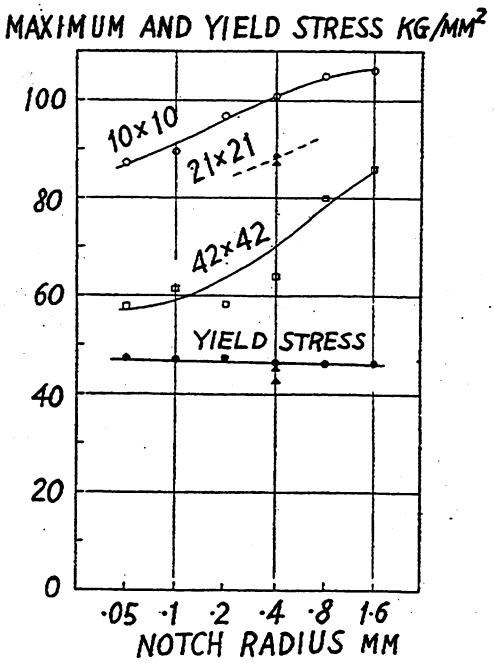

Fig. 2-18
Maximum and yield stress vs. notch radius in various size of specimens at 0° C, uncorrected; mild steel; from Ref. [2.12]

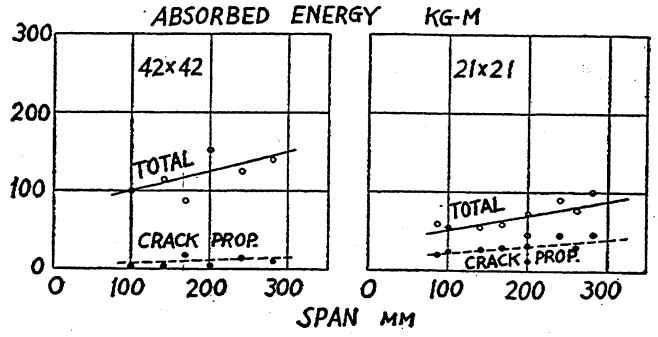

Fig. 2-19
Effect of span on absorbed energy
at 20° C; mild steel; from Ref. [2.12]

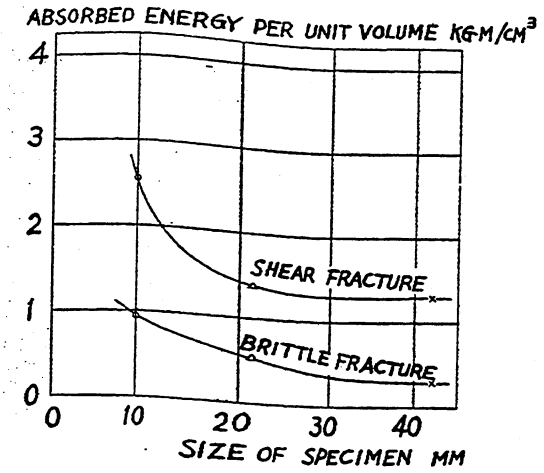

Fig. 2-20
Absorbed energy per unit volume
vs. size of specimens in shear (+80 °C)
and brittle fracture (-20 °C); scaled notch radii,
corrected span; mild steel; from Ref. [2.12]

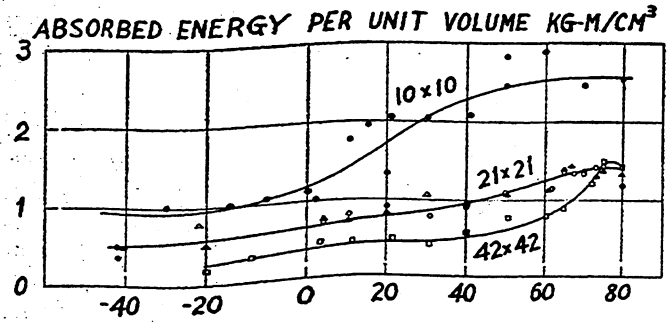

Fig. 2-21
Absorbed energy per unit volume
vs. test temperature for each size
of specimens; mild steel; from Ref. [2.12]

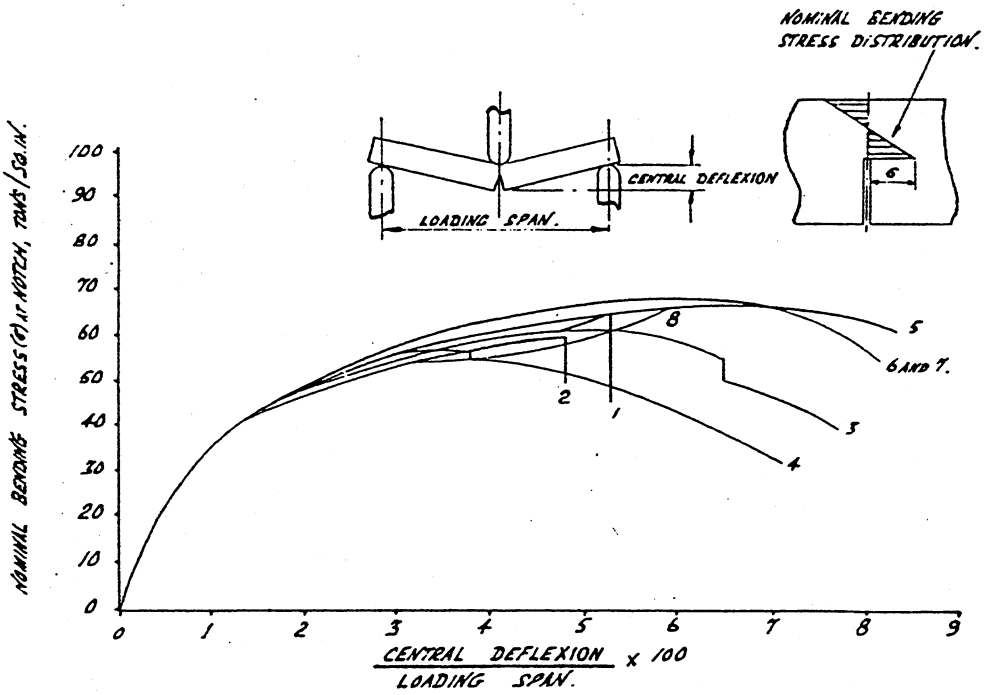

Fig. 2-22
Load deflexion curves for geometrically similar specimens; structural-quality mild steel; from Ref. [2.13]

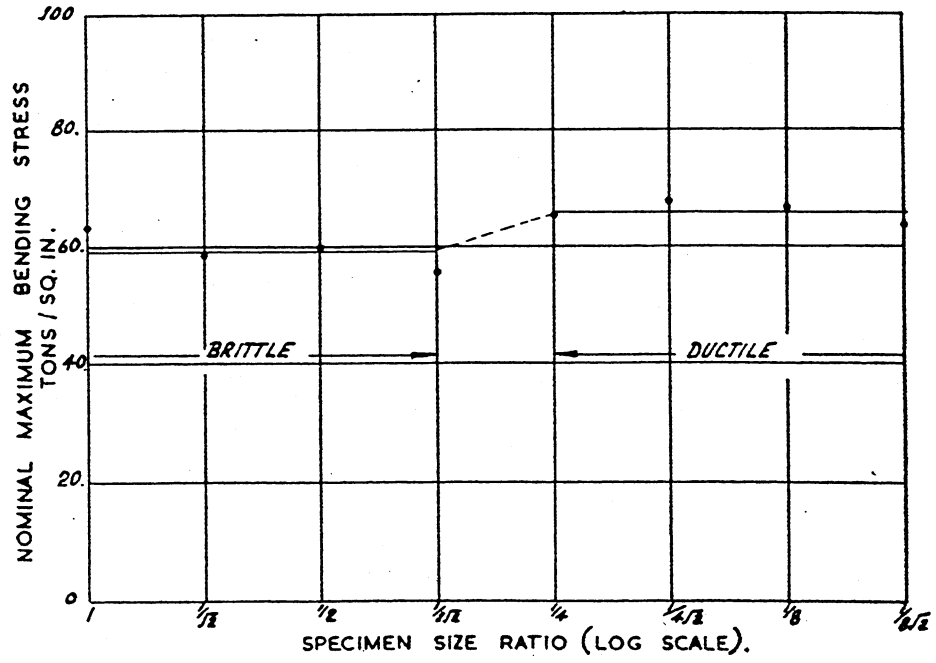

Fig. 2-23
Relation between specimen size and nominal breaking stress; structural-quality mild steel; from Ref. [2.12]

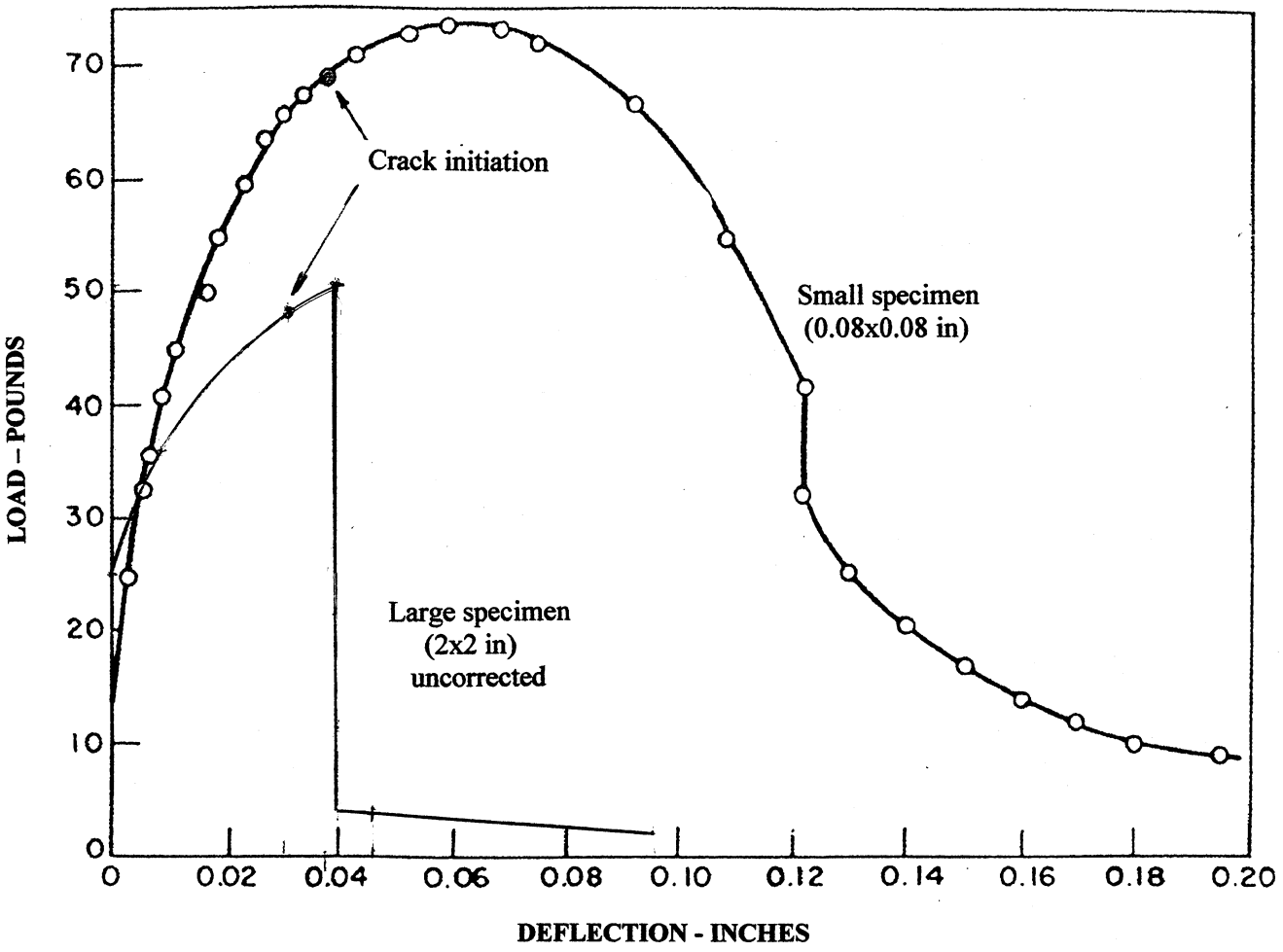

Fig. 2-24
Load-deflection curves for V-notch Charpy specimens; small (0.08 x 0.08 in, span 3/8 in) and large (2 x 2 in, span 11 in); large specimen results scaled down without correction for differences in span length; mild steel; after Ref. {[2.15]

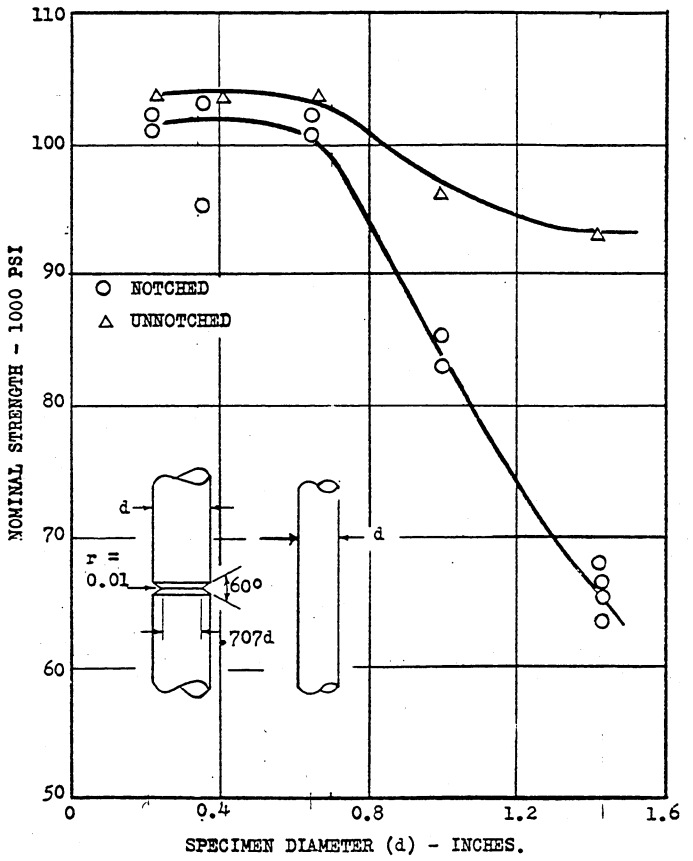

Fig. 2-25
Effect of section size on the strength of smooth and notched 7075-S-T6 aluminium tensile specimens; from Ref. [2.17]

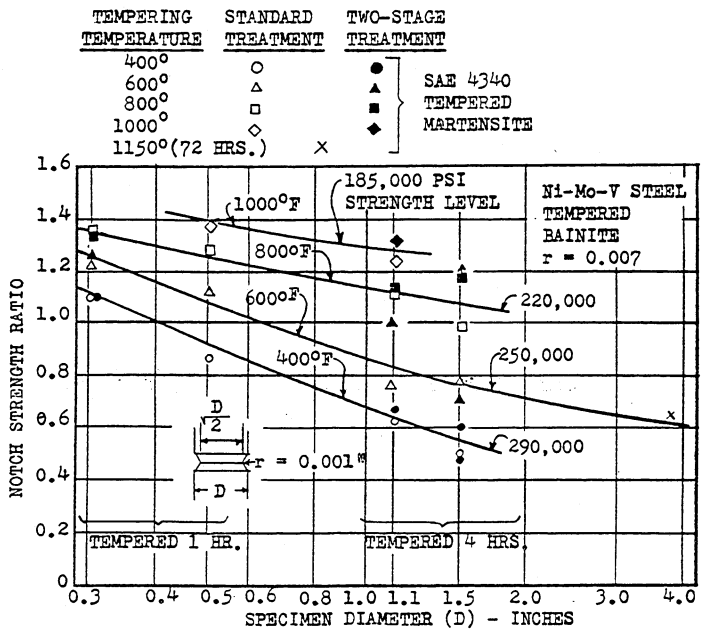

Fig. 2-26
Size effect in notched tensile tests of SAE 4340 steel quenched to martensite and tempered to various strength levels; for comparison, one notch tensile test on the Ni-Mo-V steel is also shown; from Ref. [2.17]

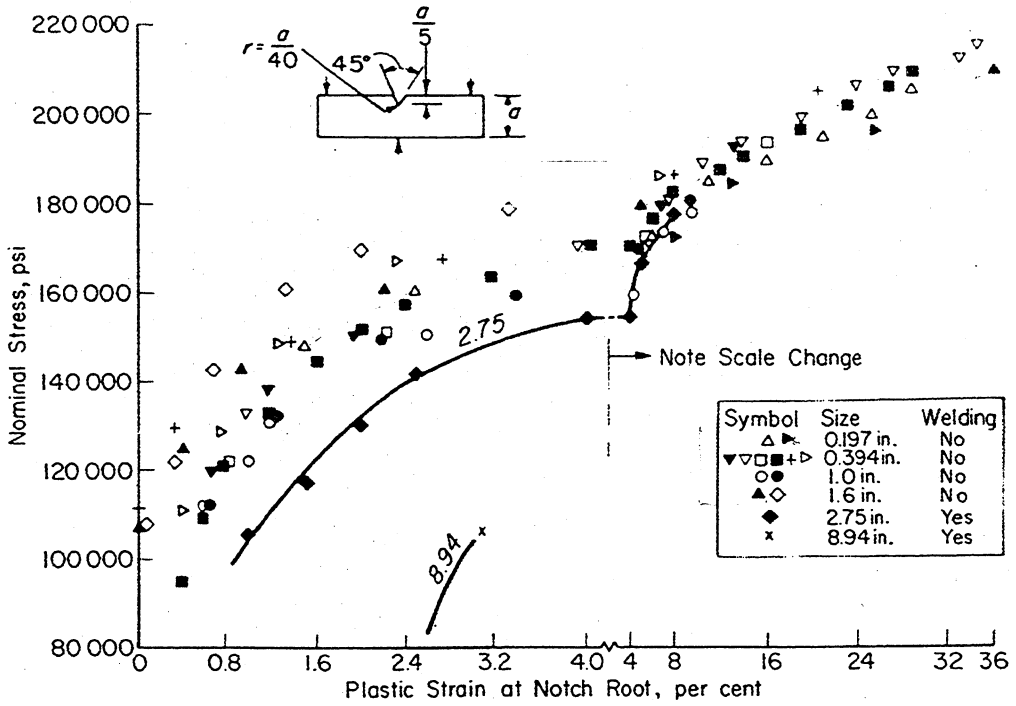

Fig. 2-27
Nominal bending stress vs. plastic strain at notch root; various sizes of geometrically similar V-notch Charpy specimens; forged generator rotor Ni-Mo-V steel; from Ref. [2.18]

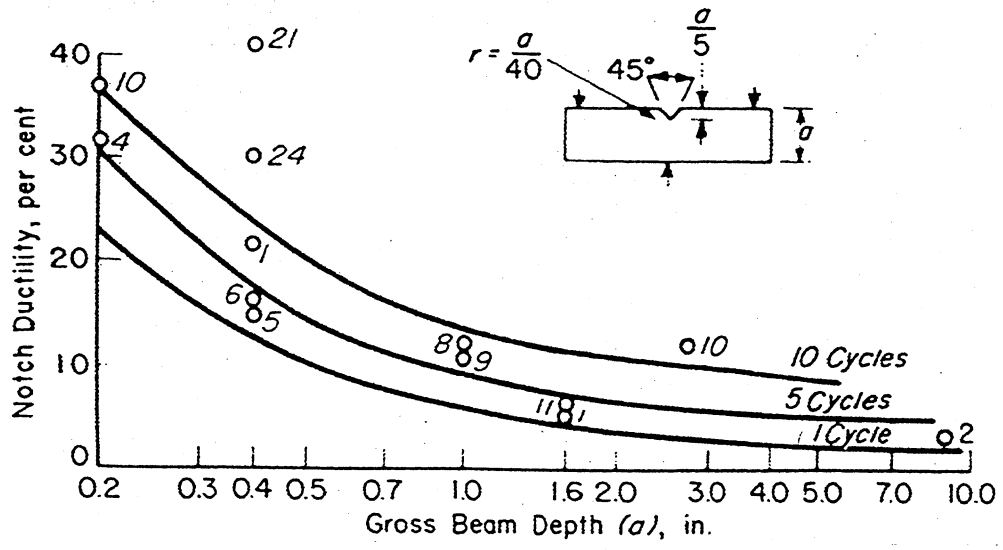

Fig. 2-28
Notch strain at fracture for slow bending of notched specimens that are geometrically similar to a V-notch Charpy impact specimen; numbers adjacent to
points are number of successive loading and complete unloading cycles prior to
fracture; forged generator rotor Ni-Mo-V steel; from Ref. [2.18]

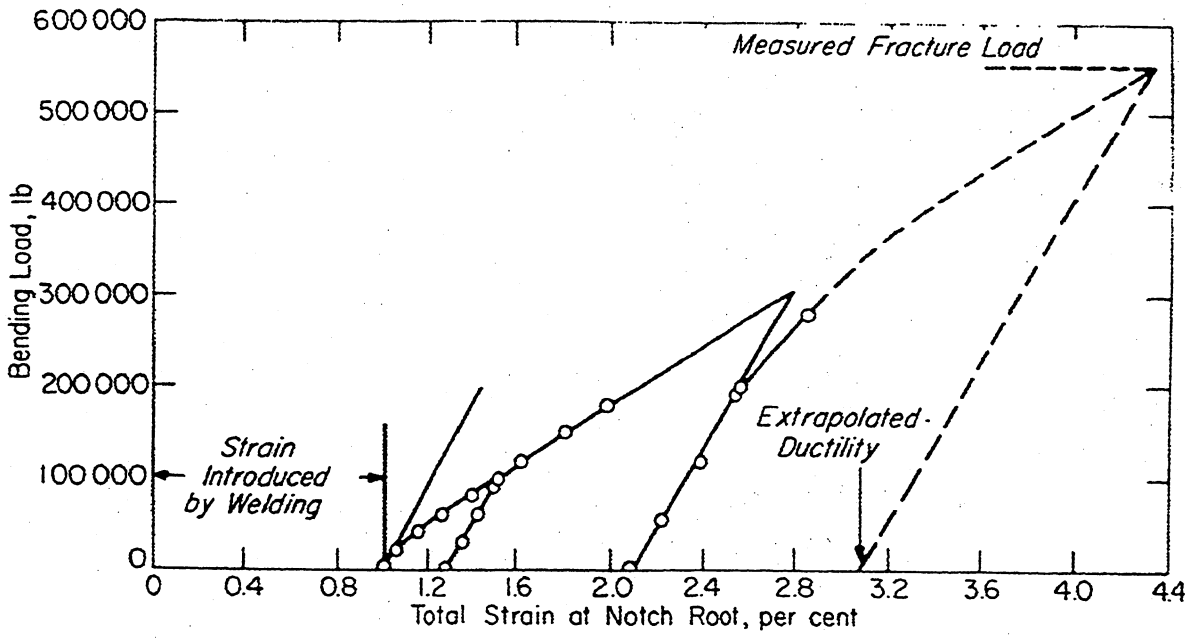

Fig. 2-29
Notch-bend test data for 8.94 in square beam with notch sharpness = 1, span: 57 in; forged generator rotor Ni-Mo-V steel; from Ref. [2.18]

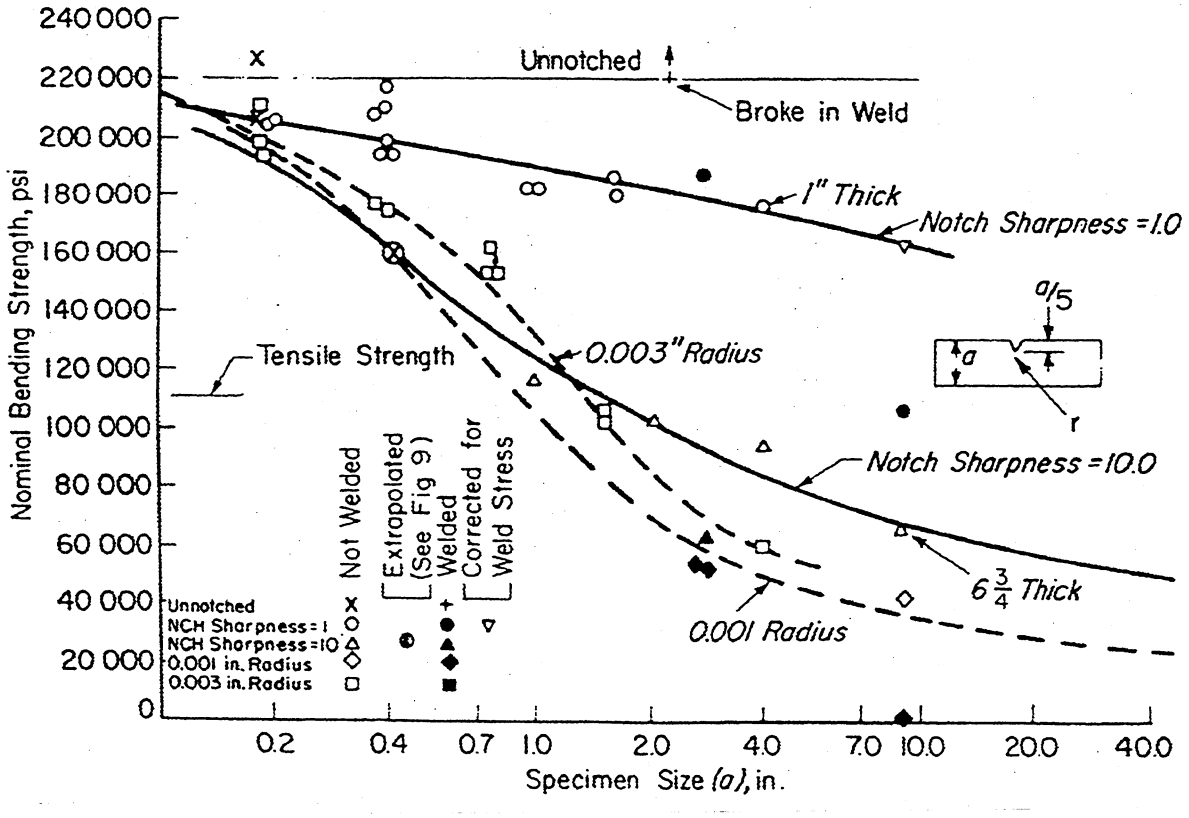

Fig. 2-30
Slow notch-bend strength vs. size and notch sharpness for 20 % notch depth; forged generator rotor Ni-Mo-V steel; from Ref. [2.18]

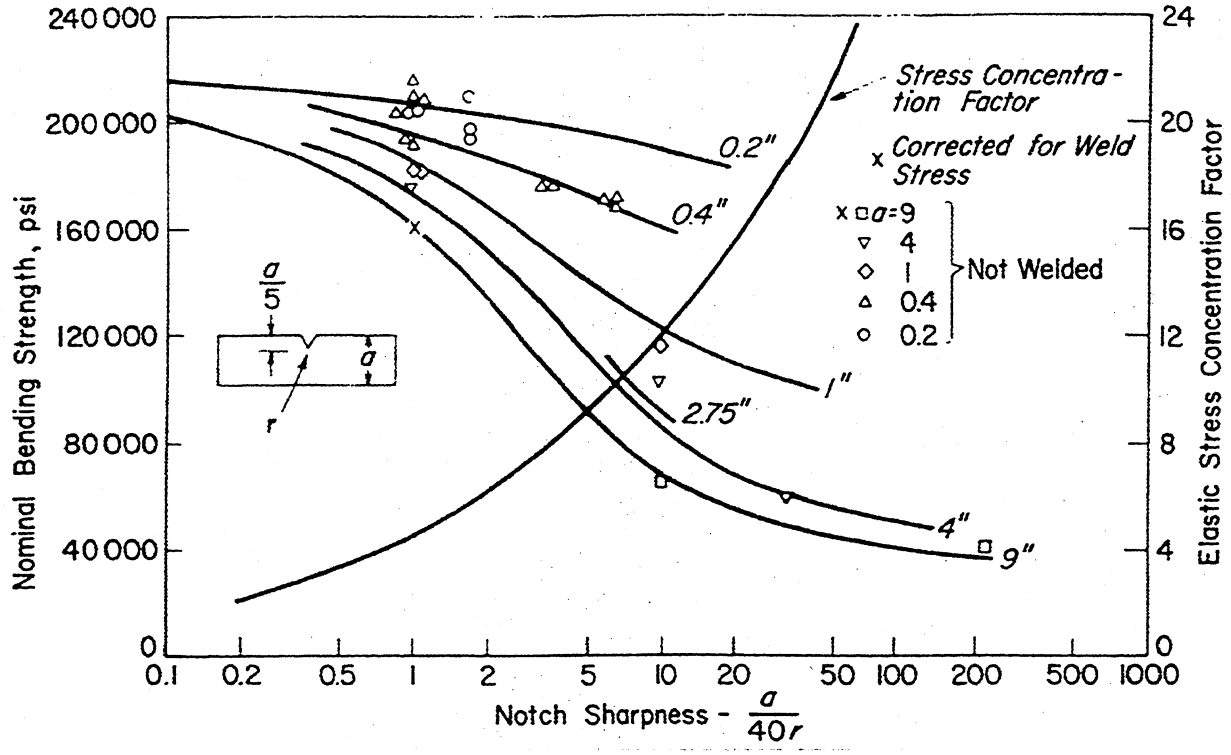

Fig. 2-31
Effect of notch sharpness on bend strength of specimens with 20 % notch depth; forged generator rotor Ni-Mo-V steel; from Ref. [2.18]

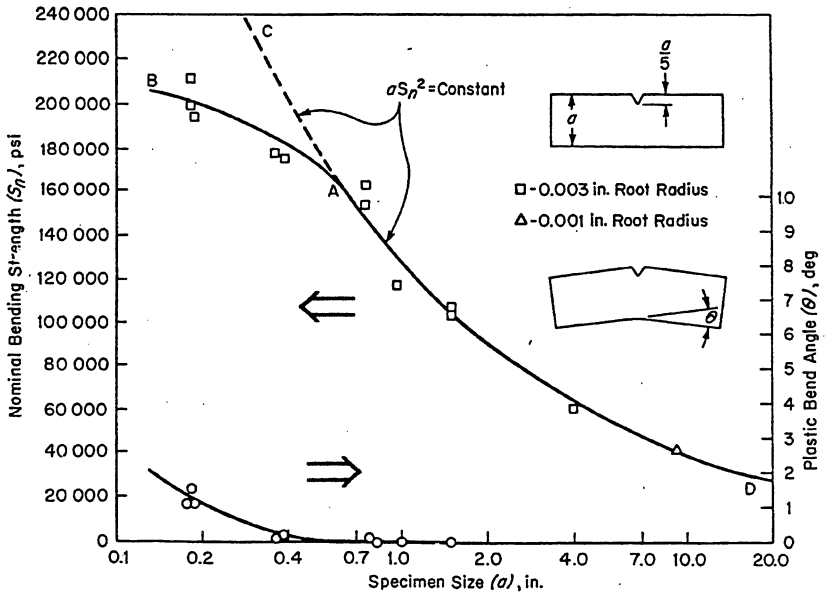

Fig. 2-32
Correlation of notch bend data with the size effect predicted by the Griffith-Irwin theory; tempered Ni-Mo-V steel forging-rotor steel; from Ref. [2.20]

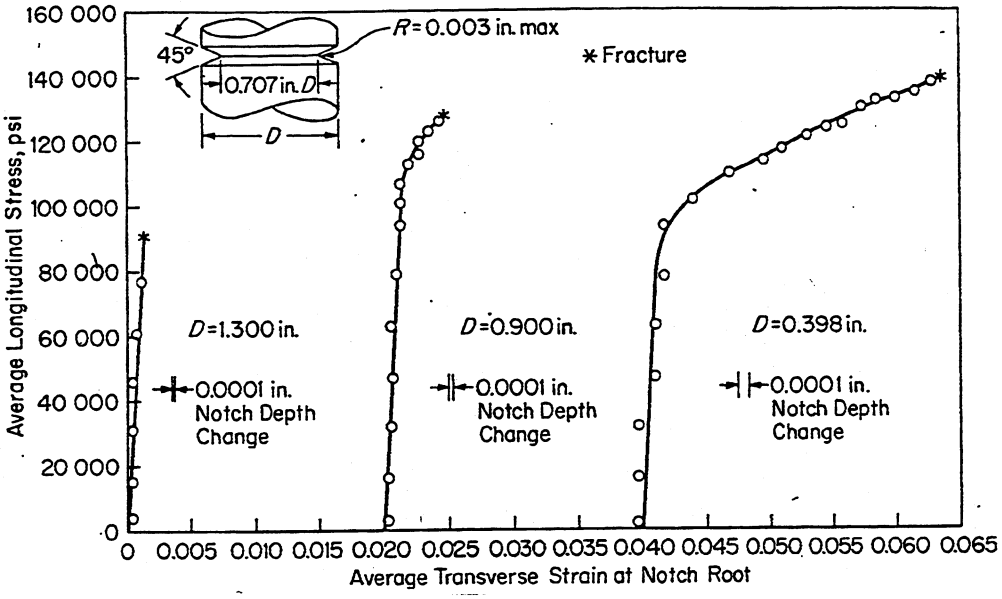

Fig. 2-33
Typical examples of stress-strain curves for notched tension test specimens; tempered Ni-Mo-V steel forging-rotor steel; from Ref. [2.20]

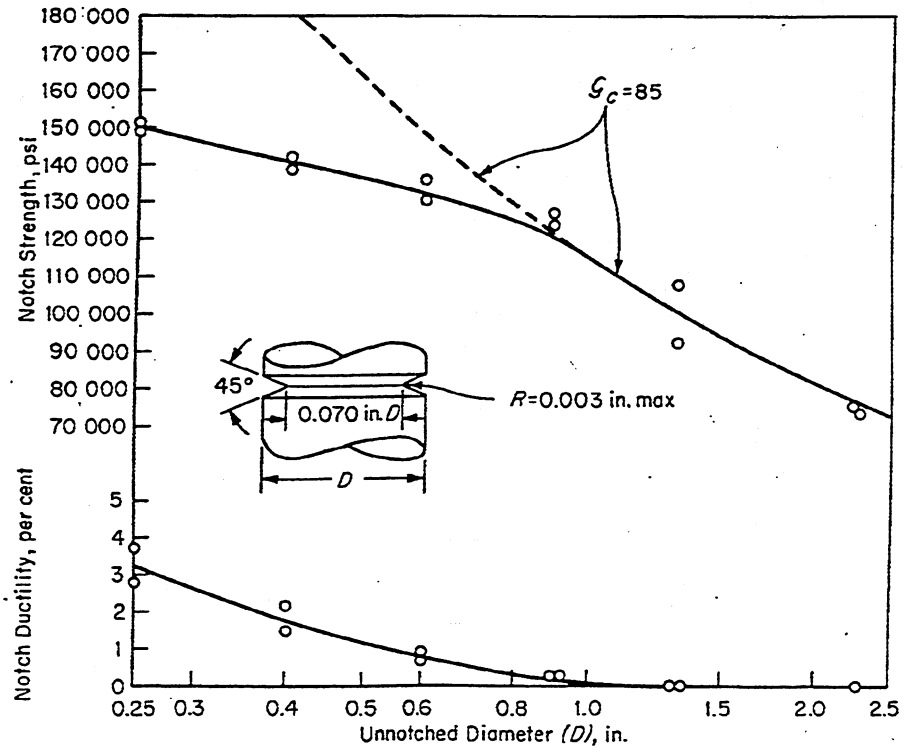

Fig. 2-34
Notch tension test results on material A; 45°, 50 % sharp V-notches; tempered Ni-Mo-V steel forging-rotor steel; from Ref. [2.20]

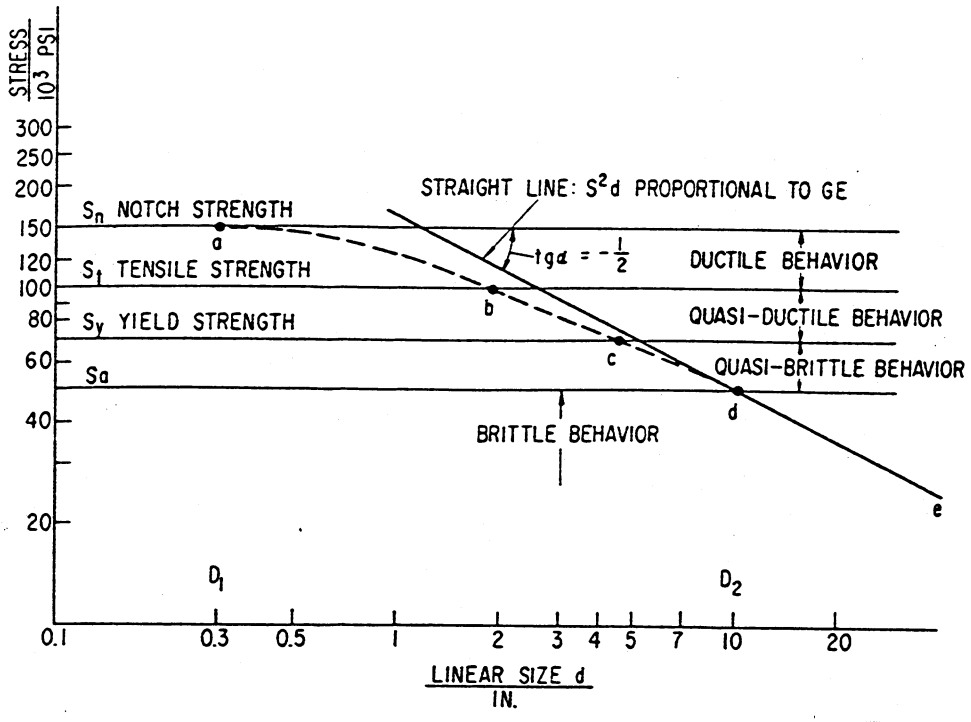

Fig. 2-35
Notch strength versus size; schematic representation; from Ref. [2.22]

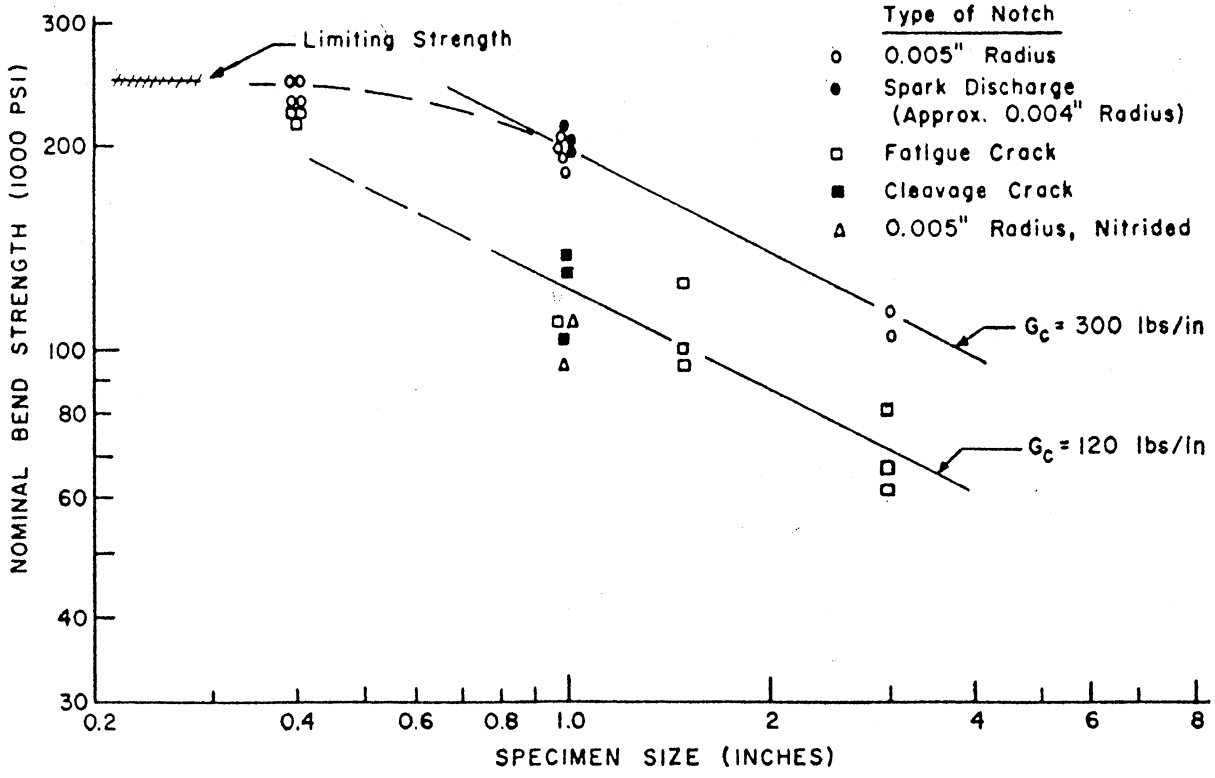

Fig. 2-36
Influence of notch preparation on the notched bend strength of various size specimens; heat treated alloy steel with course grained tempered bainitic microstructure; vacuum arc remelted alloy steel; from Ref. [2.24]

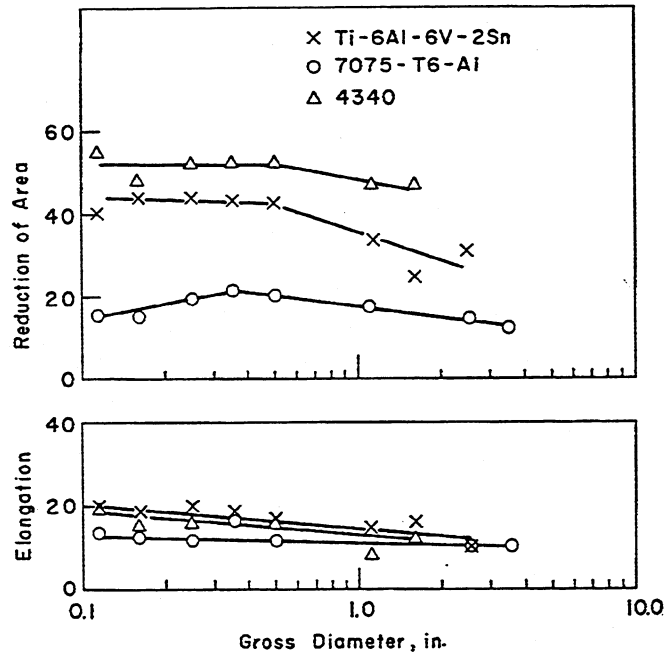

Fig. 2-37
Reduction of area and elongation of smooth specimens vs. section size; different materials; from Ref. [2.25]

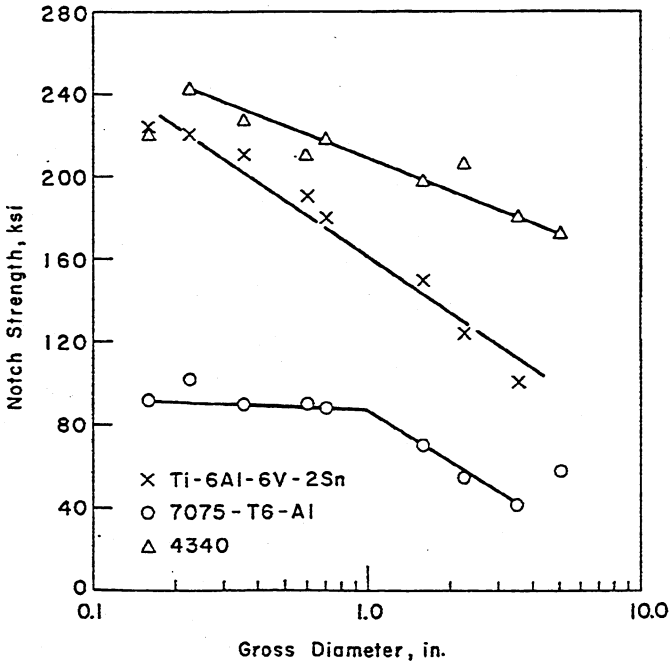

Fig.. 2-38
Notch strength versus section size; different materials; from Ref. [2.25]

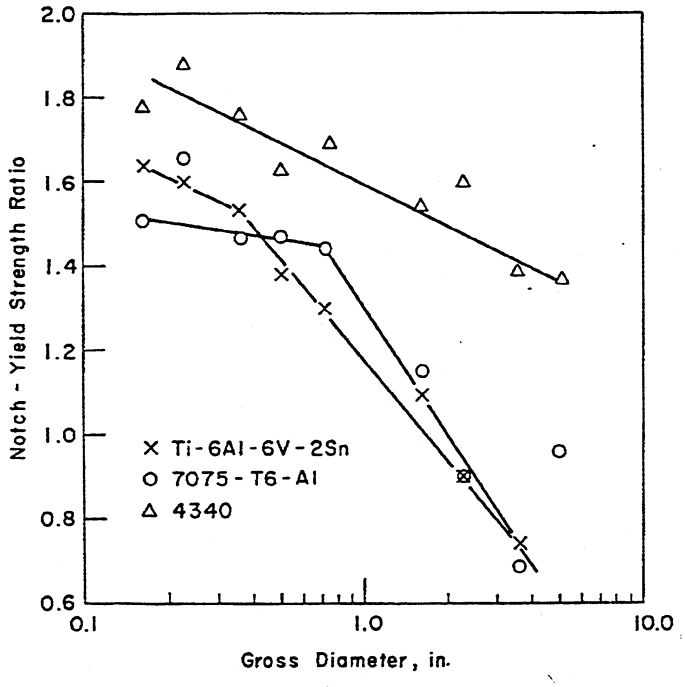

Fig. 2-39
Ratio of notch tensile strength to
the average 0.2 % yield strength;
different materials; from Ref. [2.25]

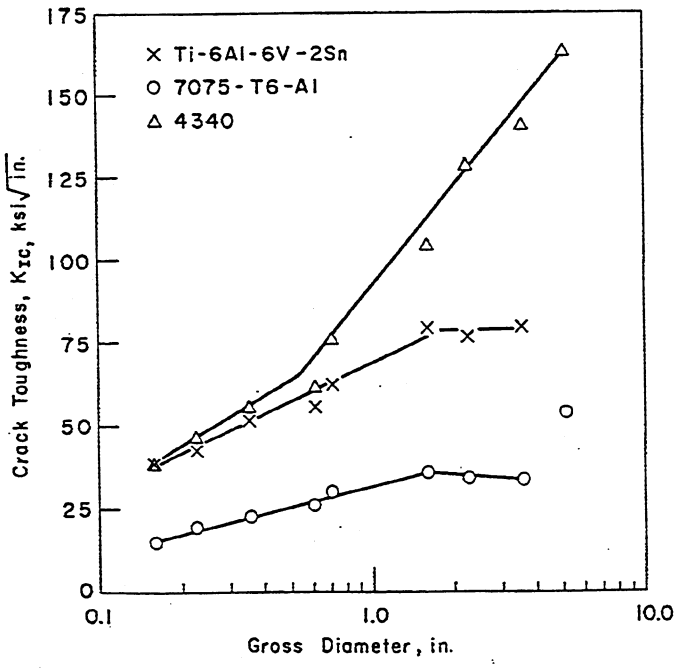

Fig. 2-40
Crack toughness K_{IC} v.s. section size;
different materials; from Ref. [2.25]

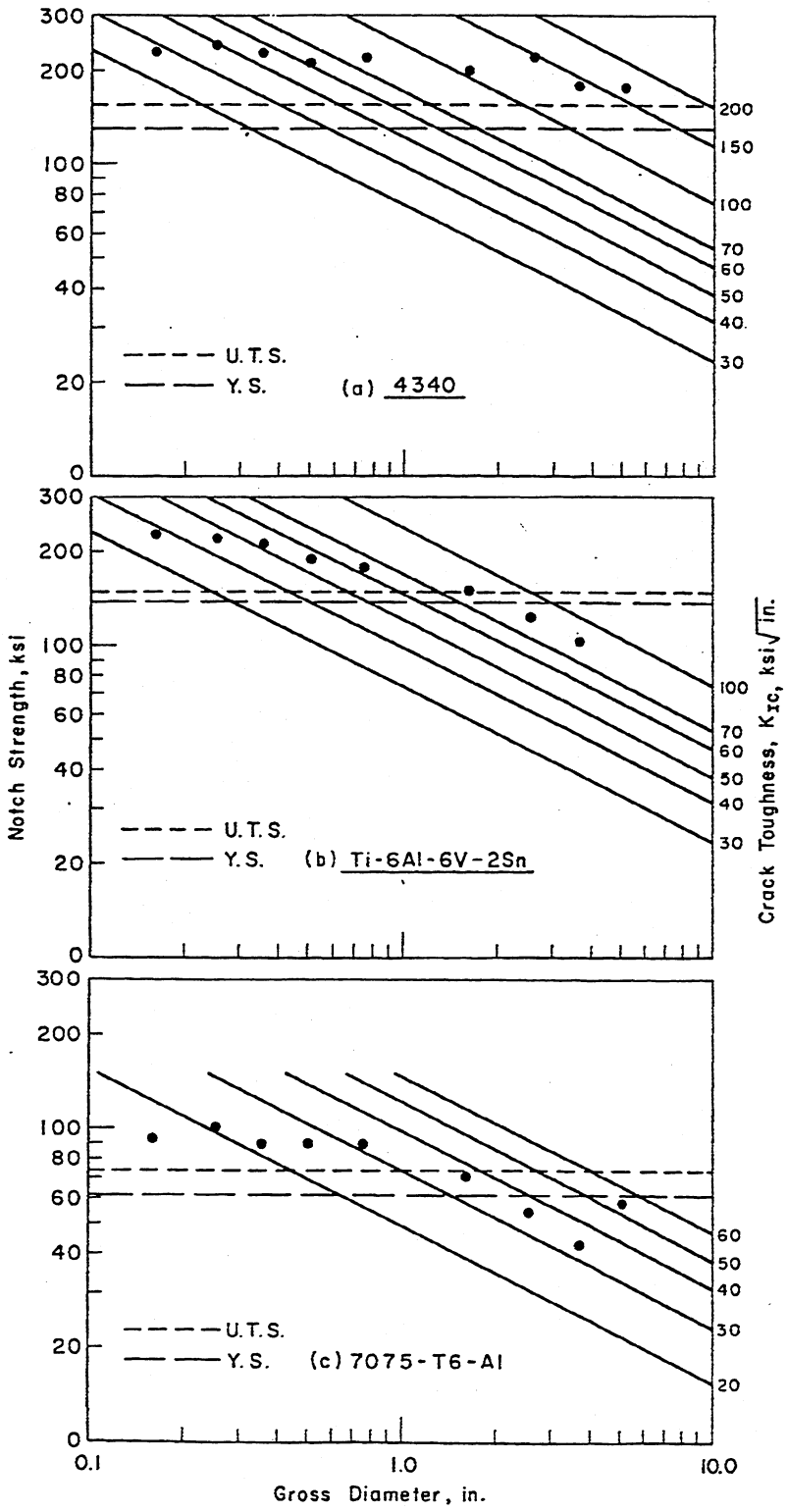

Fig. 2-41
Notch strength vs. section size
with K_{IC} as the parameter;
different materials; from Ref. [2.25]

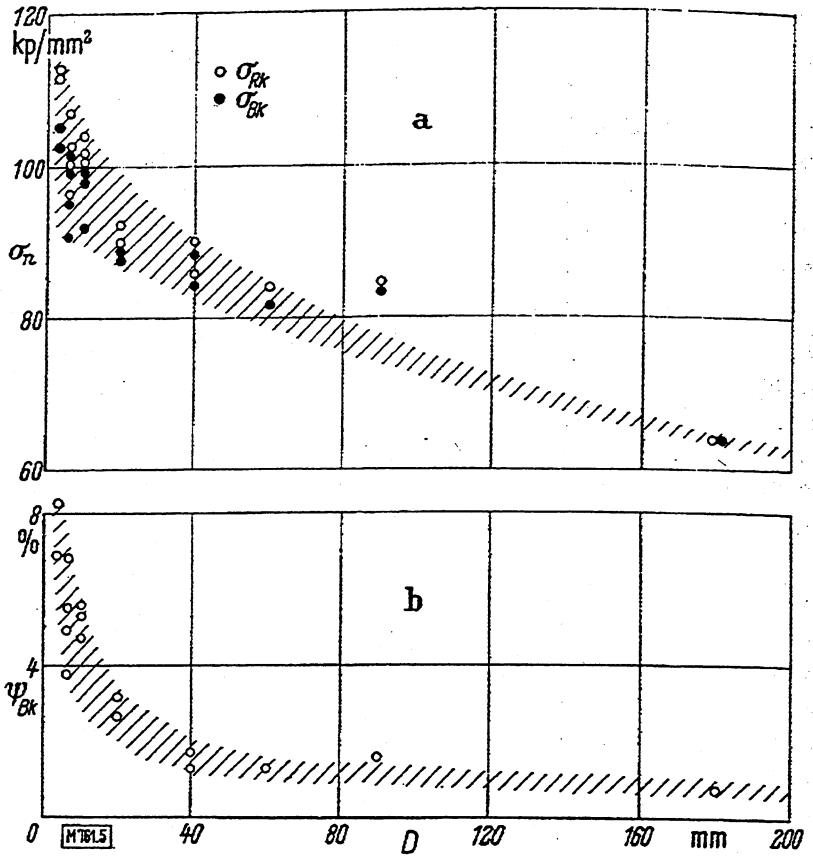

Fig. 2-42
Notch strength σ_{Bk}, true fracture stress σ_{Rk}, and percentage area reduction Ψ_{Bk} after fracture of similarly V-notched tensile bars as function of unnotched specimen diameter D; material C60-steel, quasistatic test at R.T.; from Ref. [2.26]

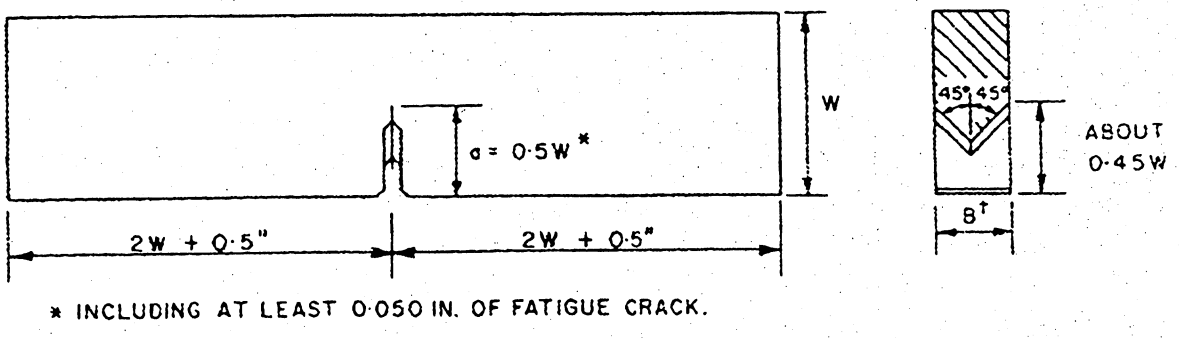

Fig. 2-43
Notch-bend specimen; from Ref. [2.27]

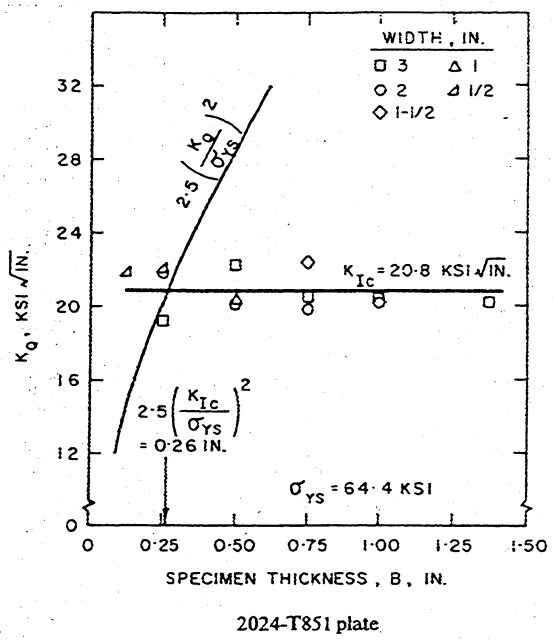

2024-T851 plate

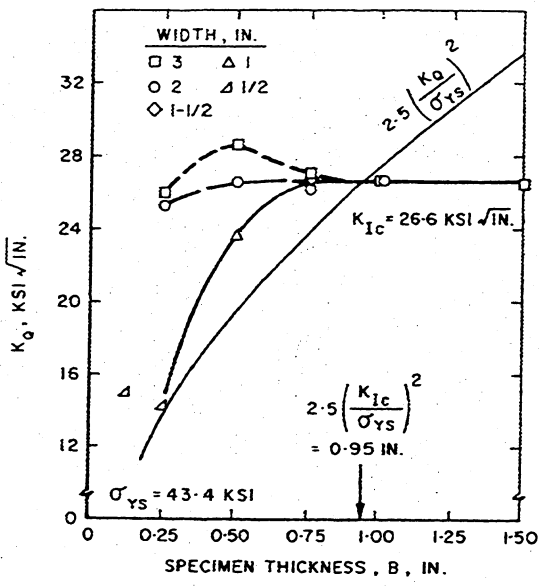

6061-T651 plate,

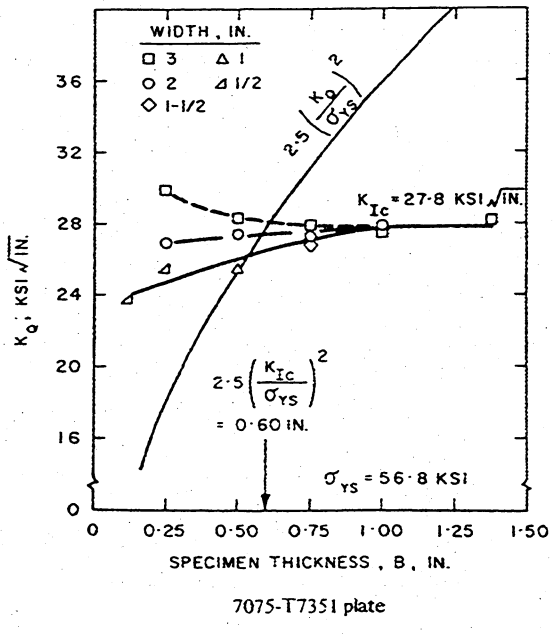

7075-T7351 plate

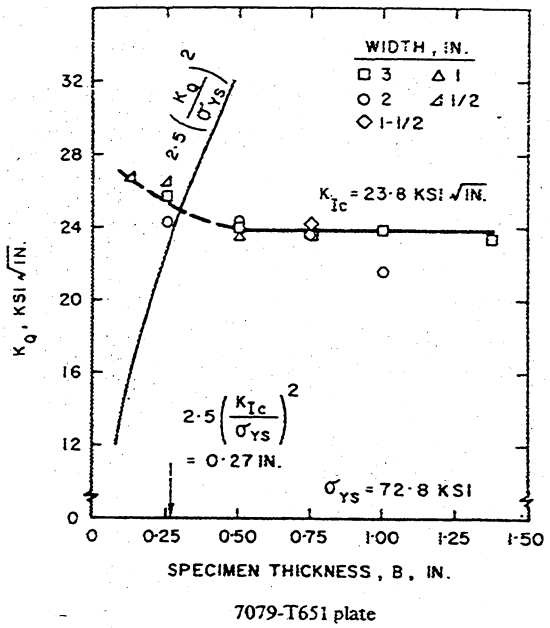

7079-T651 plate

Fig. 2-44
K_Q vs. specimen thickness B, three-point bending of proportional (see Tab. 2-27) as well as non-similar notched specimens; four different aluminium alloys; from Ref. [2.27]

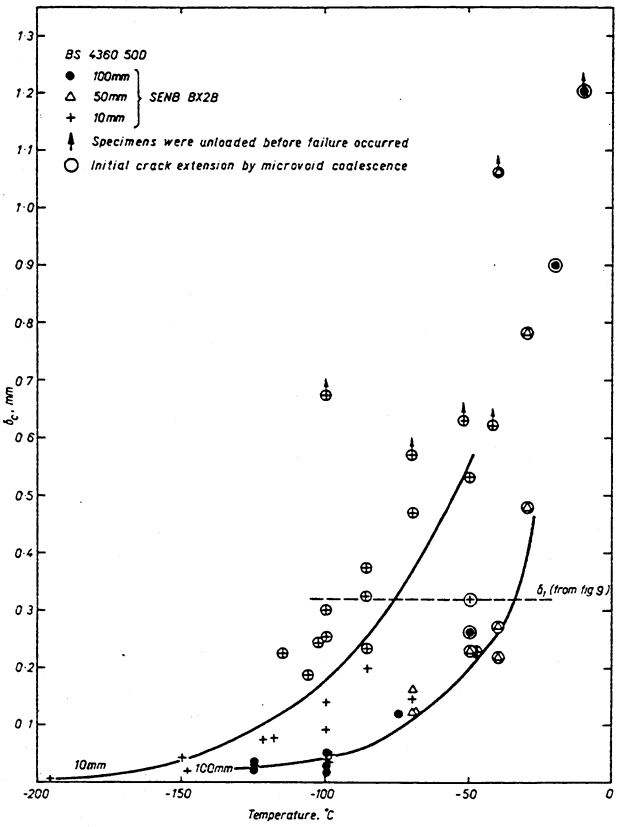

Fig. 2-45
Size effect on the COD transition curve;
carbon manganese steel; from Ref. [2.30]

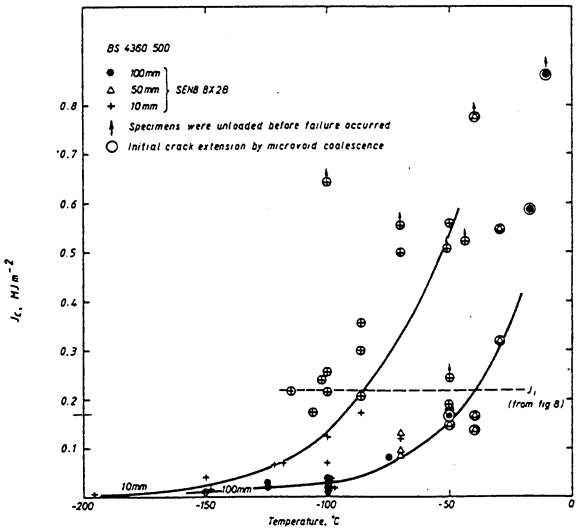

Fig. 2-46
Size influence on the J_c transition curve;
carbon manganese steel; from Ref. [2.30]

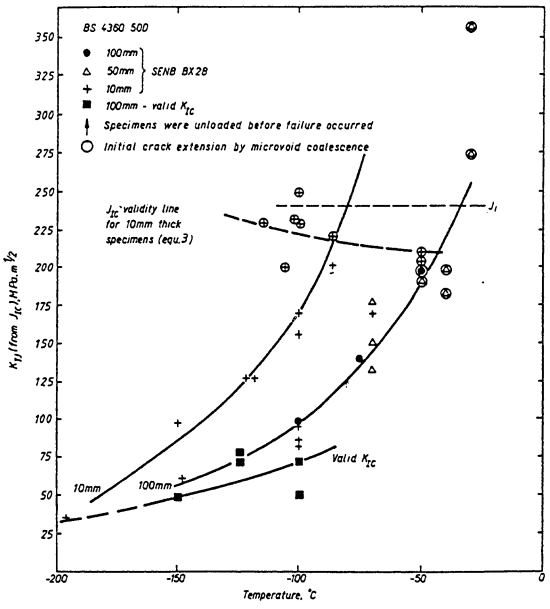

Fig. 2-47
Size effect on the K_{IJ} transition curve;
carbon manganese steel; from Ref. [2.30]

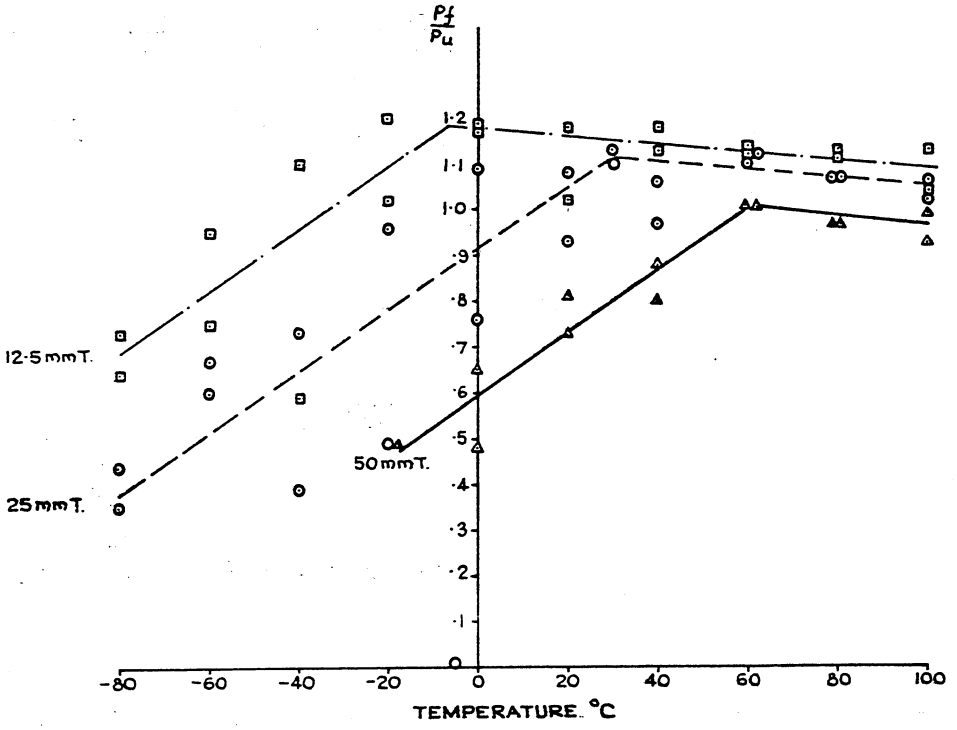

Fig. 2-48
Variation of actual failure load/calculated plane stress collapse load with temperature for compact tension specimens; turbine disc NiCrMoV steel; from Ref. [2.35]

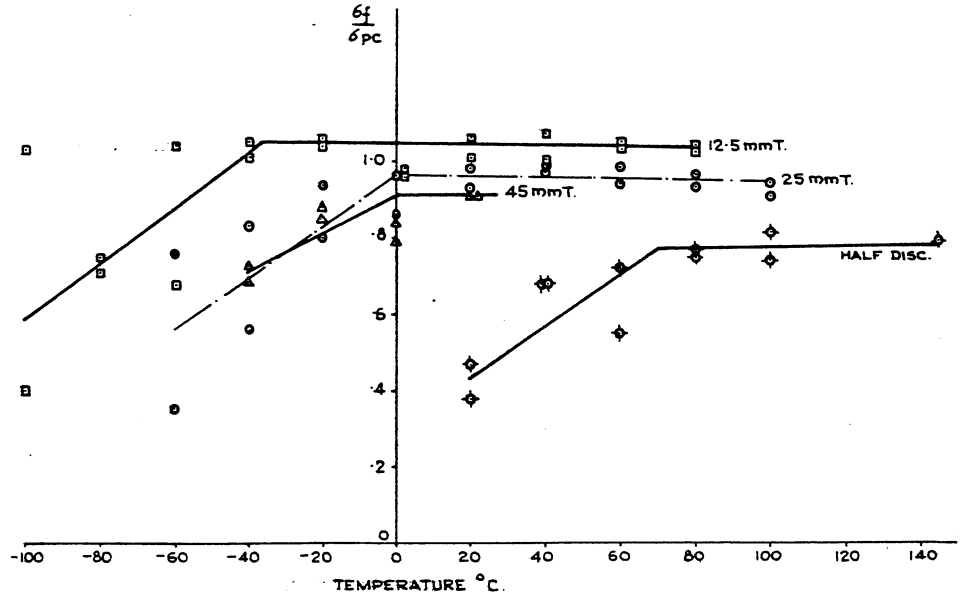

Fig. 2-49
Variation of outer fiber stress at failure/calculated outer fiber stress for plastic collapse with temperature for single-edge-notched bend specimens; turbine disc NiCrMoV steel; from Ref. [2.35]

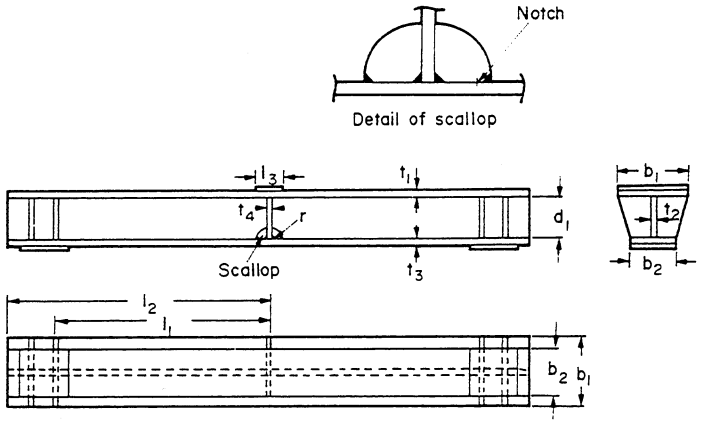

	l_1	l_2	l_3	b_1	b_2	d_1	t_1	t_2	t_3	t_4	r
M200 Series	900	1100	100	300	200	180	20	20	20	30	50
M60 Series	270	330	30	90	60	54	6	6	6	9	15
M23 Series	103	150	20	35	23	21	2.3	2.3	2.3	6	6

Size of specimen

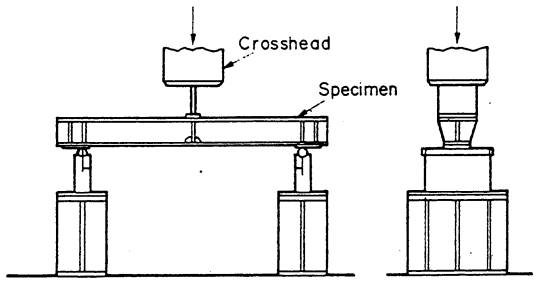

Method of test

Fig. 2-50
Shape and dimensions of I-beams, three-point bending set-up; from Ref. [2.36]

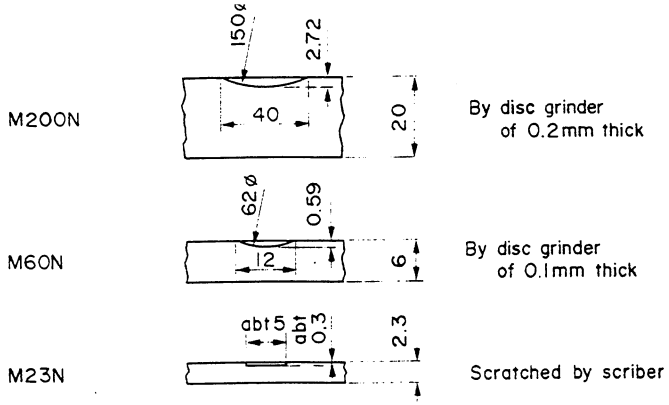

Fig. 2-51 Shape of notch at bottom flange; from Ref. [2.36]

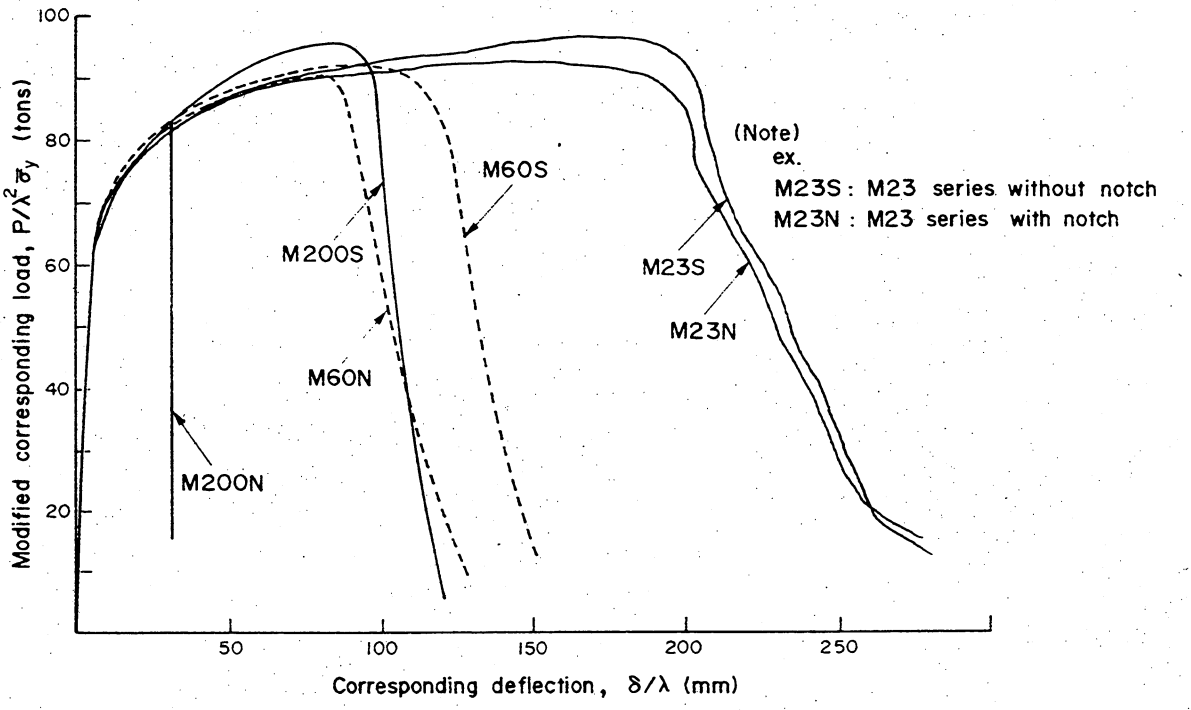

Fig. 2-52
Normalized load-deflection diagrams of un-notched and notched I-beams of three different sizes (M23, M60, & M200 ~ 2.3, 6, & 20 mm thickness of bottom flange) under quasi-static three-point bending; material: structural steels SPCC, SPHC & KAS; from Ref. [2.36]

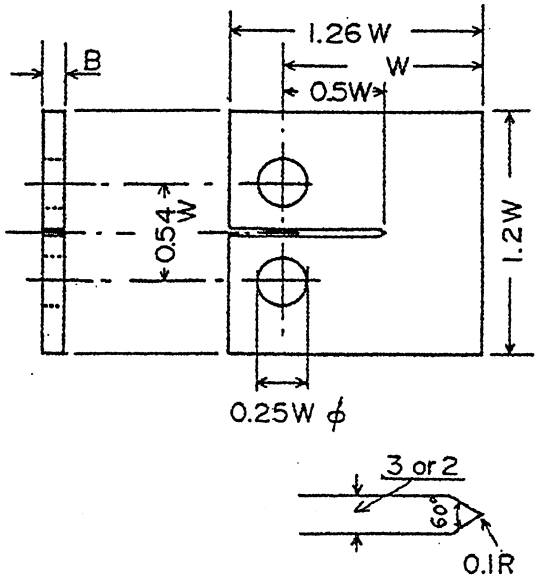

Fig. 2-53
Compact tension specimen; from Ref. [2.38]

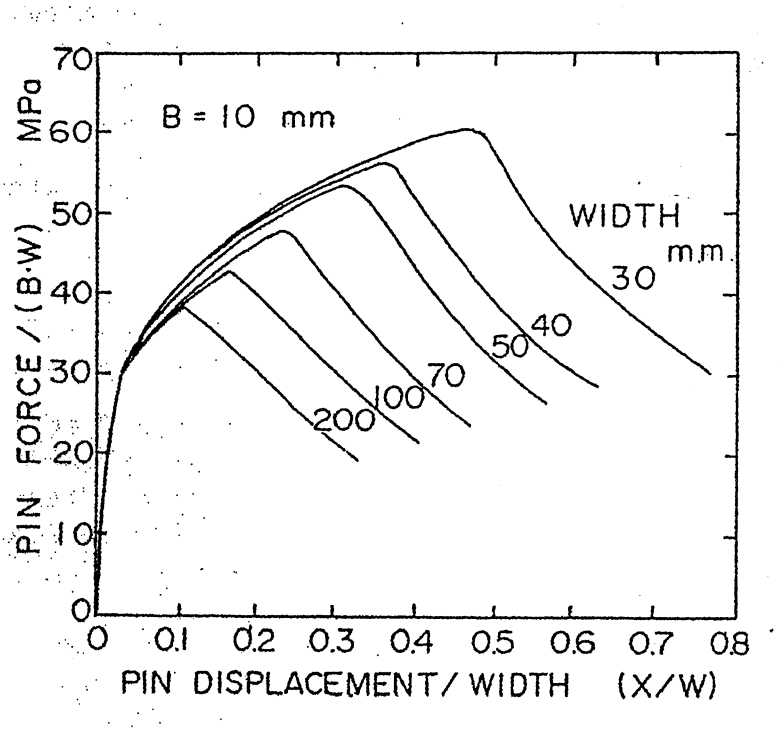

Fig. 2-54
Effect of nominal width W on load-displacement curves of compact tension specimens with a thickness of 10 mm; SUS 316 L-steel; room temperature; from Ref. [2.38]

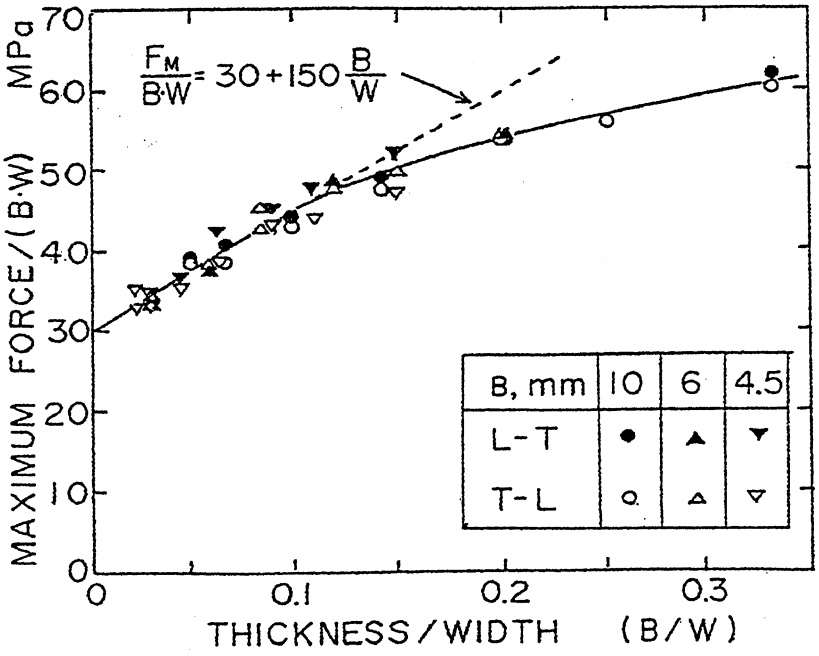

Fig. 2-55
Variation of the maximum load as a function of B/W; compact tension specimens; SUS 316 L-steel; from Ref. [2.38]

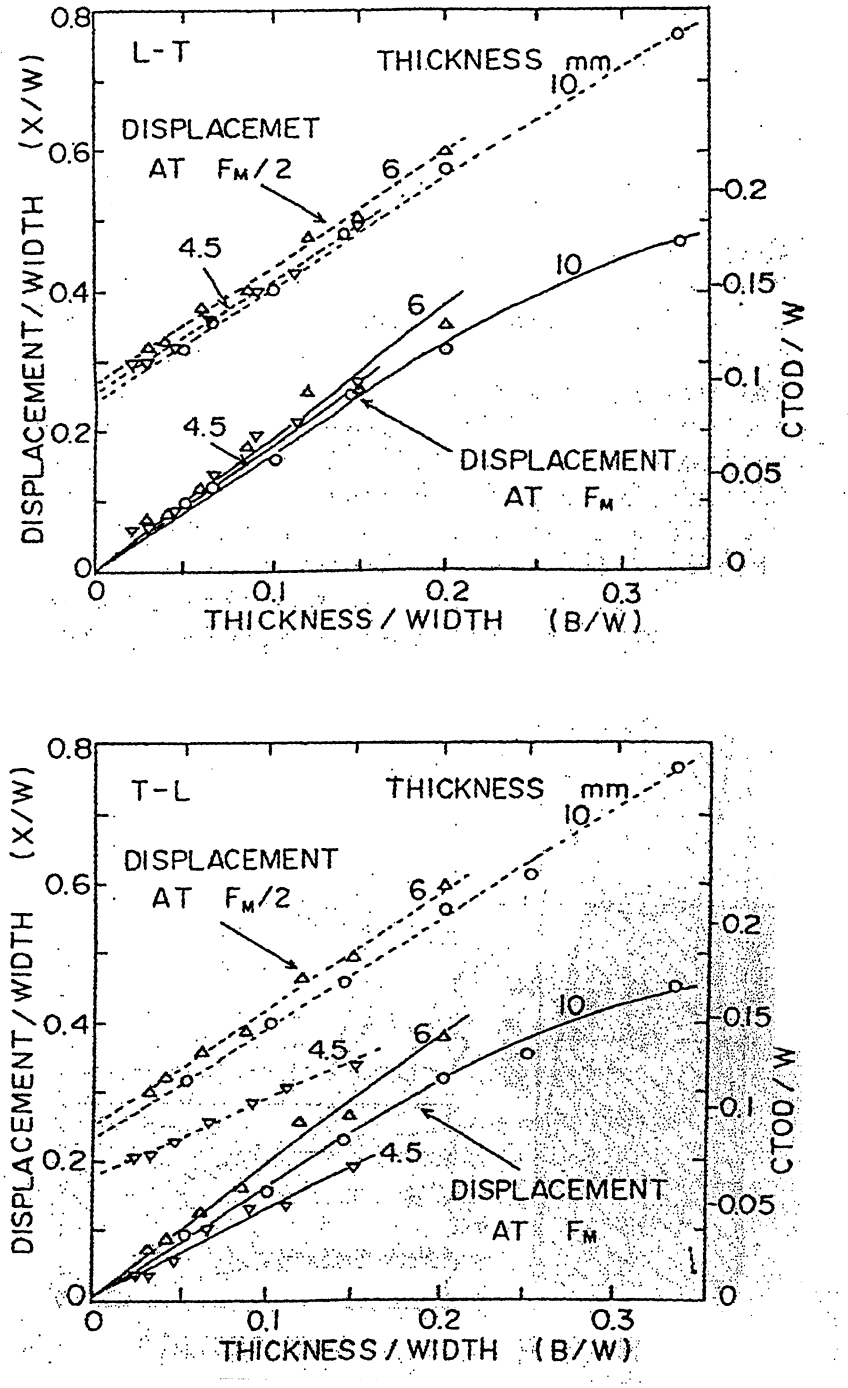

Fig. 2-56
Variation of normalized displacements X_M/W and X_H/W with B/W ratio; compact tension specimens; SUS316L-steel; room temperature; from Ref. [2.38]

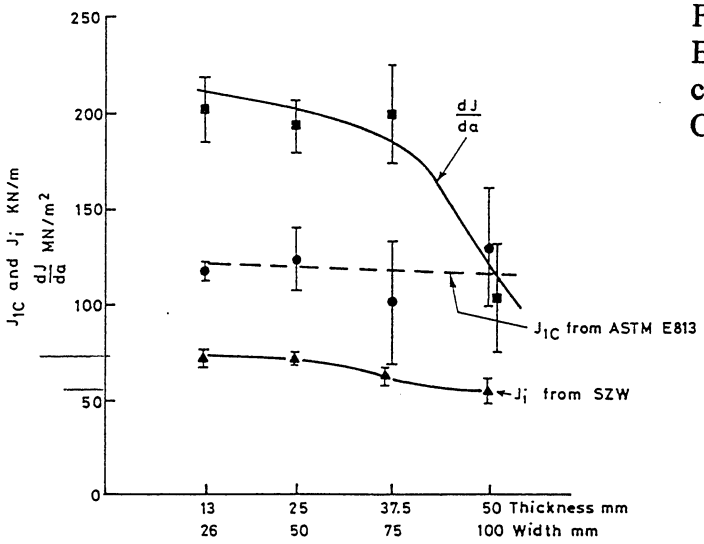

Fig. 2-57
Effect of size for non-side grooved compact specimens; normalized C-Mn steel; from Ref. [2.40]

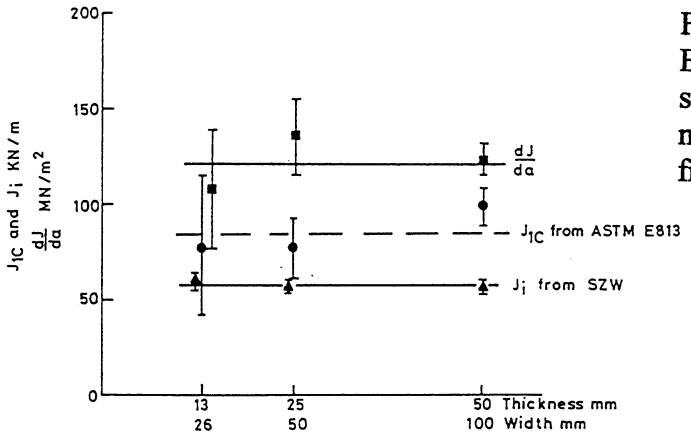

Fig. 2-58
Effect of size for compact specimens side grooved to a depth of 25 percent; normalized C-Mn steel; from Ref. [2-40]

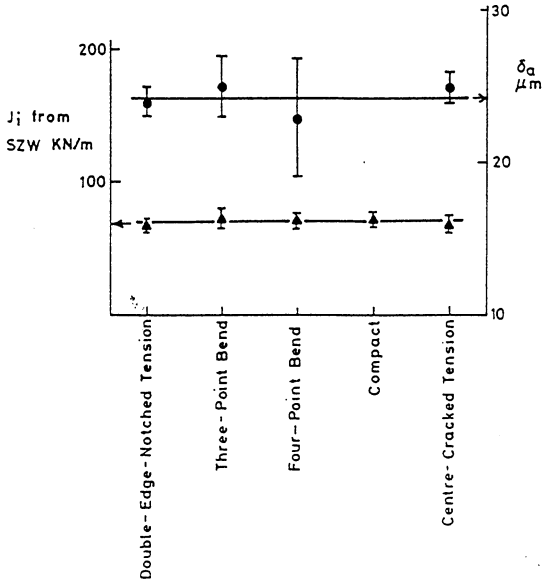

Fig. 2-59
Effect of specimen geometry on J_i and δ_a for non-side grooved specimens 25 mm thick; normalized C-Mn steel; from Ref. [2.40]

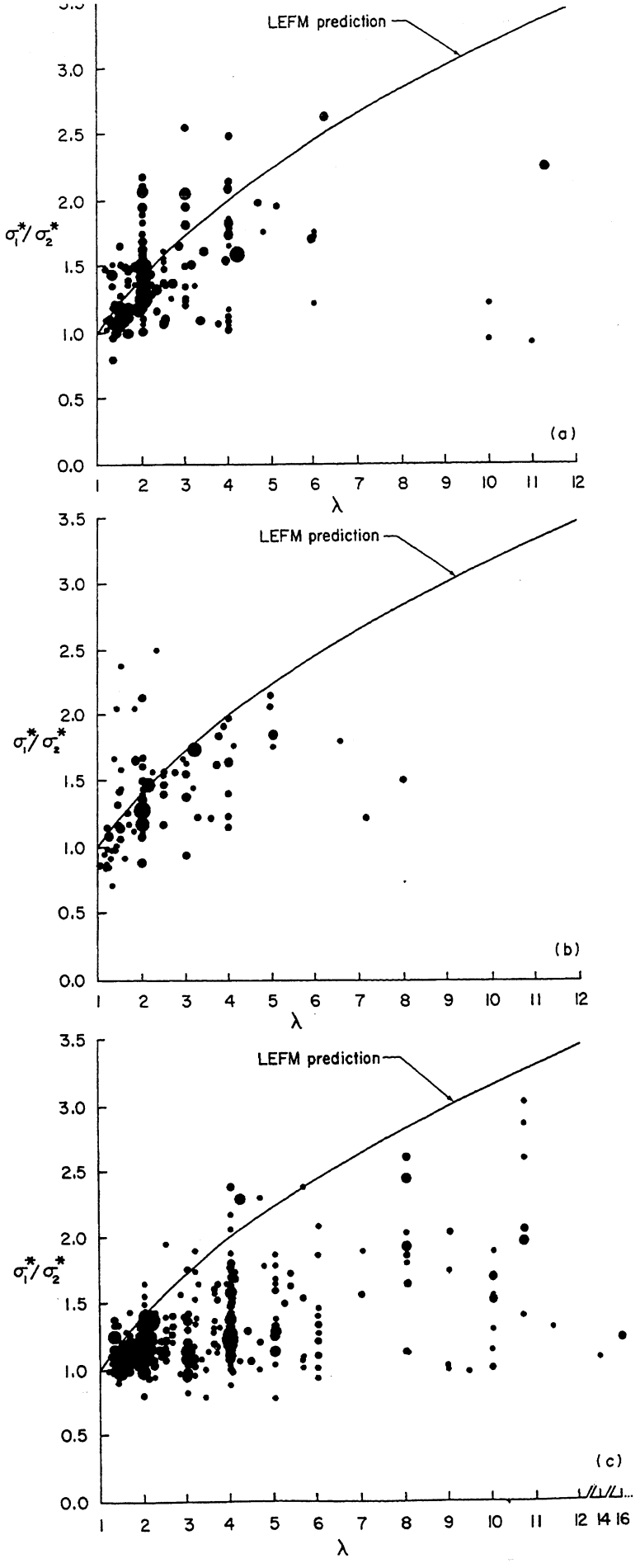

Fig. 2-60
Comparison of test data with LEFM predictions of strength size dependence:
(a) plane strain, brittle;
(b) plane strain, brittle-ductile;
(c) plane strain, ductile;
from Ref. [2.45]

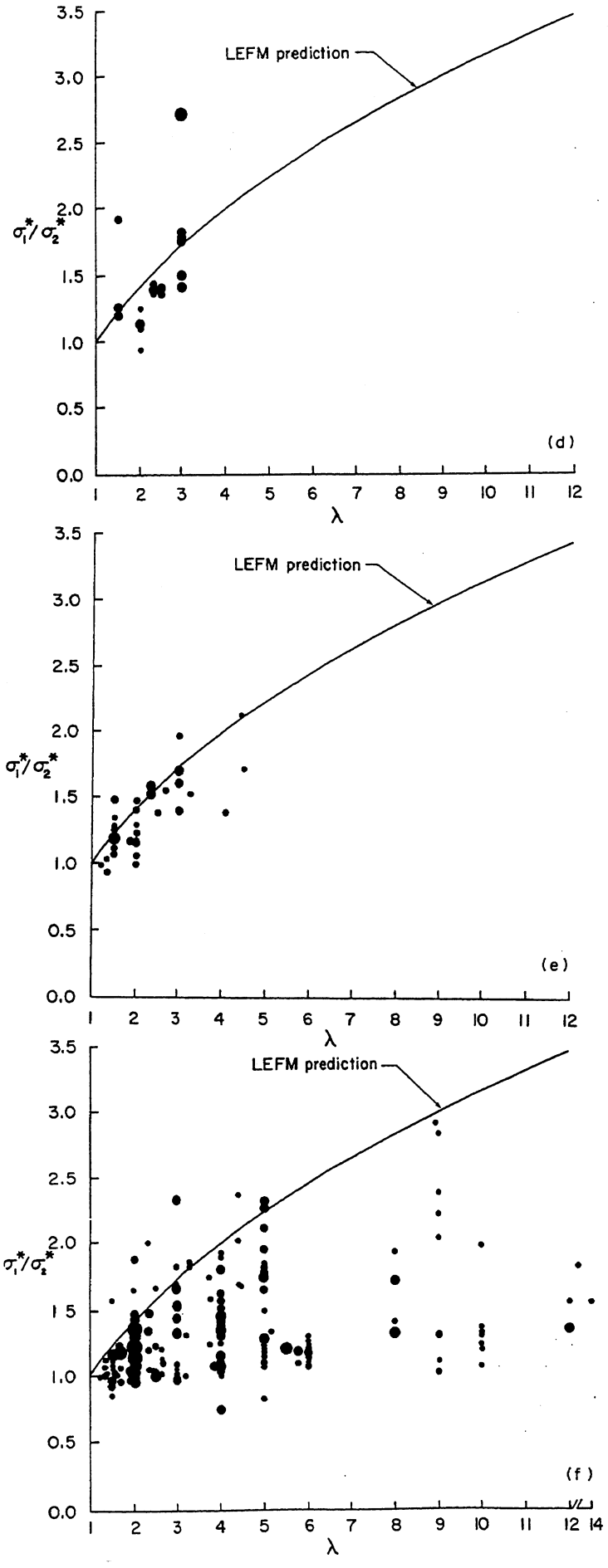

Fig. 2-61
Comparison of test data with LEFM predictions of strength size dependence:
(d) plane stress, brittle;
(e) plane stress, brittle-ductile;
(f) plane stress, ductile;
from Ref. [2.45]

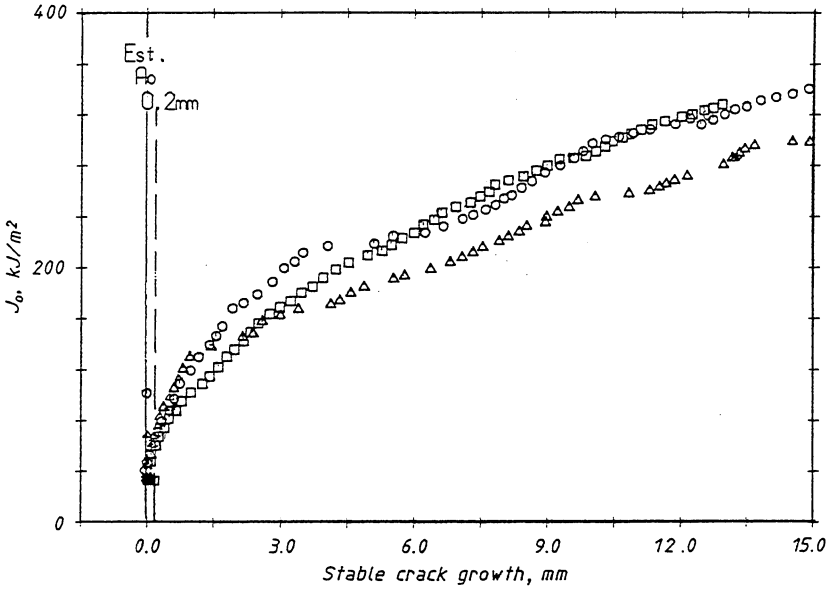

Fig. 2-62
Comparison of J_0 R-curves for 20 x 80 mm SENB specimens;
Ti-3Al-2V alloy; from Ref. [2.46]

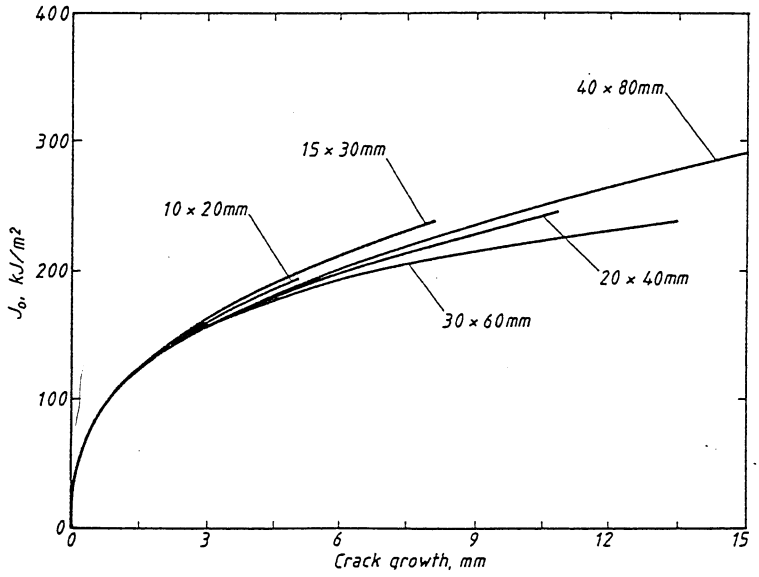

Fig. 2-63
Comparison of J_0 R-curves (size effects programme);
Ti-3Al-2V alloy; from Ref. [2.46]

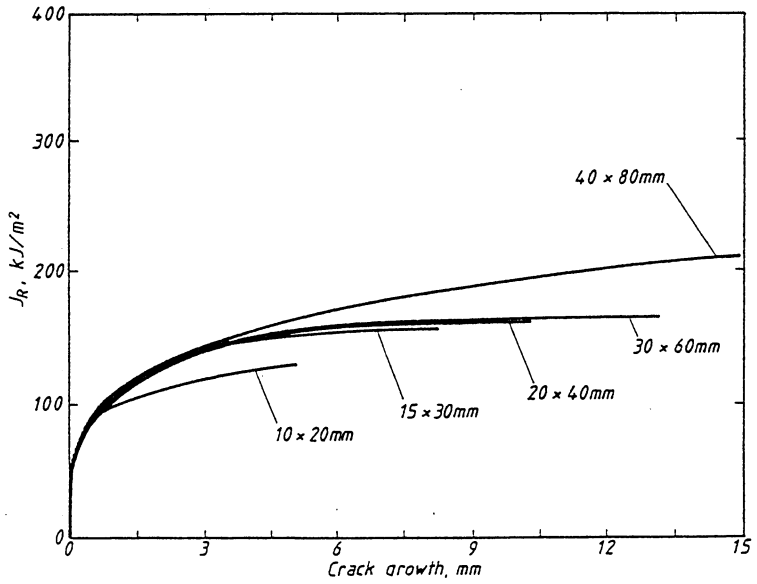

Fig. 2-64
Comparison of J_R R-curves (size effects programme);
Ti-3Al-2V alloy; from Ref. [2.46]

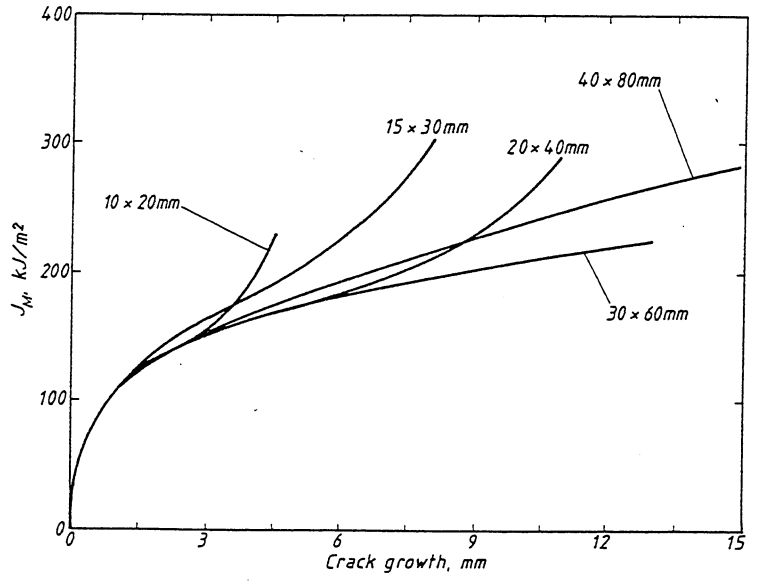

Fig. 2-65
Comparison of J_M R-curves (size effects programme);
Ti-3Al-2V alloy; from Ref. [2.46]

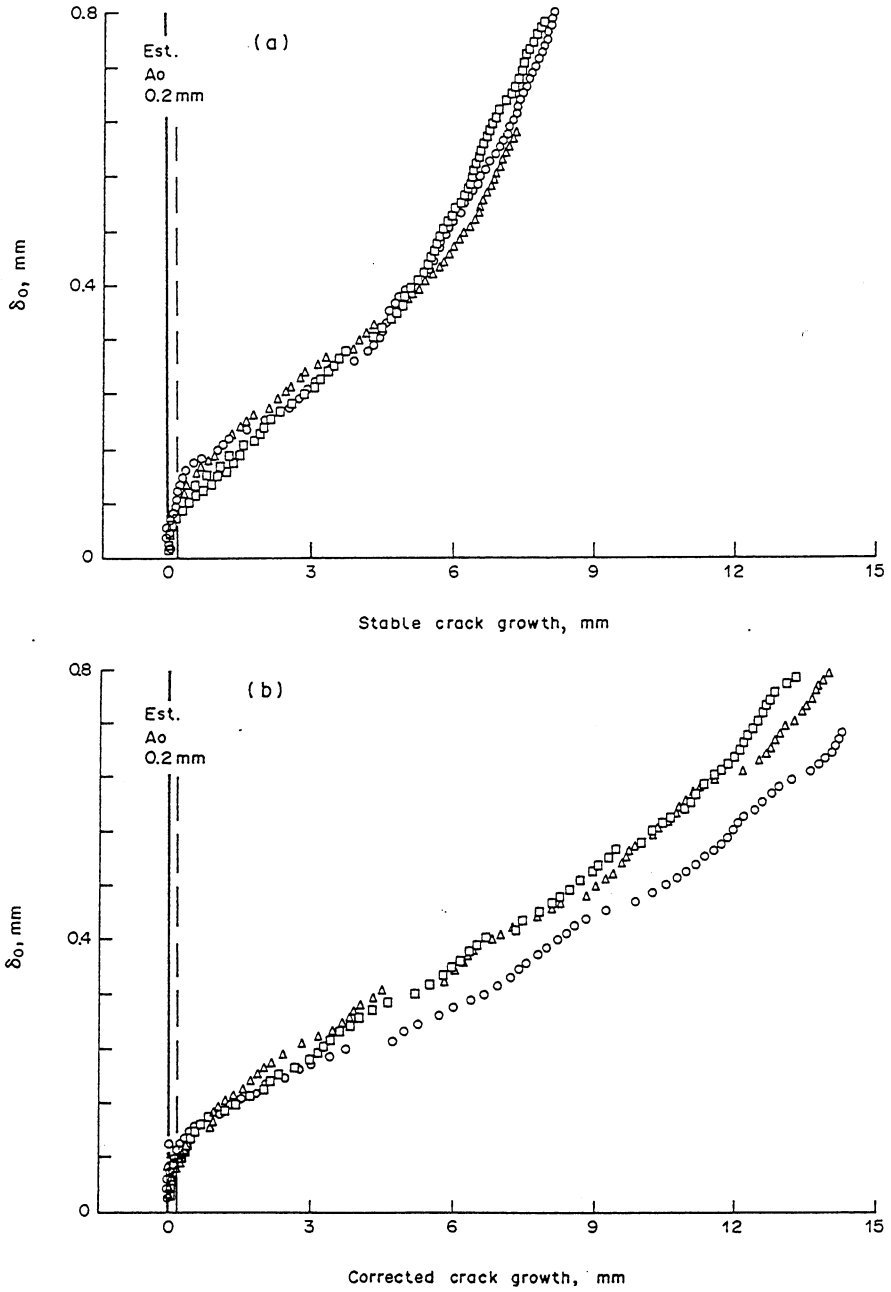

Fig. 2-66
Comparison of δ_0 R-curves from : (a) 15 x 30 mm SENB specimens; (b) 20 x 60 mm SENB specimens; Ti-3Al-2V alloy; from Ref. [2.47]

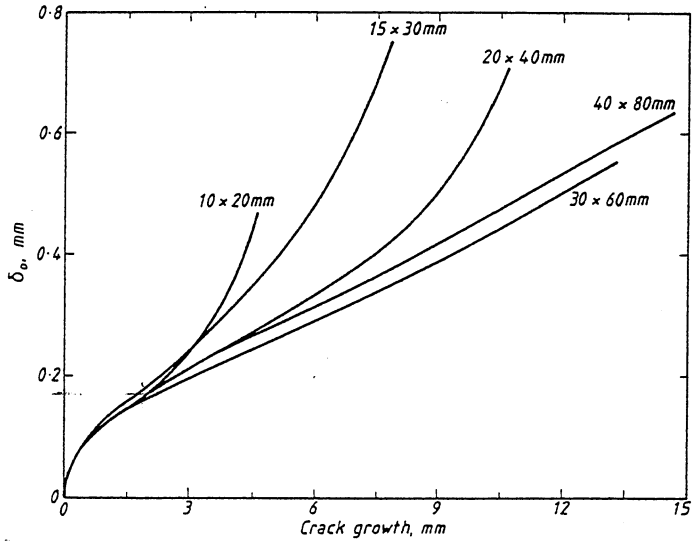

Fig. 2-67
Comparison of δ_0 R-curves (size effects programme);
Ti-3Al-2V alloy; from Ref. [2.47]

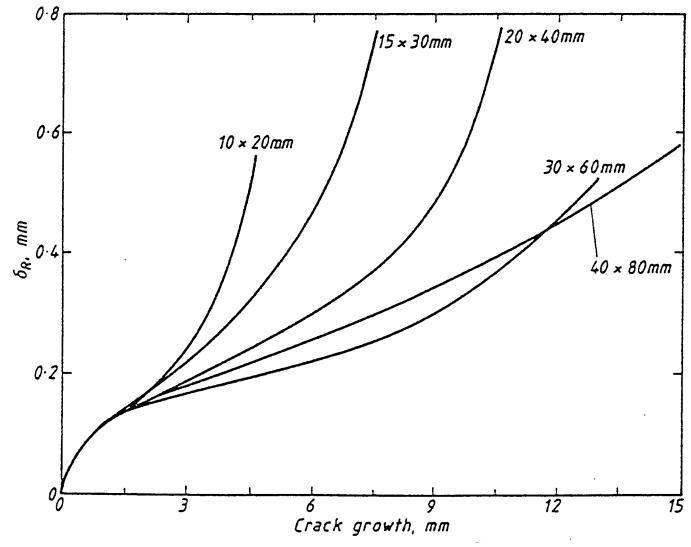

Fig. 2-68
Comparison of δ_R R-curves (size effects programme);
Ti-3Al-2V alloy; from Ref. [2.47]

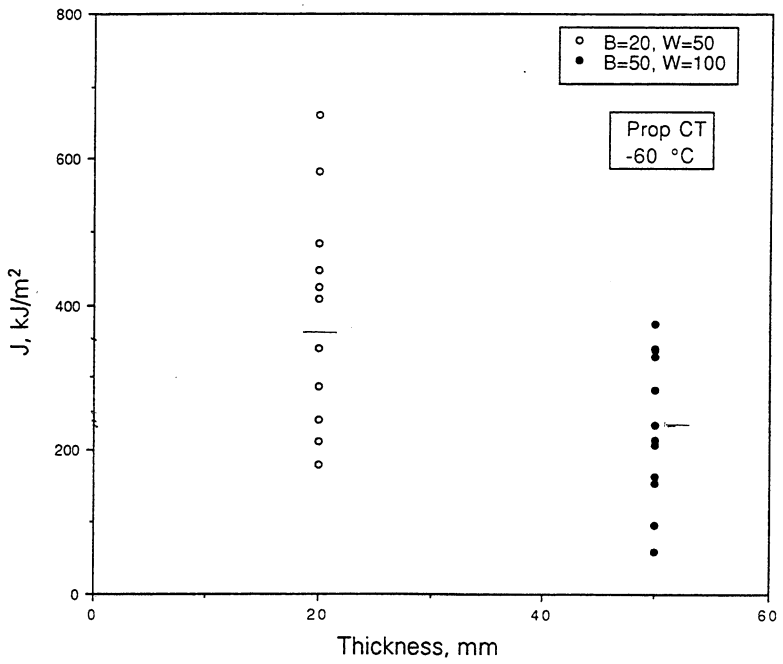

Fig. 2-69
J-integral for cleavage vs. thickness; geometrically similar CT specimens at -60 °C; material: 20 MnMoNi55 (code: PVS, pressure vessel steel tested by GKSS); from Ref. [2.49]

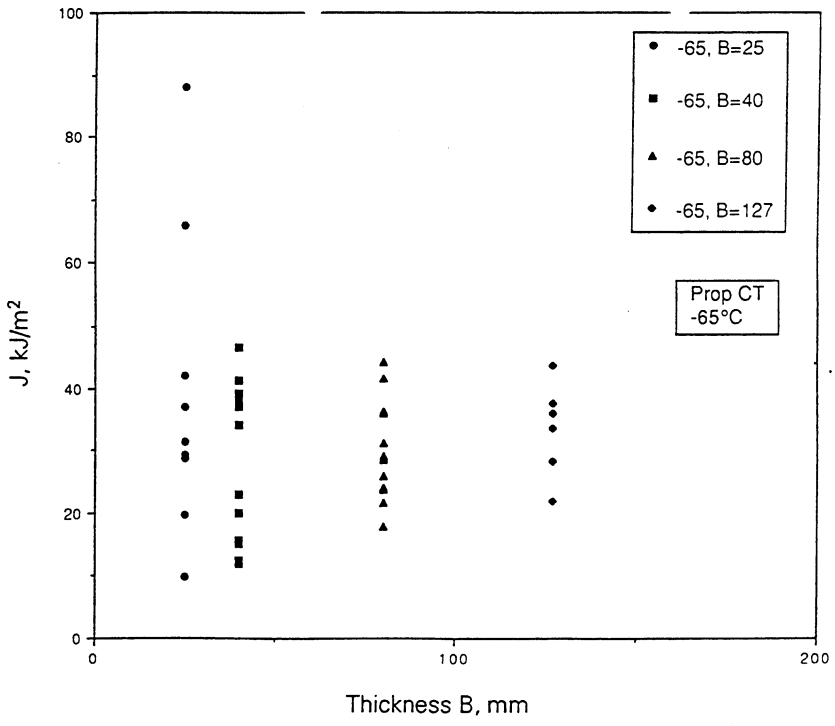

Fig. 2-70
J-integral for cleavage vs. thickness; geometrically similar CT specimens at -65 °C; material: A533B (code: Morland TH, pressure vessel steel tested by UKAEA); from Ref. [2.49]

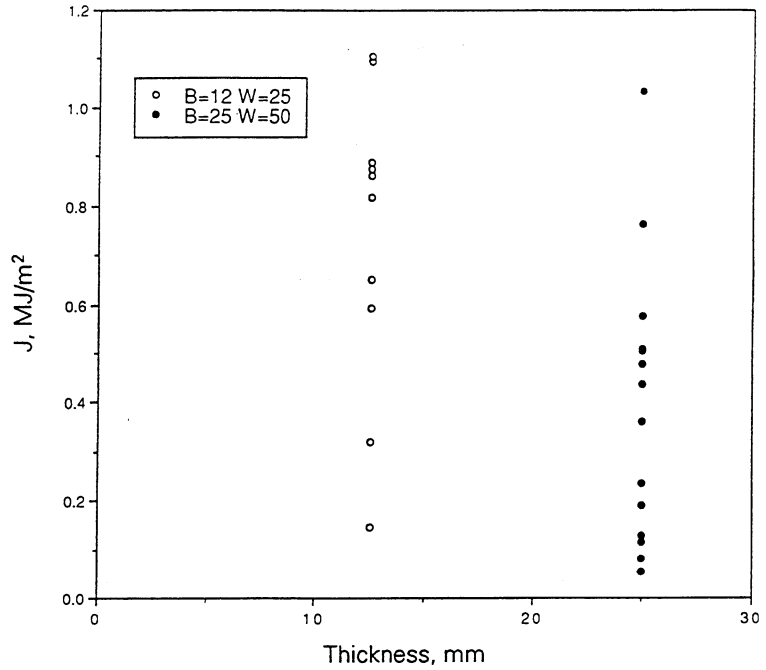

Fig. 2-71
J-integral for cleavage vs. thickness; geometrically similar CT specimens at -30 °C; material: A533B (code: Morland SG, pressure vessel steel tested by UKAEA); from Ref. [2.49]

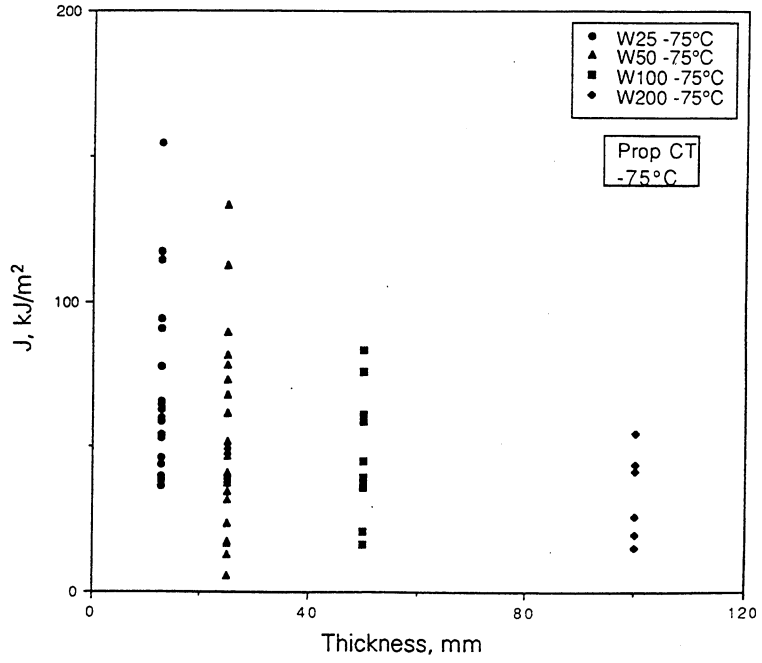

Fig. 2-72
J-integral for cleavage vs. thickness; geometrically similar CT specimens at -75 °C; material: A533B (code: McCabes data, pressure vessel steel tested by ORNL); from. Ref. [2.49]

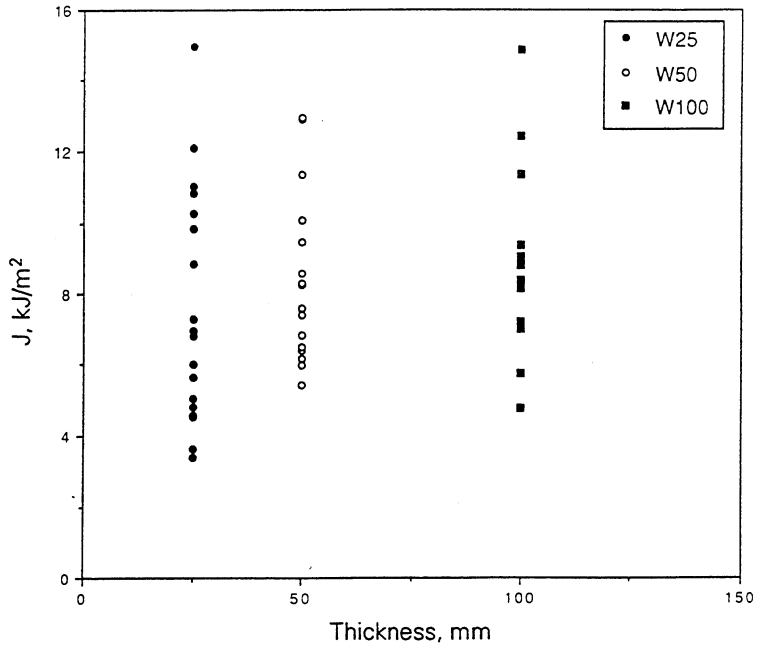

Fig. 2-73
J-integral for cleavage vs. thickness; geometrically similar CT specimens at -150 °C; material: A533B (code: McCabes data, pressure vessel steel tested by ORNL);
from Ref. [2.49]

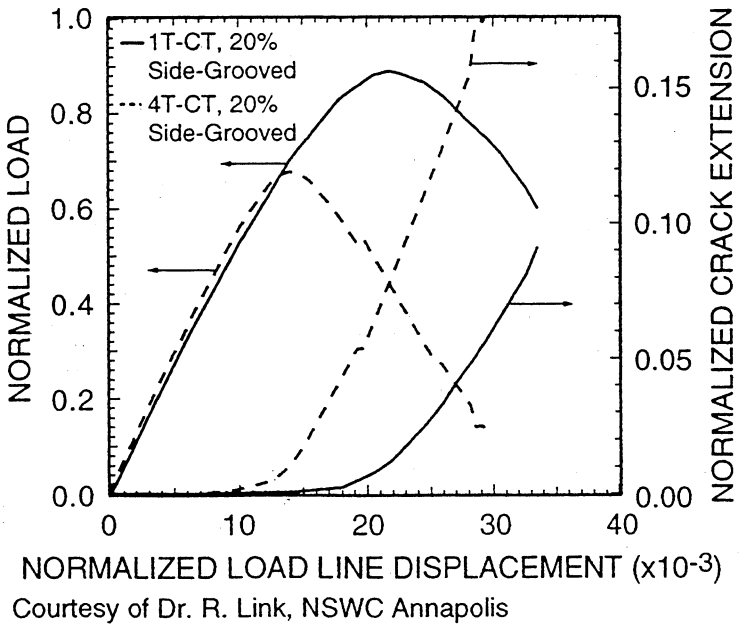

Courtesy of Dr. R. Link, NSWC Annapolis

Fig. 2-74
Size influence on the normalized load and crack extension vs. load-line displacement curves of single fracture tests with 1T and 4T compact tension (CT) specimens (20 % sidegrooved, a/W=0.70-0.71); material: high strength HY-130 steel; from Ref. [2.51]

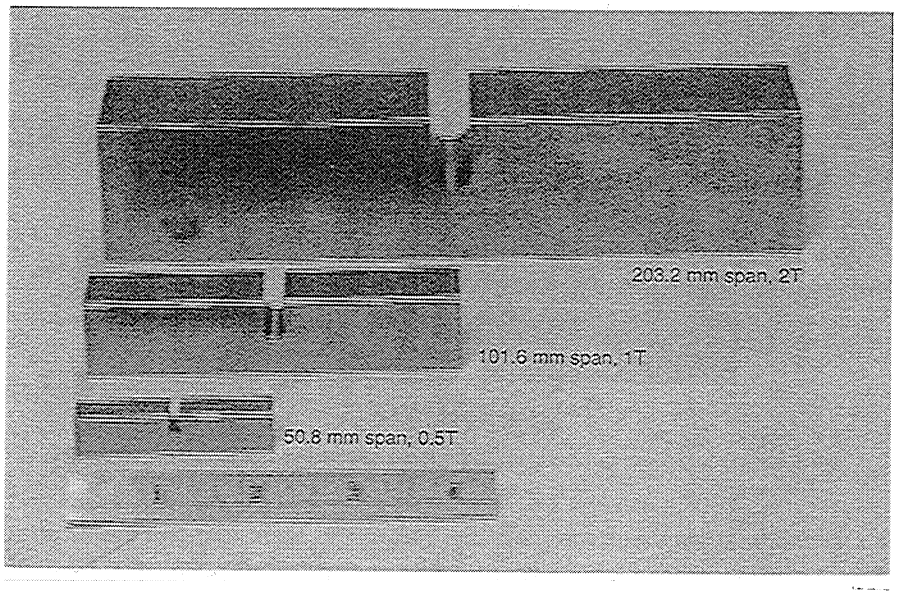

Fig. 2-75
Geometrically similar blunt notched three-point-bend specimens; from Ref. [2.52]

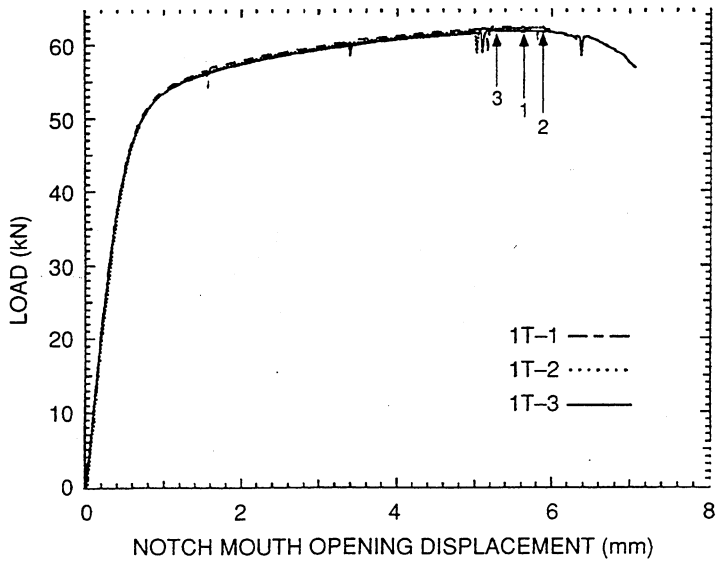

Fig. 2-76
Load vs. notch-mouth-opening displacement for three nominally identical 1T blunt-notched three-point-bend specimens (arrow markers correspond to crack initiations); material: high strength HY-130 steel; from Ref. [2.52]

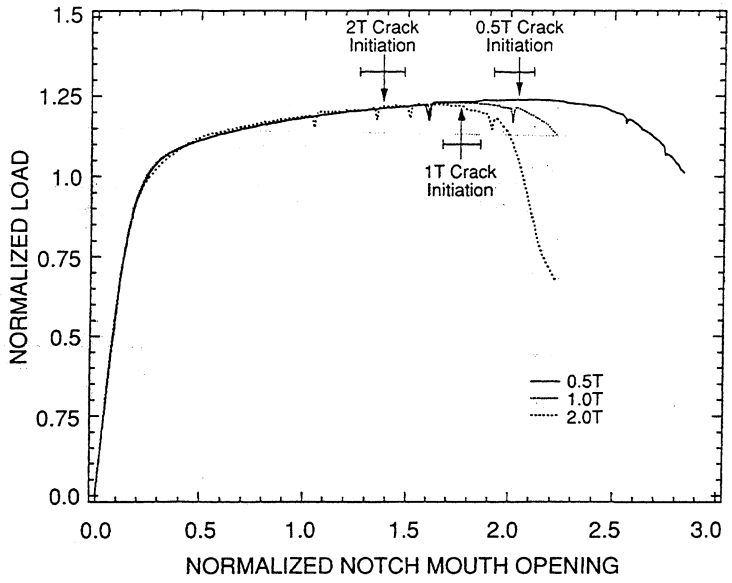

Fig. 2-77
Size influence on the normalized load vs. notch-mouth-opening curves and on crack initiation for three sizes (0.5T, 1.0T, 2.0T) of blunt-notched three-point-bend specimens; material: high strength-low hardening HY-130 steel; from Ref. [2.52]

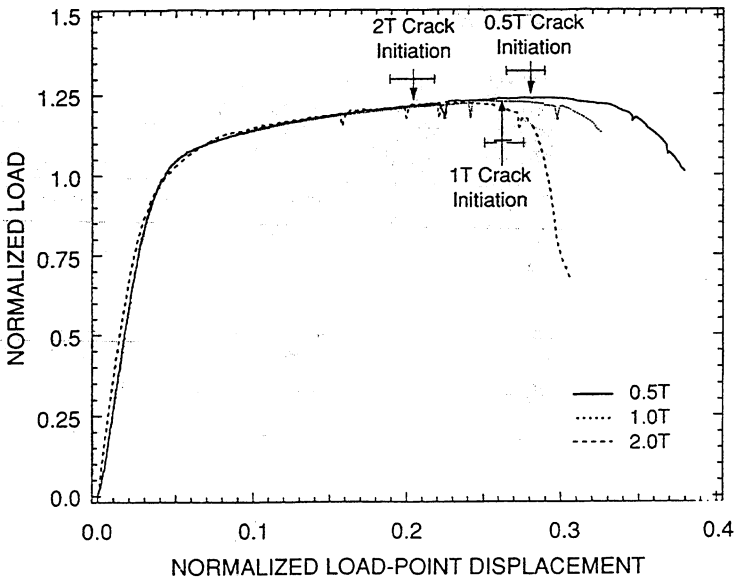

Fig. 2-78
Size influence on the normalized load vs. load-point displacement curves and on crack initiation for three sizes (0.5T, 1.0T, 2.0T) of blunt-notched three-point-bend specimens; material: high strength-low hardening HY-130 steel; from Ref. [2.52]

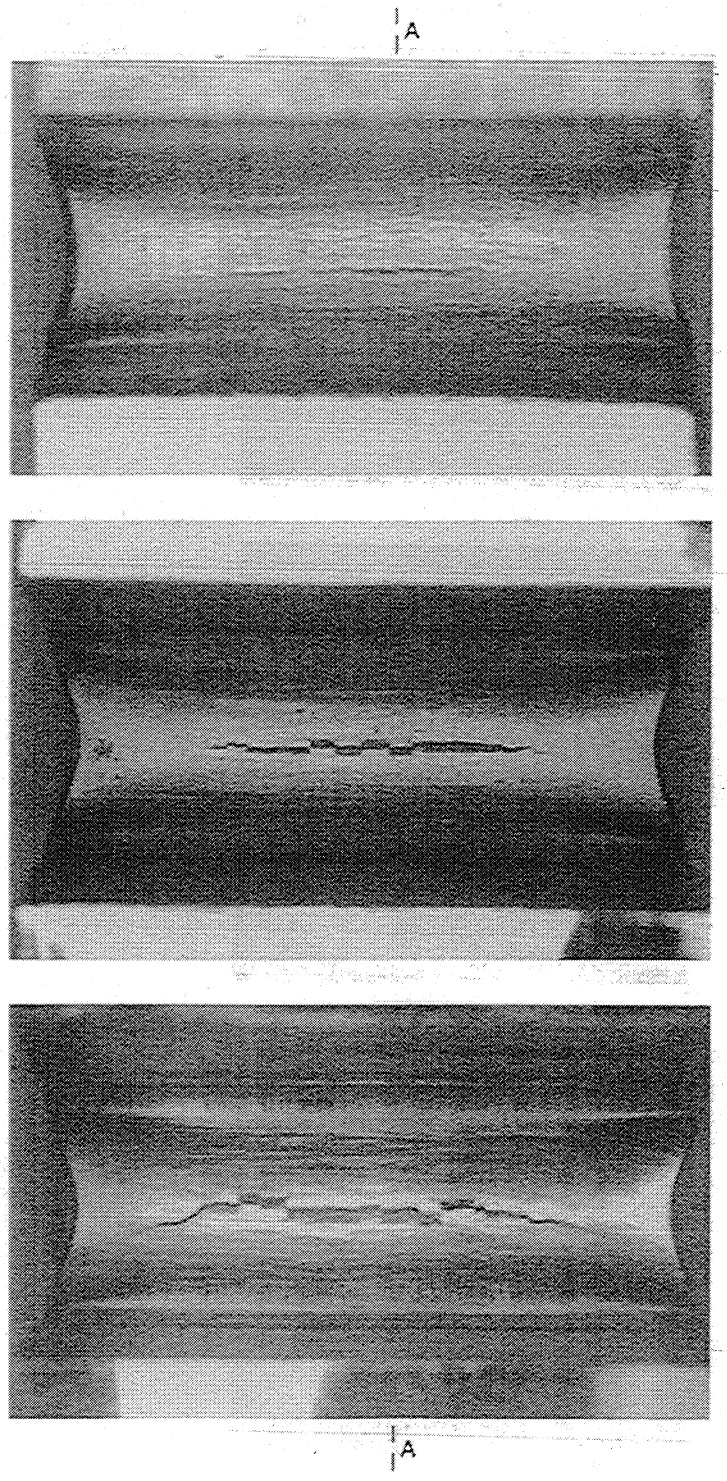

Fig. 2-79
Extend of cracking at the notch root of geometrically similar blunt-notched three-point-bend specimens, bend to approximately equal residual angles α; material: high strength-low hardening steel HY-130 steel; from Ref. [2.52]

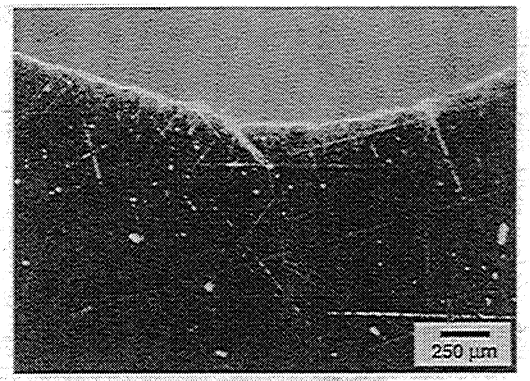

(a) Specimen 0.5T-1, α = 17.8°

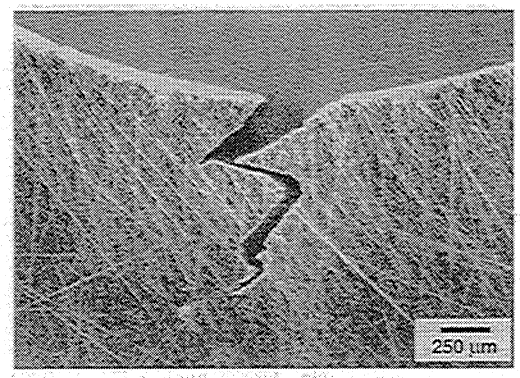

(b) Specimen 1T-3, α = 18.0°

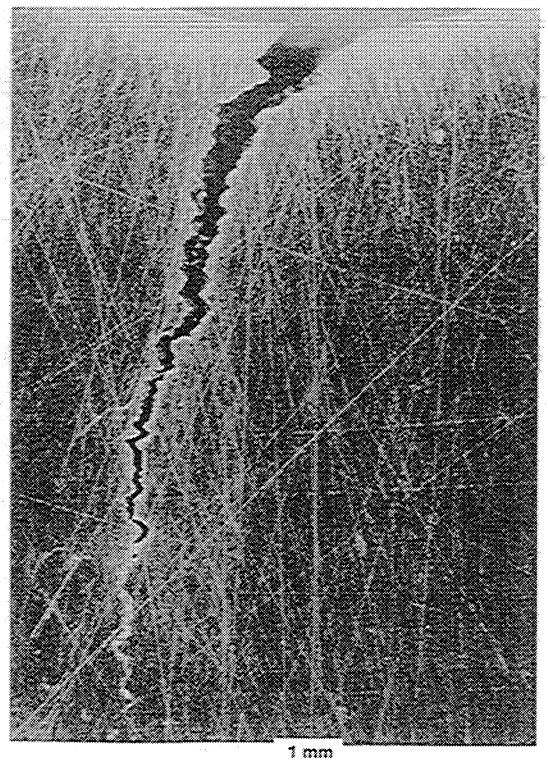

(c) Specimen 2T-3, α = 17.0°

Fig. 2-80
Maximum crack penetration at mid thickness for three specimen sizes (specimens 0.5 T-1, 1 T-3, 2 T-3 at approximately the same bend angle α), material: high strength-low hardening HY-130 steel; from Ref. [2.52]

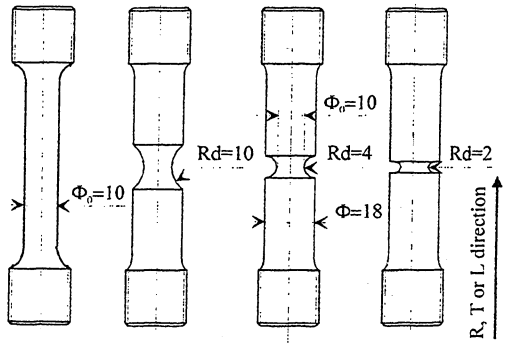

Fig. 2-81
Geometry of smooth and notched tensile specimens; from Ref. [2.56]

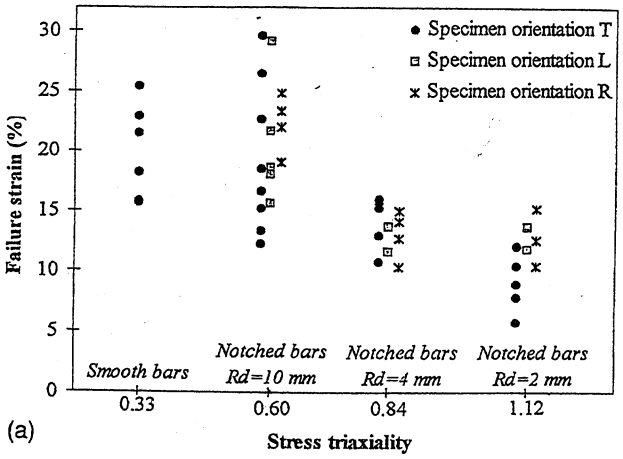

Fig. 2-82
Experimental data of the logarithmic diametric failure strain at the neck or notch root for smooth and notched axisymmetric tensile specimens; initial minimum diameter ϕ_0= 10 mm; thermally embrittled duplex stainless steel CF8M; from Ref. [2.56]

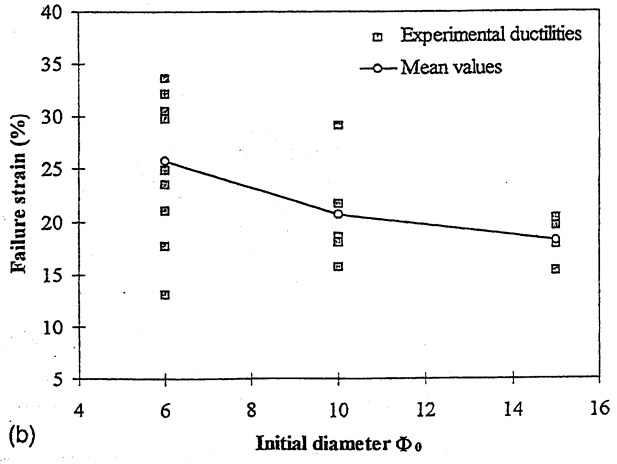

Fig. 2-83
Experimental data of the logarithmic diametric failure strain at the notch root of a family of geometrically similar notched axisymmetric tensile specimens (ϕ_o/R_d=1); specimen orientation L; thermally embrittled duplex stainless steel CF8M; from Ref. [2.56]

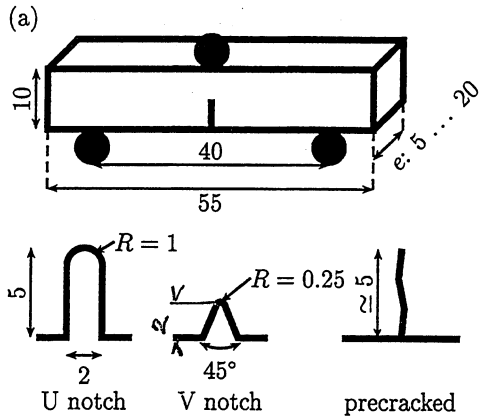

Fig. 2-84
Dimensions (mm) of Charpy type U-, V- and precracked specimens under three-point bending; from Ref. [2.58]

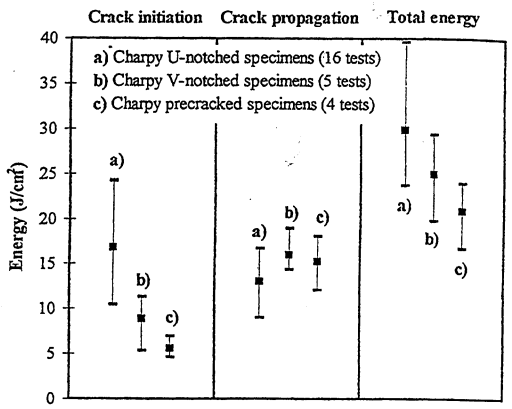

Fig. 2-85
Mean values and scatter of surface specific energies for "crack initiation" and "-propagation"; Charpy type U-notched, V-notched and precracked specimens; thermally embrittled duplex stainless steel CF8M; from Ref. [2.56]

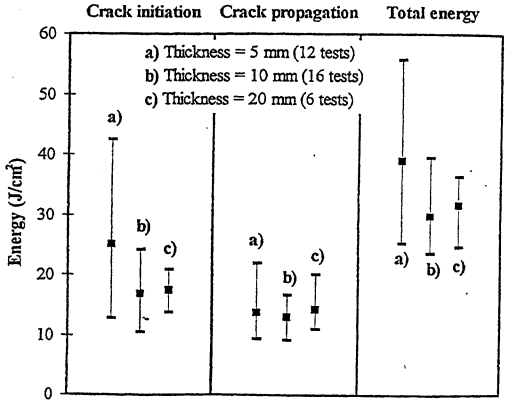

Fig. 2-86
Mean values and scatter of surface specific energies for "crack initiation" and "-propagation", Charpy type U-notched specimens with different thicknesses; thermally embrittled duplex stainless steel; from Ref. [2.56]

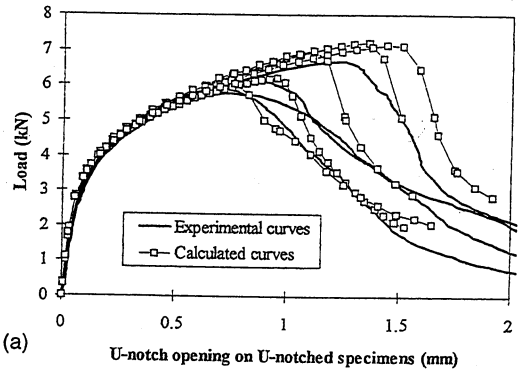

Fig. 2-87
Scatter of experimental and calculated load vs. notch-mouth opening curves for Charpy type U-notched specimens under three-point bending; thermally embrittled duplex stainless steel CF8M; from Ref. [2.56]

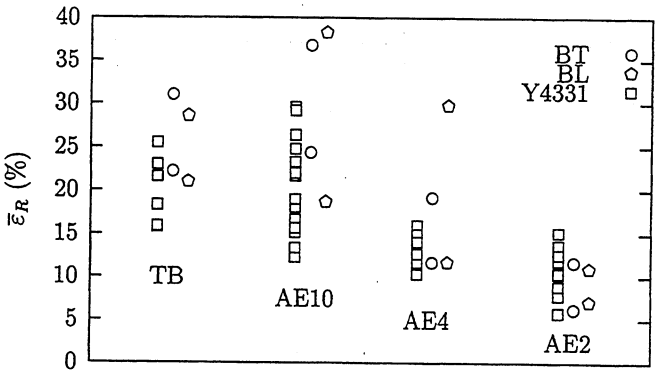

Fig. 2-88
Experimental data of the logarithmic diametric failure strain at the neck or notch root for smooth (TB) and notched axisymmetric tensile specimens (AE10, AE4, AE2); initial minimum diameter ϕ_o= 10 mm for material Y4331 and ϕ_o= 6 mm for materials BT and BL; thermally embrittled duplex stainless steels; from Ref. [2.58]

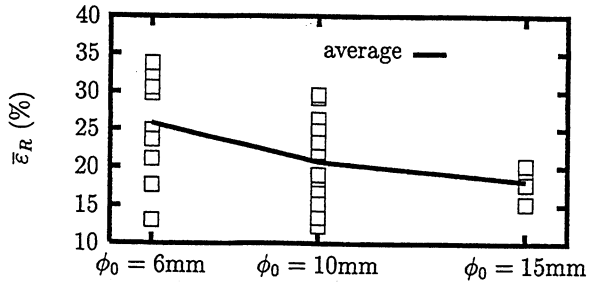

Fig. 2-89
Experimental data of the logarithmic diametric failure strain at the notch root of a family of geometrically similar notched axisymmetric specimens (ϕ_o/R_d=1); thermally embrittled duplex stainless steel Y4331; from Ref. [2.58]

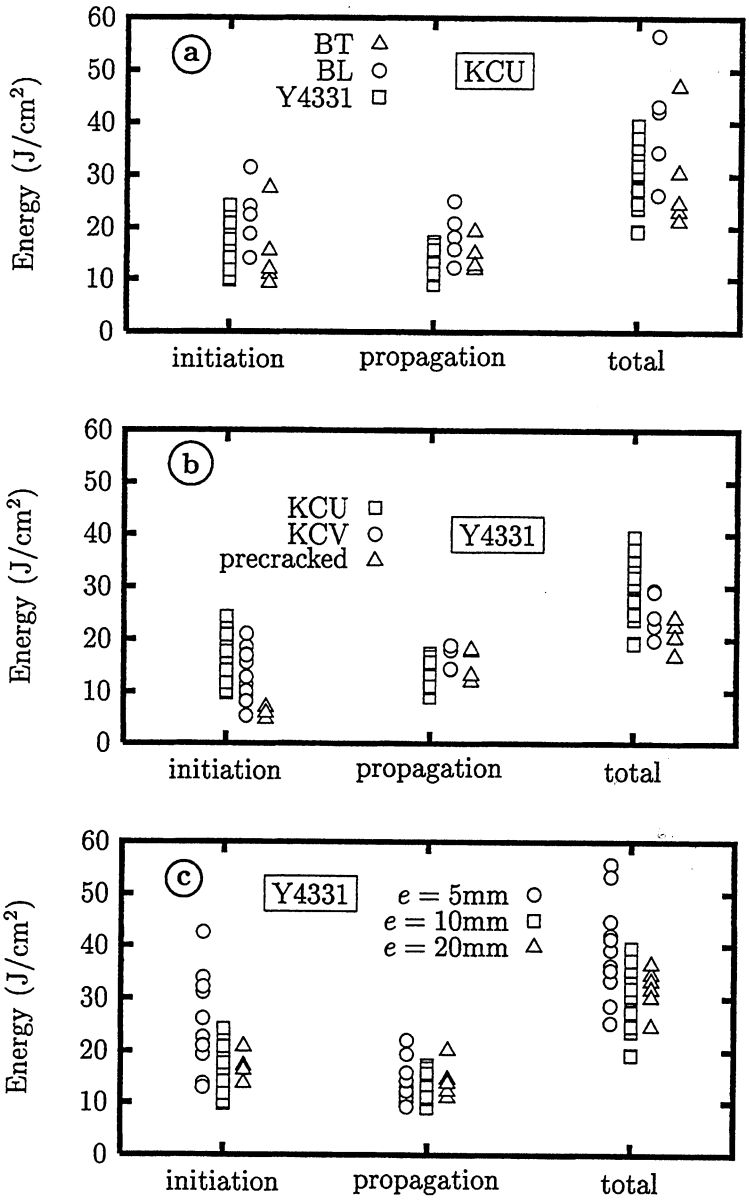

Fig. 2-90
Crack initiation, -propagation and total energies of different Charpy type specimens under three-point bending: (a) U-notched specimen of materials Y4331, BT and BL (cast duplex stainless steels), (b) U- and V-notched and precracked specimens for material Y4331, (c) U-notched specimens for material Y4331 of various thicknesses; from Ref. [2.58]

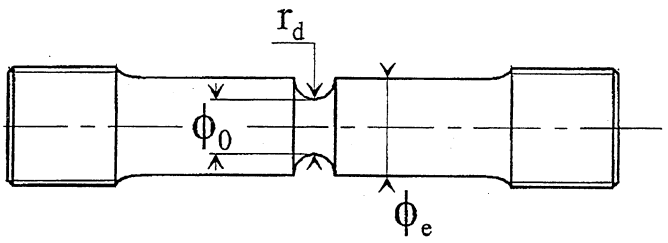

tranverse direction

(a)

	AE2 ϕ_0 =10 mm	AE4 ϕ_0 =10 mm	AE10 ϕ_0 =10 mm
r_d (mm)	2	4	10
ϕ_e (mm)	18	18	18

(b)

	AE4 ϕ_0 =3.75 mm	AE4 ϕ_0 =6 mm	AE4 ϕ_0 =10 mm	AE4 ϕ_0 =15 mm
r_d (mm)	1.5	2.4	4	6
ϕ_e (mm)	6.75	10.8	18	27

Fig. 2-91
Geometry and dimensions of the notched tensile specimens (a) for different geometries AE2, AE4, AE10, (b) for the different sizes of a AE4 type specimen with ϕ_o= 3.75, 6, 10 and 15 mm; from Ref. [2.63]

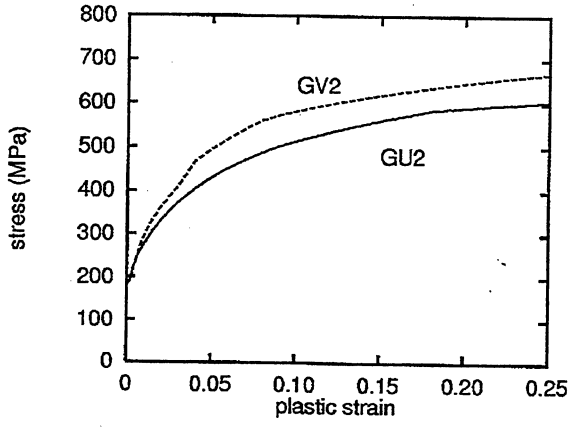

Fig. 2-92
Stress-strain curves of material GV2 (used for size effect tests) and GV2 (used for geometry effect-notch radius variation-tests); C-Mn steel; from Ref. [2.63]

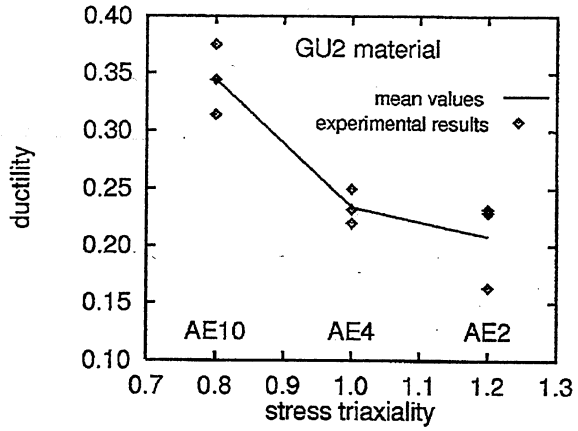

Fig. 2-93
Effect of notch radius variation on diametrical strain at failure; notched tensile specimens type AE10, AE4, AE2, notch radii Rd=10, 4, 2 mm, initial minimum diameter ϕ_o= 10 mm; C-Mn steel; from Ref. [2.63]

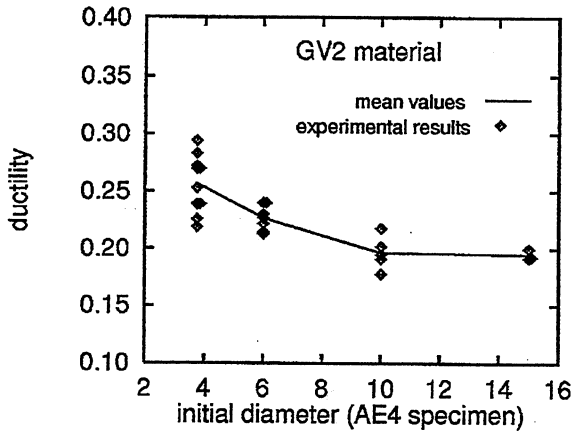

Fig. 2-94
Effect of size variation on diametrical strain at failure; notched tensile specimens type AE4, initial minimum diameter ϕ_o= 3.75, 6, 10, 15 mm; C-Mn steel; from Ref. [2.63]

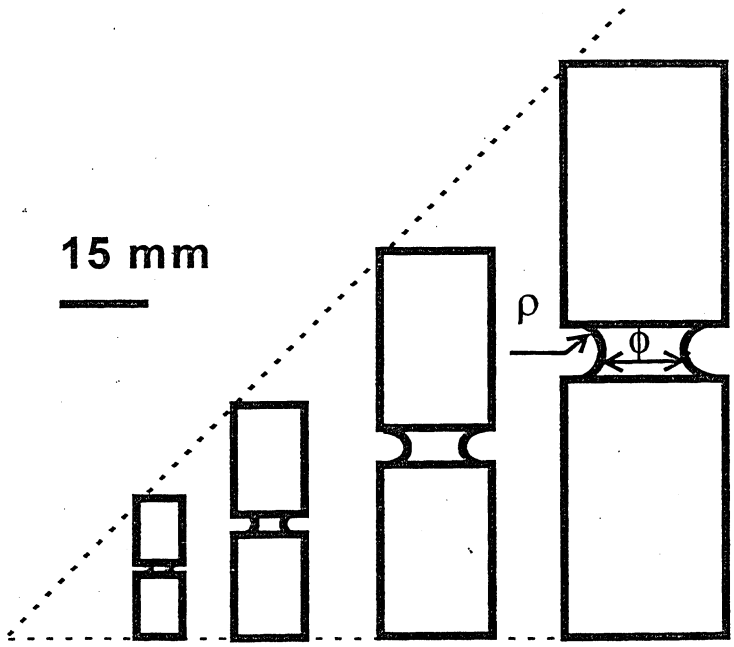

Fig. 2-95
Geometrically similar notched round tension specimens AE4-3.6, AE4-6, AE4-10 and AE4-15; C-Mn steel; from Ref. [2.64]

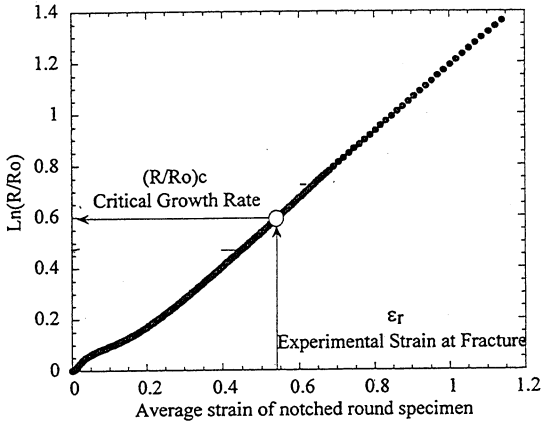

Fig. 2-96
Evaluation of cavity radius ratio and determination of the critical ratio from an experimental average diametrical strain at fracture; notched round specimens; C-Mn steel at 100 °C; from Ref. [2.64]

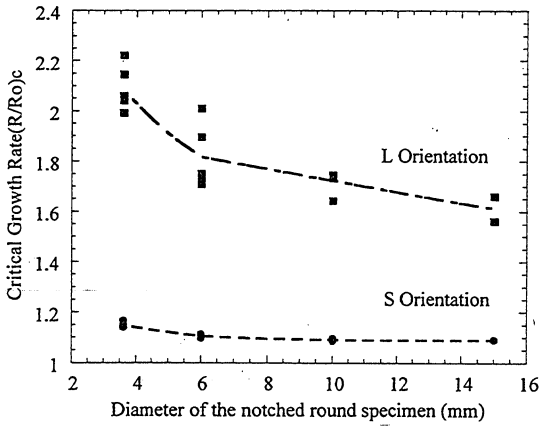

Fig. 2-97
Size dependence of critical cavity radius ratio for specimens along longitudinal (L) and radial (S) direction of a pipe component; C-Mn steel at 100 °C; from Ref. [2.64]

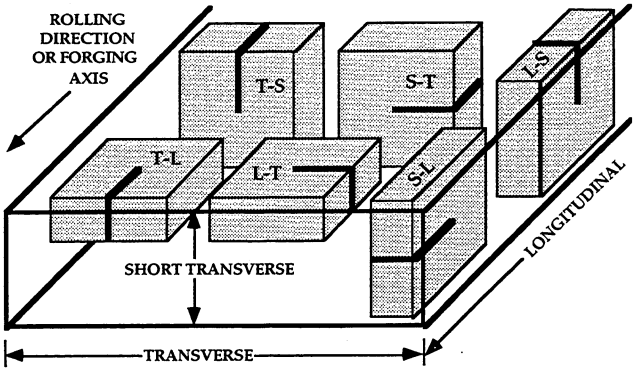

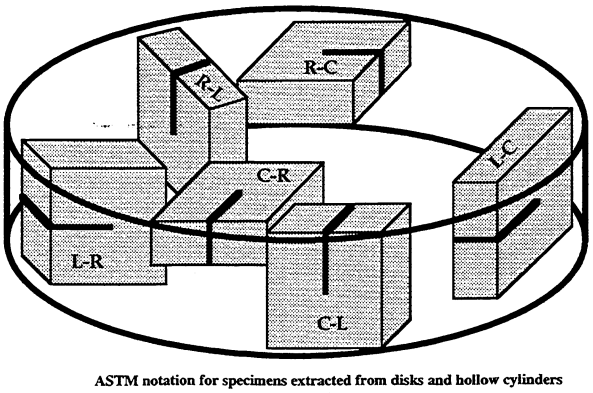

Fig. 2-98
ASTM notation for specimens cut from plates and hollow cylinders or circular disks; from Ref. [2.28]

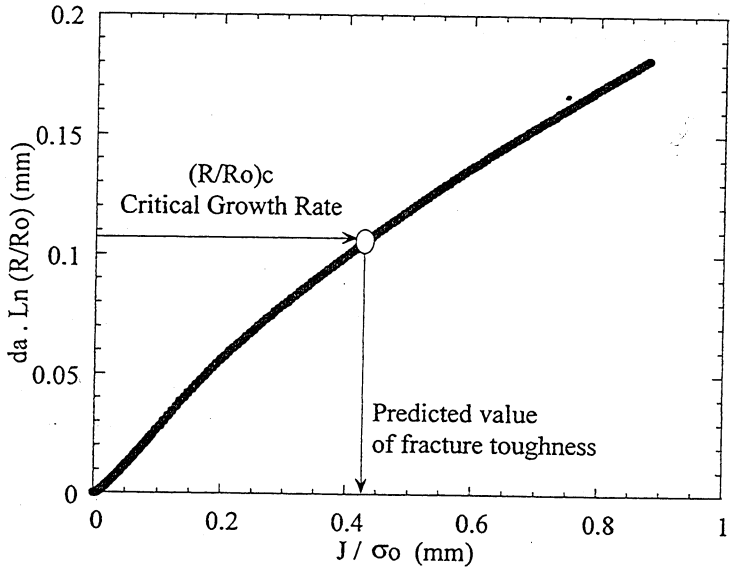

Fig. 2-99
Relation between numerically computed $\ln(R/R_o)$-values and J/σ_o at crack initiation for a 1T CT-specimen; C-Mn steel; from Ref. [2.64]

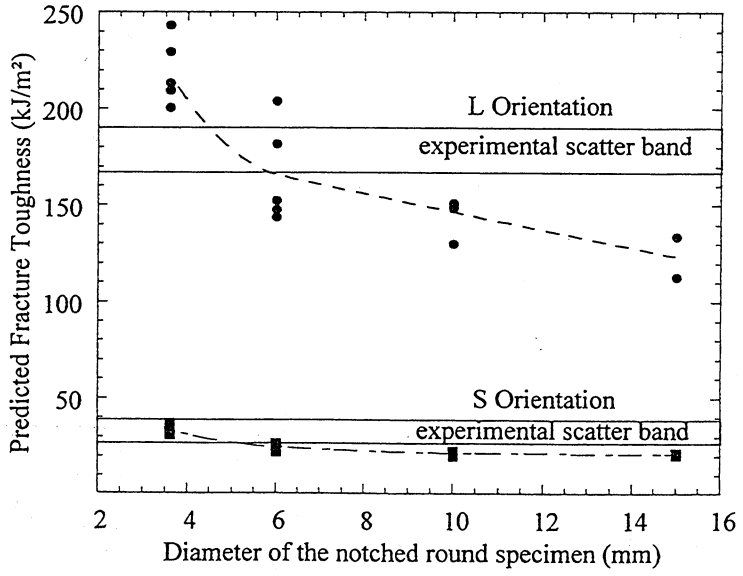

Fig. 2-100
Comparison of the predicted and experimental values for the fracture toughness J of CT-specimens; predicted values depend on the size of the round notched tension specimens used to determine the critical cavity radius ratio $(R/R_o)_c$; C-Mn steel at 100 °C; from Ref . [2-64]

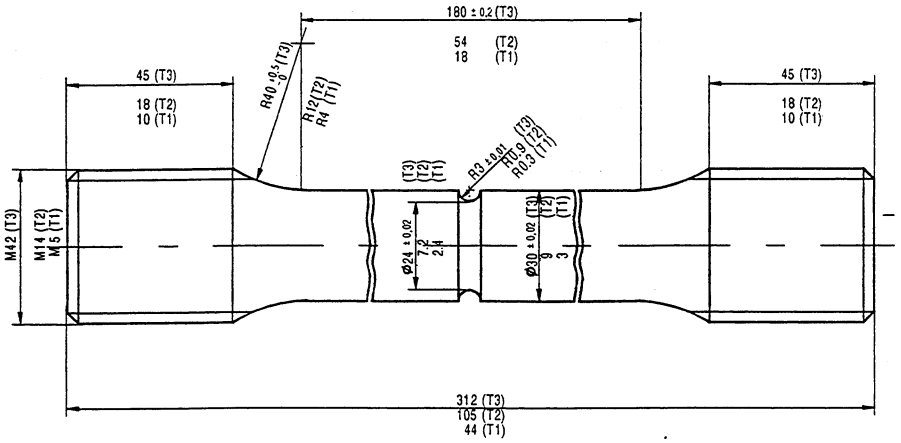

Fig. 2-101
Blunt-notched tensile specimens T1, T2, T3; dimensions are given in millimetre; from Ref. [2.72]

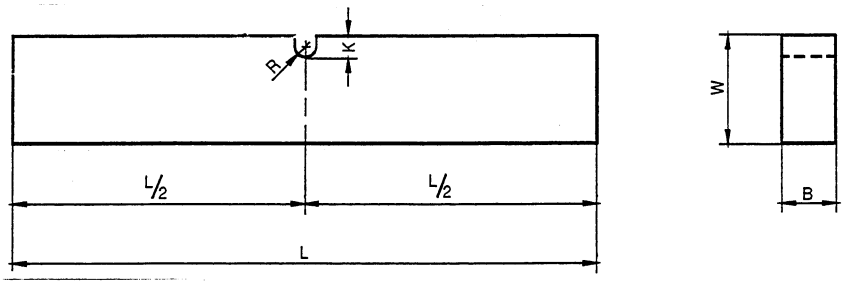

Type	Abbr.	W	B	L	L/2	K	R
1	S1	10 ± 0,1	5 ± 0,1	(55)	27,5 ± 0,1	3 ± 0,1	1 ± 0,05
2	S2	25 ± 0,1	12,5 ± 0,1	(137,5)	68,75 ± 0,2	7,5 ± 0,1	2,5 ± 0,05
3	S3	140 ± 0,1	70 ± 0,1	(770)	385 ± 0,5	42 ± 0,1	14 ± 0,05

Fig. 2-102
Three-point-bend bars with semicircular notch; from Ref. [2.76]

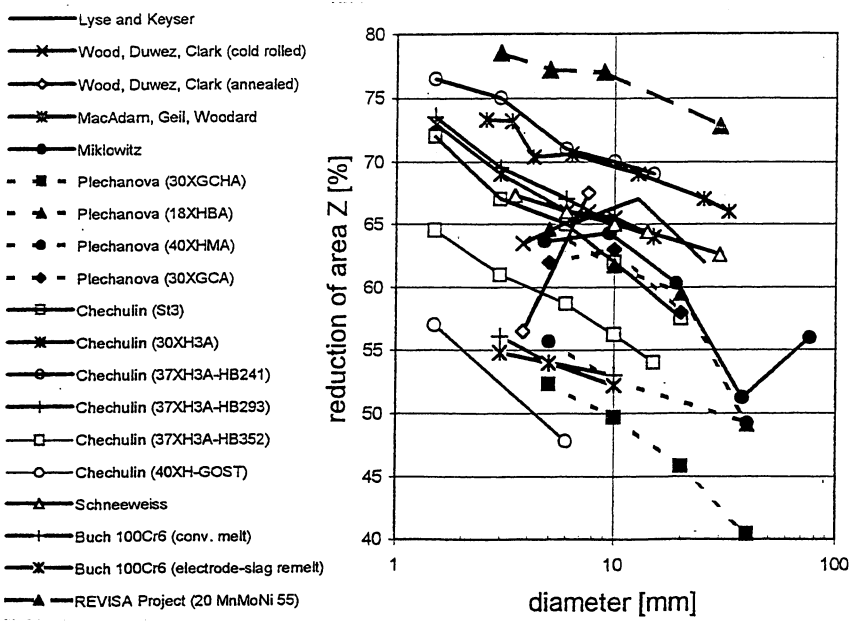

Fig. 2-103
Size dependence of the reduction of area at fracture for smooth circular tension specimens; R.T. and quasi –static strain rates; from Ref. [2.66]

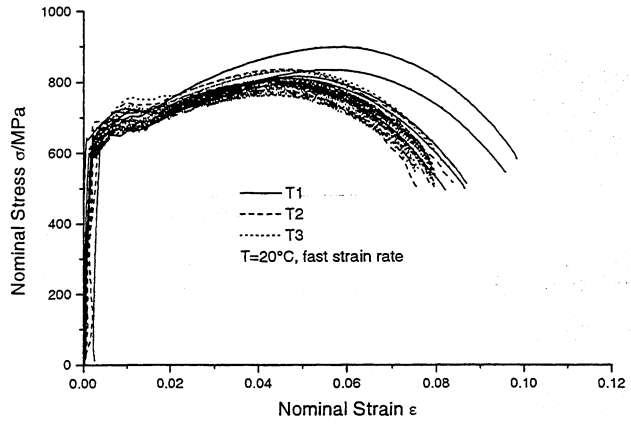

Fig. 2-104
Nominal stress vs. nominal longitudinal strain in the gauge section for the notched tensile specimens T1, T2, T3 at R.T.; fast strain rate $10^{-3}s^{-1}$; material: ferritic steel 20 MnMoNi 55; from Ref. [2.72]

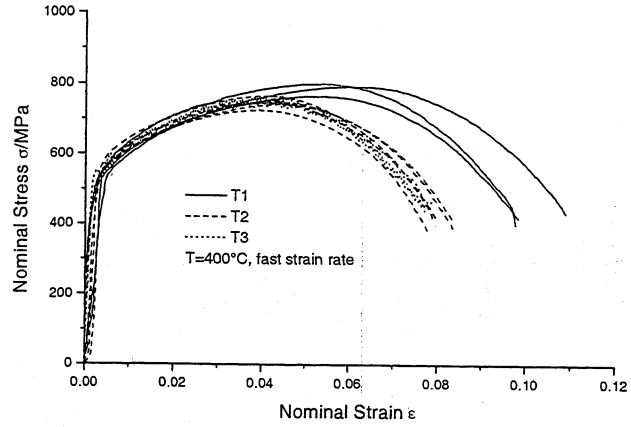

Fig. 2-105
Nominal stress vs. nominal longitudinal strain in the gauge section for the notched tensile specimens T1, T2, T3 at 400 °C; fast strain rate $10^{-3}s^{-1}$; material: ferritic steel 20 MnMoNi 55; from Ref. [2.72]

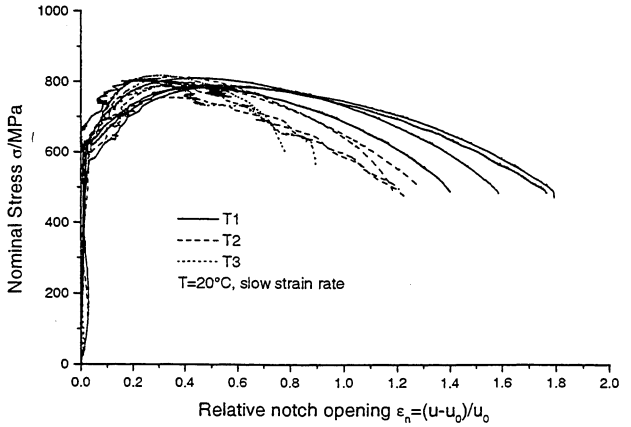

Fig. 2-106
Nominal stress vs. relative notch opening for the notched tensile specimens T1, T2 and T3 at R.T.; slow strain rate $2\cdot10^{-5}s^{-1}$; material: ferritic steel 20 MnMoNi 55; from Ref. [2.72]

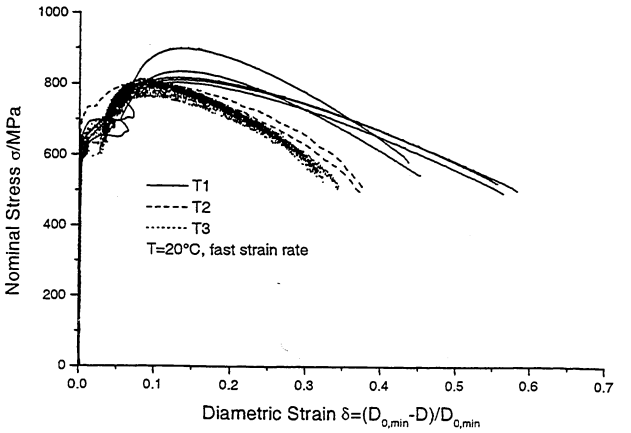

Fig. 2-107
Nominal stress vs. diametric strain for the notched tensile specimens T1, T2, and T3 at R.T.; fast strain rate $10^{-3}s^{-1}$; material: ferritic steel 20 MnMoNi 55 ; from Ref. [2.72]

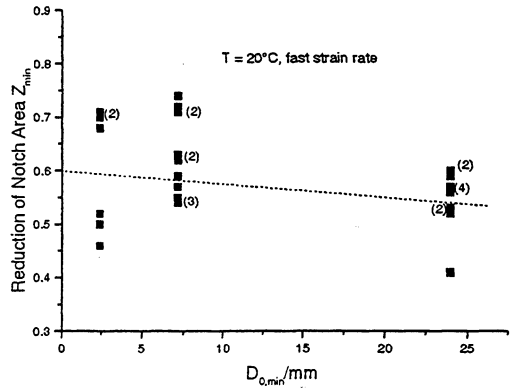

Fig. 2-108
Reduction of notch area vs. minimum initial diameter for the notched tensile specimens T1, T2, T3 at R.T.; fast strain rate $10^{-3}s^{1}$; material: ferritic steel 20 MnMoNi 55; from Ref. [2.72]

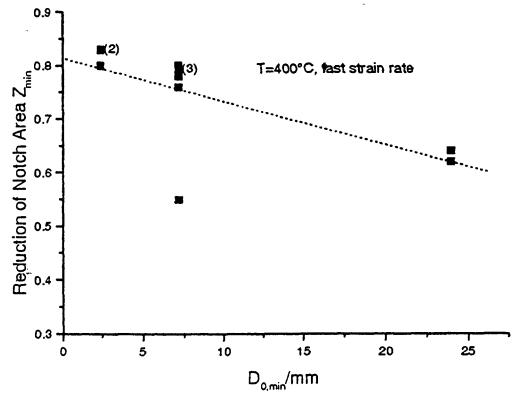

Fig. 2-109
Reduction of notch area vs. minimum initial diameter for the notched tensile specimens T1, T2, T3 at 400 °C; fast strain rate $10^{-3}s^{1}$; material: ferritic steel 20 MnMoNi 55; from Ref. [2.72]

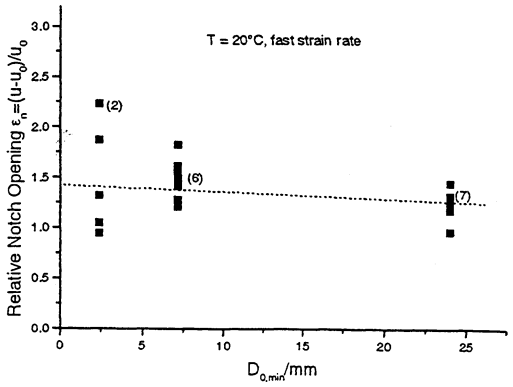

Fig. 2-110
Relative notch opening at fracture vs. minimum initial diameter for the notched tensile specimens T1, T2, T3 at R.T.; fast strain rate $10^{-3}s^{-1}$, material: ferritic steel 20 MnMoNi 55; from Ref. [2.72]

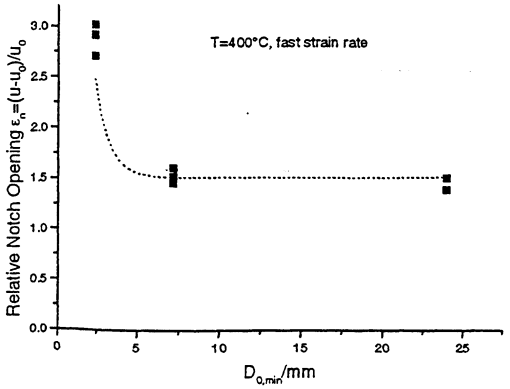

Fig. 2-111
Relative notch opening at fracture vs. minimum initial diameter for the notched tensile specimens T1, T2, T3 at 400 °C.; fast strain rate $10^{-3}s^{-1}$; material: ferritic steel 20 MnMoNi 55; from Ref. [2.72]

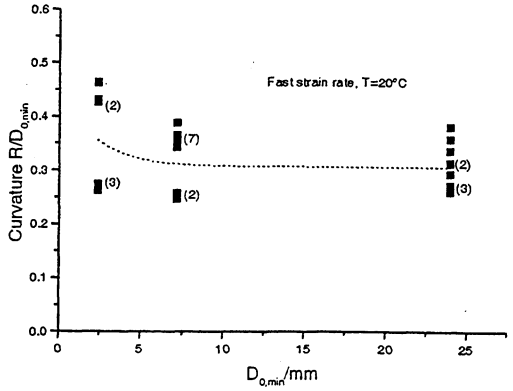

Fig. 2-112
Normalized radius of curvature vs. minimum initial diameter for the notched tensile specimens T1, T2, T3 at R.T.; fast strain rate $10^{-3}s^{-1}$; material: ferritic steel 20 MnMoNi 55; from Ref. [2.72]

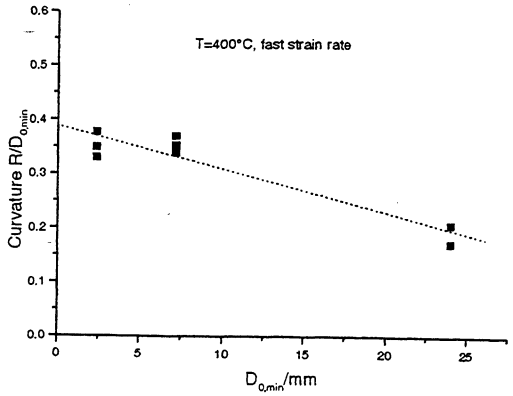

Fig. 2-113
Normalized radius of curvature vs. minimum initial diameter for the notched tensile specimens T1, T2, T3 at R.T. ; fast strain rate $10^{-3}s^{-1}$; material: ferritic steel 20 MnMoNi 55; from Ref. [2.72]

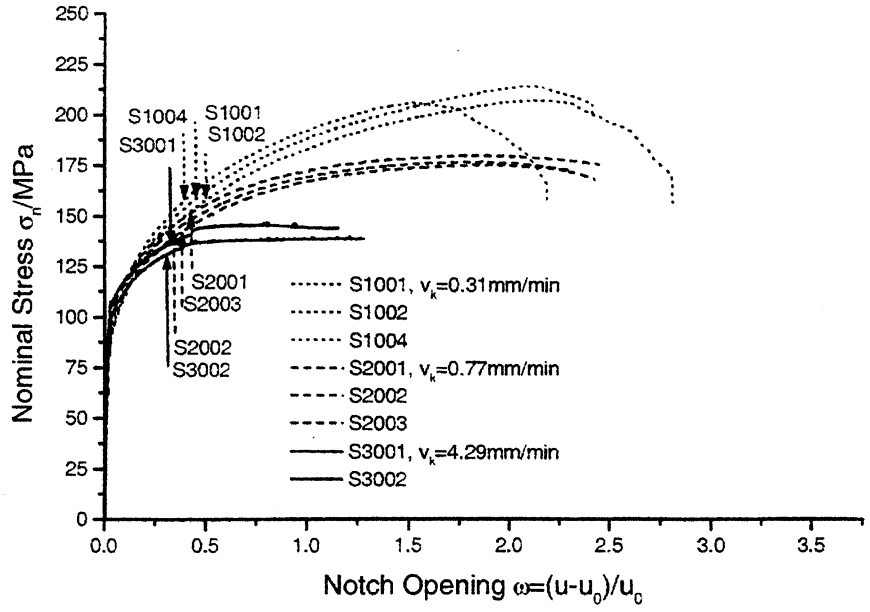

Fig. 2-114
Nominal stress vs. relative notch opening; indication of crack initiation; notched bending specimens at R.T.; fast scaled cross-head speeds; material: 20 MnMoNi 55; from Ref. [2.73]

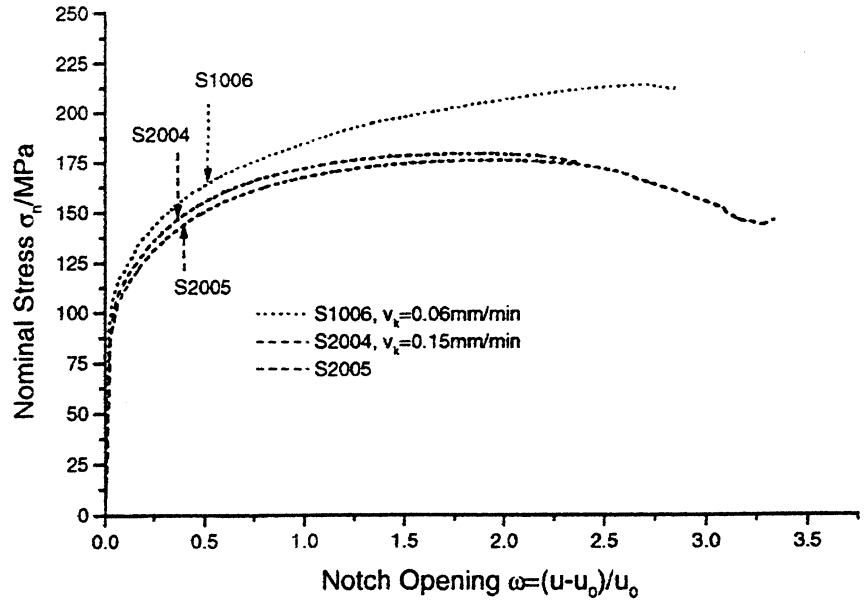

Fig. 2-115
Nominal stress vs. relative notch opening; indication of crack initiation; notched bending specimens at R.T.; slow scaled cross-head speeds; material: 20 MnMoNi 55; from Ref. [2.73]

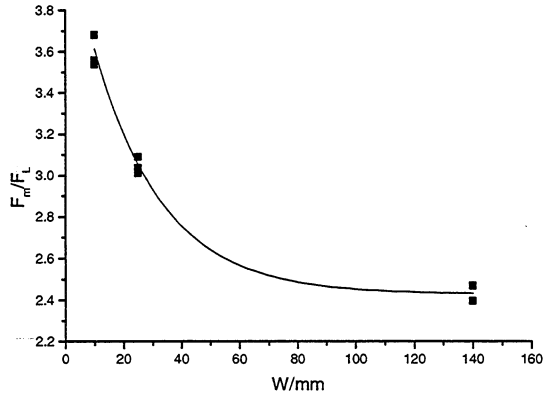

Fig. 2-116
Normalized maximum load F_m/F_L vs. specimen width W; notched bending specimens at R.T.; slow and fast tests; material: ferritic steel 20MnMoNi55; from Ref. [2.76]

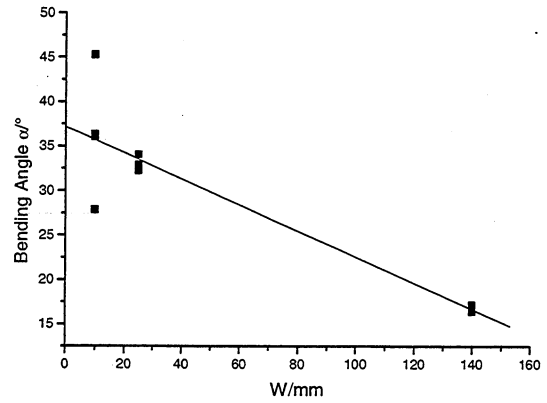

Fig. 2-117
Bending angle α at maximum load vs. specimen width W; notched bending specimens at R.T.; slow and fast tests; material: ferritic steel 20MnMoNi55; from Ref. [2.76]

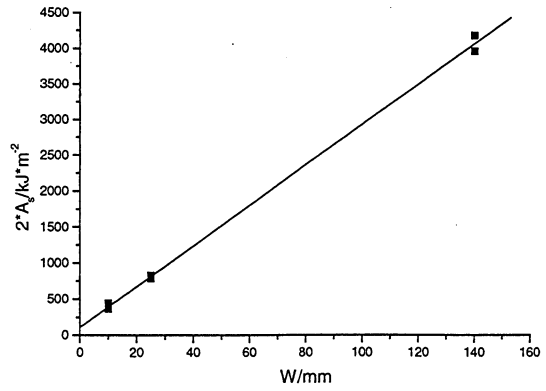

Fig. 2-118
Area specific work A_s for crack initiation vs. beam width W; notched bending specimens at R.T.; slow and fast tests; material: ferritic steel 20 MnMoNi 55; from Ref. [2.73]

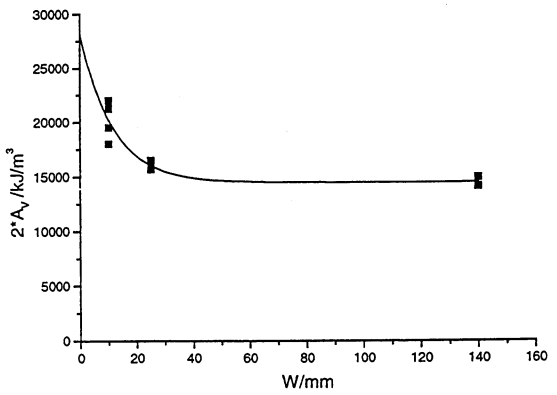

Fig. 2-119
Volume specific work A_v for crack initiation vs. beam width W; notched bending specimens at R.T.; slow and fast tests; material: ferritic steel 20 MnMoNi 55; from Ref. [2.73]